Systems metabolic engineering of *Corynebacterium glutamicum* for extended substrate utilization in biorefinery applications

Dissertation

zur Erlangung des Grades

der Doktors der Ingenieurwissenschaften

der Naturwissenschaftlich-Technischen Fakultät

der Universität des Saarlandes

von

Peng Cao

Saarbrücken

2023

Tag des Kolloquiums:	8. Dezember 2023
Dekan:	Prof. Dr. Ludger Santen
Berichterstatter:	Prof. Dr. Christoph Wittmann
	Prof. Dr. Andriy Luzhetskyy
Vorsitz:	Prof. Dr. Uli Kazmaier
Akad. Mitarbeiter:	Dr. Ruth Kiefer

Publications

Partial results of this work have been published in advance authorized by the Institute of Systems Biotechnology (Universität des Saarlandes) represented by Prof. Dr. Christoph Wittmann.

Peer-reviewed articles

Goldbeck, O., Desef, D. N., Ovchinnikov, K. V., Perez-Garcia, F., Christmann, J., Sinner, P., Crauwels, P., Weixler, D., **Cao, P.**, Becker, J., Kohlstedt, M., Kager, J., Eikmanns, B. J., Seibold, G. M., Herwig, C., Wittmann, C., Bar, N. S., Diep, D. B., Riedel, C. U. (2021). Establishing recombinant production of pediocin PA-1 in *Corynebacterium glutamicum*. *Metab Eng*. 68, 34-45.

Christmann, J., **Cao, P.**, Becker, J., Desiderato, C. K., Goldbeck, O., Riedel, C. U., Kohlstedt, M., Wittmann, C. (2023). High-efficiency production of the antimicrobial peptide pediocin PA-1 in metabolically engineered *Corynebacterium glutamicum* using a microaerobic process at acidic pH and elevated levels of bivalent calcium ions. *Microb Cell Fact*. 22, 41.

Cao, P, Christmann, J., Kohlstedt, M., Gläser, L., Fritz, M., Goldbeck, O., Riedel, C. U., Becker, J., Wittmann, C. Metabolically engineered *Corynebacterium glutamicum* co-consumes the biomass sugars glucose, mannose, galactose, xylose, L-arabinose, and L-rhamnose to valorize spent sulfite liquor into the bulk chemical glutaric acid. **In preparation.**

Conference contributions

Cao, P, Schwechheimer, S., Becker, J., Wittmann, C. Metabolic engineering of *Corynebacterium glutamicum* for SSL valorization. Ph.D. day, 2019, Saarland, Germany.

Cao, P, Schwechheimer, S., Becker, J., Wittmann, C. Metabolic network analysis of mannose-grown *Corynebacterium glutamicum*. 6th Joint Conference of the DGHM & VAAM, 2020, Leipzig, Germany.

Cao, P, Christmann, J., Schwechheimer, S., Schulze, D., Becker, J., Wittmann, C. Metabolic network analysis of mannose-grown *Corynebacterium glutamicum*. 4th GASB, 2020, Virtual.

Cao, P, Christmann, J., Kohlstedt, M., Becker, J., Wittmann, C. Systems metabolic engineering of *Corynebacterium glutamicum* towards extension of the substrate spectrum for biorefinery applications. Metabolic Engineering 15, 2023, Singapore.

Acknowledgment

It is a long PhD journey with many challenges and difficulties, but of course also enjoyable and memorable moments. Here, I would like to take this opportunity to acknowledge all those who have been with me and supported me on this journey.

First and foremost, I would like to thank my supervisor. Many thanks, Christoph, for giving me the opportunity to work at iSBio, and I am really happy to be here for the last few years. Thanks for always being supportive and patient, guiding me through this journey with your knowledge and advice. Thanks for correcting my thesis so carefully. In addition, I will never forget the times and moments we had together talking about football and watching it, what a joy.

Thanks, Prof. Dr. Andriy Luzhetskyy for being my second supervisor to support my work and reviewing my thesis. Many thanks!

Thanks, Jens for working together with me, and helping me a lot for many things, like calling cellphone, handling with daily affairs for me. Also, it is a great pleasure to share the moments we enjoyed football together. Thanks, Judith for sharing your knowledge and experience, you will always be in my heart. Thanks, Michael for the help and contribute to my work. Thanks, Michel for the help and support for the analysis. Thanks, Susanne for taking care all the administration things. Thanks for the help from all those in the iFermenter project.

There are many amazing people I met at iSBio. I would like to thank Lars, Martin, Dennis for sharing the office with me, teaching me a lot, no matter good and bad, helping me to integrate into iSBio and Germany. Thanks to Demian, I had an amazing experience at Rock am Ring with you, Lars and Martin, thanks a lot for dealing with the car things for me. Thanks to Julian, we had a great time playing golf together. Thanks to Balkan girls, Sofija and Selma, for the unforgettable moments we had together. Thanks, Kyo, Iza and Anna, for the interesting talk, for enjoying the food together. Thanks, David for being my first student and help from both academic and life. I would like to thank everyone in iSBio for their help through this journey.

I must express my sincere thanks to my buddy from China. Muzi, thanks for being here and sharing the journey with me. Wei and Hanling, thanks for having common hobbies and taking holidays together with me. Yunsheng and Mei, such a luck to meet you here again after university. You all deserve my special thanks.

Finally, thanks to my mom and dad, for understanding my decision, for being supportive all the time.

Table of Contents

Summary ..... **VII**

Zusammenfassung ..... **VIII**

1 Introduction **1**

2 Objectives **3**

3 Theoretical Background **4**

3.1 The soil bacterium *Corynebacterium glutamicum* 4

3.1.1 Discovery of the microbe and pioneering research 4
3.1.2 *Corynebacterium glutamicum* as a versatile cell factory 5
3.1.3 Glutarate as important bio-plastic monomer and precursor for green solvents 7
3.1.4 Pediocin PA-1 as a potent bacteriocin for food preservation 9
3.1.5 Natural substrate spectrum of *C. glutamicum* 10

3.2 Metabolic engineering *C. glutamicum* towards an extended substrate spectrum… 13

3.2.1 Hexoses 13
3.2.2 Pentoses 16
3.2.3 Disaccharides 19
3.2.4 Organic acids 20
3.2.5 Organic alcohols 21
3.2.6 Feedstocks and raw materials 23

3.3 Industrial waste stream – Spent sulfite liquor 25

3.3.1 Spent sulfite liquor - Waste stream from pulp and paper industry 25
3.3.2 Chemical composition of spent sulfite liquor 26
3.3.3 Valorization of spent sulfite liquor 30

4 Material and Methods **33**

4.1 Strains 33

4.2 Plasmids and primers 36

4.3 Chemicals 39

4.4 Medium composition 39

4.4.1 Complex medium 39
4.4.2 Minimal medium 40
4.4.3 SSL medium 43

4.5 Strain preservation 45

4.6 Strain construction 45

4.6.1 Polymerase chain reaction 45
4.6.2 Gel electrophoresis 46
4.6.3 DNA fragment purification and concentration 47
4.6.4 Enzymatic digestion 47
4.6.5 Construction of transformation vectors 48
4.6.6 Generation of heat shock competent *E. coli* cells 49
4.6.7 Transformation of *E. coli* competent cells by heat shock 49
4.6.8 Isolation of plasmid DNA 49
4.6.9 Generation of electro competent *C. glutamicum* cells 50
4.6.10 Transformation of *C. glutamicum* cells 50
4.6.11 Second recombination of *C. glutamicum* 51
4.6.12 Codon optimization 51
4.7 Cultivation 51
4.7.1 Shake flask cultivation in minimal medium 51
4.7.2 Shake flask cultivation in SSL medium 52
4.7.3 Fed-batch fermentations in stirred tank bioreactors 52
4.8 Analytical methods 53
4.8.1 Quantification of cell concentration 53
4.8.2 Quantification of sugars 53
4.8.3 GC-MS analysis of sugars 54
4.8.4 Quantification of organic acids and inhibitors 54
4.8.5 Quantification of glutarate 55
4.8.6 Quantification of amino acids 55
4.8.7 Quantification of pediocin PA-1 activity 55
4.9 Separation and purification of mannose 56
4.9.1 Separation sugar from SSL using preparative flash chromatography 56
4.9.2 Purification and crystallization of mannose 57
5 Results and Discussion 58
5.1 System metabolic engineering of *C. glutamicum* for the consumption of seven biomass sugars 58
5.1.1 The wild type exhibits high robustness during growth on spent sulfite liquor-based medium 58
5.1.2 A first optimization round aims at plasmid-based expression of the catabolic pathways 62
5.1.3 Genome-based overexpression of *manA* for enhanced mannose utilization 64
5.1.4 Genome-based implementation of xylose catabolism 65
5.1.5 Streamlining *C. glutamicum* to utilize L-arabinose 68
5.1.6 Enabling genome-based galactose catabolism in *C. glutamicum* 70
5.1.7 Fine-tuning the multi-substrate use in *C. glutamicum* at the level of the transcriptional regulator IolR 72
5.1.8 Introducing L-rhamnose catabolism into *C. glutamicum* 75
5.1.9 Overexpression of the fructose permease PtsF for improved mannose co-utilization 78

5.2 Engineered *C. glutamicum* co-consumes the seven major biomass sugars ..80

5.2.1 Co-utilization of the six sugars contained in the globally accumulating waste stream spent sulfite liquor 80

5.2.2 Benchmarking *C. glutamicum* MSU-8B on a mixture with the seven major biomass sugars……84

5.3 Towards industrial application: Valorization of spent sulfite liquor using the advanced *C. glutamicum* MSU strain family.....86

5.3.1 Metabolically engineered *C. glutamicum* utilizes all sugar-based carbon in spent sulfite liquor 86

5.3.2 Creating a multi-substrate-using cell factory for glutarate-production 92

5.3.3 Benchmarking glutarate production from spent sulfite liquor in batch and fed-batch processes 94

5.4 Production of the antimicrobial peptide pediocin PA-1 from spent sulfite liquor…….....98

5.4.1 Re-engineering of the multi-substrate use in a genome-reduced *C. glutamicum* chassis……..98

5.4.2 Pediocin production from spent sulfite liquor 99

5.5 Selective recovery of high-value sugars from spent sulfite liquor using *C. glutamicum* cell factories with a fine-tuned substrate spectrum.....101

5.5.1 Recovery of mannose, a supplement to treat and prevent urinary tract infections…… 102

5.5.2 Recovery of galactose, a dietary supplement 107

5.5.3 Enrichment of L-rhamnose, a precursor in the flavor and perfume industry, along with glutarate production 111

6 Conclusion and Outlook.....115

7 Appendix.....117

7.1 Primers 117

7.2 Codon optimization 118

7.3 Detoxification of furfural, 5-HMF, and sulfite by *C. glutamicum*.....128

7.4 Calculation of specific consumption rate on synthetic sugar mixture 129

7.5 The genomic layout of the created *C. glutamiucm* strain family.....131

7.6 Separation results using flash and prep ion exchange chromatography.....132

8 Abbreviations and Symbols 134

9 References.....138

Summary

C. glutamicum is a robust industrial workhorse for chemical production. However, due to its narrow substrate spectrum, the microbe is mainly applied on using first-generation edible crops, unfavorably competing with food supply. In this regard, the present work aimed at systems metabolic engineering of *C. glutamicum* towards an extended substrate spectrum. Starting from the wild type, several rounds of optimization genomically introduced and evaluated various catabolic sugar modules. Ultimately, this provided a multi-substrate-use cell factory, designated *C. glutamicum* MSU8-B. The novel strain co-consumed glucose and fructose together with various second-generation sugars, such as mannose, xylose, L-arabinose, galactose, and L-rhamnose. MSU-8B, furthermore, harnessed all six sugars contained in spent sulfite liquor (SSL), a global industrial waste stream from the pulp and paper industry, providing a milestone towards biorefinery applications of the microbe. Afterwards, the sugar modules were successfully transferred into the genome-based cell factory *C. glutamicum* GTA-4, enabling production of up to 30 g L^{-1} of the plastic monomer glutarate from SSL in a fed-batch process. Furthermore, variants with a streamlined substrate spectrum which consumed all substrates except one enabled the recovery of single high-value sugars from SSL.

Zusammenfassung

C. glutamicum ist ein robustes industrielles Arbeitspferd für die chemische Produktion. Aufgrund seines schmalen Substratspektrums wird die Mikrobe jedoch hauptsächlich auf essbaren Pflanzen der ersten Generation eingesetzt, was eine ungünstige Konkurrenz für die Lebensmittelversorgung darstellt. Vor diesem Hintergrund zielte die vorliegende Arbeit darauf ab, den Stoffwechsel von *C. glutamicum* auf ein erweitertes Substratspektrum umzustellen. Ausgehend vom Wildtyp wurden in mehreren Optimierungsrunden verschiedene katabole Zuckermodule genomisch eingeführt und bewertet. Dies führte schließlich zu einer Zellfabrik mit mehreren Substraten, die als MSU8-B bezeichnet wurde. Der neuartige Stamm verbrauchte Glucose und Fructose zusammen mit Zuckern der zweiten Generation, wie Mannose, Xylose, L-Arabinose, Galactose und L-Rhamnose. MSU-8B nutzte darüber hinaus alle sechs Zucker, die in verbrauchter Sulfitablauge (SSL), einem industriellen Abfallstrom aus der Zellstoff- und Papierindustrie, enthalten sind, was einen Meilenstein in Richtung Bioraffinerieanwendungen der Mikrobe darstellt. Anschließend wurden die Zuckermodule erfolgreich in die genombasierte Zellfabrik GTA-4 übertragen, was die Produktion von bis zu 30 g L^{-1} des Kunststoffmonomers Glutarat aus SSL in einem Fed-Batch-Prozess ermöglichte. Darüber hinaus ermöglichten Varianten mit einem gestrafften Substratspektrum, die alle Substrate bis auf eines verbrauchten, die Gewinnung von hochwertigen Einzelzuckern aus SSL.

1 Introduction

With the identification of L-glutamate as a flavor enhancer over 100 years ago, and its following wide application in human nutrition (Ikeda, 2002; Lindemann et al., 2002), the increasing demand for this amino acid led to the development of a L-glutamate production process (Eggeling and Bott, 2005). In this regard, the gram-positive soil bacterium *Corynebacterium glutamicum*, capable of secreting L-glutamate naturally, was isolated in 1957 (Kinoshita et al., 1957; Udaka, 1960). Shortly after its discovery, *C. glutamicum* was employed as robust industrial workhorse to produce L-glutamate (Kumagai, 2000), as well as the essential amino acid L-lysine (Eggeling and Bott, 2015; Wittmann and Becker, 2007). Over the last six decades, the microbe has been upgraded into a versatile cell factory to produce a broad range of added-value compounds, e.g., amino acids, bulk and fine chemicals, fuels, materials, and pharmaceuticals, laying its pivotal role in industrial biotechnology and bioeconomy (Becker and Wittmann, 2012a; Becker and Wittmann, 2015). As examples, the production of the high-volume bulk chemical glutarate as bioplastic monomer and solvent precursor for the chemical industry (Diaz, 1997; Li et al., 2020), and the high-value antimicrobial peptide pediocin PA-1 with application in the food industry (Papagianni and Anastasiadou, 2009; Rodriguez et al., 2002), by *C. glutamicum* were successfully demonstrated (Christmann et al., 2023; Rohles et al., 2018). Current industrial production processes by *C. glutamicum* are mainly based on well-known first-generation feedstocks, such as starch and molasses, from expensive and edible food crops, however, unfavorably competing with human nutrition (Kimura, 2005). Accordingly, alternative novel non-edible feedstocks, in particular second-generation renewables lignocellulosic biomass, have attracted interest towards an environmentally sustainable and economically feasible process (Lee and Lavoie, 2013). As the most abundant biomass on earth, lignocellulose is yielded up to 1.3 billion tons per year, mainly consisting of three components, i.e., lignin (15-20%), cellulose (40-50%), and hemicellulose (25-35%) (Baruah et al., 2018; Malherbe and Cloete, 2002). The depolymerization of lignin generates aromatics, whereas cellulose is a homopolymer of glucose, hemicellulose is composed of various fermentable hexoses (glucose, mannose, galactose, and L-rhamnose) and pentoses (xylose and L-arabinose) (Sun et al., 2016). The use of these units, especially lignocellulosic sugars, is thereby a crucial prerequisite for the utilization of lignocellulosic biomass (Buschke et al., 2013b). Naturally, *C. glutamicum* utilizes a variety of substrates, such as first-generation sugars, glucose, fructose, sucrose at high rate (Leßmeier et al., 2015), whereas mannose, rich in softwood, at low rate (Sasaki et al., 2011). The microbe is also able to grow on common inhibitors in lignocellulosic hydrolysates (Chandel et al., 2013), such as organic acids, acetic acid (Wendisch et al., 2000), and lactic acid (Stansen et al., 2005), as well as

aromatics, e.g., benzoate, phenol, vanillin, and 4-hydroxybenzoate (Shen et al., 2005; Weiland et al., 2023). In addition, given that *C. glutamicum* exhibits weak carbon catabolite repression, it appears as a suitable host for the simultaneous utilization of different carbon sources (Baritugo et al., 2018; Leßmeier et al., 2015). However, the wild type *C. glutamicum*, particularly ATCC 13032 strain, lacks the ability to utilize most second-generation sugars, e.g., xylose, L-arabinose, galactose, and L-rhamnose (Baritugo et al., 2018). In this context, metabolic engineering *C. glutamicum* towards a broadened substrate spectrum could fully exploit the potential of this microbe within the biorefinery value chain (Baritugo et al., 2018; Leßmeier et al., 2015). Recently, the catabolic pathways and involved genes of second-generation sugars in different bacteria have been clearly elucidated, for example, xylose catabolism in *E. coli* (Domingues et al., 2021), arabinose assimilation in *C. glutamicum* ATCC 31831 (Kawaguchi et al., 2009), and galactose utilization in *L. lactis* (Grossiord et al., 2003). Meanwhile, enormous progress has been made for engineering these pathways in *C. glutamicum*, creating recombinant strains capable of utilizing xylose, L-arabinose, and galactose as sole carbon source, and providing promising cell factories to be integrated into second-generation biorefinery (Baritugo et al., 2018; Buschke et al., 2013b; Choi et al., 2019; Leßmeier et al., 2015).

The pulp and paper industry plays an important role for utilization of lignocellulosic biomass (FAO). As one of the major wood pulping processes, sulfite pulping provides cellulose fibers in almost pure form, while spent sulfite liquor (SSL) is released as industrial waste stream during the process, accumulating 30-50 billion liters per year (Marques et al., 2009; Sjöström, 1993). This stream contains vast amounts of sugars, including glucose, mannose, xylose, L-arabinose, galactose, and L-rhamnose, thereby appearing as a suitable feedstock for second-generation biorefinery (Marques et al., 2009). However, SSL is mostly burned for energy nowadays, wasting valuable carbon sources (Ek et al., 2009). In this regard, developing new strategies and processes to valorize sugars in SSL is of great interest (Daniel et al., 2012; Rueda et al., 2015). Given the excellent traits of *C. glutamicum*, i.e., the industrial workhorse, utilization of diverse substrates, as well as the robustness towards several inhibitors, favor it as an attractive platform for utilization of SSL. Furthermore, producing high-value products from this sugar stream using metabolically engineered *C. glutamicum* holds great promise, which could improve the profitability of the process, envisioning even more attractive and sustainable bioeconomy (Cherubini, 2010; Ohara, 2003).

2 Objectives

The overall aim of this thesis was to systems metabolic engineering *C. glutamicum* towards a broadened substrate spectrum, creating strains which could utilize multiple substrates, particularly second-generation sugars. As a proof-of-principle, the obtained strains should be evaluated in the industrial waste stream-spent sulfite liquor (SSL), aimed at valorization all sugars present in SSL. In this regard, the wild type *C. glutamicum* ATCC 13032 should be taken as a starting point. The first objective of the work was to assess the performance of the wild type *C. glutamicum* on SSL, aimed at robust growth. Given that mannose is enriched in SSL, the naturally inefficient mannose utilization in *C. glutamicum* should be enhanced. Following implementation of xylose catabolism, L-arabinose catabolism, galactose catabolism, and L-rhamnose catabolism into *C. glutamicum* should be conducted using a range of carefully designed synthetic modules to optimize the sugar utilization. These created strains with streamlined substrate spectrum should be further assessed on synthetic sugar mixtures to gain insights into the simultaneous utilization of multiple carbon sources. Subsequently, investigation strains performance on SSL, and valorization SSL into high-value glutarate and pediocin PA-1 by transferring the streamlined sugar modules into superior glutarate producer and pediocin PA-1 producer was a further objective of the work. In addition, recovery of single valuable sugars from SSL using engineered *C. glutamicum* with streamlined substrate spectrum should also valorize this waste stream.

3 Theoretical Background

3.1 The soil bacterium *Corynebacterium glutamicum*

3.1.1 Discovery of the microbe and pioneering research

L-Glutamate, the world's most important food amino acid nowadays (Ikeda, 2003), was identified as a taste-enhancer in Japan more than hundred years ago, and the compound was soon widely applied as additive in human nutrition (Ikeda, 2002; Lindemann et al., 2002). After World War II, the Japanese population was suffering from malnutrition due to food shortage, including algae as the natural glutamate source. Thus, the innovation was set to develop a fermentative L-glutamate production process, aiming to provide better-tasting food to the people (Eggeling and Bott, 2005). In this regard, *Corynebacterium glutamicum (*initially named *Micrococcus glutamicus)*, was isolated from soil during a screening program for L-glutamate producing microorganisms by Kinoshita and colleagues of the Japanese enterprise Kyowa Hakko Kogyo Co. in 1957 (Kinoshita et al., 1957; Udaka, 1960). The microbe was found naturally capable to secrete the amino acid into the culture medium. Its further use and development enabled the first industrial L-glutamate production process laid the foundation of the meanwhile global amino acid fermentation industry (Kumagai, 2000).

Figure 3-1: Raster electron micrograph of *Corynebacterium glutamicum* on minimal glucose medium (Bolten, 2010).

Phylogenetically, *C. glutamicum* is a Gram-positive (Figure 3-1), rod-shaped, non-endotoxin, non-sporulating bacterium, belonging to the class of *Actinobacteria*, the order of *Actinomycetales*, the suborder of *Corynebacterineae* and the family of *Corynebacteriaceae* (Liebl, 2005; Stackebrandt et al., 1997). Moreover, *C. glutamicum* is non-pathogenic and products obtained by this microbe have been awarded as generally recognized as safe (GRAS) by the US Food and Drug Administration (FDA)

(Liebl, 2005). Overall, the microbe is widely applied as robust industrial workhorse for the production of numerous amino acids by fermentation (Becker and Wittmann, 2012b; Becker and Wittmann, 2017; Eggeling and Bott, 2015; Lee et al., 2016; Wittmann and Becker, 2007).

3.1.2 *Corynebacterium glutamicum* as a versatile cell factory

Since almost six decades, *C. glutamicum* has been intensively studied as important model microorganism and industrial cell factory, respectively. Over the years, biotechnological techniques such as molecular cloning and genetic manipulation have contributed to the establishment of efficient genetic engineering tools of *C. glutamicum* (Jager et al., 1992; Schafer et al., 1994; Schwarzer and Puhler, 1991). DNA sequencing has provided the entire genome sequence of *C. glutamicum* (3,282,708 bp from Bielefeld University; 3,309,401 bp from Kyowa Hakko Kogyo Co.) and a detailed insight into its genetic repertoire (3,052 genes from Bielefeld University; 3,084 genes from Kyowa Hakko Kogyo Co.) (Ikeda and Nakagawa, 2003; Kalinowski et al., 2003). Later, functional genomics tools including transcriptomics (Kromer et al., 2004; Wendisch, 2003), proteomics (Hermann et al., 2001; Schaffer et al., 2001), metabolomics (Kromer et al., 2004; Strelkov et al., 2004), and fluxomics (Kiefer et al., 2004; Kromer et al., 2004; Wittmann and Heinzle, 2001; Wittmann et al., 2004) have greatly contributed to the comprehensive understanding of the basic physiology and biochemistry of the microbe and its tailored engineering into efficient producer strains using systems metabolic engineering (Becker and Wittmann, 2012a).

Meanwhile, *C. glutamicum* has become a robust cell factory for the production of almost one-hundred value-added compounds, including amino acids, bulk and fine chemicals, fuels, materials, and various healthcare products (Becker et al., 2018b; Becker and Wittmann, 2012a; Becker and Wittmann, 2015).

Besides L-glutamate, *C. glutamicum* has been employed to produce L-lysine, an essential amino acid with applications as feed additive and food supplement (Becker et al., 2011; Eggeling and Bott, 2015; Wittmann and Becker, 2007). In addition, *C. glutamicum* was engineered to overproduce other amino acids such as L-methionine (Li et al., 2016; Park et al., 2007), L-alanine (Jojima et al., 2010), L-valine (Blombach et al., 2007; Chen et al., 2015), L-isoleucine (Yin et al., 2012), L-tryptophan (Ikeda and Katsumata, 1999), L-serine (Zhu et al., 2015), and L-histidine (Mizukami et al., 1994), as well as different non-proteinogenic amino acids, including γ-aminobutyric acid (Jorge et al., 2016; Jorge et al., 2017) , 5-aminovalerate (Rohles et al., 2022; Rohles et al., 2016), L-pipecolic acid (Pauli

et al., 2023; Perez-Garcia et al., 2017a), and ectoine (Becker et al., 2013; Giesselmann et al., 2019). Furthermore, systems metabolic engineering of *C. glutamicum* enabled the synthesis of various organic acids as monomers for bio-based materials, e.g. D-lactate as building block for polylactic acid (Tsuge et al., 2015), succinate (Chung et al., 2017), glutarate (Rohles et al., 2018), and *cis,cis*-muconic acid as building blocks for polyesters, polyurethanes, and polyamides for the bioplastic industry (Becker et al., 2018a). In addition, engineered strains of *C. glutamicum* were applied for high-level production of diamines such as 1, 5-diaminopentane and 1, 4-diaminobutane, important monomers for bio-polyamides (Kim et al., 2018; Kind et al., 2010; Li et al., 2018). In addition, *C. glutamicum* was improved to produce bio-based fuels, such as ethanol (Inui et al., 2004; Jojima et al., 2015), isobutanol (Yamamoto et al., 2013), 1-propanol (Siebert and Wendisch, 2015), and 1, 2-propanediol (Lange et al., 2017; Siebert and Wendisch, 2015).

On the other hand, *C. glutamicum* has emerged as a promising platform to produce diverse and complex molecules for high-value application (Wolf et al., 2021): the extremolytes ectoine and hydroxyectoine for cosmetics and medicals (Giesselmann et al., 2019; Jungmann et al., 2022), terpenoids, e.g. astaxanthin, patchoulol, and coenzyme Q_{10} as pharmaceuticals and nutraceuticals (Burgardt et al., 2021; Henke and Wendisch, 2019; Henke et al., 2018), plant (poly)phenols, e.g. cyanidin 3-O-glucoside, resveratrol, and salidroside for the food and healthcare industry (Kallscheuer et al., 2019; Kallscheuer et al., 2017; Zha et al., 2018), antibiotics such as roseflavin (Mora-Lugo et al., 2019), and antimicrobial peptides such as pediocin (Goldbeck et al., 2021) and nisin (Weixler et al., 2022).

The extensive investigations and developments on *C. glutamicum* led to an explosion of its product portfolio, including high-volume chemicals as well as high-value bio-actives (Becker et al., 2018b). Without doubt, *C. glutamicum* plays a vital role in industrial biotechnology and bio-based economy (Becker et al., 2018b; Becker and Wittmann, 2012a). The manufacturing of these products is based on first-generation sugars, unfavorably competing with human nutrition. The focus of this thesis, therefore, was to improve *C. glutamicum* to use mixed sugar-containing waste-streams for production instead. This should be demonstrated for two relevant products, the high-volume bulk chemical glutarate as bioplastic monomer and solvent precursor for the chemical industry, and the high-value antimicrobial peptide pediocin PA-1 with application in the food industry. Therefore, these two products will be illustrated in more detail in the following.

3.1.3 Glutarate as important bio-plastic monomer and precursor for green solvents

Glutarate is a saturated five-carbon dicarboxylic acid of recognized commercial value. Traditionally, glutarate is produced from petroleum through a cascade of chemical conversions, including ring-opening from γ-butyrolactone (Figure 3-2 a) (Paris et al.) and oxidation of cyclopentene (Figure 3-2 b) (Vafaeezadeh and Hashemi, 2016). Notably, the γ-butyrolactone route starts from petroleum and its pyrolysis into two-carbon acetylene, followed by increasing of the carbon chain length and hydrogenation to synthesize 1, 4-butanediol which requires further dehydrogenation to generate γ-butyrolactone. The consequent ring-opening reaction of γ-butyrolactone eventually increases the carbon backbone to five carbons. Further acidification then yields glutarate (Paris et al.). Alternatively, cyclopentene is first obtained by steam cracking of petroleum, and then oxidized to glutarate (Vafaeezadeh and Hashemi, 2016). Unfavorably, this type of production requires fossil resources, hazardous chemicals, and massive amounts of energy (Matar and Hatch, 2001) .

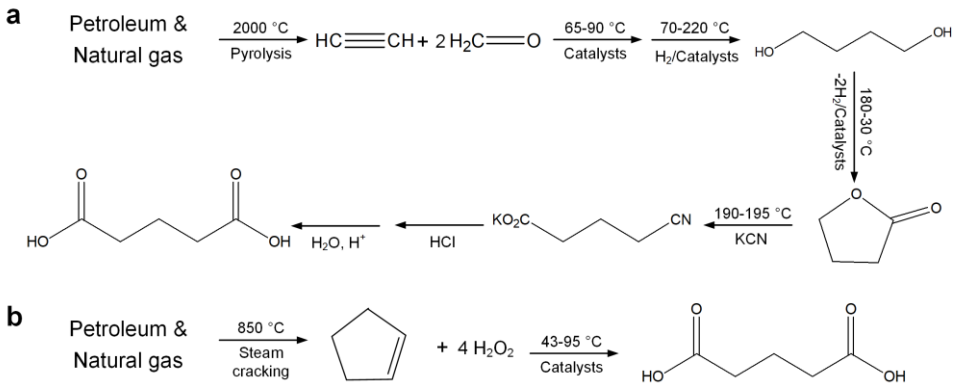

Figure 3-2: Chemical synthesis of glutarate. Route of ring-opening from γ-butyrolactone (**a**) (Paris et al.); route of oxidation of cyclopentene (**b**) (Vafaeezadeh and Hashemi, 2016).

On the product side, glutarate can be reduced into the corresponding five-carbon alcohol 1, 5-pentanediol using hydrogenation (Werle et al.). Both chemicals are valuable monomers to derive polyesters, polyurethanes, and polyamides, which have wide applications in adhesives, sealants, coatings, and reins (Li et al., 2020; Napoleon, 1997; Zheng et al., 2022). In addition, glutarate can be converted into dimethyl-glutarate, a widely applied cleaning solvent (Diaz, 1997).

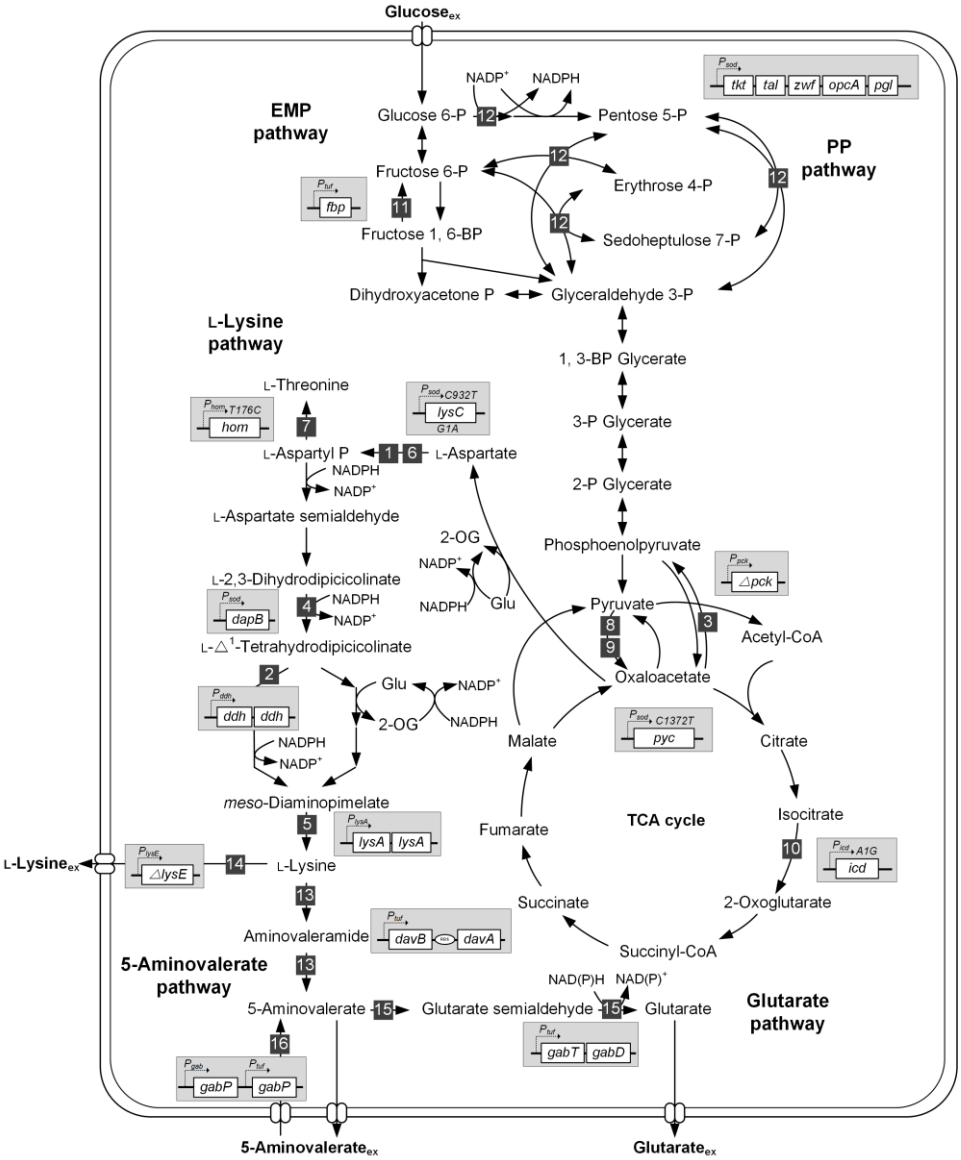

Figure 3-3: Metabolic pathway for the production of glutarate in *C. glutamicum* GTA-4. The following genome-based modifications displayed in gray boxes were implemented in wild type *C. glutamicum* ATCC 13032: 1, nucleotide exchange in *lysC* (*lysC*^{T311I}); 2, additional copy of *ddh* (2x *ddh*); 3, deletion of *pck* (*⊿pck*); 4, overexpression of *dapB* (*P*$_{sod}$ *dapB*); 5, additional copy of *lysA* (2x *lysA*); 6, overexpression of *lysC* (*P*$_{sod}$ *lysC*^{T311I}); 7, nucleotide exchange in *hom* (*hom*^{V95A}); 8, nucleotide exchange in *pyc* (*pyc*^{P485S}); 9, overexpression of *pyc* (*P*$_{sod}$ *pyc* ^{P485S}); 10, replacement of start codon of *icd* (*icd*^{GTC}); 11, overexpression of *fbp* (*P*$_{tuf}$ *fbp*); 12, overexpression of *tkt*-operon (*P*$_{sod}$ *tkt*); 13, integration of *davBA* (*P*$_{tuf}$ *davBA*); 14, deletion of *lysE* (*⊿lysE*); 15, overexpression of *gabTD* (*P*$_{tuf}$ *gabTD*); 16, additional copy of *gabP* (*P*$_{gab}$ *gabP P*$_{tuf}$ *gabP*). EMP pathway: Embden–Meyerhof–Parnas pathway; PP pathway: Pentose Phosphate pathway; TCA cycle: Tricarboxylic Acid cycle. Figure adapted from (Becker et al., 2011; Rohles et al., 2018).

Given the drawbacks of petrochemical production, different alternative biosynthetic routes have been investigated to derive glutarate from renewable resources instead. Biochemically, glutarate is an intermediate of the 5-aminovalerate (AVA) pathway that is present in different *Pseudomonas* species to catabolize L-lysine (Revelles et al., 2005).

Hereby, L-lysine is first converted to AVA by L-lysine 2-monooxygenase (DavB) and 5-aminovaleramidase (DavA). Then, AVA is further metabolized into glutarate by 5-aminovalerate aminotransferase (DavT) and glutarate semialdehyde dehydrogenase (DavD) (Revelles et al., 2005). Toward glutarate overproduction, this heterologous pathway was successfully introduced into *E. coli* (Adkins et al., 2013; Park et al., 2013) and *C. glutamicum* (Han et al., 2020; Kim et al., 2019; Rohles et al., 2022; Rohles et al., 2018). Because the route starts from L-lysine, L-lysine overproducing *C. glutamicum* strains appeared as excellent hosts (Becker et al., 2011; Wittmann and Becker, 2007). The strategy allowed to generate high-efficiency glutarate-overproducers through rational systems metabolic engineering, spearheaded by *C. glutamicum* GTA-4 that comprised a systematically streamlined metabolism to derive glutarate up to 90 g L^{-1} and a yield of 70%, reflecting more than 90% of the theoretical maximum (Rohles et al., 2018). Starting from the non-producing wild type ATCC 13032, 12 genomic modifications first generated the L-lysine hyper-producing strain *C. glutamicum* LYS-12 (Becker et al., 2011) by increasing the flux through L-lysine biosynthesis, enhancing precursor supply, attenuating competing pathways, and increasing redox power supply. Afterwards, subsequent genomic engineering integrated the 5-aminovalerate pathway to redirect L-lysine to AVA and create *C. glutamicum* AVA-2 (Rohles et al., 2016). Lastly, final metabolic engineering increased the flux to glutarate, and optimized metabolite transport, yielded *C. glutamicum* GTA-4 (Figure 3-3). This strain produced glutarate in an attractive titer of 90 L^{-1}, yield of 0.70 mol mol^{-1} and a maximum productivity of 1.8 g L^{-1} h^{-1} in a fed-batch process from glucose setting a benchmark for bio-based glutarate production (Rohles et al., 2018). Notably, a downstream purification strategy was developed, providing glutarate from the fermentation broth at 99% purity. This development allowed the use of bio-based glutarate for the synthesis of a novel bio-polyamide PA5.6, which exhibited similar characteristics with the petrochemical based polymer, e.g. a molecular weight about 10,000 g mol^{-1}, a melting temperature of 241 °C, a crystallization enthalpy of about 80 J g^{-1}, and thermal stability up to 330 °C (Rohles et al., 2018).

3.1.4 Pediocin PA-1 as a potent bacteriocin for food preservation

Among microbial products for the food industry are various bacteriocins, i.e. antimicrobial peptides that act against food-borne pathogens. They have found vital applications for food-preservation. Pediocin PA-1 is a prominent bacteriocin (Figure 3-4), given its antimicrobial activity against a wide spectrum of Gram-positive bacteria, especially *Listeria monocytogenes*, a foodborne pathogen. Therefore, pediocin has attracted

interest for food preservation, and, furthermore, as promising alternative to commonly used antibiotics (Papagianni and Anastasiadou, 2009; Rodriguez et al., 2002).

Naturally, pediocin is produced by lactic acid bacteria (LAB), including *Pediococcus* spp. and *Lactobacillus* spp. (Ennahar et al., 1996; Papagianni and Anastasiadou, 2009). The biosynthesis of the peptide is encoded by the gene cluster *pedABCD* (Marugg et al., 1992). Within the cluster, *pedA* is the structural gene for ribosomal synthesis of pre-pediocin, whereas *pedB* is encoding an immunity protein and *pedC* and *pedD* are essential for processing, cleavage and secretion of mature pediocin (Marugg et al., 1992; Venema et al., 1995). It has been shown that *C. glutamicum* can grow in the presence of high concentrations of pediocin, while no significant degradation was observed (Goldbeck et al., 2021). Notably, heterologous expression of a codon optimized *pedACD*^{Cgl} operon in the host *C. glutamicum* enabled pediocin production to significant level (Goldbeck et al., 2021). Subsequently, optimization of the bioprocess, i.e., fine-tuning of oxygen supply, optimization of the medium, the use of an acidic environment, and supplementation with calcium chloride boosted production to 66 mg L^{-1}, the highest titer achieved so far (Christmann et al., 2023). *C. glutamicum* thereby appears as a suitable platform for antimicrobial peptide production. However, production so far relied on the use of first-generation sugar and expensive complex ingredients such as yeast extract and peptone, leaving space for improvement (Christmann et al., 2023).

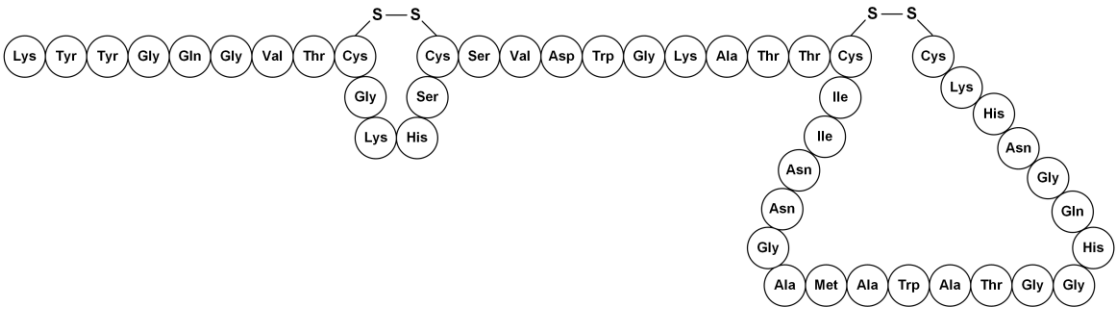

Figure 3-4: Amino acids sequence of pediocin PA-1. Figure adapted from (Umu et al., 2017).

3.1.5 Natural substrate spectrum of *C. glutamicum*

With the rising prices and considerable environmental problems caused by the massive industrial use of non-sustainable fossil resources, alternative processes have to be developed (Lee and Lavoie, 2013). In particular, biorefinery approaches that employ microbial cell factories for the production of chemicals, materials and fuels and rely on sustainable and environmentally friendly biomass feedstocks hold a great promise towards a more sustainable future (Cherubini, 2010; Ohara, 2003).

C. glutamicum as a robust industrial workhorse is one of the most promising microorganisms for biorefinery applications (Baritugo et al., 2018). Naturally, the microbe utilizes a variety of carbon sources (Figure 3-5) (Blombach and Seibold, 2010; Leßmeier et al., 2015). Among others, it uses the so-called first-generation sugars, glucose, fructose, and sucrose, commonly available from starch (corn) and molasses (sugarbeed and sugarcane) in the bio-industry (Kimura, 2005; Leßmeier et al., 2015). Other sugars are not efficiently used or not used at all. Growth of the wild type on mannose is much slower when compared with that on glucose, making this sugar a unsuitable carbon source for fermentation at high rate (Sasaki et al., 2011). Ribose (Nentwich et al., 2009), as well as disaccharides such as maltose (Seibold et al., 2009) are also consumed by *C. glutamicum.* Furthermore, organic acids, such as lactic acid (Stansen et al., 2005) and acetic acid (Wendisch et al., 2000), and organic alcohols, such as ethanol (Arndt et al., 2008), arabitol (Laslo et al., 2012) are native carbon sources. Notably, *C. glutamicum* also grows on aromatic compounds such as benzoate, phenol, vanillate, vanillin, and 4-hydroxybenzoate (Shen et al., 2005; Weiland et al., 2023; Weiland et al., 2022), common inhibitors in lignocellulosic hydrolysates (Chandel et al., 2013). Interestingly, *E. coli* (Kremling et al., 2009), *B. subtilis* (Hueck and Hillen, 1995) and *S. cerevisiae* (Gancedo, 1998), show strong carbon catabolite repression, causing diauxic growth and sequential utilization of carbon sources in the presence of glucose. Unlike these microorganisms, *C. glutamicum* exhibits only weak carbon catabolite repression which partially enables the simultaneous utilization of different nutrients (Baritugo et al., 2018; Leßmeier et al., 2015). For example, mixtures of glucose with fructose (Dominguez et al., 1997), and acetate (Wendisch et al., 2000), respectively, are co-consumed. These traits make *C. glutamicum* a suitable host for industrial fermentation (Baritugo et al., 2018).

Nevertheless, current industrial production processes using first-generation sugars from expensive and edible crops are competing with human food supply (Naqvi and Yan). Therefore, second-generation biorefineries, based on lignocellulosic biomass, have been developed to improve the environmental sustainability and economic feasibility of the production processes (Lee and Lavoie, 2013). Lignocellulosic biomass, the structural material and building block of terrestrial plants, is the most abundant and renewable biomass on earth, and up to 1.3 billion tons is yielded per year (Baruah et al., 2018; Kuhad and Singh, 1993; Malherbe and Cloete, 2002). It mainly consists of three components: the aromatic polymer lignin (15-20%), and the two polysaccharides hemicellulose (25-35%) and cellulose (40-50%). Notably, depolymerization of lignin generates aromatic units, whereas hydrolysis of cellulose and hemicellulose yields several fermentable sugars, such as pentoses and hexoses (Baruah et al., 2018; Malherbe and Cloete, 2002; Sun et al., 2016). Many studies have been conducted to

valorize lignin (Barton et al., 2018; Becker et al., 2018a; Becker and Wittmann, 2019; Kohlstedt et al., 2018; Kohlstedt et al., 2022; Weiland et al., 2022), hemicellulose (Buschke et al., 2011; Choi et al., 2019; Mao et al., 2018; Yim et al., 2016), and cellulose (Lynd et al., 2005; Lynd et al., 2002; Oh and Jin, 2020). In addition, third-generation biorefineries based on algal (microalgae and macroalgae) biomass from marine are investigated (Bhatia et al., 2022; Poblete-Castro et al., 2020).

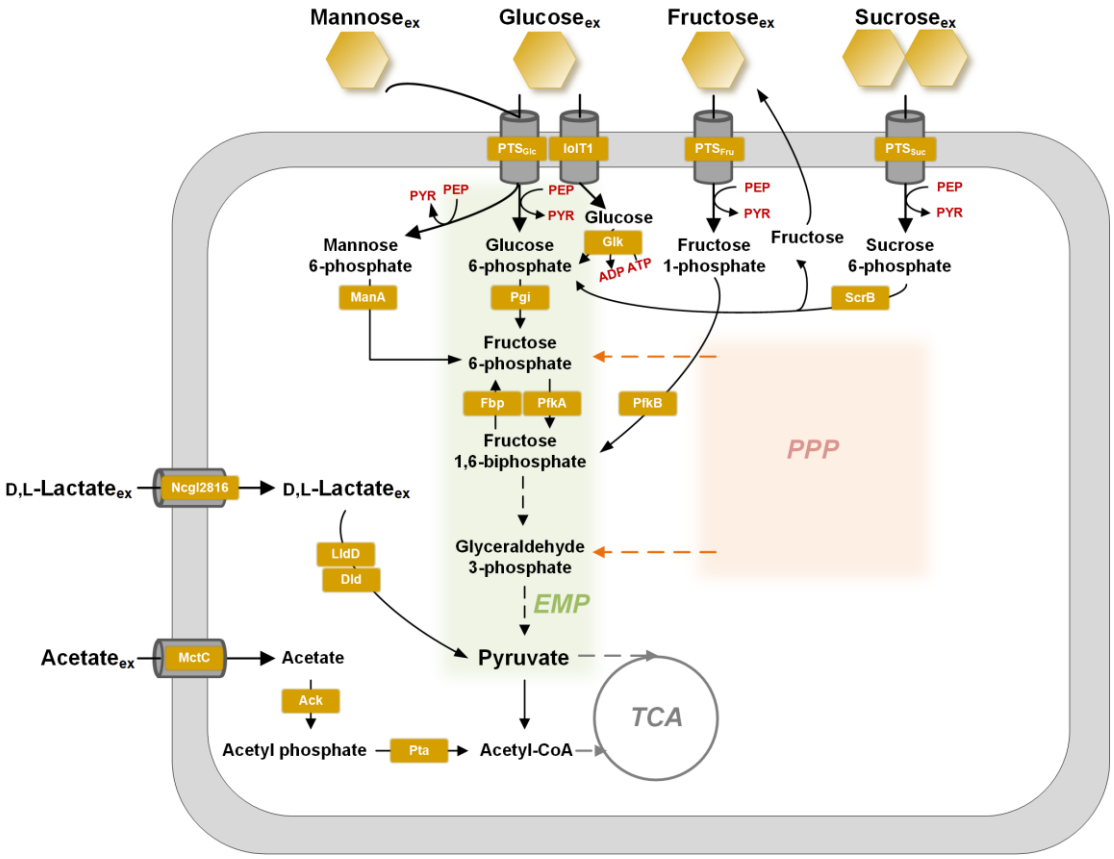

Figure 3-5: Natural substrate spectrum of *C. glutamicum* ATCC 13032. Hexagons represent hexoses; two hexagons represent disaccharides. Ack: ATP-dependent acetate kinase; Dld: D-lactate dehydrogenase; Fbp: fructose 1, 6-bisphosphatase; Glk: glucokinase; IolT1: myo-inositol transporter; LldD: L-lactate dehydrogenase; ManA: mannose 6-phosphate isomerase; MctC: monocarboxylic acid transporter; Ncgl2816: lactate permease; PfkA: 6-phosphofructokinase; PfkB: 1-phosphofructokinase; Pgi: phosphoglucose isomerase; Pta: phosphotransacetylase; PTS$_{Fru}$: fructose-specific phosphotransferase system; PTS$_{Glc}$: glucose-specific phosphotransferase system; PTS$_{Suc}$: sucrose-specific phosphotransferase system; ScrB: sucrose-6-phosphate hydrolase. (Baritugo et al., 2018; Becker et al., 2018b; Becker and Wittmann, 2015).

Unfavorably, the wild type, particularly the strain *C. glutamicum* ATCC 13032, lacks the ability to utilize most second-generation and third-generation substrates, e.g. xylose, L-arabinose, galactose, and mannitol (Baritugo et al., 2018). To fully exploit the potential of *C. glutamicum*, increasing interest have focused on optimizing and extending the

substrate spectrum of *C. glutamicum* towards novel cheap feedstocks from non-food biomass (Baritugo et al., 2018; Buschke et al., 2013b). Different metabolic engineering strategies have been developed to optimize and enhance the utilization of natural substrates (Baritugo et al., 2018; Blombach and Seibold, 2010). Moreover, engineering *C. glutamicum* towards broad substrate spectrum is an important issue. Heterologous expression of essential genes have extended the substrates spectrum of *C. glutamicum* to non-natural substrates, such as hexoses (galactose), pentoses (xylose, L-arabinose), disaccharides (lactose, cellobiose), organic alcohols (mannitol, glycerol), and polymeric feedstocks (starch, hemicellulose, cellulose, industrial waste streams) (Baritugo et al., 2018; Buschke et al., 2013b; Choi et al., 2019; Leßmeier et al., 2015). The optimization and extension of substrate spectrum of *C. glutamicum* will be described in more detail in the following sections.

3.2 Metabolic engineering *C. glutamicum* towards an extended substrate spectrum

3.2.1 Hexoses

Glucose is the most abundant sugar in starch and lignocellulosic biomass, and displays the dominating carbon source in industry (Kimura, 2005). Glucose uptake in *C. glutamicum* occurs mainly via the glucose-specific phosphotransferase system (PTS_{Glc}) (Malin and Bourd, 1991; Moon et al., 2007; Parche et al., 2001). However, it was reported that the presence of gluconeogenic carbon sources, such as acetate and pyruvate, inhibits the glucose uptake in *C. glutamicum*, owing to transcriptional repression of the glucose-specific transporter gene *ptsG* by the regulator SugR (Engels and Wendisch, 2007). In contrast, the *ptsG* expression level is significantly increased in the presence of maltose, resulting in increased glucose utilization (Krause et al., 2010). One approach to accelerate glucose uptake is based on constitutive overexpression of the gene *ptsG* (Lindner et al., 2013; Xu et al., 2016). Moreover, PTS-independent glucose uptake systems were identified in *C. glutamicum,* by which glucose is transported by myo-inositol transporter (IolT1/IolT2) into the cytoplasm and then phosphorylated via native glucokinases (Lindner et al., 2011). The transcriptional regulator gene *iolR* located upstream of the *iol* gene cluster, was shown to be involved in the repression of the *iol* genes (Klaffl et al., 2013). The introduction of a frameshift mutation (320delA) in the gene *iolR* in PTS-deficient *C. glutamicum* strains, allowed the obtained mutants to grow on glucose through the IolT uptake system (Ikeda et al., 2011). In addition, adaptive laboratory evolution was applied for *C. glutamicum* on glucose minimal medium,

obtaining a mutant with a 20% increased growth rate after 100 generations (Pfeifer et al., 2017).

Fructose, one of main sugars in molasses, is particularly important for industrial amino acid production (Kimura, 2005). Fructose uptake in *C. glutamicum* occurs majorly via the fructose-specific phosphotransferase system (PTS_{Fru}), which generates fructose 1-phosphate. A minor fraction of fructose is then phosphorylated via the PTS_{Glc} , generating fructose 6-phosphate (Dominguez et al., 1998; Ikeda, 2012; Parche et al., 2001). Additionally, the myo-inositol transporter (IolT1/IolT2) transports fructose, however at low affinity (Baumchen et al., 2009). Notably, the L-lysine yield on fructose is significantly lower than that on glucose due to the high requirement for NADPH, majorly generated in the pentose phosphate (PP) pathway (Kiefer et al., 2002; Kiefer et al., 2004). The overexpression of fructose 1, 6-bisphosphatase (FBP) in *C. glutamicum* has been shown to increase the carbon flux into the PP pathway and increase the supply of NADPH, resulting in significantly increased lysine yields on fructose (Becker et al., 2005a). PtsG-mediated conversion of fructose to fructose 6-phosphate is thus a promising target towards increased lysine production on fructose. One study demonstrated that the deletion of the genes *ptsF* and *pfkB* (encoding fructose 1-phosphate kinase) in a lysine producing *C. glutamicum* strain directed fructose to enter the cell as fructose 6-phosphate via the PTS_{Glc}, resulting in a 96% higher the NADPH pool and approximately 300% higher L-lysine yield, compared to the control strain (Wang et al., 2016). Following this strategy, overexpression of the genes *zwf* and *gnd*, encoding glucose 6-phosphate dehydrogenase and 6-phosphogluconate dehydrogenase, respectively, further boosted the NADPH pool and lysine productivity (Wang et al., 2016). Moreover, through adaptive evolution of PTS_{Fru} deficient strain on fructose minimal medium, PtsG variants were obtained, which revealed faster fructose uptake, and increased lysine production (Krahn et al., 2021).

Mannose is widely present in lignocellulosic biomass and particularly abundant in softwood hydrolysates (Galbe and Zacchi, 2002). Mannose uptake in *C. glutamicum* occurs primarily via the PTS_{Glc}, whereby mannose is phosphorylated into mannose 6-phosphate, which is then converted to fructose 6-phosphate by mannose 6-phosphate isomerase (ManA). The fructose specific PTS_{Fru} was proven to function as substitute of the PTS_{Glc} for the uptake of mannose, when the PTS_{Glc} was absent (Lee et al., 1994; Sasaki et al., 2011). Although mannose is a natural substrate for *C. glutamicum,* the wild type *C. glutamicum* exhibits considerably slower growth on mannose than glucose (Malin and Bourd, 1991). Moreover, *C. glutamicum* utilizes glucose prior to mannose when grown in a mixture. This may be due to the higher specificity of the PTS_{Glc} to glucose than

mannose (Sasaki et al., 2011). Previous studies showed that ManA plays an essential role for growth on mannose. Interestingly, constitutive overexpression of the gene *manA* in *C. glutamicum* doubled the mannose consumption rate compared to wild type under oxygen-deprived conditions. Additional constitutive overexpression of the gene *ptsF* together with *manA* enabled simultaneous consumption of glucose and mannose in *C. glutamicum* under both aerobic and oxygen-deprived conditions (Sasaki et al., 2011).

The hexose galactose is widely contained in lignocellulosic biomass (Perez et al., 2002). Besides, galactose, together with glucose, forms the disaccharide lactose which is abundant in whey, a waste product of the dairy industry (Marwaha and Kennedy, 1988; Yang and Silva, 1995). Efficient utilization of galactose is a prerequisite for the utilization of lignocellulosic hydrolysates and valorization of the wasted carbon source whey. Naturally, *C. glutamicum* cannot consume galactose due to the lack of galactose catabolic genes. Heterologous expression of the essential genes from *Lactococcus lactis* subsp. *cremoris* MG1363 involved in galactose utilization pathway, the Leloir pathway, enabled *C. glutamicum* to consume galactose (Barrett et al., 2004). In the Leloir pathway, β-galactose is first transported into the cytoplasm via galactose permease (GalP), followed by conversion to α-galactose by aldose 1-epimerase (GalM). Galactokinase (GalK) phosphorylates galactose to galactose 1-phosphate, which is further converted to glucose 1-phosphate by hexose 1-phosphate uridylyltransferase (GalT), and UDP-glucose 4-epimerase (GalE), catalyzing the reversible epimerization of UDP-glucose to UDP-galactose (Grossiord et al., 2003). The galactose utilizing genes *galMKTE* along with the lactose utilization genes were expressed in plasmid, allowing recombinant *C. glutamicum* strain to grow on galactose as sole carbon source (Barrett et al., 2004). Further studies to overcome the disadvantage of plasmid instability were conducted by introduction of the genes into the chromosome, resulting in growth on galactose, although at low rate (Shen et al., 2019).

Rhamnose is a 6-deoxy-hexose, predominantly occurring in nature in L-form as L-rhamnose. L-Rhamnose is widely present in plants like *Rhamnus* and microalgae (Brown, 1991; Jiang et al., 2021). It is a non-natural substrate for *C. glutamicum.* Studies on utilization of L-rhamnose in *C. glutamicum* are rare, and the consumption of L-rhamnose in *C. glutamicum* has not been established so far. Nevertheless, the catabolic pathway of L-rhamnose in some microorganisms has been elucidated, such as *E. coli* (Baldoma and Aguilar, 1988; Power, 1967). In *E. coli*, α-rhamnose is first transported into the cytoplasm via rhamnose-proton symporter (RhaT) (Tate et al., 1992), followed by its convertion to β-rhamnose by rhamnose mutarotase (RhaM) (Ryu et al., 2004). Subsequently, rhamnose isomerase (RhaA) catalyzes the isomerization of β-rhamnose

to rhamnulose (Takagi and Sawada, 1964a), which is further phosphorylated into rhamnulose 1-phosphate by rhamnulokinase (RhaB) (Takagi and Sawada, 1964b). Lastly, rhamnulose 1-phosphate aldolase (RhaD) (Sawada and Takagi, 1964) catalyzes rhamnulose 1-phosphate to yield dihydroxyacetone phosphate and lactaldehyde. Therefore, introduction of the structural genes of L-rhamnose catabolic pathway from *E. coli* or other microorganisms, into *C. glutamicum* appears as promising strategy for utilization of L-rhamnose by *C. glutamicum*.

3.2.2 Pentoses

Xylose is the predominant pentose sugar and the second most abundant sugar in lignocellulosic biomass. Thus valorization of xylose is essential for the efficient utilization of lignocellulosic biomass (Jagtap and Rao, 2018; Qin et al., 2012). Most bacteria metabolize xylose via the xylose isomerase pathway. In this pathway, xylose is imported into the cell by a xylose transporter and further isomerized into xylulose by xylose isomerase (XylA). Xylulokinase (XylB) mediates the conversion of xylulose to xylulose 5-phosphate, an intermediate of PP pathway (Domingues et al., 2021; Hochster and Watson, 1954; McClintock and Zhang, 2017). Notably, the gene *xylB* is present in *C. glutamicum*. Natively, *C. glutamicum* cannot consume xylose due to a low expression level of the gene and the lack of the gene *xylA* (Kawaguchi et al., 2006). Several studies have been conducted to enable xylose utilization in *C. glutamicum.* The gene *xylA* from *E. coli* has been employed preferably since the encoded protein has a high specific activity (Buschke et al., 2013a; Buschke et al., 2011; Gopinath et al., 2011; Kawaguchi et al., 2006). However, a *C. glutamicum* mutant harboring the *xylA gene* from *Xanthomonas campestris* exhibited faster growth and higher biomass concentration (0.14 h^{-1}, 3.37 g CDW L^{-1}) than that using *xylA* gene from *E. coli* (0.09 h^{-1}, 2.79 g CDW L^{-1}) (Meiswinkel et al., 2013a). This is might due to similar codon usage between *xylA* from *X. campestris* to that of *C. glutamicum* (Mao et al., 2018). Additional co-expression of *xylB* together with *xylA* enhanced growth on xylose (Kawaguchi et al., 2006).

In addition, the transport of xylose should also not be ignored. Although *C. glutamicum* is capable of transporting xylose into the cell, xylose uptake in *C. glutamicum* is not fully understood, while a xylose specific transporter has not been identified so far. It was, however, reported that the myo-inositol-proton symporter IolT1 contributes to the xylose uptake in *C. glutamicum,* in which deletion of the transcriptional regulator IolR enabled a higher growth rate compared to the reference strain on xylose (Brusseler et al., 2018). Expression of the specific xylose-proton symporter gene *xylE*, along with the genes *xylA* and *xylB* from *E. coli*, following optimization of the expression level using synthetic

promoters of different strength, yielded *C. glutamicum* recombinant strains with a high specific growth rate of 0.37 h^{-1} on xylose (Yim et al., 2016). Furthermore, the L-arabinose-proton symporter AraE has been investigated for xylose uptake. Introduction of the gene *araE* from *Bacillus subtilis* (Mao et al., 2018), or *C. glutamicum* ATCC 31831 (Chen et al., 2017; Sasaki et al., 2009) not just improved xylose consumption rate, but also allowed simultaneous utilization of glucose and xylose in *C. glutamicum*. Interestingly, the overexpression of the PP pathway genes *tal* (encoding transaldolase) (Jo et al., 2017; Mao et al., 2018), *tkt* (encoding transketolase) (Mao et al., 2018), and *gnd* (encoding 6-phosphogluconate dehydrogenase) (Jo et al., 2017), was shown to improve xylose utilization. This might be due to the increased flux from the PP pathway into the glycolytic pathway (Matsushika et al., 2012; Zhou et al., 2012).

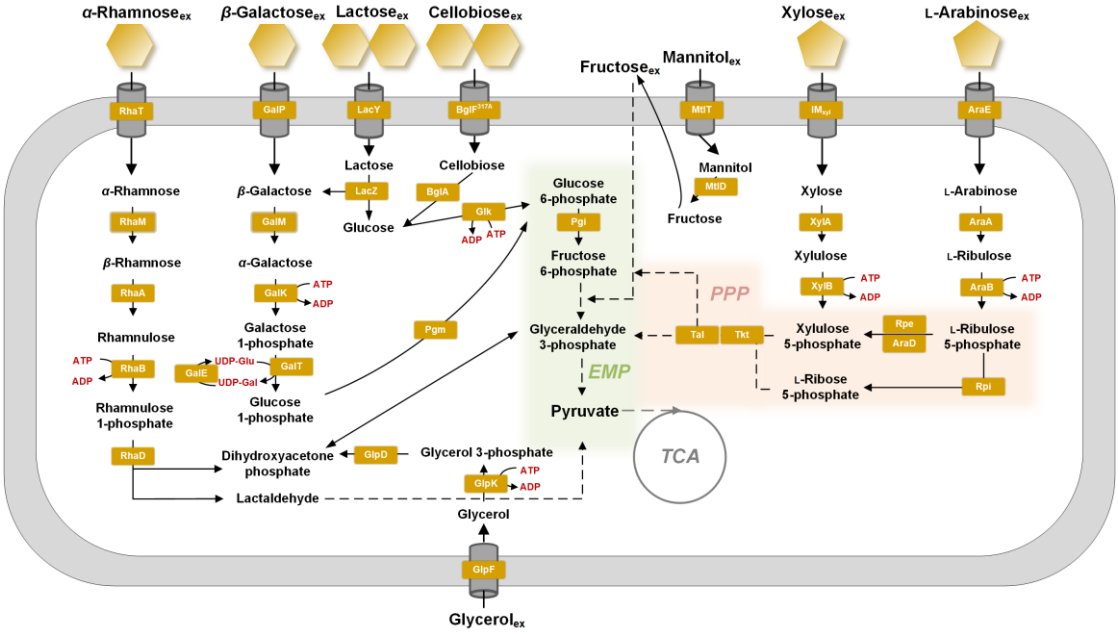

Figure 3-6: Extension of the substrate spectrum of *C. glutamicum* to non-native substrates. Pentagons represent pentoses; hexagons represent hexoses; two hexagons represent disaccharides. AraA: L-arabinose isomerase; AraB: L-ribulokinase; AraD: L-ribulose 5-phosphate 4-epimerase; AraE: L-arabinose-proton symporter; BglA: phospho-β-glucosidase; BglF^{317A}: β-glucoside-specific permease; GalE: UDP-glucose 4-epimerase; GalK: galactokinase; GalM: aldose 1-epimerase; GalP: galactose permease; GalT: hexose 1-phosphate uridylyltransferase; Glk: glucokinase; GlpD: glycerol 3-phosphate dehydrogenase; GlpF: glycerol transport facilitator; GlpK: glycerokinase; IM$_{xyl}$: xylose symporter; LacY: lactose permease; LacZ: β-galactosidase; MtlD: mannitol-2-dehydrogenase; MtlT: mannitol transporter; Pgi: phosphoglucose isomerase; Pgm: phosphoglucomutase; RhaA: rhamnose isomerase; RhaB: rhamnulokinase; RhaD: rhamnulose 1-phosphate aldolase; RhaM: rhamnose mutarotase; RhaT: rhamnose-proton symporter; Rpe: ribulose 5-phosphate-3-epimerase; Rpi: ribose 5-phosphate isomerase; Tal: transaldolase; Tkt: transketolase; XylA: xylose isomerase, XylB: xylulokinase. (Baritugo et al., 2018; Becker et al., 2018b; Becker and Wittmann, 2015).

Besides the xylose isomerase pathway, the alternative Weimberg pathway which catabolizes xylose without carbon loss, has also been implemented in *C. glutamicum*. In this pathway, xylose is converted to α-ketoglutarate in the TCA cycle (Weimberg, 1961). Heterologous expression of the structural operon *xylXABCD*, encoding enzymes for Weimberg pathway from *Caulobacter crescentus*, yielded a recombinant *C. glutamicum* strain that grew on xylose as sole carbon and energy source (Brusseler et al., 2018; Radek et al., 2014; Radek et al., 2017). Notably, *C. glutamicum* has been engineered to produce amino acids (Gopinath et al., 2011; Meiswinkel et al., 2013a), ectoine (Perez-Garcia et al., 2017b), 1, 5-diaminopentane (Buschke et al., 2013a), 3-hydroxypropionic acid (Mao et al., 2018), succinate (Jo et al., 2017) and isobutanol (Lange et al., 2018) from xylose.

Next to xylose, L-arabinose is the second abundant pentose in lignocellulosic biomass (Qin et al., 2012; Seiboth and Metz, 2011). The *C. glutamicum* strains ATCC 13032 and R are not able to consume L-arabinose, different to *C. glutamicum* ATCC 31831. In *C. glutamicum* ATCC 31831, L-arabinose is first imported into the cell by the L-arabinose-proton symporter (AraE), followed by conversion to L-ribulose by L-arabinose isomerase (AraA). Then, L-ribulokinase (AraB) phosphorylates L-ribulose to L-ribulose 5-phosphate which is further converted to xylulose 5-phosphate by L-ribulose 5-phosphate 4-epimerase (AraD) (Kawaguchi et al., 2009). The introduction of the heterologous gene cluster *araBAD* from *E. coli* into strains ATCC 13032 and R has been shown sufficient to enable L-arabinose consumption (Gopinath et al., 2011; Kawaguchi et al., 2008; Meiswinkel et al., 2013a; Schneider et al., 2011). This finding indicates a so far unidentified endogenous L-arabinose transporter, present in strains ATCC 13032 and R. Nevertheless, the additional expression of L-arabinose transporter gene *araE*, together with the gene cluster *araBAD* could further increase L-arabinose utilization under both aerobic and oxygen-deprived conditions (Sasaki et al., 2009). Besides the L-arabinose catabolic genes, pyruvate kinase has been identified as a bottleneck for L-arabinose metabolism in *C. glutamicum* ATCC 31831 using metabolome analysis. Following overexpression of this enzyme in combination with the deletion of *araR*, encoding repressor of the L-arabinose catabolic genes, enabled simultaneous utilization of glucose and L-arabinose at the same rate (Kawaguchi et al., 2018). Moreover, the production of amino acids (Meiswinkel et al., 2013a; Schneider et al., 2011), ectoine (Perez-Garcia et al., 2017b), succinate (Chen et al., 2014) and isobutanol (Lange et al., 2018) from L-arabinose by metabolic engineered *C. glutamicum* have been established.

3.2.3 Disaccharides

The disaccharide sucrose, composed of glucose and fructose, is one of main sugars in molasses (Kimura, 2005). In *C. glutamicum*, sucrose uptake occurs via the sucrose-specific phosphotransferase system (PTS_{Suc}) in which sucrose is phosphorylated into sucrose 6-phosphate. Sucrose 6-phosphate is then hydrolyzed to glucose 6-phosphate and free fructose, mediated by sucrose 6-phosphate hydrolase (ScrB) (Dominguez and Lindley, 1996; Engels et al., 2008; Moon et al., 2005). Unlike other bacteria, such as *Streptococcus lactis* (Thompson and Chassy, 1981) and *Clostridium acetobutylicum* (Tangney and Mitchell, 2000), *C. glutamicum* does not contain fructokinase (ScrK) to convert fructose into fructose 6-phosphate (Dominguez and Lindley, 1996). Therefore, in *C. glutamicum,* fructose is exported by a so far unidentified mechanism and re-imported into cells via the PTS_{Fru} and PTS_{Glc} in its phosphorylated form (Dominguez and Lindley, 1996; Wittmann et al., 2004). It was reported that the deletion of the gene *ptsF* in *C. glutamicum* caused poor growth and fructose accumulation in sucrose containing media (Moon et al., 2005). The expression of the heterologous gene *scrK* from *C. acetobutylicum* modified the intracellular fructose entry into metabolism, so that fructose was efficiently phosphorylated into fructose 6-phosphate without any fructose efflux (Moon et al., 2005). Further on, introduction of fructokinase into *C. glutamicum* has successfully improved amino acid production on sucrose, such as L-lysine (Xu et al., 2020) and L-serine (Zhang et al., 2017). Due to the fructose moiety of sucrose, metabolic engineering strategies, found beneficial for the increase of the NADPH pool and the lysine yield on fructose also work on sucrose. Hereby, the overexpression of fructose 1, 6-bisphosphatase in *C. glutamicum* led to a 30% increased lysine yield on sucrose (Becker et al., 2005a), and the double deletion of the genes *ptsF* and *pfkB* resulted in higher sucrose consumption rate and lysine yield (Wang et al., 2016).

Lactose, composed of glucose and galactose as mentioned above, is present in whey at a concentration up to 40-50 g L^{-1} (Marwaha and Kennedy, 1988; Yang and Silva, 1995). The utilization of lactose for fermentation provides a possibility for the valorization of whey (Siso, 1996). To enable growth on lactose, the *E. coli* lactose operon was introduced into *C. glutamicum* strain R163 previously (Brabetz et al., 1991). The heterologous expression of lactose permease (LacY) and β-galactosidase (LacZ) enabled growth of *C. glutamicum* on lactose as the sole carbon source, whereby LacY mediated the uptake of lactose and LacZ catalyzed the breakdown of lactose into glucose and galactose. However, only the glucose moiety of lactose was metabolized, whereas galactose was accumulated in the culture due to the lack of a galactose utilization pathway (Brabetz et al., 1991). Further studies reported that the expression of

the lactose catabolic genes *lacYZ* from *Lactobacillus delbrueckii* subsp. *bulgaricus* ATCC 11842, together with the galactose operon *galMKTE* from *L. lactis* as described above, enabled complete lactose utilization from whey in *C. glutamicum* (Barrett et al., 2004). In addition, adaptive laboratory evolution was applied, whereby the lactose operon *lacSZ* from *Streptococcus thermophilus* was expressed along with galactose operon from *L. lactis*, obtaining a fast-growing mutant in which a proline-148 to leucine amino acid change in the lactose permease (LacS) was identified (Shen et al., 2019).

Cellobiose, the β-1, 4 linked glucose dimers, is a partial degradation product of cellulose (Beguin and Aubert, 1994). Cellobiose is not a natural substrate for wild type *C. glutamicum*. However, adaptive mutants of *C. glutamicum* strain R which can utilize cellobiose have been reported. The mutation of either valine-317 to alanine or methionine in the β-glucoside-specific permease (BglF), was identified, allowing the mutants to transport cellobiose. Subsequent degradation of cellobiose into glucose is mediated by phospho-β-glucosidase (BglA) (Kotrba et al., 2003). Integration of the genes $bglF^{317A}$ and *bglA* under control of a constitutive promoter, together with the xylose catabolic genes, into the genome of *C. glutamicum* strain R, enabled simultaneous utilization of cellobiose, xylose and glucose (Sasaki et al., 2008). Moreover, constructing β-glucosidase secreting and surface displaying *C. glutamicum* strains are other strategies to allow cellobiose utilization. As example, the β-glucosidases from *Saccharophagus degradans* were successfully expressed in *C. glutamicum* using cell surface display which yielded a mutant to use cellobiose as sole carbon source (Adachi et al., 2013). Secretory expressing β-glucosidases derived from *Thermobifida fusca* YX endowed cellobiose utilization by *C. glutamicum* (Matsuura et al., 2019; Sato et al., 2020), later enabling to produce L-lysine (Adachi et al., 2013), 1, 5-diaminopentane (Matsuura et al., 2019) and shikimic acid (Sato et al., 2020) from cellobiose.

3.2.4 Organic acids

Lactate has wide applications, particularly in food and pharmaceuticals. It is also a potential carbon and energy source for bio-based production and the monomer for polylactic acid (PLA), a biodegradable biopolymer (Baritugo et al., 2018; Castillo Martinez et al., 2013). *C. glutamicum* contains three enzymes related to lactate catabolism. Lactate is transported into the cell via lactate permease (encoded by NCgl2816). The quinone-dependent L-lactate dehydrogenase (LldD) and D-lactate dehydrogenase (Dld), respectively, mediate the conversion of lactate to pyruvate (Kato et al., 2010; Stansen et al., 2005). Notably, *lldD* is inducible whereas *dld* is constitutively expressed at low level (Scheer et al., 1988), so that the wild type *C. glutamicum* efficiently

utilizes only L-lactate (Neuner and Heinzle, 2011). The overexpression of *dld* led to complete D, L-lactate consumption at an increased uptake rate. The additional overexpression of the genes encoding pyruvate carboxylase (PycA) and malic enzyme (MalE) further increased the growth rate on lactate (Neuner and Heinzle, 2011). Interestingly, constitutive overexpression of the *ldh* gene in *C. glutamicum*, encoding NAD^+-dependent lactate dehydrogenase, was reported to complement the LldD deficiency. This finding indicated Ldh as a promising target for improved lactate utilization (Sharkey et al., 2011). Furthermore, lactate has been employed to produce L-glutamate (Stansen et al., 2005) and L-lysine (Neuner and Heinzle, 2011).

Acetate is a common inhibitor generated during the pre-treatment of lignocellulosic biomass (Chandel et al., 2013). Acetate enters the central metabolism at the level of acetyl-CoA, which is an important precursor for synthesis of value-added products, such as polyhydroxybutyrate and succinate (Baritugo et al., 2018). Notably, *C. glutamicum* naturally catabolizes acetate as sole carbon source. In *C. glutamicum*, acetate is taken up into the cell via monocarboxylic acid transporter (MctC) (Jolkver et al., 2009), followed by its phosphorylation to acetyl phosphate by ATP-dependent acetate kinase (Ack). Subsequently, phosphotransacetylase (Pta) catalyzes the conversion of acetyl phosphate to acetyl-CoA (Gerstmeir et al., 2003; Reinscheid et al., 1999). In contrast to inactive glyoxylate cycle on glucose, the anaplerotic function is fulfilled by this cycle when growing *C. glutamicum* on acetate (Wendisch et al., 2000). Surprisingly, *C. glutamicum* strain ATCC 13032 exhibited strong tolerance to acetate whereby a growth rate of 0.24 h^{-1} on 10 g^{-1} acetate was observed (Wendisch et al., 2000). Moreover, growth was observed at high concentration of up to 60 g^{-1} acetate of *C. glutamicum* although inhibition occurred (Kiefer et al., 2021). Therefore, *C. glutamicum* appears as a promising host for utilization of lignocellulosic biomass due to its capacity for metabolizing high-level acetate. Furthermore, the heterologous expression of acetyl-CoA synthetase (AcsA) from *B. subtilis* improved the acetate recycling and succinate production in *C. glutamicum* (Zhu et al., 2013). Overexpression of the gene *pta* enhanced acetate reuse which is a byproduct for 3-hydroxypropionic acid production by *C. glutamicum* (Chang et al., 2020).

3.2.5 Organic alcohols

Mannitol is one of the most abundant organic alcohols found in nature. In particular, mannitol is a major constituent of algal biomass which makes up to 30% of dry weight in brown seaweeds (Iwamoto and Shiraiwa, 2005). The utilization of mannitol thus could open new possibilities for third generation biorefineries. The wild type *C. glutamicum*

lacks the capacity to catabolize mannitol although its arabitol operon was harnessed for mannitol utilization (Peng et al., 2011). The encoding gene cluster contains three genes in the order of *mtlR*, *mtlT* and *mtlD*. The gene *mtlR* encodes an autoregulatory DeoR-type transcriptional repressor, causing constitutive repression of two structural genes *mtlT* and *mtlD*. The gene *mtlT* encodes a MFS-type transporter for mannitol uptake, and *mtlD* encodes a NAD-dependent mannitol-2-dehydrogenase which mediates the conversion of mannitol to fructose. Through deletion of *mtlR*, the expression level of *mtlT* and *mtlD* were significantly upregulated, allowing growth on mannitol (Peng et al., 2011). The expression level of *mtlD* was shown as the rate-limit step for mannitol utilization instead of *mtlT* after deletion of *mtlR* (Sheng et al., 2021). Notably, the generated intracellular fructose from mannitol was secreted and subsequently taken up again into the cells (Hoffmann et al., 2018). Therefore, modulating fructose catabolism appeared crucial for efficient mannitol utilization. Beneficially, heterologous expression of fructokinase from *E. coli* in lysine producing *C. glutamicum* resulted in decreased efflux of fructose into the medium and increased the lysine production on mannitol (Hoffmann et al., 2018). In addition, the overexpression of the native fructose 1-phosphate kinase (PfkB) promoted mannitol utilization and L-ornithine production by *C. glutamicum* (Nie et al., 2022; Sheng et al., 2021).

Glycerol is the main by-product (10% w/w) from the biodiesel industry (Monteiro et al., 2018; Yang et al., 2012). Thus, developing a new sustainable process for utilization glycerol to valorize this waste stream is imperative. *C. glutamicum* ATCC 13032 contains two structural genes for glycerol utilization, i.e., the gene *glpK* encoding glycerokinase which mediates the phosphorylation of glycerol to glycerol 3-phosphate, and the gene *glpD* encoding glycerol 3-phosphate dehydrogenase which oxidizes glycerol 3-phosphate to dihydroxyacetone 3-phosphate. However, the strain lacks the ability to grow on glycerol as sole carbon source, owing to the low enzymatic activities of the pathway (Meiswinkel et al., 2013b; Rittmann et al., 2008). Heterologous overexpression *glpK* and *glpD* from *E. coli* was shown to be sufficient to enable glycerol utilization in *C. glutamicum* at a growth rate of 0.22 h^{-1}. Furthermore, the co-expression of the gene *glpF* from *E. coli*, encoding a facilitator for glycerol transport, together with the two structural genes, resulted in a faster growth rate of 0.28 h^{-1} (Rittmann et al., 2008). In addition, plasmid-based overexpression of the native genes *glpK* and *glpD* enabled *C. glutamicum* to grow on glycerol. However, the growth rate of 0.12 h^{-1} was almost twofold slower than that using the *E. coli* based genes (Meiswinkel et al., 2013b). Notably, recombinant *C. glutamicum* strains exhibited robust growth on different crude glycerol streams from industry (Meiswinkel et al., 2013b). Glycerol-based production towards amino acids

(Rittmann et al., 2008), succinate (Litsanov et al., 2013), and the diamine putrescine (Meiswinkel et al., 2013b) have been established in *C. glutamicum.*

3.2.6 Feedstocks and raw materials

The hydrolysis and saccharification of starch into monomeric glucose is a common step prior to fermentation (Kimura, 2005). Alternatively, the direct utilization of starch, resulting in a simplified overall process and reduced capital costs, has been studied. Consolidated bioprocessing (CBP) which combines saccharolytic and fermentative abilities in one host, aims at direct production from biomass (Olson et al., 2012). Heterologously introducing α-amylase (Amy) from *Streptomyces griseus* in *C. glutamicum* yielded a recombinant strain that used soluble starch as carbon and energy source. This strain secreted α-amylase into the medium to degrade starch to glucose, maltose and other high-molecular-weight carbohydrates (Seibold et al., 2006). In addition, expression of α-amylase (AmyA) from *Streptococcus bovis* enabled *C. glutamicum* to utilize raw corn starch and raw wheat starch (Tateno et al., 2007a). Moreover, developing the cell-surface displaying system for α-amylase is another effective strategy. Display of α-amylase on the surface of *C. glutamicum* cells enabled growth on starch and established production towards L-lysine (Tateno et al., 2007b), glutamate (Yao et al., 2009), poly-hydroxybutyrate (Song et al., 2013) from starch.

To enable direct utilization of cellulose, degradation of cellulose by several types of cellulolytic enzymes into fermentable carbohydrates is essential (Beguin and Aubert, 1994). First study of developing the CBP for cellulose in *C. glutamicum* has been demonstrated by constructing an endoglucanase-secreting *C. glutamicum* (Tsuchidate et al., 2011). Different endoglucanases, digesting amorphous region of the cellulose chain to generate reducing sugars, were successfully expressed in *C. glutamicum* and the candidate (Clocel3242) from *Clostridium cellulovorans* exhibited highest activity. Using the endoglucanase-secreting *C. glutamicum* strain, together with the addition of β-glucosidase which degrades the oligosaccharides to glucose, achieved glutamate production from β-glucan (Tsuchidate et al., 2011). Next, co-expression of endoglucanase (encoded by *XCC2387*) from *X. campestris* and β-glucosidase (encoded by *Sde1394*) from *S. degradans* allowed *C. glutamicum* to grow on carboxymethyl cellulose and cellobiose (Anusree et al., 2016). Furthermore, formation of mini-cellulosomes, the macromolecular complexes, have enabled *C. glutamicum* to hydrolyze cellulose. The expression of the assembled mini-cellulosomes, consisting of scaffolding protein CbpA from *C. cellulovorans* and the endoglucanase CelE from *C. thermocellum*,

led to a higher hydrolysis efficiency of carboxymethyl cellulose compared to that only expressing endoglucanase (Hyeon et al., 2011).

The CBP for hemicellulose starts with efficient saccharification of hemicellulose to fermentable sugars. In particular, xylan as the major type of the hemicellulose, is considered as the second most abundant polysaccharides after cellulose, consisting mainly of xylose residues (Rennie and Scheller, 2014). Previously, one study engineered the enzymatic degradation of xylan to xylose in *C. glutamicum*. Two enzymes, endoxylanase (XlnA) from *Streptomyces coelicolor*, breaking down xylan to yield xylose and xylo-oligosaccharides, and xylosidase (XynB) from *Bacillus pumilus*, hydrolyzing xylo-oligosaccharides to xylose, were expressed and optimized in *C. glutamicum*, obtaining a mutant efficiently hydrolyzing xylan into xylose (Yim et al., 2016). Additional co-expression xylose utilization gene *xylAB* and xylose transporter *xylE* from *E. coli,* enabled faster cell growth on xylan (Yim et al., 2016). Moreover, using the same strategy, xylonic acid production based on xylan in *C. glutamicum* has been demonstrated by the overexpression of the genes *xlnA*, *xynB* and *xylE*, together with the genes *xdh* (encoding xylose dehydrogenase) and *xylC* (encoding xylonolactonase) from *Caulobacter crescentus* which mediated the conversion of xylose to xylonic acid (Yim et al., 2017).

Biorefineries provide an environmental friendly and economic feasible platform for management and valorization of the industrial waste streams (Ferreira et al., 2019). Metabolically engineered *C. glutamicum* strains harboring lactose and galactose catabolic genes has been demonstrated towards the production of L-lysine and ethanol from whey, the waste from diary industry (Barrett et al., 2004; Shen et al., 2019). Engineering lactate utilization pathway enabled novel strains to produce L-lysine on silage juices, considered as agricultural waste (Neuner et al., 2013). Crude glycerol, generated as waste during biodiesel production, has been valorized for the production of amino acids and the diamine putrescine by recombinant strains (Meiswinkel et al., 2013b). *C. glutamicum* also exhibited growth and robustness on spent sulfite liquor (SSL), the waste stream from pulp and paper industry (Lira-Parada et al., 2022). In this regard, *C. glutamicum* appears as a promising host for the utilization of various industrial waste streams.

3.3 Industrial waste stream – Spent sulfite liquor

3.3.1 Spent sulfite liquor - Waste stream from pulp and paper industry

The pulp and paper industry is one of largest industries of the world. Based on the Food and Agriculture Organization (FAO) of the United Nations, the global annual production of paper and paperboard is over 400 million tons (FAO). Furthermore, roughly 50% paper and paperboard is produced from wood pulp, whereas other 50% is produced from recovered paper (FAO). Using wood as raw material to produce paper and paperboard plays an important role for utilization of lignocellulose biomass. Different methods, mainly mechanical pulping and chemical pulping, are developed to generate pulp from wood materials (Biermann, 1996). Mechanical pulping only uses mechanical actions and no chemicals to separate the wood fibers. This process produces short and fragile fibers containing high amounts of lignin. It is used to produce low grade paper, such as newspaper and magazines (Höglund, 2009). Chemical pulping instead uses different chemicals to treat wood materials. Although the yield of chemical pulping is low (about 45%) compared to mechanical pulping (over 90%), the cellulose fibers are long and intact, and lignin is removed. Therefore, the paper obtained from chemical pulping maintains a higher strength which makes chemical pulping dominant in the pulp and paper industry (Ek et al., 2009; FAO). Currently, sulfur based chemical pulping is the most applied technology. Major processes are Kraft pulping (sulfate process) and sulfite pulping. The Kraft process uses alkaline conditions to produce strong fibers. It accepts all types of raw materials, including resinous types of wood and non-wood species. Additionally, almost all pulping chemicals can be recycled by the recovery boiler in the Kraft process (Biermann, 1996; Ek et al., 2009). In contrast, the sulfite process uses acidic conditions. It digests more cellulose and yields weaker fibers which can be easily bleached, however, it accepts only a limited number of wood species compared to the Kraft process (Biermann, 1996; Ek et al., 2009). More than 3 million tons of sulfite pulp was generated in 2019, widely applied to produce writing paper, print paper and tissue (FAO).

During the sulfite process (Figure 3-7), the wood materials are cooked in batch digesters with sulfite/bisulfite salt solutions, using calcium (Ca^{2+}), magnesium (Mg^{2+}), sodium (Na^{+}) and ammonium (NH_4^{+}) as alkali cations (Annergren and Germgard, 2014; Biermann, 1996; Ek et al., 2009). For the building block lignocellulose biomass, the existing strong covalent cross-linkages between lignin and carbohydrates (cellulose and hemicellulose) are cleaved by the chemicals (Ek et al., 2009). Hereby, cellulose is separated to produce cellulose pulp, whereas chemically-treated lignin along with hemicellulose is dissolved in the aqueous phase, generating huge amount of waste named spent sulfite liquor (SSL) (Ek et al., 2009). Thus, more than 50% of the wood material is contained in the waste

stream, resulting in more than 1 ton of solid waste contained in SSL when 1 ton of pulp is produced. Containing about 11-14% solids, the thin and weak liquor accumulates at approximately 30-50 billion liters worldwide (Lawford and Rousseau, 1993; Marques et al., 2009; Sjöström, 1993). Usually it is thickened and concentrated via several rounds of evaporation and concentration, and, usually burned for chemical and energy recovery, wasting valuable carbon (Ek et al., 2009). SSL, containing large amounts of lignin and hemicellulose hydrolysates, therefore appears as a suitable and renewable feedstock for second-generation biorefineries.

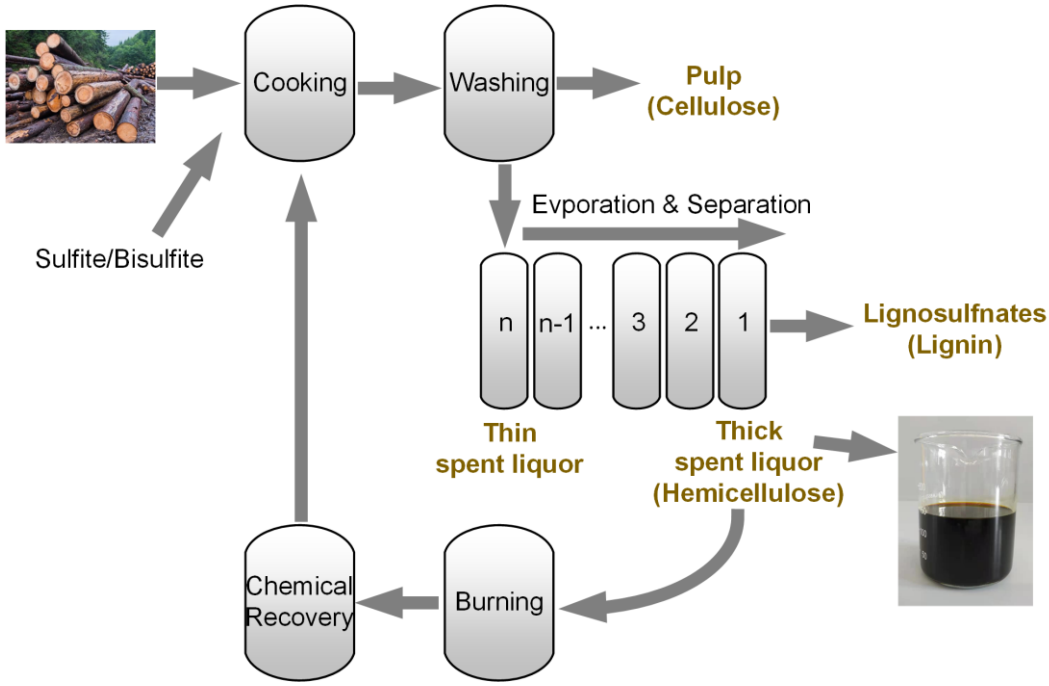

Figure 3-7: General scheme of sulfite wood pulping process with SSL release. Figure adapted from (Pereira et al., 2013).

3.3.2 Chemical composition of spent sulfite liquor

The composition of SSL is complex and varies depending on the employed operational conditions and the type of wood material used (Fatehi and Ni, 2011). Under chemical treatment, lignin is mainly converted to lignosulfonates which display 50-80% of total solids in SSL (Marques et al., 2009; Sjöström, 1993). Lignosulfonates are polydisperse polymers with a wide range of molecular mass. Given their unique properties, lignosulfonates have found different low-value uses as dispersant additives, flocculants, metal adsorbents, dust suppressants, and so on (Aro and Fatehi, 2017; Gonçalves et al., 2021; Lora, 2008; Vishtal and Kraslawski, 2011).

Apart from the lignosulfonates, the polysaccharide hemicellulose is hydrolyzed into diverse monosaccharides, which form up to 30% of total solids in thin SSL (Sjöström,

1993) (Marques et al., 2009). There are more than 1 million tons of sugars generated and contained in SSL worldwide per year (FAO). Previous studies reported that the main sugars contained in SSL are glucose, mannose, xylose, L-arabinose, galactose and L-rhamnose (Rødsrud et al., 2012; Sjöström, 1993). Notably, the sugar composition in SSL depends on the type of wood. For coniferous softwood, such as Spruce, the obtained SSL is rich in mannose (50% of all sugar) (Lawford and Rousseau, 1993; Sjöström, 1993), whereas deciduous hardwood, such as Eucalyptus, yields SSL rich in xylose (more than 70% of total sugar) (Marques et al., 2009; Xavier et al., 2010). The SSL-contained sugars are promising fermentable substrates for microorganisms to produce chemicals, materials, and fuels.

Table 3-1: Chemical composition of spent sulfite liquor.

Components	Concentration [g L^{-1}]			
	Hardwood SSL		Softwood SSL	
	(Marques et al., 2009)	(Xavier et al., 2010)	(Björling and Lindman, 1989)	(Holmgren and Sellstedt, 2008)
pH	2.9	3.4	-	2.3
Dry solids	128	148	220	-
Lignosulphonates	59	78.2	120	110
Glucose	3.0	2.3	7.0	9.7
Mannose	1.0	8.5	21.0	27
Xylose	21.0	24.6	9.0	11.0
L-Arabinose	1.0	7.8	2.0	0.7
Galactose	5.0	4.5	6.0	4.7
L-Rhamnose	1.0	1.6	-	-
Furfural	2.0	≤ 0.1	0.2	-
Acetic acid	8.0	8.2	3.0	-
Ash	28.0	19.8	-	-

Moreover, some of the sugars contained in SSL have a value on their own. Mannose is used as dietary supplement in food, as auxiliary moisturizing agent in cosmetics, and as feed additive (Hu et al., 2016). In addition, mannose binds pathogenic *E. coli* strains that cause inflammation in the urinary tract, yielding a complex that is flushed out, allowing mannose to treat and prevent urinary tract infections (UTIs) (De Nunzio et al., 2021; Kranjcec et al., 2014; Porru et al., 2014). Galactose has been shown to support early human development and prevent diseases, especially diseases involved in brain function, leading to its name as the "brain sugar" (Coelho et al., 2015; Roser et al., 2009; Salkovic-Petrisic et al., 2014). L-Rhamnose is a precursor for the industrial synthesis of the aroma furaneol (Hecquet et al., 1996) and a valuable sugar residue in cardiac glycosides for the synthesis of cardiac drugs (Brown and Thomas, 1983; Prassas and Diamandis, 2008). Xylose and L-arabinose are low caloric pentoses, while xylose is widely used as sweetener in food and beverage (Xu and Luo, 2012), and L-arabinose has been reported as functional food addictive, nutritional supplement, and precursor for pharmaceuticals (Hu et al., 2018). In addition, various derivatives can be easily obtained from these sugars, involving e.g. the conversion of galactose to tagatose, used as an artificial sweetener (Levin, 2002), and the conversion of xylose to xylitol, applied in food, odontology, and pharmaceuticals (Ur-Rehman et al., 2015). Given the wide application of these sugars, their separation and purification from SSL seems also an attractive approach to valorize this waste stream.

Besides lignosulfonates and sugars, various inhibitors are inevitably generated during the acid treatment of lignocellulosic biomass in the sulfite process (Chandel et al., 2013; Palmqvist and Hahn-Hägerdal, 2000b; Pereira et al., 2013). Based on their origin, these inhibitors are classified into the following groups: sugar-derived inhibitors, lignin-derived inhibitors, weak acids, raw material extractives, and heavy metal ions (Chandel et al., 2013; Mussatto and Roberto, 2004). Sugar-derived inhibitors are mainly furans, such as furfural (generated from the dehydration of pentoses, particularly xylose) (Dunlop, 1948), and 5-hydroxymethylfurfural (HMF) (generated from the dehydration of hexoses) (Ulbricht et al., 1984). Furans are toxic to microorganisms. It was reported that the growth of *S. cerevisiae* was inhibited, by 47%, 81%, and 90% at furfural concentrations of 0.5, 1 and 2 g L^{-1}, and by 65%, 83%, and 89% at 5-HMF concentrations of 1, 3 and 5 g L^{-1}, respectively. Similar inhibitory effect were also observed for *Candida shehatae*, *Pichia stipitis* and *Zymomonas mobilis* (Delgenes et al., 1996). In addition to the inhibition of cell growth, furans have a negative effect on product formation. Previous studies showed that the addition of 1.5 g L^{-1} of furfural decreased ethanol yield and productivity by 90% and 85%, respectively (Nigam, 2001). Several lignin-derived inhibitors, including aromatics, polyaromatics, phenolics and aldehyde, are formed during the hydrolysis

process (Marques et al., 2009; Pereira et al., 2013). Among these inhibitors, phenolics, such as vanillin, phenol, 4-hydroxybenzaldehyde and syringaldehyde, exhibited the most toxic effect on microorganisms which impaired the cell membrane, causing reduction of cell growth and sugar assimilation (Delgenes et al., 1996; Heipieper et al., 1994; Klinke et al., 2004; Larsson et al., 2000; Zhang et al., 2012). Regarding weak acids and raw material extractives, such as acetic acid, formic acid, levulinic acid, tannic and terpene acids, they have least toxic effect on the cells compared to furans and phenolics (Chandel et al., 2013; Mussatto and Roberto, 2004). Notably, the addition of low concentrations of acids can have a beneficial effect on the fermentation process (Felipe et al., 1995; Larsson et al., 1999a; Palmqvist et al., 1999). In one study, an increased acetic acid concentration up to 10 g L^{-1} increased ethanol production by yeasts (Palmqvist et al., 1999). Similar effects were observed when adding formic acid and levulinic acid at low concentration (Larsson et al., 1999a). Heavy metal ions, such as iron, chromium, nickel and copper that are released during corrosion of the process reactors inhibit enzyme activities involved in various metabolic reactions (Mussatto and Roberto, 2004; Watson et al., 1984). More importantly, the presence of several inhibitors might cause synergistic effects leading to even stronger inhibition (Chandel et al., 2013; Mussatto and Roberto, 2004). One research showed that the individual addition of furfural, lignin derivatives, and acetic acid, respectively, led to a reduction of the ethanol productivity by 13%, 45% and 60%, respectively, while the addition of all three inhibitors together decreased the ethanol productivity by 83% (Nigam, 2001).

To obtain an effective and successful fermentation process, the inhibition effects have to be reduced or preferentially even removed. Different detoxification methods have been developed and employed, including physical, chemical and biological treatment (Chandel et al., 2013; Larsson et al., 1999b; Palmqvist and Hahn-Hägerdal, 2000a). Physical methods, such as evaporation effectively removes volatile compounds including acetic acid and furfural (Converti et al., 2000), whereas non-volatile inhibitors, phenolics in particular, are accumulated (Parajó et al., 1997). Chemical methods (such as $Ca(OH)_2$ overliming) have been widely used and displayed as one of the most efficient detoxification methods. $Ca(OH)_2$ overliming treatment increases the pH of the hydrolysates to 9 – 10, resulting in precipitation and removal of most inhibitors, including furfural, 5-HMF, phenolics, acetic acid and soluble lignin compounds (Amartey and Jeffries, 1996; Helle et al., 2008; Martinez et al., 2001; Martinez et al., 2000). Regarding biological methods, there are two strategies including enzymatic and microbial treatment. The use of the enzymes laccase (Martín et al., 2002) and peroxidases (Cho et al., 2009) was shown effective to remove of phenolics. Several microorganisms were applied for the detoxification of lignocellulosic hydrolysates, e.g., *Trichoderma reesei* decreased

furans, phenolics, and the weak acid content (Palmqvist et al., 1997), *Coniochaeta ligniaria* metabolized furfural and 5-HMF (Lopez et al., 2004). With the development of metabolic engineering and systems biology, the construction of ideal microorganisms capable to metabolize and detoxify the inhibitors while simultaneously conducting product formation, appears as a promising strategy, allowing simultaneous detoxification and fermentation (Chandel et al., 2013). Nevertheless, given the high complexity of inhibitors, and the varied tolerance of different microorganisms for different inhibitors, as well as increased economic cost of the detoxification treatment, the detoxification methods have to be carefully chosen to acquire satisfactory process conditions.

3.3.3 Valorization of spent sulfite liquor

Many processes have been established to produce value-added products from SSL over last few decades (Rødsrud et al., 2012). Lignosulfonates dominate 80-90% of the commercial lignin market and the globally annual production of lignosulfonates was estimated to about 1.5 million tons in 2025, whereby Borregaard is the main supplier (Dessbesell et al., 2020). Currently, lignosulfonates are separated from SSL, whereby the molecular mass of the lignosulfonates is much higher than that of the other compounds in SSL, facilitating efficient separation (Marques et al., 2009). Commercial separation and recovery of lignosulfonates from SSL involves membrane filtration (Pabby et al., 2008; Restolho et al., 2009). In particular, ultrafiltration, widely used in the calcium bisulfite pulping process, yields up to 95% pure lignosulfonates (Aro and Fatehi, 2017). Other separation methods such as the Howard method, amine extraction, ion-exchange resin, and reverse osmosis, respectively, have been developed at laboratory scale, but, so far, have been rarely applied in the industry (Aro and Fatehi, 2017). The aromatic compound vanillin, employed in food, beverages and pharmaceuticals, is another value-added product from SSL, although at low volume (Hocking, 1997). Due to low economic costs of alternative chemical synthesis routes, Borregaard seems to be the only supplier for the production of bio-vanillin from SSL nowadays. Hereby, vanillin is generated by oxidation of purified lignosulfonates (Bjørsvik and Minisci, 1999).

Regarding fermentable sugars in SSL, the lignosulfonates-free spent liquor, containing the sugars, is still majorly burned (Ek et al., 2009). Although this reduces the overall energy consumption of the sulfite pulping process, vast amounts of carbon are inevitably wasted. Over the last years, several studies have focused on the production of bioethanol from fermentable sugars in SSL (Branco et al., 2019; Daniel et al., 2012; Pereira et al., 2013; Rueda et al., 2015), which is currently generated from fermentation of first-generation sugar crops, i.e., sugar cane and corn gain (Gray et al., 2006). Hereby,

given high productivity, and tolerance many inhibitors (Almeida et al., 2007; Ma and Liu, 2010), as well as the GRAS trait, *S. cerevisiae* has been employed for ethanol production from SSL sugar (Helle et al., 2004; Johansson et al., 2011; Johansson et al., 2014). Nevertheless, native *S. cerevisiae* cannot grow on xylose as sole carbon source, the predominant sugar in hardwood SSL, despite the presence of a xylose metabolic pathway (Batt et al., 1986). Different metabolic engineering strategies have been applied to enable xylose utilization in *S. cerevisiae*, including engineering heterologous xylose isomerase (XI) (Karhumaa et al., 2005; Kuyper et al., 2003), and engineering heterologous xylose reductase (XR), xylitol dehydrogenase (XDH) and xylulokinase (XK) (Bengtsson et al., 2009; Jeppsson et al., 2006). In addition, adaptive evolution for selection of superior xylose utilizing *S. cerevisiae* strains has been conducted as attractive alternative since strains generated by this approach are not regarded GMO (Attfield and Bell, 2006; Pitkanen et al., 2005). Besides *S. cerevisiae*, *P. stipitis* has gained attention for ethanol production from SSL owing to its xylose utilization capacity (Bajwa et al., 2009; Henriques et al., 2018; Xavier et al., 2010). However, *P. stipitis* was found sensitive towards the inhibitors in SSL, requiring intensive detoxification pretreatment for successful fermentation, a bottleneck for industrial application (Pereira et al., 2012; Takahashi et al., 2013). Adaptive evolution, however, generated *P. stipitis* mutants with higher tolerance (Huang et al., 2009; Pereira et al., 2015). Other yeasts like *Candida shehatae* (Yu et al., 1987) and bacteria such as *E. coli* (Lawford and Rousseau, 1993) were also shown to produce ethanol from SSL. Apart from ethanol, xylitol as commercial sweetener is another promising product (Ur-Rehman et al., 2015). The current industrial production of xylitol is conducted through chemical hydrogenation of xylose, derived from hemicellulosic hydrolysates (Mikkola et al., 2000). Thus, hardwood SSL, containing a higher percentage of xylose, seems an ideal raw material for xylitol production. Some laboratories have reported production of xylitol using SSL as the raw material (Lai and Bura, 2012; Miura et al., 2015; Rodrigues et al., 2008). Furthermore, SSL based production of polyhydroxybutyrate (PHB) using halophilic microorganisms (Weissgram et al., 2015), succinic acid using *Actinobacillus succinogenes* and *Basfia succiniciproducen*s (Alexandri et al., 2017; Ladakis et al., 2018) has been developed.

Regarding the inhibitors, furfural is an important chemical feedstock for other furan-based chemicals, such as furfuryl alcohol, furoic acid, and furfurylamine which have potential applications in the chemical industry (Zeitsch, 2000). Today, furfural is industrially produced through the dehydration of pentose, mainly using agricultural residues as a feedstock (Dashtban et al., 2012). SSL could be a feasible raw material (Montastruc et al., 2011; Xing et al., 2011).

The mentioned processes, however, undergo different developments nowadays. Processes including lignosulfonate recovery and ethanol production from SSL are widely and partially applied in industry, respectively. Vanillin and acetic acid production were performed in the past but have been stopped in most pulp mills due to competition from fossil equivalents. PHB and succinic acid production are being conducted at laboratory scale and are not applied in industry so far (Rødsrud et al., 2012; Rueda et al., 2015). Moreover, based on the price of residual sugar (\$ 0.5 kg^{-1}, from Borregaard) and ethanol (\$ 0.4-0.6 kg^{-1}, from NASDAQ), ethanol production does not appear cost-efficient and economically feasible. Therefore, it is critical to develop new strategies and processes, particularly utilizing the high amounts valuable sugar in SSL since they are mostly wasted. Novel microorganisms effectively utilizing all sugars in SSL is a crucial prerequisite for efficient fermentation, where systems metabolic engineering could play an essential role for the novel strain development (Buschke et al., 2013b). One should also consider the tolerance of selected microorganisms to inhibitors to achieve successful fermentation. In brief, further studies should focus on conversion of all sugars contained in SSL to produce value-added compounds by robust industrial workhorse, paving the way for valorization of this waste stream from pulp and paper industry. Here, the excellent traits, i.e., the industrial workhorse, utilization of diverse substrates, as well as the robustness towards several inhibitors, favor *C. glutamicum* as an attractive platform for valorization of SSL and will be studied in detail.

4 Material and Methods

4.1 Strains

The wild type *C. glutamicum* ATCC 13032 (DSM 20300) was obtained from the German Collection of Microorganisms and Cell Cultures (DSMZ, Braunschweig, Germany). The genome reduced chassis strain *C. glutamicum* CR099 (Baumgart et al., 2018) and the advanced glutaric acid producer *C. glutamicum* GTA-4 (Rohles et al., 2018), previously developed from the wild type ATCC 13032, were taken from previous work. The *E. coli* strains DH5α and NM522 were obtained from Invitrogen (Karlsruhe, Germany) and used as hosts for plasmid amplification and methylation, respectively. All strains used and created in this work are listed in Table 4-1.

Table 4-1: Strains used in this work. Jens Christmann contributed to the construction of MSU-9 and MSU-18.

Strains	Description	Reference
E. coli		
E. coli DH5α	Heat shock competent cells for the amplification of the transformation vector	Invitrogen
E. coli NM522	Heat shock competent cells for the amplification and methylation of the transformation vector	Invitrogen
C. glutamicum		
ATCC 13032	Wild type	ATCC
MSU-1	ATCC 13032 + episomal expression of *manA* (NCgl0716) from *C. glutamicum* ATCC 13032 under control of *tac* promoter + episomal expression $xylA_{Xc}$ (XCC1758) from *X. campestris* pv. *campestris* ATCC 33913 and *xylB* (NCgl0111) from *C. glutamicum* ATCC 13032, under control of *tac* promoter	This work
MSU-2	ATCC 13032 + overexpression of *manA* by replacement of the natural promoter with the *tuf* promoter	This work
MSU-3A	MSU-2 + genome-based integration of $xylA_{Xc,\ co}$ from *X. campestris* pv. *campestris* ATCC 33913 (codon optimized for *C. glutamicum*) under control of *tuf* promoter into upstream of *xylB* locus	This work
MSU-3B	MSU-2 + genome-based integration of native $xylA_{Xc}$ from *X. campestris* pv. *campestris* ATCC 33913 under control of *tuf* promoter into upstream of *xylB* locus	This work

Table 4-1: (Continued from previous page) Strains used in this work.

Strains	Description	Reference
MSU-3C	MSU-2 + genome-based integration of native *xylA*$_{Xc}$ from *X. campestris* pv. *campestris* ATCC 33913 under control of *tac* promoter into upstream of *xylB* locus	This work
MSU-4A	MSU-3B + genome-based integration of *araBDAE*$_{Cg,\ co}$ from *C. glutamicum* 31831 (codon optimized for *C. glutamicum* ATCC 13032) under control of *tuf* promoter into *iolR* locus (NCgl0154)	This work
MSU-4B	MSU-3B + genome-based integration of *araBDAE*$_{Ec,\ co}$ (*araB*: b0063; *araD*: b0061; *araA*: b0062; *araE*: b2841) from *E. coli* K12 MG1655 (codon optimized for *C. glutamicum*) under control of *tuf* promoter into *iolR* locus	This work
MSU-4C	MSU-3B + genome-based integration of native *araBDAE*$_{Cg}$ from *C. glutamicum* 31831 (Accession number AB447371) under control of *tuf* promoter into *iolR* locus	This work
MSU-5A	MSU-4C + genome-based integration of *galPMKTE*$_{Ll,\ co}$ from *L. lactis* subsp. *cremoris* MG1363 (codon optimized for *C. glutamicum*) under control of *tuf* promoter into *crtEb* locus (NCgl0594)	This work
MSU-5B	MSU-4C + genome-based integration of native *galPMKTE*$_{Ll}$ from *L. lactis* subsp. *cremoris* MG1363 (Accession number AJ011653) under control of *tuf* promoter into *crtEb* locus	This work
MSU-5C	MSU-4C + genome-based integration of native *galPMKTE*$_{Ll}$ from *L. lactis* subsp. *cremoris* MG1363 into *crtEb* locus, *galPMKT* under control of *tuf* promoter, *galE* under control of native *galE* promoter	This work
MSU-6	MSU-3B + deletion of *iolR*	This work
MSU-7A	MSU-4C + recovery of *iolR*, gene *iolR* in the upstream of arabinose operon	This work
MSU-7B	MSU-5B + recovery of *iolR*, gene *iolR* in the upstream of arabinose operon	This work
MSU-8A	MSU-7B + genome-based integration of *rhaTBADM*$_{Ec,\ co}$ from *E. coli* K12 MG1655 (codon optimized for *C. glutamicum*) under control of *tuf* promoter into *crtB* locus (NCgl2347)	This work
MSU-8B	MSU-7B + genome-based integration of native *rhaTBADM*$_{Ec}$ (*rhaT*: b3907, *rhaB*: b3904, *rhaA*: b3903, *rhaD*: b3902, *rhaM*: b3901) from *E. coli* K12 MG1655 under control of *tuf* promoter into *crtB* locus	This work
MSU-8C	MSU-7B + genome-based integration of native *rhaTBADM*$_{Lm}$ (*rhaT*: lmo2850, *rhaB*: lmo2849, *rhaA*: lmo2848, *rhaD*: lmo2847, *rhaM*: lmo2846) from *L. monocytogenes* EGD-e under control of *tuf* promoter into *crtB* locus	This work

Table 4-1: (Continued from previous page) Strains used in this work.

Strains	Description	Reference
MSU-9	MSU-4C + overexpression of *ptsF* by replacement of the natural promoter with the *tuf* promoter	This work
GTA-4	Glutarate hyper-producing strain with 16 genome-based modifications	(Rohles et al., 2018)
MSU-10	GTA-4 + overexpression of *manA* by replacement of the natural promoter with the *tuf* promoter	This work
MSU-11	MSU-10 + genome-based integration of native $xylA_{Xc}$ from *X. campestris* pv. *campestris* ATCC 33913 under control of *tuf* promoter into upstream of *xylB* locus	This work
MSU-12	MSU-11 + genome-based integration of native $araBDAE_{Cg}$ from *C. glutamicum* 31831 under control of *tuf* promoter into *iolR* locus	This work
MSU-13	MSU-12 + genome-based integration of native $galPMKTE_{Ll}$ from *L. lactis* subsp. *cremoris* MG1363 under control of *tuf* promoter into *crtEb* locus	This work
CR099	Genome-reduced strain; ATCC 13032 *ΔCGP123ΔISCg1ΔISCg2*	(Baumgart et al., 2018)
MSU-14	CR099 + overexpression of *manA* by replacement of the natural promoter with the *tuf* promoter	This work
MSU-15	MSU-14 + genome-based integration of native $xylA_{Xc}$ from *X. campestris* pv. *campestris* ATCC 33913 under control of *tuf* promoter into upstream of *xylB* locus	This work
MSU-16	MSU-15 + genome-based integration of native $araBDAE_{Cg}$ from *C. glutamicum* 31831 under control of *tuf* promoter into *iolR* locus	This work
MSU-17	MSU-16 + genome-based integration of native $galPMKTE_{Ll}$ from *L. lactis* subsp. *cremoris* MG1363 under control of *tuf* promoter into *crtEb* locus	This work
MSU-18	MSU-17 + episomal expression of $pedACD^{Cg}$ operon, under control of *tac* promoter	This work
MAN-1A	MSU-7B + deletion of *ptsH* (NCgl1862)	This work
MAN-1B	MSU-7B + deletion of *manA*	This work
MAN-1C	MSU-7A + deletion of *ptsH*	This work
MAN-2	MSU-8B + deletion of *manA*	This work
GAL-1	MSU-7A + genome-based integration of native $rhaTBADM_{Ec}$ from *E. coli* K12 MG1655 under control of *tuf* promoter into *crtB* locus	This work
GAL-2A	ATCC 13032 + empty episomal plasmid pClik 5a MCS	This work
GAL-2B	ATCC 13032 + episomal expression of *galP* from *L. lactis* subsp. *cremoris* MG1363 under control of *tuf* promoter	This work

Table 4-1: (Continued from previous page) Strains used in this work.

Strains	Description	Reference
GAL-2C	ATCC 13032 + episomal expression of *galMKTE* from *L. lactis* subsp. *cremoris* MG1363 under control of *tuf* promoter	This work
GAL-2D	MSU-4C + episomal expression of *galMKTE* from *L. lactis* subsp. *cremoris* MG1363 under control of *tuf* promoter	This work
RHA-1	MSU-13 + recovery of *iolR*, gene *iolR* in the upstream of arabinose operon	This work

4.2 Plasmids and primers

For genomic modification of *C. glutamicum*, the integrative plasmid pClik int *sacB* was applied (Becker et al., 2005b). This vector contained a multiple cloning site, an origin of replication (ORI) for *E. coli*, kanamycin resistance (Kan^R), and the *sacB* gene from *Bacillus subtilis*, encoding levansucrase, as a selection marker, respectively. The plasmid pTC, encoding the DNA methyltransferase for *C. glutamicum*, was used for DNA methylation (Kind et al., 2010). The vector also contained an ORI for *E. coli* and tetracycline resistance (Tet^R). To add the DNA methylation pattern of *C. glutamicum* to plasmid DNA, pTC was co-expressed in *E. coli* NM522. For initial growth tests on xylose and mannose containing media, the episomal plasmids pVWEx1 *manA* and pEKEx3 $xylA_{Xc}$ $xylB_{Cg}$ obtained from Ulm University were used. For pediocin production, the plasmid pXMJ19-$pedACD^{Cg}$ was obtained from Ulm University within the framework of the European iFermenter project. It contained the pediocin operon *pedACD* from *P. acidilactici* PAC1.0 under control by the IPTG–inducible P_{tac} promoter and chloramphenicol resistance gene (Goldbeck et al., 2021). In addition, the genes of interest were overexpressed using the episomal plasmid pClik 5a MCS (Buschke et al., 2011; Hoffmann et al., 2018), which contained a multiple cloning site, origins of replication for *E. coli* and *C. glutamicum*, and kanamycin resistance (Kan^R). For plasmids and primers design, the SnapGene software (www.snapgene.com) was used. All plasmids used in this work are listed in Table 4-2 and all primers are shown in the appendix Table 7-1.

Table 4-2: Plasmids used in this work for strain engineering of *C. glutamicum*. Jens Christmann contributed to the construction of pClik int *sacB* P_{tuf}*ptsF*.

Plasmids	Description	Reference
pTC	Expression vector for DNA-methyltransferase of *C. glutamicum*, containing ORI for *E. coli* and tetracycline resistance as selection marker	(Kind et al., 2010)
pClik 5a MCS	Episomal replicating vector with origins of replication (ORI) for *C. glutamicum* and *E. coli*, and Kan^R as a selection marker	(Hoffmann et al., 2018)
pClik int *sacB*	Integrative transformation vector for genome-based modification of *C. glutamicum* with MCS, ORI for *E. coli*, and Kan^R and *sacB* as selection markers	(Becker et al., 2005b)
pVWEx1_*manA*	Episomal vector for expression of *manA* from *C. glutamicum* ATCC 13032 under control of *tac* promoter	(Perez-Garcia et al., 2021)
pEKEx3_$xylA_{Xc}$ $xylB_{Cg}$	Episomal vector for expression of native $xylA_{Xc}$ from *X. campestris* pv. *campestris* ATCC 33913 and *xylB* from *C. glutamicum* ATCC 13032, under control of *tac* promoter	(Meiswinkel et al., 2013a; Perez-Garcia et al., 2021)
pClik int *sacB* P_{tuf} *manA*	Integrative vector for overexpression of gene *manA,* under control of *tuf* promoter	This work
pClik int *sacB* P_{tuf} $xylA_{Xc,\ co}$	Integrative vector for integration of the gene $xylA_{Xc,\ co}$ from *X. campestris* pv. *campestris* ATCC 33913 (codon optimized for *C. glutamicum*), under control of *tuf* promoter upstream of *xylB* locus	This work
pClik int *sacB* P_{tuf} $xylA_{Xc}$	Integrative vector for integration of native gene $xylA_{Xc}$ from *X. campestris* pv. *campestris* ATCC 33913 under control of *tuf* promoter upstream of *xylB* locus	This work
pClik int *sacB* P_{tac} $xylA_{Xc}$	Integrative vector for integration of native gene $xylA_{Xc}$ from *X. campestris* pv. *campestris* ATCC 33913 under control of *tac* promoter upstream of *xylB* locus	This work
pClik int *sacB* P_{tuf} $araBDAE_{Cg,\ co}$	Integrative vector for integration of the genes $araBDAE_{Cg,\ co}$ from *C. glutamicum* 31831 (codon optimized for *C. glutamicum*) under control of *tuf* promoter into *iolR* locus	This work
pClik int *sacB* P_{tuf} $araBDAE_{Ec,\ co}$	Integrative vector for integration of the genes $araBDAE_{Ec,\ co}$ from *E. coli* K12 MG1655 (codon optimized for *C. glutamicum*) under control of *tuf* promoter into *iolR* locus	This work
pClik int *sacB* P_{tuf} $araBDAE_{Cg}$	Integrative vector for integration of native genes $araBDAE_{Cg}$ from *C. glutamicum* 31831 under control of *tuf* promoter into *iolR* locus	This work

Table 4-2: (Continued from previous page) Plasmids used in this work for strain engineering of *C. glutamicum*.

Plasmids	Description	Reference
pClik int *sacB* P_{tuf} *galPMKTE*$_{Ll,\ co}$	Integrative vector for integration of the genes *galPMKTE*$_{Ll,\ co}$ from *L. lactis* subsp. *cremoris* MG1363 (codon optimized for *C. glutamicum*) under control of *tuf* promoter into *crtEb* locus	This work
pClik int *sacB* P_{tuf} *galPMKTE*$_{Ll}$	Integrative vector for integration of native genes *galPMKTE*$_{Ll}$ from *L. lactis* subsp. *cremoris* MG1363 under control of *tuf* promoter into *crtEb* locus	This work
pClik int *sacB* P_{tuf} *galPMKTE*$_{Ll\_PgalE}$ from *L. lactis* subsp. *cremoris* MG1363 into *crtEb* locus, genes *galPMKT* under control of *tuf* promoter and *galE* under control of native promoter	Integrative vector for integration of native genes *galPMKTE*$_{Ll}$ P_{galE} *galE*	This work
pClik int *sacB* *ΔiolR*	Integrative vector for deletion of gene *iolR*	This work
pClik int *sacB* int_*iolR*	Integrative vector for recovery of gene *iolR*, integrate *iolR* to original locus, which is in the upstream of arabinose operon	This work
pClik int *sacB* P_{tuf} *rhaTBADM*$_{Ec,\ co}$	Integrative vector for integration of the genes *rhaTBADM*$_{Ec,\ co}$ from *E. coli* K12 MG1655 (codon optimized for *C. glutamicum*) under control of *tuf* promoter into *crtB* locus	This work
pClik int *sacB* P_{tuf} *rhaTBADM*$_{Ec}$	Integrative vector for integration of native genes *rhaTBADM*$_{Ec}$ from *E. coli* K12 MG1655 under control of *tuf* promoter into *crtB* locus	This work
pClik int *sacB* P_{tuf} *rhaTBADM*$_{Lm}$	Integrative vector for integration of native genes *rhaTBADM*$_{Lm}$ from *L. monocytogenes* EGD-e under control of *tuf* promoter into *crtB* locus	This work
pClik int *sacB* P_{tuf} *ptsF*	Integrative vector for overexpression of gene *ptsF* under control of *tuf* promoter	This work
pXMJ19-*pedACD*^{Cg}	Episomal vector for expression of *pedACD*^{Cg} operon from *P. acidilactici* PAC1.0 (codon optimized for *C. glutamicum*), under control of *tac* promoter, for recombinant production of pediocin PA-1	(Goldbeck et al., 2021)
pClik int *sacB* *ΔptsH*	Integrative vector for deletion of gene *ptsH*	This work
pClik int *sacB* *ΔmanA*	Integrative vector for deletion of gene *manA*	This work
pClik 5a MCS *galP*	Episomal replicating vector for expression of gene *galP* from *L. lactis* subsp. *cremoris* MG1363 under control of *tuf* promoter promotor	This work
pClik 5a MCS *galMKTE*	Episomal replicating vector for expression of genes *galMKTE* from *L. lactis* subsp. *cremoris* MG1363 under control of *tuf* promoter promotor	This work

4.3 Chemicals

Brain heart infusion (BHI) medium, agar, peptone, yeast extract, and beef extract were purchased from Difco Laboratories (Detroit, MI, USA). All other chemicals were obtained from Sigma-Aldrich (Steinheim am Albuch, Germany), Merck (Darmstadt, Germany), Fluka (Buchs, Switzerland) or Carl Roth GmbH (Karlsruhe, Germany). Spent sulfite liquor ultrafiltration (SSL-UF) was provided from Borregaard (Sarpsborg, Norway) within the framework of the European iFermenter project.

4.4 Medium composition

All media and solutions used in this work were prepared in ultrapure water. Solid medium for plate cultures was prepared by adding 20 g L^{-1} of agar. Sterilization was performed by autoclaving at 121 °C for 30 min or by filtration. If required, kanamycin (50 µg mL^{-1}) and spectinomycin (50 µg mL^{-1}) were added as selection markers. Likewise, isopropyl β-D-1-thiogalactopyranoside (IPTG; 1 mM) was added as inducer into the medium, as given below.

4.4.1 Complex medium

For cultures of *E. coli* and first pre-cultures of *C. glutamicum*, BHI medium (Table 4-3) was used.

Table 4-3: Composition of the complex medium BHI.

BHI	37 g
Add 1 L H_2O	
Autoclave	

For the preparation of electro-competent *C. glutamicum* cells, BHI^{++} medium was used. In short, 37 g BHI was dissolved in 870 mL water followed by autoclaving. Afterwards, 50 mL of autoclaved 2 M $(NH_4)_2SO_4$ and 80 mL of autoclaved 50% glucose were added to yield the final medium.

For cell regeneration of *C. glutamicum* after electroporation with plasmid DNA, BHIS medium was used. Hereby, 37 g BHI was dissolved in 750 mL water, autoclaved, and mixed with 250 mL of autoclaved 2 M sorbitol.

For *C. glutamicum* selection cultures during second recombination events for strain construction, a CM^{Sac} agar medium was used. CM medium, sucrose, glucose and urea were sterilized separately and mixed together afterwards (Table 4-4).

Table 4-4: Composition of the complex medium CM^{Sac}.

CM medium	
Peptone	10 g
Beef extract	5 g
Yeast extract	5 g
NaCl	2.5 g
Add 730 mL H_2O	
Autoclave	
Sucrose (500 g L^{-1}), autoclaved	200 mL
Glucose (500 g L^{-1}), autoclaved	20 mL
Urea (40 g L^{-1}), sterile-filtered	50 mL

4.4.2 Minimal medium

To cultivate and characterize *C. glutamicum* strains in shake flasks with pure sugar substrates, chemically defined minimal medium was used for second pre-cultures and main cultures. The minimal medium consisted of different stock solutions which were prepared and sterilized separately (Table 4-5).

Table 4-5: Composition of the stock solutions of the minimal medium used for cultivation of *C. glutamicum.*

Solution A	
NaCl	20 g
$CaCl_2$	1.1 g
$MgSO_4 \cdot 7\ H_2O$	4 g
Add up to 1 L with H_2O	
Autoclave	

Solution B	
$(NH_4)_2SO_4$	150 g
Adjust pH 7 with NaOH; Add up to 1 L with H_2O	
Autoclave	

Buffer solution	
P1: K_2HPO_4	348.23 g
Add up to 1 L with H_2O	
P2: KH_2PO_4	272.16 g
Add up to 1 L with H_2O	
P1 and P2 were prepared separately, add P2 to P1 until pH 7.8 for final solution	
Autoclave	

Vitamin solution	
Biotin	25 mg
Thiamin · HCl	50 mg
Ca-Pantothenate	50 mg
Add up to 1 L with H_2O	
Filtration, Store at 4 °C	

Iron solution	
$FeSO_4 \cdot 7\ H_2O$	20 mg
Adjust pH 1 with HCl; Add up to 10 mL with H_2O	
Filtration, Store at 4 °C	

DHB solution	10 mL
3,4-Dihydroxybenzoic acid	300 mg
NaOH (6 M)	500 µL
Add up to 10 mL with H_2O, Filtration, Store at 4 °C	

Trace element solution	
$FeCl_3 \cdot 6\ H_2O$	200 mg
$MnSO_4 \cdot H_2O$	200 mg
$ZnSO_4 \cdot H_2O$	50 mg
$CuCl_2 \cdot 2\ H_2O$	20 mg
$Na_2B_4O_7 \cdot 10\ H_2O$	20 mg
$(NH_4)_6Mo_7O_{24} \cdot 4\ H_2O$	10 mg
Add up to 1 L with H_2O	
Filtration, Store at 4 °C	

To prepare substrate stock solutions, the individual sugar substrates were prepared separately. Glucose was prepared at a concentration of 500 g L^{-1} and sterilized by autoclaving. Mannose, xylose, L-arabinose, galactose, L-rhamnose and fructose were prepared at a concentration of 100 g L^{-1} and sterilized by filtration.

The stock solutions were mixed freshly before use as listed in Table 4-6.

Table 4-6: Composition of the minimal medium used for cultivation of *C. glutamicum.*

Minimal medium	
Solution A	50 mL
Solution B	100 mL
Buffer solution	100 mL
Vitamins	20 mL
Trace elements	10 mL
Iron solution	10 mL
DHB solution	1 mL
Substrate solution	Adding based on requirement
Add up to 1 L with H_2O	

Different sugar substrates (glucose, mannose, xylose, L-arabinose, galactose, L-rhamnose and fructose) were added either as sole carbon source at a final concentration of 10 g L^{-1} or as mixtures (each sugar at a final concentration of 5 g L^{-1}) to the medium, as specified below.

4.4.3 SSL medium

To cultivate *C. glutamicum* in shake flasks with SSL as substrate, SSL medium was used for second pre-cultures and main cultures. The SSL medium consisted of different stock solutions which were prepared and sterilized separately (Table 4-7).

Table 4-7: Composition of the stock solutions of the SSL medium used for cultivation of *C. glutamicum* on SSL.

Salt solution	MOPS based	MES based
$(NH_4)_2SO_4$	25 g	33.33 g
Urea	6.25 g	8.33 g
KH_2PO_4	1.25 g	1.67 g
K_2HPO_4	1.25 g	1.67 g
$MgSO_4 \cdot 7\ H_2O$	0.3125 g	0.4167 g
$CaCl_2$	12.5 mg	16.7 mg
MOPS buffer	52.5 g	-
Adjust pH 6.5 with NaOH; Add to 1 L with H_2O Autoclave		
MES buffer	-	250 mM

When MES buffer was applied, MES (1 M) was prepared by filtration separately from other salts. After autoclaving other salts, 333 mL MES (1 M) buffer was immediately mixed together with 1 L of other salts to get the final salt solution.

Biotin solution	
Biotin	200 mg
Add up to 1 L with H_2O	
Filtration, Store at 4 °C	

DHB solution	10 mL
3,4-Dihydroxybenzoic acid	300 mg
NaOH (6 M)	500 µL
Add up to 10 mL with H_2O	
Filtration, Store at 4 °C	

Trace element solution	
$FeSO_4 \cdot 7\ H_2O$	10 g
$MnSO_4 \cdot H_2O$	10 g
$ZnSO_4 \cdot 7\ H_2O$	1 g
$CuSO_4$	200 mg
$NiCl_2 \cdot 6\ H_2O$	20 mg
Adjust pH 1 with NaOH; Add up to 1 L with H_2O	
Filtration, Store at 4 °C	

SSL-UF from Borregaard solution was sterilized by filtration and stored at 4°C.

The stock solutions were mixed freshly before use as listed in Table 4-8.

Table 4-8: Composition of the SSL medium used for cultivation of *C. glutamicum* on SSL.

SSL medium	
Salt solution	800 mL
Trace elements	1 mL
Biotin solution	1 mL
DHB solution	1 mL
SSL-UF solution	100 mL or 200 mL as required
Add up to 1 L with H_2O	

For fed-batch fermentations in a 1 L stirred tank bioreactors using SSL as substrate, SSL medium was applied as described above. Pure SSL-UF solution was used as the feed solution.

4.5 Strain preservation

To preserve bacterial strains, *E. coli* or *C. glutamicum* strains were cultivated in baffled shake flasks (10% filling volume) on a rotary shaker (30 °C, 230 rpm, 5 cm shaking diameter, Infors, Bottmingen, Switzerland). If required, antibiotics were added. During exponential growth, 1 mL culture was harvested mixed with 1 mL sterile 60% (v/v) glycerol, the mixture was stored at -80 °C.

4.6 Strain construction

4.6.1 Polymerase chain reaction

To amplify desired DNA fragments for vector construction, polymerase chain reaction (PCR) was performed using the Phusion High-Fidelity PCR Master Mix (Thermo Fisher Scientific, MA, USA), containing a proofreading polymerase. To verify *E. coli* and *C. glutamicum* mutants for the correct genetic modification, a Phire Green Hot Start II PCR Master Mix was used. In short, colonies were picked by a toothpick and suspended in ultrapure water, serving as template DNA. The PCR was prepared based on the composition listed in Table 4-9 and performed according to the program listed in Table 4-10.

Table 4-9: Composition of prepared PCR mixture.

Component	Volume [µL]
2x Phusion High-Fidelity PCR Master Mix or Phire Green Hot Start II PCR Master Mix	10
Forward primer (10 µM)	0.5
Reverse primer (10 µM)	0.5
DNA template	1
DMSO	0.6
Add up to 20 µL with H_2O	

Table 4-10: Performed temperature and time program used for PCR.

Step	Temperature [°C]	Time [min]	Cycle
Initial denaturation	98	10	1
Denaturation	98	0.5	
Annealing	*	0.5	30
Elongation	72	**	
Final elongation	72	5	1
Storage	8	∞	1

*Annealing temperature depends on the used primers

**Elongation time depends on the length of amplified fragment and employed polymerase

The annealing temperature of each primer was calculated using the SnapGene software (www.snapgene.com). The obtained PCR products were verified, purified, and quantified as described below.

4.6.2 Gel electrophoresis

Products from PCR or from the enzymatic digestion of plasmids were separated and evaluated for fragment size by electrophoresis in 1% agarose. Th electrophoresis was performed in 1x TAE buffer which was prepared from dilution of a 50x TAE stock solution (Table 4-11). Before loading a sample into the gel, it was mixed with GelPilot Loading Dye 5x (Qigen, Hiden, and Germany). The 1 kb/1000 bp BLUE DNA Ladder (GeneON, Ludwigshafen, Germany) was used as size standard.

Table 4-11: Composition of 50x TAE stock solution.

Component	
Tris	242.28 g
Acetic acid (100%)	57 mL
EDTA (0.5 M, pH 8.0)	100 mL
Add up to 1 L with H_2O	

Gel electrophoresis was run at 130 V for 40-60 min (Owl Easycast B1A, Thermo Fisher Scientific, MA, USA; PowerPac Basic Power Supply, Bio-Rad, CA, USA). Afterwards,

the gel was stained for 20 min in a 2.5 mg L^{-1} solution of ethidium bromide. DNA fragments were detected and visualized by UV-illumination using the ChemiDoc XRS+ System (Bio-Rad, City, CA, USA).

4.6.3 DNA fragment purification and concentration

PCR products and enzymatically digested plasmid DNA were purified and concentrated using the Wizard SV Gel and PCR Clean-Up System (Promega Madison, WI, USA) according to the manufacturer's instructions. Afterwards, the obtained DNA concentration was determined by the NanoDrop 1000 spectrophotometer (Thermo Fisher Scientific, MA, USA).

4.6.4 Enzymatic digestion

Enzymatic digestion was used to linearize empty plasmids for the construction of transformation vectors and the validation of constructed plasmids. The digestion was performed at 37 °C for 1 h using fast digest restriction enzymes (Thermo Fisher Scientific, MA, USA) (Table 4-12).

Table 4-12: Composition of the reaction mixture used for enzymatic digestion.

Component	Volume [µL]	Concentration
DNA template	-	Up to 1 µg
10x FastDigest Buffer	2	
Enzyme I/II	1	
Add up to 20 µL with H_2O		

For linearization of empty plasmids, using one restriction enzyme was sufficient. For validation constructed plasmids, one or two specific restriction enzymes were applied to obtain the desired inserted fragment.

4.6.5 Construction of transformation vectors

Gibson assembly was performed to construct transformation vectors. Primers, containing at least 20 bp of homologous overlapping sequence to the plasmid or to the corresponding fragment, respectively, were employed to amplify the desired DNA fragment. The purification of the PCR products and linearized empty plasmids was performed as described above. Afterwards, 100 ng of linearized empty-plasmid DNA and an equimolar amount of the chosen PCR products were mixed together with 15 µL of Gibson master mix to a final volume of 20 µL. The composition of the Gibson assembly buffer and the Gibson master mix was prepared is listed in Table 4-13 and Table 4-14, respectively.

Table 4-13: Composition of 5x Gibson assembly buffer.

Component	
Tris-HCl (1 M; pH 7.5)	3 mL
$MgCl_2$ (1 M)	300 µL
Each dNTP (100 mM)	60 µL
DTT (1 M)	300 µL
PEG-8000	1.5 g
NAD	20 mg
Add up to 6 mL with H_2O	

Table 4-14: Composition of Gibson master mix.

Component	
5x Gibson assembly buffer	320 µL
T5 exonuclease	0.64 µL
Phusion polymerase	20 µL
Taq ligase	160 µL
Add up to 1200 µL with H_2O	

Gibson assembly was performed at 50 °C for 1 h. Afterwards, the reaction mixture was directly used for the transformation of *E. coli* competent cells or stored at -20 °C.

4.6.6 Generation of heat shock competent *E. coli* cells

To prepare heat shock competent *E. coli* (DH5α and NM522) cells, one single colony from a plate culture (pre-grown for 1 day) was incubated in 5 mL LB medium overnight (37 °C, 230 rpm). For *E. coli* NM522, carrying the pTC plasmid, 12.5 µg L^{-1} tetracycline was added to the medium. Then, 1 mL of the overnight cultured *E. coli* cells was inoculated in 100 mL LB medium in a 500 mL shake flask and incubated until an OD_{600} value of 0.25 – 0.3 was reached. Subsequently, the culture was chilled on ice for 15 min. Then cells were harvested by centrifugation (4000 *xg*, 10 min, 4 °C), using pre-cooled 50 mL falcon tubes. The cell pellet was resuspended in 40 mL pre-cooled 0.1 M $CaCl_2$ and kept on ice for 30 min. Then, cells were centrifuged and harvested again, and resuspended in 5 mL pre-cooled 0.1 M $CaCl_2$ solution containing 15% (v/v) glycerol. Finally, 200 µL aliquots of the cell suspension were dispensed into pre-cooled 1.5 mL tubes and stored at -80 °C.

4.6.7 Transformation of *E. coli* competent cells by heat shock

Heat shock was used for transformation of DNA into *E. coli* competent cells. Competent cells were first thawed on ice. Then, 100 – 500 ng plasmid DNA was added, and the mixture was incubated on ice for 30 min. Heat shock was performed at 45 °C for 45 sec in a water bath. Then, the cells were incubated on ice for 2 minutes. Subsequently, 900 µL BHI medium was added and cell regeneration was performed at 37 °C for 60 min in a thermomixer (Eppendorf, Hamburg, Germany) at 800 rpm. Afterwards, the cell pellet was harvested by centrifugation (5000 *xg*, 5 min, room temperature) and resuspended in 100 µL medium. The cells were then plated on BHI^{Kan} or $BHI^{Kan+Tet}$ agar for selection and incubated at 37 °C for 1 day. Obtained colonies were verified by PCR and, after plasmid isolation, by enzymatic digestion as described above.

4.6.8 Isolation of plasmid DNA

For isolation of plasmids from *E. coli*, the QIAprep Spin Miniprep Kit (Qiagen, Hilden, Germany) was used according to the manufacturer's instructions. *E. coli* strains carrying plasmids were inoculated in baffled shake flasks (BHI medium at 10% filling volume) and grown overnight (37 °C, 230 rpm), followed by plasmid isolation. Plasmid DNA obtained from *E. coli* DH5α was used for transformation of *E. coli* NM522 competent cells. Plasmid DNA obtained from *E. coli* NM522 was used for transformation of *C. glutamicum*

competent cells. In cases, the concentration of the obtained plasmid DNA was determined prior to further use as described above.

4.6.9 Generation of electro competent *C. glutamicum* cells

To prepare electro competent *C. glutamicum* cells, one single colony from a freshly prepared agar plate was incubated in 5 mL BHI^{++} medium and grown overnight (30 °C, 230 rpm). Then, the cells were harvested and used as inoculum for the main culture in 50 mL BHI^{++} medium at an initial OD_{660} of 0.3. When the OD_{660} reached values between 1.2 – 1.5, cells were harvested by centrifugation (6500 *xg*, 4 min, 4 °C) using pre-cooled 50 mL falcon tubes. The cell pellet was resuspended and washed twice with 10 mL pre-cooled 10% (v/v) glycerol. Subsequently, the cell pellet was resuspended in 4 mL 10 % (v/v) glycerol per gram cell wet weight, and 200 µL aliquots of the cell suspension were dispensed into pre-cooled 1.5 mL tubes. To maintain high transformation efficiency, electro competent *C. glutamicum* cells were always freshly prepared.

4.6.10 Transformation of *C. glutamicum* cells

Electroporation was used for the transformation of plasmid DNA into competent *C. glutamicum* cells. For this purpose, 200 µL cell suspension was mixed with plasmid DNA (5 µg for integrative plasmids, 0.5 µg for episomal plasmids) and transferred into an electroporation cuvette (Gene Pulser Cuvette, 0.2 cm, Bio-Rad, CA, USA). A mixture without DNA was used as negative control. Then, 400 µL 10% (v/v) glycerol was added on top, and the mixture was incubated on ice for 2 min. Subsequently, the cells were electroporated (3 kV, 25 µF, 400 Ω, GenePulser XCell, Bio-Rad, CA, USA). After the electroporation, 900 µL BHIS medium was added, and the mixture was quickly transferred into a 15 mL falcon tube that contained 4 mL BHIS, pre-heated to 46 °C. The mixture was then exposed to heat shock at 46 °C for 6 min, and then further incubated at 30 °C for 2 – 2.5 h for cell regeneration. Finally, cells were harvested by centrifugation (6500 *xg*, 4 min; Temperature), and resuspended in 100 µL medium. The cells were then plated on $BHIS^{Kan}$ agar and inoculated at 30 °C for 2 days. The obtained colonies were verified by PCR. Positive clones that contained the desired genomic modification were taken further to the second recombination.

4.6.11 Second recombination of *C. glutamicum*

To obtain marker-free *C. glutamicum* mutants, a second recombination event was required to remove the vector backbone that had been introduced during the electroporation. Single positive colonies, obtained from first recombination, were grown in 10 mL BHI medium with kanamycin at 30 °C overnight. Then, cells were plated on CM^{Sac} agar and inoculated at 30 °C for 2 days. The protein levansucrase encoded *sacB* from *Bacillus subtilis*, is lethal for *C. glutamicum*. So that cells that had lost the vector backbone containing *sacB* should be able to grow on the sucrose containing CM^{Sac} medium. Single colonies that had grown on CM^{Sac} agar were picked by a toothpick and patched on CM^{Sac} and BHI^{Kan} raster plates. These plates were incubated at 30 °C for 1 day. Colonies that were able to grow on CM^{Sac} agar but not on BHI^{Kan} agar were randomly picked for PCR verification. If successful, further validation was conducted by sequencing (GENEWIZ Germany GmbH, Leipzig, Germany).

4.6.12 Codon optimization

To optimize heterologous gene expression at the translational level, codon optimization was conducted to adapt the codon usage of introduced genes to that of *C. glutamicum*. Codon optimization and gene synthesis was performed by Biocat GmbH (Heidelberg, Germany) or GenScript Biotech (Rijswijk, Netherlands), using the company's bioinformatics algorithms, and sequences are shown in the appendix 7.2.

4.7 Cultivation

4.7.1 Shake flask cultivation in minimal medium

To characterize *C. glutamicum* strains on single substrates, cultivation was conducted in minimal medium in baffled shake flasks with 10% filling volume on a rotary shaker (shaking diameter 5 cm, Infors, Bottmingen, Switzerland) at 30 °C and 230 rpm. Cells from a glycerol stock were spread on BHI agar and incubated for 2 days at 30 °C. In a first step, *C. glutamicum* was inoculated from the plate culture into a liquid pre-culture (BHI medium) and grown overnight. Cells were harvested by centrifugation (8000 *xg*, room temperature, 5 min), resuspended in minimal medium, used to inoculate the second pre-culture in minimal medium, and incubated again until the exponential growth phase reached. Subsequently, cells were harvested (8000 *xg*, room temperature, 5 min) and used to inoculate the main culture in the same minimal medium in triplicate. The initial optical density of the second pre-culture and the main culture was adjusted to 0.2

and 0.5, respectively. If appropriate, kanamycin (50 µg mL-1) or spectinomycin (50 µg mL-1) was added as selection marker before inoculation, while IPTG (1 mM) was added as inducer during the cultivation.

4.7.2 Shake flask cultivation in SSL medium

Cultivation was conducted in baffled shake flasks with 10% filling volume on a rotary shaker at 30 °C and 230 rpm. As described above, *C. glutamicum* cells were grown in complex BHI medium as first pre-culture and then shifted to SSL medium for the second pre-culture and the subsequent main culture. The initial optical density of second pre-culture and main culture were set to 1 - 3 and 1 - 3 depending on the characterized strain, respectively.

4.7.3 Fed-batch fermentations in stirred tank bioreactors

For glutarate production from SSL, the performance of *C. glutamicum* strains was assessed in a fed-batch process using 1 L bioreactors (SR0700ODLS, DASGIP AG, Jülich, Germany), respectively. The first pre-culture was grown for 12 h at 30 °C in 1 L baffled flasks, filled with 100 mL BHI medium. Cells were harvested (8000 x*g*, room temperature, 5 min), resuspended in SSL medium, inoculated into a second pre-culture in SSL medium and incubated again until the exponential growth phase was reached. Subsequently, cells were harvested (8000 x*g*, room temperature, 5 min), and resuspended in 5 mL of batch medium and then used as inoculum for the process. The batch medium was SSL medium as described above, additionally supplemented with 5 g L^{-1} of yeast exact. The batch process was started with 300 mL of medium. During the process, the temperature was kept at 30 °C ± 0.1 (CWD4 bioblock, DASGIP AG, Jülich, Germany). For pH online monitoring, a pH electrode (Mettler Toledo 405-DPAS-SC-K8S/225, Mettler Toledo, Giessen, Germany) was used. The pH was uncontrolled in the initial phase to simulate the conditions in shake flasks, and later kept constant at 7.0 ± 0.1 or 6.5 ± 0.1 as described below by automated addition of 6 M NaOH (MP8 pump system, Eppendorf, Hamburg, Germany). The dissolved oxygen level (pO2) was monitored using a pO2 electrode (VisiFerm DO 225; Hamilton, Höchst, Germany) and maintained above 30% of saturation by adjusting the stirrer speed, the aeration rate, and the oxygen fraction of the gas inflow. The composition of the exhaust gas (CO_2 and O_2) was measured online (GA4, DASGIP AG, Jülich, Germany). The initial stirrer speed was set to 800 rpm, and the aeration rate was set to 18 sL h^{-1}. Pure SSL UF was used as feed. It was added pulse-wise when the sugars in the reactor were nearly depleted. The

volume of the added feed was adjusted to the liquid volume in the reactor at the time point of addition. As example, a level of 10% SSL-UF by a feed pulse, the added volume matched 11.1% (v/v) of the liquid volume in the reactor. To reach a level of 20% SSL-UF by a feed-pulse, the pulse matched 25% (v/v) of the liquid volume. Data acquisition and process control were conducted by DASGIP control software (DASGIP AG, Jülich, Germany).

4.8 Analytical methods

4.8.1 Quantification of cell concentration

For determination of the cell optical density, 0.5 - 1 mL sample was collected under sterile condition and transferred into a 1.5 mL tube. The optical density was determined spectrophotometrically at 660 nm (VWR, Hannover, Germany) using water as reference. If necessary, samples were diluted to OD_{660} values below 0.3. The dilution factor was monitored on an analytical balance. Dilutions and measurements were performed in duplicate.

For gravimetrical determination, a 15 mL falcon tube was first dried at 80 °C until constant weight (48 h). Then, the tube was cooled down in a desiccator for 30 min, and its weight was determined on a balance. Then, 10 – 15 mL culture sample was collected under sterile conditions and transferred into the pre-dried 15 mL falcon tube. The exact sample amount was determined on a balance. Subsequently, cells were harvested by centrifugation (9800 x*g*, 4 °C, 10 min) and washed three times with water. Finally, the cell pellet was dried at 80 °C until constant weight (72 h) and weighed again. The corresponding correlation between CDW and optical density was determined with three biological replicates, and a linear correlation factor was obtained. A correlation between cell dry weight and optical density CDW [g L^{-1}] = 0.32 x OD_{660} was obtained.

4.8.2 Quantification of sugars

Glucose, mannose, xylose, L-arabinose, galactose, L-rhamnose and fructose were quantified by HPLC (Agilent 1260 Infinity Series, Agilent Technologies, Darmstadt, Germany). Single sugars were analyzed on an Agilent Metacarb 87C column (85 °C, 300 x 7.8 mm, Agilent Technologies, CA, USA), using water as the mobile phase at a flow rate of 0.5 mL min^{-1}. Complex sugar mixtures were separated on an VA 300/7.8 NUCLEOGEL® Sugar Pb column (MACHEREY-NAGEL, Düren, Germany). The separation was carried out at 80 °C using water as the mobile phase at a flow rate of 0.4

mL min^{-1}. In both cases, refraction index measurement was used for detection, and external standards were used for quantification. If appropriate, samples were diluted prior to analysis.

4.8.3 GC-MS analysis of sugars

To further identify sugars in biological samples, gas chromatography–mass spectrometry (GC-MS) (GC 7890b, 5977A mass selective detector, Agilent Technologies) was used. In short, 10 µL sample was dried under a nitrogen stream for 30 min. Then, 50 µL 2 % methoxylamine in pyridine was added to the sample, and the mixture was kept for 25 min at 80 °C. Afterwards, 50 µL *N*, *O*-bis(trimethylsilyl)trifluoroacetamide (BSTFA) or *N*-methyl-*N*-(trimethylsilyl)trifluoroacetamide (MSTFA) was added. The mixture was kept for 30 min at 80 °C, yielding the oxime trimethylsilyl derivatives of the sugars. The supernatant was then used for GC-MS analysis. GC-MS analysis was conducted as previously described using a HP-5 column (Kiefer et al., 2002). Mannitol was added as internal standard, and the samples were analyzed in the scan mode. Gas chromatography was used for detection of the total ion chromatogram and external standards were used for identification of relevant sugars.

4.8.4 Quantification of organic acids and inhibitors

Organic acids, including lactate, formate, acetate and levulinic acid were quantified by HPLC (Agilent 1260 Infinity Series, Agilent Technologies, Darmstadt, Germany). Separation was carried out on an Aminex HPX-87H column (300 × 7.8 mm, Bio-Rad, CA, USA) with a guard cartridge holder (30 x 4.6 mm cartridge, Bio-Rad, CA, USA) at 45 °C with 12 mM H_2SO_4 as mobile phase and a flow rate of 0.5 mL min^{-1}. Refraction index was used for detection and external standards were used for quantification. If appropriate, samples were diluted prior to analysis.

Furfural, 5-hydroxymethylfurfuryl (5-HMF), and their derivatives, were quantified by HPLC (Agilent 1260 Infinity Series, Agilent Technologies, Darmstadt, Germany) (Heer and Sauer, 2008). Separation was carried out on Aminex HPX-87H column (300 × 7.8 mm, Bio-Rad, CA, USA) with a guard cartridge holder (30 x 4.6 mm cartridge, Bio-Rad, CA, USA) at 20 °C with 12 mM H_2SO_4 as mobile phase and a flow rate of 0.6 mL min^{-1}. Diode-array detection of UV absorption at 210 nm, 250 nm and 280 nm were applied and external standards were used for quantification. Furfuryl alcohol and 5-(hydroxymethyl)furfuryl alcohol was measured and analyzed at 210 nm; 2-furoic acid and

5-hydroxymethyl-2-furancarboxylic acid was measured and analyzed at 250 nm; furfuryl and 5-hydroxymethylfurfuryl was measured and analyzed at 280 nm. If appropriate, samples were diluted prior to analysis.

4.8.5 Quantification of glutarate

Glutarate was quantified by HPLC (Agilent 1260 Infinity Series, Agilent Technologies, Darmstadt, Germany) (Rohles et al., 2018). Separation was carried out on an Aminex HPX-87H column (300 × 7.8 mm, Bio-Rad, CA, USA) at 60 °C with 3.5 mM H_2SO_4 as mobile phase and a flow rate of 0.8 mL min^{-1}. Refraction index was used for detection and external standards were used for quantification. If appropriate, samples were diluted prior to analysis.

4.8.6 Quantification of amino acids

Amino acids, including 5-aminovaleric acid and L-lysine, respectively, were quantified by HPLC (Agilent 1260 Infinity Series, Agilent Technologies, Darmstadt, Germany) (Rohles et al., 2016). The culture supernatant was diluted 1:10 with α-amino butyric acid (222 µM) as internal standard and used for analysis. Separation was carried out on a reversed phase column (Gemini, 5 µm, C18, 110A, 150 x 4.6 mm, Phenomenex, Aschaffenburg, Germany). Pre-column derivatization with *o*-phthalaldehyde (OPA) was conducted automatically, then separation was performed with gradient of eluent A (40 mM NaH_2PO_4, pH 7.8) and eluent B (45% (v/v) methanol, 45% (v/v) acetonitrile, 10% (v/v) water) at 40 °C with a flow rate of 1 mL min^{-1}. Detection was performed by fluorescence measurement (340 nm excitation, 540 nm emission, fluorescence detector G1312A, Agilent Technologies) and internal standard of α-amino butyric acid was used for quantification.

4.8.7 Quantification of pediocin PA-1 activity

The biological activity of pediocin PA-1 was determined using a growth inhibition assay as previously described (Christmann et al., 2023; Goldbeck et al., 2021; Holo et al., 1991). The sensor strains *Listeria. innocua pIMK2* and *L. innocua pNZ44* were first inoculated overnight using BHI medium in glass tubes with 20% filling volume on a rotary shaker at 37 °C and 230 rpm. The samples, culture supernatant from pediocin producer, were stepwise diluted with BHI medium in a 96-well microtiter plate, yielding a twofold dilution

series (final volume of 100 µL for each dilution). Then, the *L. innocua* culture was diluted 1:25-fold (adding 2 mL *L. innocua* strain culture into 48 mL BHI medium*)* in fresh BHI medium, obtaining the indictor strain solution which was further mixed 1:1 (100 µL indictor strain solution with 100 µL diluted sample, reaching final volume of 200 µL for each well) with each diluted sample. Subsequently, the filled microtiter plate was incubated at 37 °C, 230 rpm for 6 h. The cell concentration in each well was quantified at 595 nm by a plate reader (Labsystems iEMS Reader MF, Thermo Fisher, Waltham, MA, USA). Finally, the pediocin PA-1 activity was calculated from the growth inhibition data (Holo et al., 1991), using software-based parameter fitting with the sigmoidal dose response tool (Origin 2021, Northampton, UK). In this study, the activity is given as bacteriocin units per mL (BU mL^{-1}) (Christmann et al., 2023). The cultivation of the pediocin producer and the quantification of pediocin PA-1 activity was conducted by Jens Christmann (Saarland University).

4.9 Separation and purification of mannose

4.9.1 Separation sugar from SSL using preparative flash chromatography

To separate sugar fraction from SSL or fermentation broth, preparative flash chromatography was applied using a Reveleris® PREP Purification System from BÜCHI Labortechnik GmbH (Essen, Germany). This system is equipped with a fraction collector for 20 mL tubes. A plunger glass column (49 x 400 mm) with a thermostatic jacket was utilized for chromatographic purification by packing the column with different ion exchange resins. Gel-type, monodisperse, strongly acidic cation exchange resins (SAC) from Lanxess (Lewatit MDS 1268 K 350, Lewatit MDS 1268 Ca 290, and H^+ resin) were used as specified below. There resins are based on a styrene-divinylbenzene copolymer with sulfonic acid as functional groups and these groups serve as binding sites for the respective cation, which interacts with the hydroxyl groups of different analytes depending on their steric orientation. HPLC grade water was used as eluent at a flow rate of 7 mL min^{-1} and column temperature was maintained at 60 °C or 85 °C as specified below. The chromatograms were recorded with an ELSD and a UV detector at the three detectable absorption maxima of sugars, SSL-UF and inhibitors (200, 263 and 280 nm). The collected fraction volume was set to 7 mL. For pure SSL-UF, samples were directly injected into the system. For fermentation broth, the broth was collected by centrifugation (8000 x*g*, 4 °C, 10 min) after fermentation process finished, centrifugation was conducted by three times to remove all cells and supernatant was collected, then the supernatant was used and injected into the system. For regeneration or reload of a resin, an

appropriate amount of salt solution with the respective ion was applied to the packed column followed by washing with water. The collected fractions from flash chromatography were lastly analyzed and quantified using different HPLCs as described above. The flash chromatography analysis was conducted by Melanie Fox from MyBiotech GmbH (Überherrn, Germany).

4.9.2 Purification and crystallization of mannose

The obtained fractions in 20 mL tubes from flash chromatography that contain mannose were collected and mixed together into a bottle and used for crystallization. The mannose solution (100 mL) was first treated with 12% (w/v) activated carbon and stirred at 500 rpm for 1 h at room temperature to remove the color in solution. The activated carbon was later removed by filtration (Whatman filter paper, Grade 3, Sigma-Aldrich). Then, the color removed solution was evaporated in a rotational vacuum concentrator (RVC 233 CDplus, Christ, Osterode am Harz, Germany) at 20 mbar, 40 °C, 200 rpm until the water was nearly depleted (about 96 h), and the mannose concentrate was obtained. Subsequently, adding 100 mL of ethanol (≥ 95%) to the concentrate to re-dissolve mannose in ethanol. If required, adding reasonable water into the ethanol solution to increase the solubility of mannose. Afterwards, a small portion of mannose (less than 1% (w/w) contained in solution) was added as seeding crystal. Ethanol was evaporated by stirring (500 rpm, room temperature) under a laboratory fume hood until it was nearly depleted (about 12 h) and the crude mannose crystals were obtained. Finally, the crude crystals were freeze at -80 °C and then lyophilized (Alpha 3-4 LSCbasic, Christ, Osterode am Harz, Germany) for generating white crystalline powder. Jens Christmann (Saarland University) contributed to the purification of mannose.

5 Results and Discussion

5.1 System metabolic engineering of *C. glutamicum* for the consumption of seven biomass sugars

5.1.1 The wild type exhibits high robustness during growth on spent sulfite liquor-based medium

Spent sulfite liquor (SSL) is a high-volume industrial waste stream. It contains massive amounts of fermentable sugars (over 1 million tons per year) but is majorly simply burned for energy generation, thereby wasting valuable carbon source (Lawford and Rousseau, 1993; Sjöström, 1993). It appears thus crucial to develop new strategies processes to better valorize this stream. Towards this goal, ultrafiltrated SSL (SSL-UF), provided from Borregaard, was first analyzed for its composition (Table 5-1).

Table 5-1: Chemical composition of spent sulfite liquor ultrafiltration permeate (SSL-UF). The pH value of the liquid raw material was 4.5. n=3.

Compound	Concentration [mM]	Concentration [g L^{-1}]
Glucose	218.7 ± 6.0	39.4 ± 1.1
Mannose	566.9 ± 17.2	102.1 ± 3.1
Galactose	133.5 ± 1.4	24.1 ± 0.3
L-Rhamnose	13.3 ± 0.6	2.2 ± 0.1
Xylose	339.3 ± 0.5	50.8 ± 0.1
L-Arabinose	94.9 ± 8.8	15.1 ± 1.3
Furfural	3.0 ± 0.5	0.3 ± 0.0
5-HMF	1.4 ± 0.0	0.2 ± 0.0
Acetic acid	118.1 ± 0.1	7.1 ± 0.0
Formic acid	11.7 ± 0.0	0.5 ± 0.0
Levulinic acid	12.8 ± 0.0	1.5 ± 0.0
SO_3^{2-}	174.9 ± 12.7	14.0 ± 1.0
SO_4^{2-}	18.1 ± 0.5	1.7 ± 0.0

As shown, liquid raw material was acidic and contained six different sugars plus several inhibitors. Mannose constituted about 45% of the total sugar, because the stream

originated from softwood (Spruce), known to be rich in this sugar (Lawford and Rousseau, 1993; Sjöström, 1993). Xylose and glucose made up another 40%, while galactose, L-arabinose, and L-rhamnose were present at lower levels and constituted the remaining fraction. Regarding inhibitors, sulfite was found to be present. Acidic acid was the main short-chain organic acid, whereas levulinic acid and formic acid were present in small amount. In addition, the SSL-UF contained minor level of furans, including furfural and 5-HMF.

C. glutamicum ATCC 13032 was capable to utilize glucose efficiently, while mannnose was known to be metabolized at least slowly. Furthermore, the microbe was known to be also tolerant to inhibitors, including furans (Tsuge et al., 2014), aromatics (Shen et al., 2005; Weiland et al., 2023; Weiland et al., 2022), and acetic acid (Kiefer et al., 2021; Wendisch et al., 2000). On the other hand, it lacked the abitity to utilize most the other sugars that were contained in the raw material (Baritugo et al., 2018). The extension of the substrate spectrum was therefore of great interest. First tests focused on the utilization of the two major sugars, mannose and xylose, since glucose utilization had been well studied before (Becker et al., 2011; Lindner et al., 2013; Xu et al., 2016). *C. glutamicum* ATCC 13032 was cultivated on mannose or xylose as sole carbon source, respectively. The strain metabolized mannose completely (Figure 5-1 a), however only after a long lag phase of 30 h and only at a low growth rate, far below that on glucose than that on glucose (Table 5-2) (Becker et al., 2011). Eventually, the onset of growth was linked to a spontaneous mutation that enhanced mannose metabolization, similar to recent observation for the growth of *C. glutamicum* on mannitol (Hoffmann et al., 2018; Hoffmann et al., 2021). Obviously, mannose was used only inefficiently. *C. glutamicum* ATCC13032 did not grow on xylose, as expected, because of the missing xylose isomerase (Figure 5-1 b) (Kawaguchi et al., 2006).

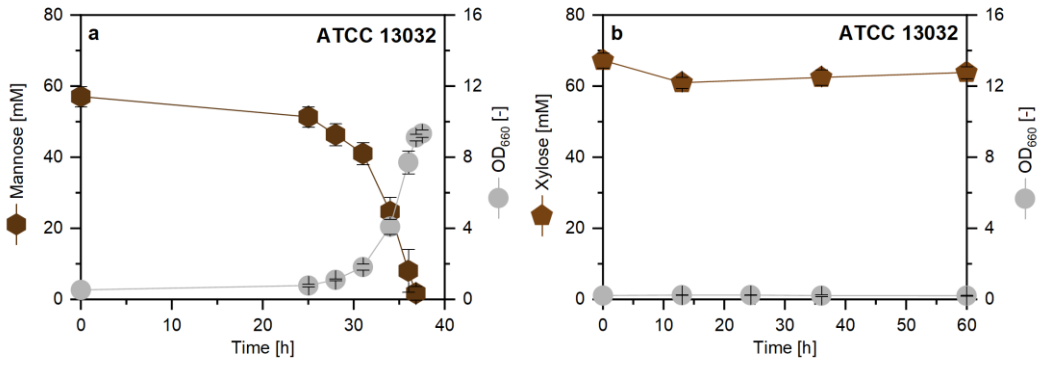

Figure 5-1: Cultivation *C. glutamicum* ATCC 13032 in shake flasks using minimal medium with either 10 g L^{-1} mannose (**a**) or 10 g L^{-1} xylose (**b**), respectively, as sole carbon source. The data comprise mean values and standard errors from three biological replicates.

The strain was then grown in a synthetic three-sugars mixture (Figure 5-2 a). It utilized glucose and mannose sequentially, whereas xylose remained untouched. The apparently diauxic growth potentially indicated underlying catabolite repression effects or simply resulted from the poor mannose utilization capacity that was also obvious from the mannose-based culture (Figure 5-1 a). In any case, it appeared necessary to improve the mannose utilization of *C. glutamicum*.

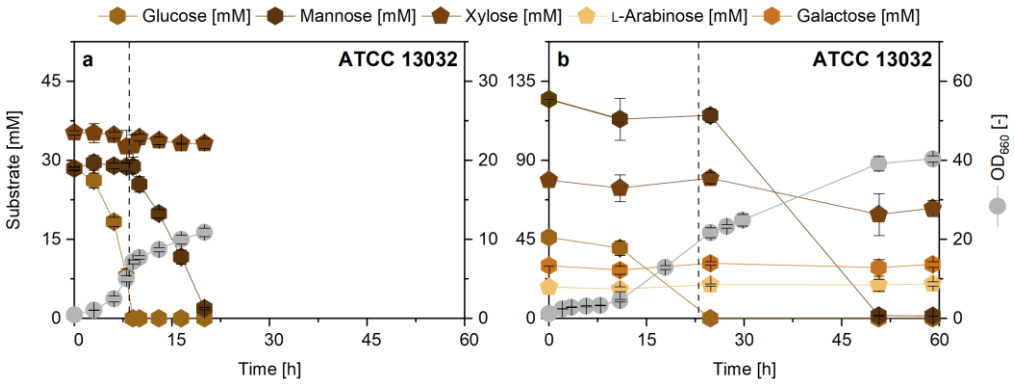

Figure 5-2: Growth characteristics *C. glutamicum* ATCC 13032 in shake flasks using minimal medium containing 5 g L^{-1} of glucose, 5 g L^{-1} of mannose and 5 g L^{-1} of xylose (initial pH 7.0) (**a**) and SSL-based medium containing 20% (v/v) SSL-UF (initial pH 6.1) (**b**). L-Rhamnose was not shown due to its low level. The vertical dashed line indicates the time point of glucose depletion. The data comprise mean values and standard errors from three biological replicates.

Next, we assessed the growth performance on SSL-based medium. For this purpose, the minimal medium, containing mineral salts, vitamins, and chelating agents, was mixed with SSL-UF at a ratio of 4:1, resulting in a fraction of 20% (v/v) of the waste material as sole source of carbon. Surprisingly, the wild type could grow on this waste-based medium (Figure 5-2 b). Hereby, it revealed a lag phase of 8 h, indicating certain inhibitory effects. Afterwards, mannose (125 mM) and glucose (46 mM) were fully consumed within 50 h, while the other sugar concentrations remained constant. Overall, a high amount of cells could be generated. The final OD_{660} of 40 corresponded to a biomass concentration of 12.8 g L^{-1} (Rohles et al., 2016; Rohles et al., 2018).

The initial medium pH was slightly acidic (pH 6.1) due to the acid nature of the waste material and at the lower range tolerated by *C. glutamicum* (Christmann et al., 2023). However, the chosen medium and changes of its composition by the metabolism of the growing cells beneficially enabled a neutral pH range throughout the process.

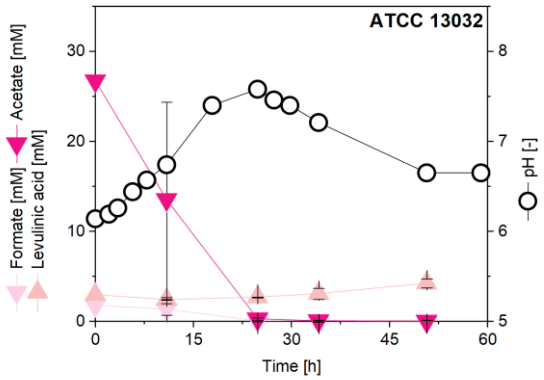

Figure 5-3: The pH change and metabolization of organic acids when cultivating *C. glutamicum* ATCC 13032 in shake flasks using SSL-based medium containing 20% (v/v) SSL-UF. The data comprise mean values and standard errors from three biological replicates.

The rapid hydrolysis of the chosen nitrogen source urea into NH_4^+, and the metabolization of acetate (27 mM) and formate (1.8 mM) beneficially increased the pH to 7.6 after 25 h (Figure 5-3) (Bull et al., 1964). Then, the pH slightly decreased to a well-tolerated pH of 6.6 after 50 h, likely caused by assimilation of the generated NH_4^+ (Wittmann et al., 1995). In addition, levulinic acid (3.0 mM) remained untouched.

The contained furans, 0.5 mM furfural and 0.1 mM 5-HMF, likely did not cause pronounced inhibition effects, as they were present significantly below levels previously found critical (Tsuge et al., 2014). Furthermore, *C. glutamicum* efficiently converted furfural into furfuryl alcohol and 2-furoic acid (appendix Figure 7-20), a well-known microbial detoxification mechanism (Tsuge et al., 2014). However, the high amount of sulfite seemed to pose a problem, although, together with sulfate, it displayed a useable sulfur source for *C. glutamicum* (Koch et al., 2005). Sulfite is toxic to cells and widely used for preservation of food (Silva and Lidon, 2016; Winkler et al., 2006). Here, sulfite was oxidized into sulfate at a high rate during the initial phase of the process (appendix Figure 7-20). The process was largely abiotic but was enhanced in the presence of cells. The oxidation likely resulted in limiting oxygen levels (Tsunogai, 1971). This might explain the initial lag phase of the aerobic bacterium, relying on efficient oxygen supply for growth. However, the presence of oxygen allowed to remove the toxic sulfite, providing a great advantage over anaerobic fermentations on sulfite-containing media, e. g. using yeasts (Dashko et al., 2014; Hahn-Hagerdal et al., 2007).

Taken together, *C. glutamicum* ATCC 13032, exhibited an in-built tolerance to grow on SSL-based medium, a promising trait to for valorization of the industrial waste stream.

However, only glucose was used efficiently out of six sugars, requiring metabolic engineering to extend the substrate spectrum and use all sugar-based carbon in SSL.

5.1.2 A first optimization round aims at plasmid-based expression of the catabolic pathways

The fastest and simplest way to achieve heterologous gene expression in *C. glutamicum* is the use of episomal plasmids (Christmann et al., 2023; Jungmann et al., 2022; Pauli et al., 2023). To this end, we used plasmid-based expression to improve the utilization of mannose and enable the utilization of xylose, the two major SSL-sugars. The episomal vector pVWEx1 *manA* contained the native gene *manA* (NCgl0716), encoding mannose 6-phosphate isomerase as the essential enzyme for efficient growth on mannose (Sasaki et al., 2011), under control of the IPTG-inducible *tac* promoter (Perez-Garcia et al., 2021). For xylose utilization, we applied the vector pEKEx3 $xylA_{Xc}$ $xylB_{Cg}$ (Meiswinkel et al., 2013a) that contained the genes *xylA* (XCC1758), encoding xylose isomerase from *X. campestris* pv. *campestris* ATCC 33913, and *xylB* (NCgl0111), encoding xylulokinase from *C. glutamicum,* both under control of *tac* promoter (Meiswinkel et al., 2013a). The two vectors were co-transformed into the wild type, resulting in strain *C. glutamicum* MSU-1.

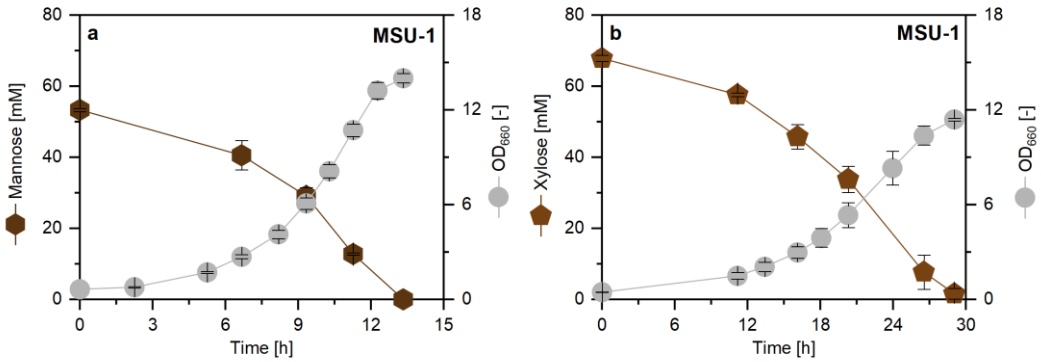

Figure 5-4: Cultivation of *C. glutamicum* MSU-1 in shake flasks using minimal medium with 10 g L^{-1} mannose (**a**) and 10 g L^{-1} xylose (**b**) as sole carbon source, respectively. The data comprise mean values and standard errors from three biological replicates.

Next, the novel mutant was cultivated on both sugars individually. The utilization of mannose was found significantly improved (Figure 5-4 a). Compared to the parent wild type, the strain MSU-1 grew without lag phase from early on and consumed the sugar within 13 h, amost two times faster. In addition, it achieved a higher specific growth rate and a higher biomass yield (Table 5-2). Xylose was used by the reombinant strain, as

expected (Figure 5-4 b). The co-expression of *xylA* and *xylB* enabled exponential growth on the pentose at a specific growth rate of 0.12 h^{-1} and a xylose uptake rate of 12.0 C-mmol g^{-1} h^{-1} (Table 5-2).

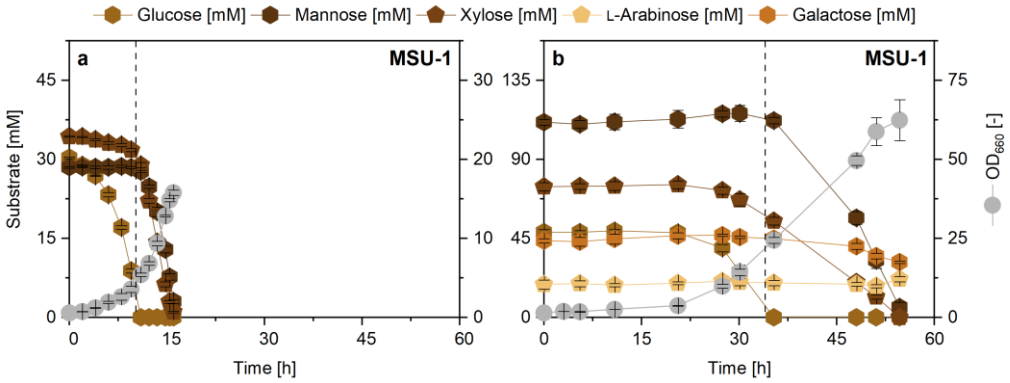

Figure 5-5: Growth characteristics of *C. glutamicum* MSU-1 on sugar mixture in shake flasks using minimal medium containing 5 g L^{-1} of glucose, 5 g L^{-1} of mannose and 5 g L^{-1} of xylose (**a**) and SSL-based medium containing 20% (v/v) SSL UF (**b**). L-Rhamnose was not shown due to its low level. The vertical dashed line indicates the time point of glucose depletion. The data comprise mean values and standard errors from three biological replicates.

When growing *C. glutamicum* MSU-1 on a synthetic mixture of glucose, mannose, and xylose all three sugars were consumed within 16 h (Figure 5-5 a). Glucose still appeared as the preferred substrate and was depleted over the first 10 h. During this phase, xylose was co-consumed to a weak extent, whereas mannose was not used. After glucose was used up, the cells increased the uptake of xylose, and started to co-consume mannose as a similar rate. Apparently, the catabolism of mannose and xylose was subjected to carbon catabolite repression by glucose. Despite the overexpression of *manA*, previously shown to enhance the growth of *C. glutamicum* on mannose (Sasaki et al., 2011), glucose and mannose were not simultaneously consumed. This might have been caused by the specificity of PTS_{Glc}, the major transporter for the two sugars, blocking mannose uptake in the presence of glucose (Sasaki et al., 2011), suggesting additional overexpression of PTS_{Fru} (Sasaki et al., 2011). Likewise, the slow xylose consumption in the presence of glucose pointed to limiting effects at the level of transport. Therefore, the introduction of a heterologous xylose importer seemed promising to enhance utilization of the pentose (Sasaki et al., 2009). Both targets were addressed at later stages (see below).

Subsequently, we benchmarked *C. glutamicum* MSU-1 on SSL medium, containing 20% of the black liquor as sole source of carbon and energy. Different to growth in minimal medium, the strain exhibited a pronounced lag-phase of more than one day (Figure 5-5

b). The three main sugars, mannose, xylose, and glucose were consumed within 55 h. Galactose, L-arabinose, and L-rhamnose remained untouched, as expected. Despite MSU-1 could utilize much more of the total sugar, contained in SSL than the wild type, its unfavorable growth delay displayed a severe bottleneck regarding growth in batch mode. The inhibition appeared also detrimental for later envisioned fed-batch processes, where pulses of SSL were supposed to be periodically added to the culture (Kohlstedt et al., 2018; Rohles et al., 2018). The harbored plasmid seemed a major reason for the observed growth inhibition. On top of the demanding industrial waste substrate, already posing a challenge to growth (Figure 5-2 b), the plasmid likely placed an additional burden on the cells (Karim et al., 2013; Wittmann et al., 2007). Moreover, plasmid-based strains are not always found stable under industrial conditions (Ensley, 1986), and the addition of selection markers increases production costs (Shaw et al., 2016). Therefore, it appeared crucial to create a stable genome-based chassis strain instead.

5.1.3 Genome-based overexpression of *manA* for enhanced mannose utilization

The first step towards a genome-based *C. glutamicum* that could co-use multiple substrates, aimed at genomic overexpression of the native *manA* gene in the wild type. For this purpose, the native promoter of the *manA* gene was replaced by the *tuf* (NCgl0480) promoter, successfully used to enable strong constitutive overexpression in the microbe (Becker et al., 2005a; Christmann et al., 2023; Jungmann et al., 2022; Rohles et al., 2016). The genetic construct for the modification comprised the 200 bp *tuf* promoter sequence, flanked by 500 bp-sized homology regions for recombination into the chromosome. Clones from the second recombination which carried the desired mutation were identified by 1257 bp fragment that resulted from PCR and could be well distinguished from the 1057 bp fragment PCR product, observed for wild type revertants. After confirming the correctness of the genetic modification by sequencing, a positive clone was was designated *C. glutamicum* MSU-2 (ATCC 13032 P_{tuf} *manA*) and studied further.

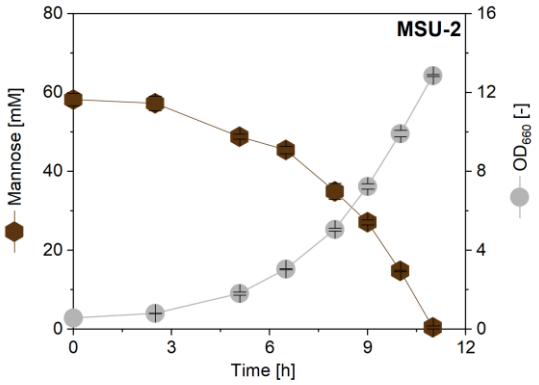

Figure 5-6: Cultivation *C. glutamicum* MSU-2 (ATCC 13032 P_{tuf} *manA*) on minimal medium with 10 g L^{-1} mannose. The data comprise mean values and standard errors from three biological replicates.

Favorably, strain MSU-2 was found much improved during grwoth on mannose as compared to its plasmid-based counterpart MSU-1 (Figure 5-6). It grew without lag phase and achieved 17% and 27% higher specific rates regarding growth and substrate uptake, respectively (Table 5-2). Interestingly, the mutant used mannose almost as efficient as it used glucose. So far, the use of mannose by *C. glutamicum* has been studied much less than that of other sugars, such as glucose, fructose, sucrose, and xylose (Baritugo et al., 2018; Buschke et al., 2013b; Choi et al., 2019; Leßmeier et al., 2015). Given the growth performance of MSU-2 on glucose and mannose, mannose, however, appeared as a suitable carbon source for *C. glutamicum*, suggesting to explore its metabolization further (Kiefer et al., 2004; Wittmann and Heinzle, 2001; Wittmann et al., 2004).

5.1.4 Genome-based implementation of xylose catabolism

Next, we focused on integrating the xylose utilization genes into the microbe. Naturally, *C. glutamicum* comprises two of the three steps for xylose utilization: uptake of the pentose into the cell, encoded by a so far unknown importer, and phosphorylation of the catabolic intermediate xylulose into xylulose 5-phoshate, encoded by *xylB* (Kawaguchi et al., 2006). Therefore, heterologous expression of xylulose isomerase, encoded by *xylA*, is sufficient to establish growth on xylose. We selected the $xylA_{Xc}$ gene from *X. campestris* pv. *campestris* ATCC 33913 (Meiswinkel et al., 2013a) for genomic integration upstream of the native *xylB* gene to create three different types of synthetic xylose operons. In all cases, the genetic constructed comprised (from 5' to 3') a 500 bp homology region, the constitutive *tuf* promoter or the inducible *tac* promotor, respectively, *xylA*, either with its native or an optimized codon usage, a 20 bp ribosomal binding site

(RBS) (Rohles et al., 2016) as intergenic region between *xylA* and *xylB*, and a second homology region. To tailor gene expression at the transcriptional and the translational level, three different genetic constructs were designed as follows: (i) P_{tuf} $xylA_{Xc,\ co}$ included the codon-optimized (co) version $xylA_{Xc,\ co}$ under control of the *tuf* promoter, (ii) P_{tuf} $xylA_{Xc}$ contained the native $xylA_{Xc}$ gene under control of the *tuf* promoter, and (iii) P_{tac} $xylA_{Xc}$ was based on the native $xylA_{Xc}$ under control of the IPTG-inducible *tac* promoter. Each construct was integrated into the genome of strain MSU-2. Positive clones from the second recombination that contained the integrated sequence were identified by PCR. The exhibited PCR product of 2648 bp for P_{tuf} $xylA_{Xc,\ co}$ and P_{tuf} $xylA_{Xc}$, 2591 bp for P_{tac} $xylA_{Xc}$, different to wild type reverants (1047 bp). After confirmation by sequencing, the novel mutants were designated MSU-3A (MSU-2 P_{tuf} $xylA_{Xc,\ co}$), MSU-3B (MSU-2 P_{tuf} $xylA_{Xc}$), and MSU-3C (MSU-2 P_{tac} $xylA_{Xc}$), respectively.

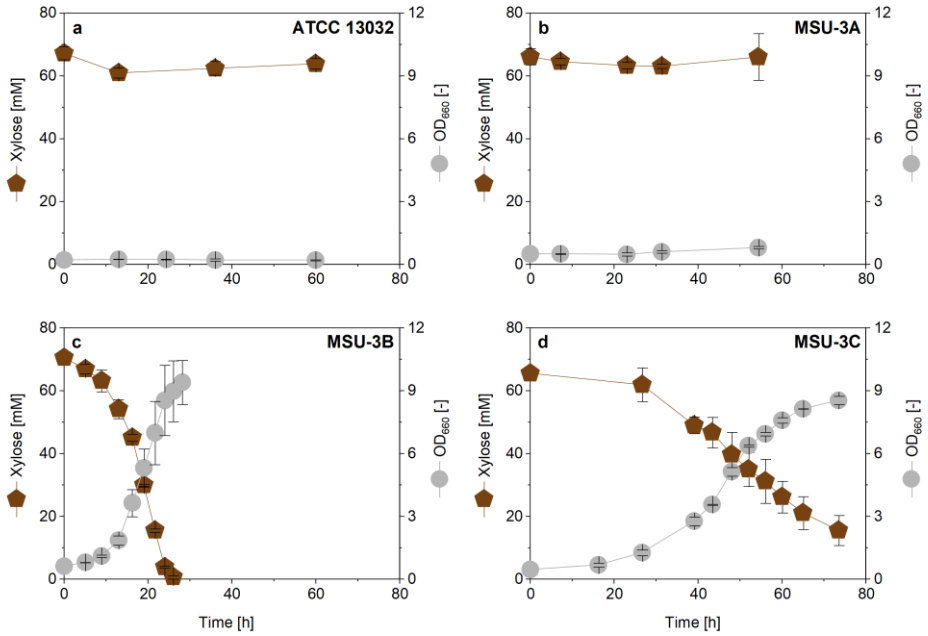

Figure 5-7: Cultivation of different *C. glutamicum* strains on minimal medium with 10 g L^{-1} xylose: wild type ATCC 13032 (**a**), MSU-3A (MSU-2 P_{tuf} $xylA_{Xc,\ co}$) (**b**), MSU-3B (MSU-2 P_{tuf} $xylA_{Xc}$) (**c**), and MSU-3C (MSU-2 P_{tac} $xylA_{Xc}$) (**d**). IPTG (1 mM) was added as inducer to the medium of MSU-3C. The wild type did not grow on the sugar, as expected (**a**). The data comprise mean values and standard errors from three biological replicates.

Both designs that were based on the native $xylA_{Xc}$ sequence, enabled xylose utilization. The best growth performance was observed for strain MSU-3B strain which expressed the $xylA_{Xc}$ *xylB* operon under control of the *tuf* promoter. The mutant used up the xylose within 30 h, whereas strain MSU-3C revealed incomplete xylose consumption of even after prolonged cultivation over 80 h. In terms of kinetics, the specific rates of growth and

substrate uptake were two- and three-fold higher, respectively, in strain MSU-3B (Table 5-2). Moreover, given the additional cost of using expensive inducer IPTG, the constitutive gene expression provides a cost-effective alternative (Hansen et al., 1998; Zhang et al., 2015). Beneficially, *C. glutamicum* MSU-3B grew significantly better than the plasmid-based strain MSU-1 (Table 5-2).

In contrast, *C. glutamicum* MSU-3A, carrying the codon-optimized version $xylA_{Xc,\ co}$, did not grow (Figure 5-7 b). Obviously, the codon optimization of *xylA* did not provide a functional XylA protein, as transcription under control of the *tuf* promoter and the ribosomal binding site, obviously worked, given the well-growing related mutant MSU-3B. Previously, the codon-optimized variants DavB and DavA from *P. putida*, revealed significantly reduced activity in *C. glutamicum* (Rohles et al., 2022), and using codon-optimized LysDH from *R. pomeroyi* caused detrimental effect on product formation (Pauli et al., 2023). Given the impact of codon usage on translation kinetics and co-translational protein folding (Liu, 2020), the codon-adapted genes might resulted in different secondary mRNA structures from native form which could have influenced expression (Wan et al., 2011), explaining the inferior phenotype.

At this stage, *C. glutamicum* MSU-3B was found efficient regarding growth on mannose and xylose. The performance on synthetic mixture and real SSL were both benchmarked at later stages (see below). As shown, the consideration of different genetic designs was crucial to bring up a well-working synthetic xylose operon. In the case of strain MSU-3B, the introduced single gene copy was obviously sufficient to provide sufficient catabolic pathway activity. In this regard, the outcome demonstrated the feasibility of basing the use of multiple substrates on a fully genome-based chassis strain, allowing to escape from detrimental metabolic burden and the use of expensive supplements.

Because strain MSU-3B performed well, we kept the design to metabolize xylose and focused the next strain engineering efforts on one of the remaining substrates to be tackled. However, one should notice different options that would be available for a further improvement of xylose utilization, e.g. in cases of raw materials such as hemicellulose-rich streams that contain elevated fractions of the pentose (Jagtap and Rao, 2018; Marques et al., 2009; Xavier et al., 2010). Such efforts could explore *xylA* genes from other donors such as *E. coli* (Buschke et al., 2013a; Gopinath et al., 2011; Kawaguchi et al., 2006) or enhanced use of the native myo-inositol/proton symporter IolT1 (Brusseler et al., 2018) and characterized heterologous transporters, such as the L-arabinose-specific transporter AraE (Chen et al., 2017; Sasaki et al., 2009), and xylose-specific transporter XylE (Yim et al., 2016). As example, deletion of the regulator *iolR* has been previously shown to contribute to fast growth of *C. glutamicum* on xylose upon

upregulation of IolT1 (Brusseler et al., 2018). On longer terms, further metabolic engineered efforts could aim at engineering the PP pathway (Jo et al., 2017; Zhou et al., 2012), although such modifications might interfere with the use of other sugars of relevance, requiring further rounds of fine-tuning.

5.1.5 Streamlining *C. glutamicum* to utilize L-arabinose

The pentose L-arabinose displayed another sugar of revelance. It was contained in SSL (Table 5-1) and known as generally abundant sugar in lignocellulosic biomass (Seiboth and Metz, 2011). The wild type could import L-arabinose by a so far unknown transporter (Kawaguchi et al., 2008) but lacked a catabolic pathway, explaining its inability to use the sugar as sole source of carbon (Figure 5-8 a). We decided to integrate the entire catabolic pathway plus a transporter into *C. glutamicum* (Kawaguchi et al., 2009). The envisioned operon comprised the genes *araB*, *araD*, and *araA*, encoding L-ribulokinase, L-ribulose 5-phosphate 4-epimerase, and L-arabinose isomerase, respectively, as well as *araE* encoding an L-arabinose transporter. The latter was selected because it offered additional xylose transport capacity, promising a beneficial co-benefit for both pentoses (Chen et al., 2017; Sasaki et al., 2009). The genetic constructs for genomic integration comprised the 200 bp *tuf* promotor sequence, followed by four structural genes in the order *araB*, *araD*, *araA* and *araE*, each separated by 20 bp ribosomal binding sites, and 500 bp flanking regions for homologous recombination. We decided to integrate the operon into the *iolR* locus, thereby eliminating the regulator for enhanced xylose uptake (Brusseler et al., 2018) and killing two birds with one stone.

Three different synthetic L-arabinose operons were designed. The first one contained a codon optimized version of the heterologous operon P_{tuf} $araBDAE_{Cg,\ co}$ from *C. glutamicum* ATCC 31831 (Accession number AB447371). A second design was based on heterologous L-arabinose operon from *E. coli* K12 MG1655 (*araB*, b0063; *araD*, b0061; *araA*, b0062; *araE*, b2841) in codon-optimized form (P_{tuf} $araBDAE_{Ec,\ co}$). Design number three comprised the heterologous operon from *C. glutamicum* ATCC 31831 with native codon usage (P_{tuf} $araBDAE_{Cg}$). Each of the three constructs was successfully integrated into the genome of *C. glutamicum* MSU-3B. After the second recombination, positive clones were identified by colony PCR. Integration of the synthetic gene cluster was inferred from the presence of 6706 bp PCR fragment for P_{tuf} $araBDAE_{Cg,\ co}$ and P_{tuf} $araBDAE_{Cg}$, 6619 bp fragment for P_{tuf} $araBDAE_{Ec,\ co}$, different from a 1572 bp fragment, expected for wild type. Correct clones were additionally validated by sequencing. The novel set of mutants was designated *C. glutamicum* MSU-4A (MSU-3B P_{tuf} $araBDAE_{Cg,}$

$_{co}$), MSU-4B (MSU-3B P_{tuf} *araBDAE*$_{Ec,\ co}$) and MSU-4C (MSU-3B P_{tuf} *araBDAE*$_{Cg}$), respectively.

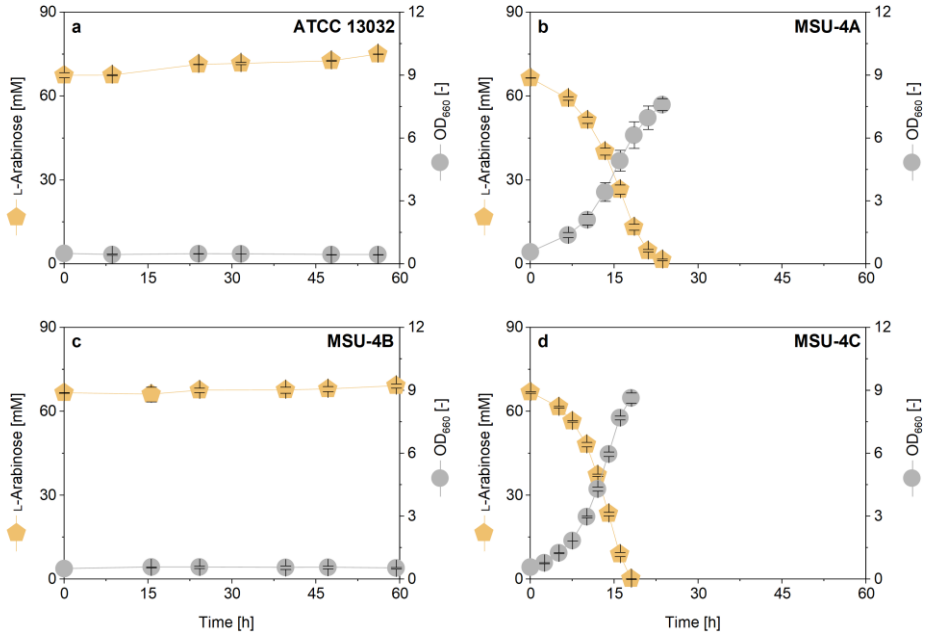

Figure 5-8: Cultivation of genome engineered *C. glutamicum* strains on minimal medium containing 10 g L^{-1} L-arabinose: wild type ATCC 13032 (**a**), MSU-4A (MSU-3B P_{tuf} *araBDAE*$_{Cg,\ co}$) (**b**), MSU-4B (MSU-3B P_{tuf} *araBDAE*$_{Ec,\ co}$) (**c**), and MSU-4C (MSU-3B P_{tuf} *araBDAE*$_{Cg}$) (**d**). The wild type did not grow as expected (**a**). The data comprise mean values and standard errors from three biological replicates.

Subsequently, the three mutants were cultivated on L-arabinose as sole carbon source. On a first glance, MSU-4A and MSU-4C completely consumed L-arabinose, whereas strain MSU-4B failed to grow or consume the sugar over a period of in 60 h (Figure 5-8 b, d). *C. glutamicum* MSU-4C exhibited the best performance (Figure 5-8 d, Table 5-2) in depleting L-arabinose within only 17 h. The mutant expressed the native gene cluster from *C. glutamicum* ATCC 31831. Obviously, codon-optimization of the L-arabinose gene cluster reduced but not increased expression strength, causing a similar detrimental effect as observed when engineereing xylose utlization (see above), providing another example that native genes can result in superior phenotypes, when expressed in their native codon use in *C. glutamicum* (Rohles et al., 2022). *C. glutamicum* MSU-4C exhibited remarkable growth and substrate uptake kinetics (Table 5-2). Obviously, the selected candidate genes for L-arabinose uptake and metabolism, as well as the chosen genetic design, created an efficient metabolic pathway for L-arabinose breakdown within the carbon core metabolism of *C. glutamicum*.

Additionally, we studied *C. glutamicum* MSU-4C on xylose (Figure 5-9). Different to expectations, strain MSU-4C exhibited almost no growth difference, when compared to the parent strain MSU-3B (Figure 5-7 c). Both strains exhibited the same specific growth rate of 0.13 h^{-1} and highly similar values for the specific xylose uptake rate (17.8 C-mmol g^{-1} h^{-1} versus 20.9 C-mmol g^{-1} h^{-1}) (Table 5-2). Obviously, the combined overexpression of *araE* and the deletion of *iolR* did not allow for improved use of the pentose, as expected based on previous findings (Brusseler et al., 2018; Chen et al., 2017; Sasaki et al., 2009). In fact, xylose metabolization seemed to operate at high capacity in the created strains.

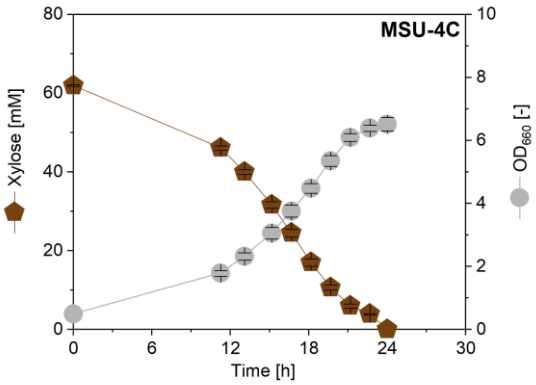

Figure 5-9: Cultivation of *C. glutamicum* MSU-4C on minimal medium with 10 g L^{-1} xylose. The data comprise mean values and standard errors from three biological replicates.

5.1.6 Enabling genome-based galactose catabolism in *C. glutamicum*

Galactose was the fourth sugar present in SSL (Table 5-1). In addition, the hexose is a prominent ingredient of dairy waste and lignocellulosic biomass (Marwaha and Kennedy, 1988; Perez et al., 2002). As expected, *C. glutamicum* ATCC 13032 could not utilize the sugar (Figure 5-10 a) due to the absence of a catabolic pathway. We decided to install the Leloir degradation route from *Lactococcus lactis* subsp. *cremoris* MG1363 (Accession number AJ011653) in the genome of *C. glutamicum* to enable galactose utilization. The operon to be expressed comprised five genes, i.e. *galP*, *galM*, *galK*, *galT* and *galE*, encoding galactose permease, aldose 1-epimerase, galactokinase, hexose 1-phosphate uridylyltransferase and UDP-glucose 4-epimerase, respectively (Grossiord et al., 2003).

Again, three different designs were realized. Two layouts followed the monocistronic design used before to install xylose and L-arabinose catabolism. In these cases, the constructs comprised two 500 bp homology regions that flanked the 200 bp *tuf* promotor

and the genes *galP*, *galM*, *galK*, *galT,* and *galE*, all separated by 20 bp ribsosomal binding sites. The first design was based on optimized codon usage (P_{tuf} *galPMKTE*$_{LI,\ co}$). The second design exhibited the native gene sequences of the donor strain (P_{tuf} *galPMKTE*$_{LI}$). The third design P_{tuf} *galPMKT*$_{LI}$ P_{galE} *galE*$_{LI}$ was bicistronic and differed in expression of *galE*. The gene was expressed under its native promotor, given the crucial role of the *galE* gene product for cell growth, related to the function of UDP-galactose for cell wall synthesis (Grossiord et al., 2003). Each cluster was synthetized and integrated into the genome of *C. glutamicum* strain MSU-4C. The *crtEb* (NCgl0594) locus, encoding lycopene elongase, was chosen for integration. Disruption of the locus upon integration facilitated the identification of correct clones by the pink color against normal yellowish colonies (Hoffmann et al., 2018). Positive clones from the second recombination were verified by formation of a 7352 bp fragment for P_{tuf} *galPMKTE*$_{LI,\ co}$ and P_{tuf} *galPMKTE*$_{LI,\ co}$, a 7448 bp fragment for P_{tuf} *galPMKT*$_{LI}$ P_{galE} *galE*$_{LI}$ during PCR analysis (wild type fragment 1864 bp). After additional confirmation by sequencing, the obtained mutants were designated *C. glutamicum* MSU-5A (MSU-4C P_{tuf} *galPMKTE*$_{LI,\ co}$), MSU-5B (MSU-4C P_{tuf} *galPMKTE*$_{LI}$), and MSU-5C (P_{tuf} *galPMKT*$_{LI}$ P_{galE} *galE*$_{LI}$), respectively.

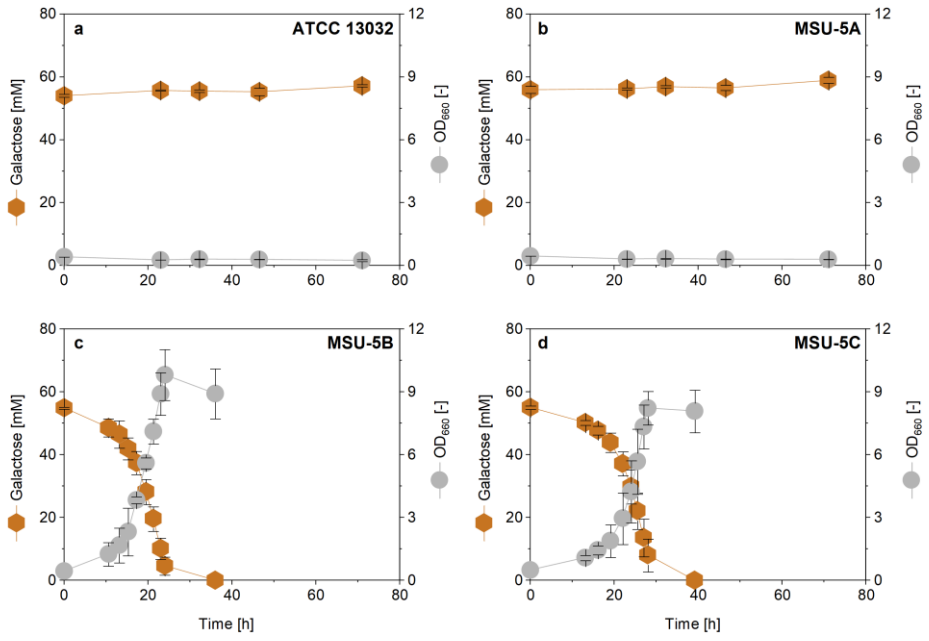

Figure 5-10: Cultivation of genome engineered *C. glutamicum* on minimal medium with 10 g L^{-1} galactose: wild type ATCC 13032 (**a**), MSU-5A (MSU-4C P_{tuf} *galPMKTE*$_{LI,\ co}$) (**b**), MSU-5B (MSU-4C P_{tuf} *galPMKTE*$_{LI}$) (**c**), and MSU-5C (MSU-4C P_{tuf} *galPMKTE*$_{LI}$ P_{galE} *galE*$_{LI}$) (**d**). The data comprise mean values and standard errors from three biological replicates.

The new fifth-generation strains were cultivated on galactose as sole carbon source. Hereby, MSU-5A carrying the codon-optimized genes was not able to metabolize

galactose over 70 h (Figure 5-10 b). However, integration of the operon with native codon usage enabled *C. glutamicum* to grow on galactose, allowing complete consumption in about 30 h (Figure 5-10 c, d). Surprisingly, codon optimized genes again did not allow functional expression in *C. glutamicum* whereas the native genes did. Notably, MSU-5B and MSU-5C performed equally well (Table 5-2), suggesting that the ribosomal binding site upstream of *galE* worked as well as the native P_{galE} promoter in enabling normal cell growth. Given its more compact design, we selected MSU-5B for further studies. Notably, galactose catabolism in *L. lactis* is subjected to catabolic repression, resulting in significant decrease of galactose uptake and galactokinase acitivity, when glucose or maltose are present (Grossiord et al., 2003). For *C. glutamicum*, poorly studied for its use of galactose, such effects are not known but might become relevant, when further streamlining *C. glutamicum* MSU-5B to grow on mixtures that contain elevated amounts of glucose and galactose. In additon, the implementation of lactose permease (LacY) and β-galactosidase (LacZ) (Barrett et al., 2004) would allow *C. glutamicum*, to directly utilize lactose, valorization of the significant streams of whey from dairy waste (Marwaha and Kennedy, 1988; Siso, 1996).

5.1.7 Fine-tuning the multi-substrate use in *C. glutamicum* at the level of the transcriptional regulator IolR

Previously, the deletion of *iolR*, the repressor of a gene cluster encoding enzymes for myo-inositol metabolism (Klaffl et al., 2013), released the repression of *iolT1*, encoding a glucose/myo-inositol permease and promoted xylose uptake in *C. glutamicum* (Brusseler et al., 2018). We therefore eliminated *iolR* from the genome of *C. glutamicum*. Different to expectations, this change did not influence the xylose uptake in the mutants of this study. On a first glance, there seemed no negative effects either but a previous transcriptome study suggested that IolR not exclusively controlled the myo-inositol catabolism of *C. glutamicum*, but that its deletion affected the expression of totally 22 genes and resulted in diverse phenotypic effects (Klaffl et al., 2013): i.e. faster growth on myo-inositol, slower growth on acetate and lactate, whereas the use of glucose appeared unchanged.

Therefore, we could not exclude additional side effects of the implemented IolR deficiency. To explore this issue further, we compared the growth of a strain that contained *iolR* (MSU-3B) and a related strain that lacked the regulator gene (MSU-4C). Because mannose was the major substrate in SSL and the metabolism of other prominent sugars such as xylose (Figure 5-9) and glucose was apparently not altered

(Klaffl et al., 2013), we studied both strains regarding growth on mannose (Figure 5-11 a, c).

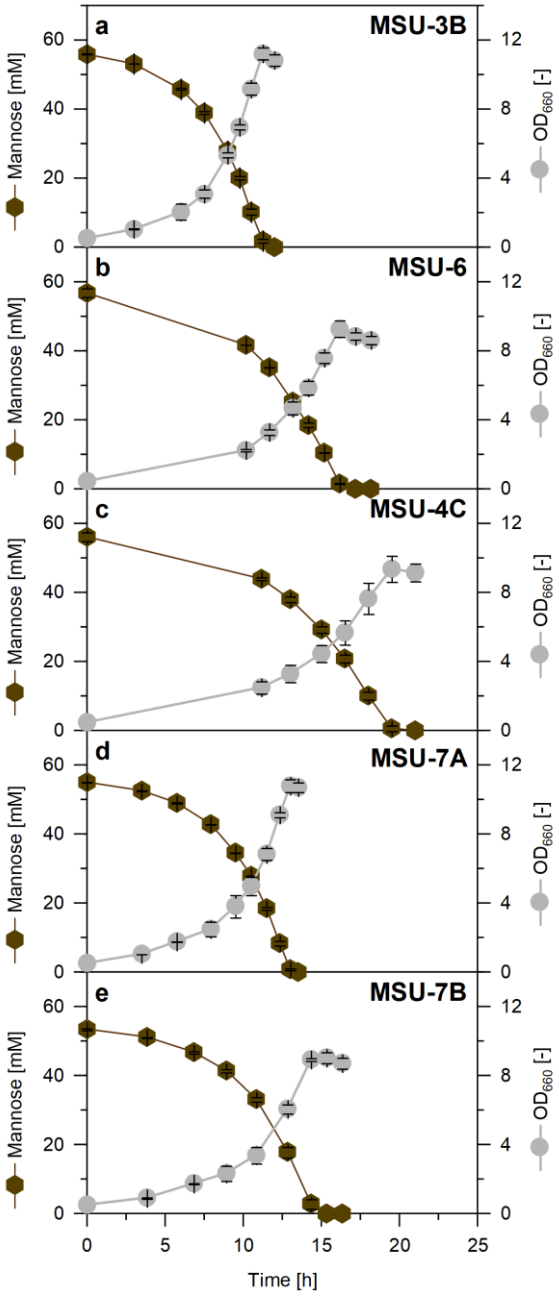

Figure 5-11: Cultivation of genome engineered *C. glutamicum* on minimal medium with 10 g L^{-1} of mannose. The strains comprise MSU-3B (**a**), MSU-6A (MSU-3B *ΔiolR*) (**b**), MSU-4C (**c**), MSU-7A (MSU-4C *iolR*) (**d**) and MSU-7B (MSU-5B *iolR*) (**e**). The data comprise mean values and standard errors from three biological replicates.

Strikingly, growth of MSU-4C on mannose was heavily impaired. The specific rates of growth (0.17 h^{-1}) and mannose consumption (19.9 C-mmol g^{-1} h^{-1}) were reduced by 51%

and 43%, compared to the values found for MSU-3B (Table 5-2). Admittedly, strain MSU-4C differed from MSU-3B not only in the absence of *iolR* but also contained the heterologous L-arabinose operon so that the exact reason for the observed impaired deficiency could not be given. To this end, we next specifically deleted *iolR* in MSU-3B. After PCR-based validation and sequencing, the desired mutant MSU-3B *ΔiolR* was designated MSU-6. Interestingly, growth of MSU-6 on mannose was remarkably impared too (Figure 5-11 b, Table 5-2), revealing that the negative growth phenotype was caused by the absence of IolR. This finding was very important towards an efficient multi-substrate using *C. glutamicum* cell factory, as it suggested to re-implement the repressor, different to the initially chosen strategy. Based on our data, we cannot suggest a specific molecular mechanism that would have caused the growth defects in the deletion strains. However, it appears interesting to study the underlying mechanisms further in the future. Obviously, IolR plays a broader role for the catabolism of carbon sources than imagined so far (Klaffl et al., 2013).

Subsequently, to further confirm the influence of the IolR repressor, we reconstituted the native *iolR* gene in its original locus in the genome of two engineered *C. glutamicum* strains. The genetic construct was composed of *iolR*, flanked by two 500 bp regions for homologous recombination. Positive clones that carried the recovered gene were verified by PCR analysis. They yielded a 1701 bp PCR fragment, different to wild type reverants (939 bp). After additional confirmation of the correct genetic change by sequencing, the obtained strains were designated *C. glutamicum* MSU-7A (MSU-4C *iolR*) and MSU-7B (MSU-5B *iolR*), respectively.

Beneficially, strain MSU-7A exhibited strongly improved growth on mannose (Figure 5-11 d), visualized by a markedly increased growth rate (0.27 h^{-1}) and specific mannose consumption rate (27.9 C-mmol g^{-1} h^{-1}), as compared to its parent strain MSU-4C (Table 5-2). Obviously, the recovery of *iolR* restored the growth deficiency on mannose. Improved growth kinetics also resulted for the mannose-grown strain MSU-7B (Table 5-2). Admittedly, despite the benefit from the presence of *iolR*, the cellular fitness of the engineered strains was not as high as that of the wild type. Obviously, the various inserted and expressed heterologous operons posed a certain metabolic burden. Similar side-effects from heterologous gene expression were observed before, particularly when expressing membrane-bound protein, eventually due to membrane disorders and interfere with metabolic pathways (Sasaki et al., 2008; Sasaki et al., 2009). Eventually, a further fine-tuning of the gene expression strength could help to alleviate such effects (Li et al., 2022).

5.1.8 Introducing L-rhamnose catabolism into *C. glutamicum*

Next, we aimed to further expand the substrate spectrum to L-rhamnose, an abundant deoxy sugar in the buckthorn plant *Rhamnus* and different microalgae (Brown, 1991; Jiang et al., 2021). The wild type *C. glutamicum* strain ATCC 13032 did not grow on L-rhamnose as sole carbon (Figure 5-12 a) due to the lack of a corresponding L-rhamnose catabolic pathway. To enable the utilization of the sugar, three different heterologous L-rhamnose operons were tested. All designs were monocistronic.

The first two set-ups were based on the five-step catabolic pathway from *E. coli* K12 MG1655 (Baldoma and Aguilar, 1988; Power, 1967), comprising the genes *rhaT* (b3907)*, rhaB* (b3904)*, rhaA* (b3903)*, rhaD* (b3902), and *rhaM* (b3901)*,* encoding an L-rhamnose-proton symporter, an L-rhamnulokinase, an L-rhamnose isomerase, an L-rhamnulose 1-phosphate aldolase, and an L-rhamnose mutarotase, respectively. The first *E. coli*-based design comprised the five codon-optimized genes under control of the *tuf* promoter (P_{tuf} *rhaTBADM*$_{Ec,\ co}$). The second design used the native genes instead (P_{tuf} *rhaTBADM*$_{Ec}$). The third design was based on the L-rhamnose operon from *Listeria monocytogenes* EGD-e (*rhaT*: lmo2850*, rhaB*: lmo2849*, rhaA*: lmo2848*, rhaD*: lmo2847, *rhaM*: lmo2846) and comprised the native gene sequences (P_{tuf} *rhaTBADM*$_{Lm}$) (Fieseler et al., 2012). In all cases, the genetic constructs for genomic modification of *C. glutamicum* comprised the P_{tuf} promoter and the genes *rhaT, rhaB, rhaA, rhaD,* and *rhaM*, seperated by 20 bp RBSs. The different L-rhamnose operons were integrated into the genome of the advanced strain MSU-7B*,* using *crtB* (NCgl2347) locus, encoding phytoene synthase (Heider et al., 2012), as integration site. Clones from the second recombination were evaluated by PCR for the presence of the desired L-rhamnose operons. Positive clones exhibited a PCR fragment of 6225 bp (P_{tuf} *rhaTBADM*$_{Ec,\ co}$ and P_{tuf} *rhaTBADM*$_{Ec}$) and 6441 bp (P_{tuf} *rhaTBADM*$_{Lm}$), respectively, all differing from wild type reverants (1879 bp). After additional confirmation by sequencing, correct clones were designated MSU-8A (MSU-7B P_{tuf} *rhaTBADM*$_{Ec,\ co}$), MSU-8B (MSU-7B P_{tuf} *rhaTBADM*$_{Ec}$) and MSU-8C (MSU-7B P_{tuf} *rhaTBADM*$_{Lm}$), respectively. Then, all new strains were evaluated for their ability to grow on L-rhamnose.

Strain MSU-8A, expressing the codon-optimized operon, was not able to consume L-rhamnose (Figure 5-12 b), while *C. glutamicum* MSU-8B (Figure 5-12 c) and MSU-8C (Figure 5-12 d) harboring the native operons, respectively, utilized this sugar. Hereby, MSU-8B almost fully depleted L-rhamnose within 200 h, whereas MSU-8C grew slower and only consumed 40% of the L-rhamnose during the same time. Notably, growth on L-rhamnose was slower than that on the other sugars, including mannose, xylose, L-arabinose, and galactose (Table 5-2). Interestingly, the entry point of L-rhamnose into

the central carbon metabolism differs from that of the other sugars. L-Rhamnose is converted into the three-carbon intermediates dihydroxyacetone phosphate, a triose phosphate of the EMP pathway (Rittmann et al., 2008), and lactaldehyde, a toxic intermediate of the methylglyoxal metabolic pathway which has to be further oxidized to lactate by an aldehyde dehydrogenase (Stansen et al., 2005), followed by reduction into pyruvate involving lactate dehydrogenase (Kato et al., 2010; Stansen et al., 2005). Notably, lactaldehyde dimerizes in aqueous solution to the corresponding 1, 4-dioxanes, eventually limiting further metabolization (Takahashi et al., 1983). Given the good growth of engineered *C. glutamicum* strains on glycerol which enters the EMP route at the level of dihydroxyacetone phosphate (Rittmann et al., 2008) and lactate (Stansen et al., 2005), the metabolization of lactaldehyde might display the major bottleneck that limits L-rhamnose utilization. It would be attractive to investigate and engineer the established catabolism on L-rhamnose further. In short, to our knowledge, this is the first study to establish L-rhamnose utilization in *C. glutamicum.*

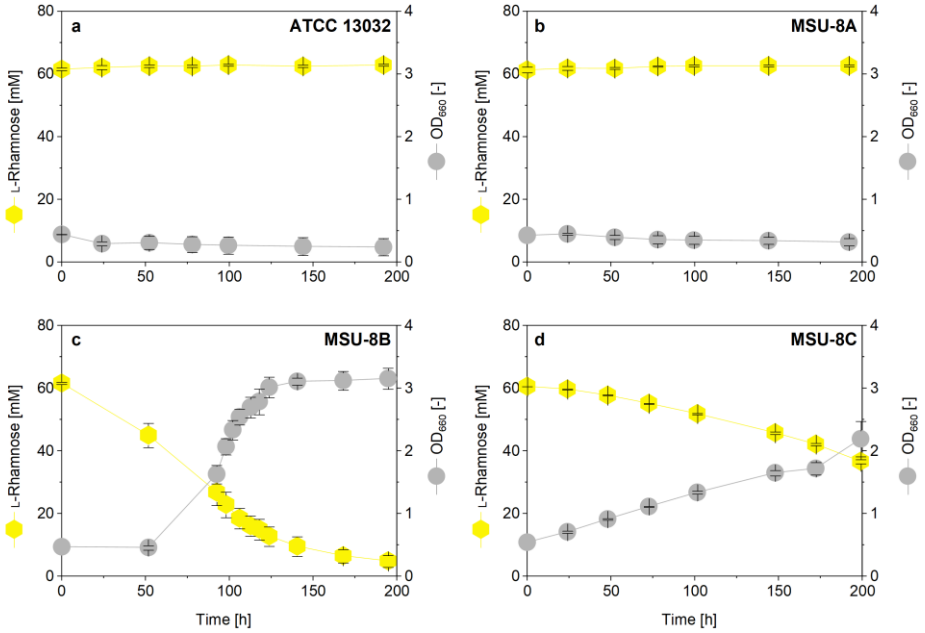

Figure 5-12: Cultivation of genome engineered *C. glutamicum* on minimal medium with 10 g L^{-1} of L-rhamnose. The strains are the wild type (a), MSU-8A (MSU-7B P_{tuf} *rhaTBADM*$_{Ec, co}$) (b), MSU-8B (MSU-7B P_{tuf} *rhaTBADM*$_{Ec}$) (c) and MSU-8C (MSU-7B P_{tuf} *rhaTBADM*$_{Lm}$) (**d**). The data comprise mean values and standard errors from three biological replicates.

Table 5-2: Growth kinetics and stoichiometry of different metabolically engineered *C. glutamicum* strains. All strains were cultivated in minimal medium with different substrate as sole carbon source. The data comprise the specific rates for growth (μ), substrate uptake (q_S), and the yield for biomass ($Y_{X/S}$). The data represent mean values and deviations from three biological replicates.

Substrate	**Strains**	**μ [h^{-1}]**	**q_S [C-mmol g^{-1} h^{-1}]**	**$Y_{X/S}$ [g C-mol^{-1}]**
Glucose	ATCC 13032	0.39 ± 0.00	28.8 ± 0.5	13.4 ± 0.3
Mannose	ATCC 13032	0.28 ± 0.01[a]	33.7 ± 0.9[a]	8.4 ± 0.2[a]
	MSU-1	0.30 ± 0.00	23.4 ± 0.5	13.0 ± 0.3
	MSU-2	0.35 ± 0.00	29.7 ± 0.5	11.7 ± 0.1
	MSU-3B	0.35 ± 0.00	34.7 ± 2.6	10.0 ± 0.2
	MSU-4C	0.17 ± 0.00	19.9 ± 2.0	8.4 ± 0.1
	MSU-6	0.24 ± 0.03	29.9 ± 1.7	8.1 ± 0.2
	MSU-7A	0.27 ± 0.04	27.9 ± 5.9	9.9 ± 0.1
	MSU-7B	0.25 ± 0.04	29.7 ± 5.6	8.6 ± 0.1
Xylose	ATCC 13032	n.g.	n.g.	n.g.
	MSU-1	0.12 ± 0.01	12.0 ± 0.6	10.2 ± 0.2
	MSU-3A	n.g.	n.g.	n.g.
	MSU-3B	0.13 ± 0.02	17.8 ± 4.5	7.3 ± 0.2
	MSU-3C	0.01 ± 0.0	5.8 ± 0.4	11.0 ± 0.4
	MSU-4C	0.13 ± 0.00	20.9 ± 1.6	6.1 ± 0.4
L-Arabinose	ATCC 13032	n.g.	n.g.	n.g.
	MSU-4A	0.14 ± 0.00	20.6 ± 1.4	6.7 ± 0.1
	MSU-4B	n.g.	n.g.	n.g.
	MSU-4C	0.17 ± 0.00	21.7 ± 0.5	7.9 ± 0.0
Galactose	ATCC 13032	n.g.	n.g.	n.g.
	MSU-5A	n.g.	n.g.	n.g.
	MSU-5B	0.17 ± 0.00	17.6 ± 2.8	9.9 ± 0.0
	MSU-5C	0.15 ± 0.01	18.0 ± 0.3	8.5 ± 0.0
L-Rhamnose	ATCC 13032	n.g.	n.g.	n.g.
	MSU-8A	n.g.	n.g.	n.g.
	MSU-8B	0.03 ± 0.01[a]	6.3 ± 0.5[a]	5.3 ± 1.2[a]
	MSU-8C	0.01 ± 0.00[a]	3.8 ± 0.4[a]	2.4 ± 0.2[a]

[a] the data were calculated during the exponential growth phase; n.g. no growth

5.1.9 Overexpression of the fructose permease PtsF for improved mannose co-utilization

The efficient co-utilization of different sugars was a desired feature of the constructed strains towards short fermentation times and fast biomass formation. While most other sugars such as xylose (Figure 5-5) and fructose (Dominguez et al., 1997) were co-utilized with glucose, mannose, however, remained untouched as long as glucose was present in the medium (Figure 5-2, 5-5). To overcome this limitation, we targeted the metabolism of fructose, structurally related to mannose. The utilization of fructose in *C. glutamicum* has been well elucidated (Kiefer et al., 2004). The uptake of the sugar is based on a fructose-specific PTS, involving the fructose-specific component PtsF. Interestingly, the transporter is also involved in the uptake of mannose by *C. glutamicum* (Sasaki et al., 2011), as, also fructose is partially assimilated by the microbe through the mannose-PTS (Kiefer et al., 2004). Here, we were interested to explore the impact of PtsF during growth of *C. glutamicum* on synthetic sugar mixtures that contained glucose, mannose, and fructose.

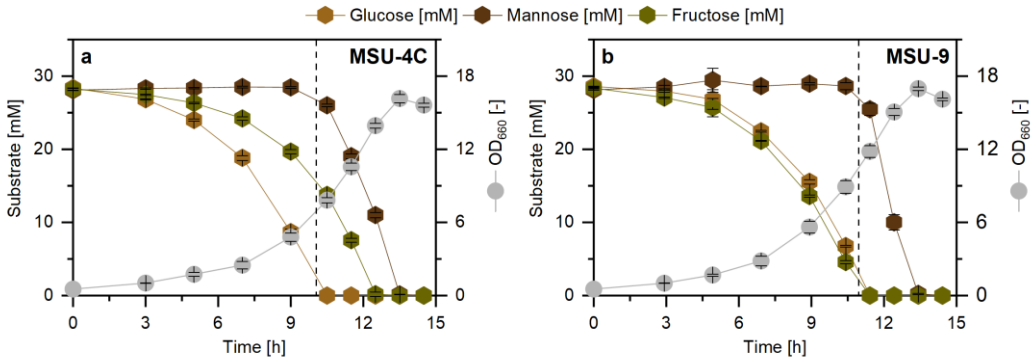

Figure 5-13: Growth characteristics of *C. glutamicum* MSU-4C (**a**) and MSU-9 (MSU-4C P_{tuf} *ptsF*) (**b**) on sugar mixtures. The cultures were grown in shake flasks using minimal medium with a mixture of 5 g L^{-1} of glucose, 5 g L^{-1} of mannose and 5 g L^{-1} of fructose. The vertical dashed line indicates the time point of glucose depletion. The data comprise mean values and standard errors from three biological replicates.

As a starting point, we tested the strain MSU-4C, which was engineered before for enhanced mannose utilization, by overexpression of the *manA* gene (see above). When grown on the three-sugars mixture (Figure 5-13 a), glucose and fructose were co-utilized during the initial phase. Thus, the utilization of fructose, involving PtsF, seemed not subjected to carbon catabolite repression by glucose (Dominguez et al., 1997). In contrast, mannose remained untouched as long as glucose was present. After glucose depletion, however, a simultaneous utilization of fructose and mannose could be observed. Assuming that PtsF was expressed from early on (to assimilate fructose), it

seemed that the system did not mediate mannose uptake during this phase. Previously, the expression of the genes *ptsF* and *manA* enabled co-utilization of glucose and mannose (Sasaki et al., 2011). Following this design, we overexpressed the *ptsF* gene in the strain MSU-4C by replacing its native promoter by the constitutive *tuf* promoter (Becker et al., 2005a; Christmann et al., 2023; Jungmann et al., 2022; Rohles et al., 2016). The genetic construct comprised a 200 bp-sized DNA fragment of the *tuf* promoter, flanked by 500 bp homologous recombination sites. Positive clones from the second recombination were verified by PCR, on basis of 1240 bp fragment which differed from that expected for wild type revertants (1040 bp). After confirmation by sequencing, the resulting strain was designated *C. glutamicum* MSU-9 (MSU-4C P_{tuf} *ptsF*).

Driven by the introduced *ptsF* overexpression, the sugar consumption pattern of the strain MSU-9 was altered (Figure 5-13 b). The utilization of fructose was found enhanced, resulting in simultaneous depletion of glucose and fructose. However, mannose was lastly consumed. Despite the overexpressed PtsF protein, mannose was not co-utilized with the other sugars. It seemed that PtsF exhibited a higher affinity to fructose than to mannose.

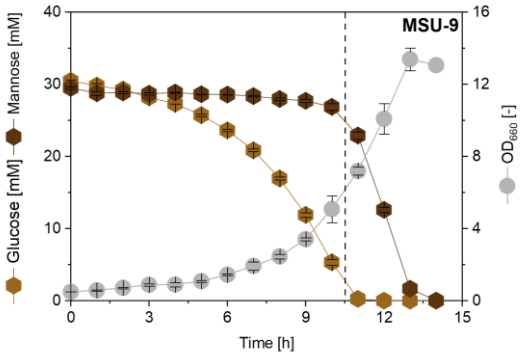

Figure 5-14: Growth characteristics of *C. glutamicum* MSU-9 on sugar mixtures. The cultures were grown in shake flasks using minimal medium with a mixture of 5 g L^{-1} of glucose and 5 g L^{-1} of mannose. The vertical dashed line indicates the time point of glucose depletion. The data comprise mean values and standard errors from three biological replicates. Jens Christmann (Saarland University) conducted this experiment.

Further on, when growing MUS-9 on a mixture containing glucose and mannose, no co-utilization was observed (Figure 5-14), different to previously reported (Sasaki et al., 2011). Given the essential role of expression level of *ptsF* for the simultaneous utilization of glucose and mannose (Sasaki et al., 2011), further fine-tuning of this gene seemed to be required. Alternatively, employing mannose-specific PTS from other donors, such as *E. coli* (Kornberg and Lambourne, 1992; Tchieu et al., 2001) and *B. subtilis* (Sun and

Altenbuchner, 2010), appears promising to reach the simultaneous utilization of glucose and mannose in *C. glutamicum*.

Taken together, we metabolically engineered *C. glutamicum* towards a broad substrate spectrum. Starting from the wild type, several rounds of optimization with carefully designed synthetic sugar modules, enabled the use of the seven major biomass sugars as sole carbon source by *C. glutamicum* strains, including the first-generation sugars glucose and fructose, and the second-generation sugars mannose, xylose, L-arabinose, galactose, and L-rhamnose.

5.2 Engineered *C. glutamicum* co-consumes the seven major biomass sugars

5.2.1 Co-utilization of the six sugars contained in the globally accumulating waste stream spent sulfite liquor

To assess the sugar utilization capacity of the metabolically engineered *C. glutamicum* MSU strains on sugar mixtures, we first tested combinations of different sugars that mimicked SSL as globally available waste stream for valorization (Table 5-1) (Marques et al., 2009; Sjöström, 1993). The mixtures comprised different combinations of glucose, mannose, xylose, L-arabinose, galactose and L-rhamnose. We evaluated the best member from each generation of the created strain genealogy: MSU-2, MSU-3B, MSU-4C, MSU-5B, MSU-7B, and MSU-8B, whereby each strain received the sugars that it could potentially use, based on the available catabolic pathways. Generally, each strain successfully consumed the expected sugar spectrum.

MSU-2 consumed glucose and mannose (Figure 5-15 a). MSU-3B utilized glucose, mannose, and xylose (Figure 5-15 b), while MSU-4B and MSU-5B and MSU-7B used up the added four and five sugars, respectively, as desired (Figure 5-15 c, d, e). The advanced strain MSU-8B depleted all six sugars within only 20 h, providing an important proof-of-value (Figure 5-15 f). It was interesting to note that the advanced strains exhibited true co-consumption of the usable sugars. Even mannose was found to be co-utilized with glucose, although at a slower rate, overcoming limitations faced by initial strains from the first generation. The more of the available sugar was used, the higher was the finally achieved cell concentration.

Considering the complexity of the network of catabolic pathways that was integrated into the microbe, it appeared impressive that all engineered strains exhibited efficient growth on the synthetic sugar mixture with high cellular fitness. The *C. glutamicum* strains

displayed promising chassis strains to be applied for the fermentative valorization of SSL. The MSU-8B strain appeared most attractive because it was able to co-utilize all sugars contained in the waste stream.

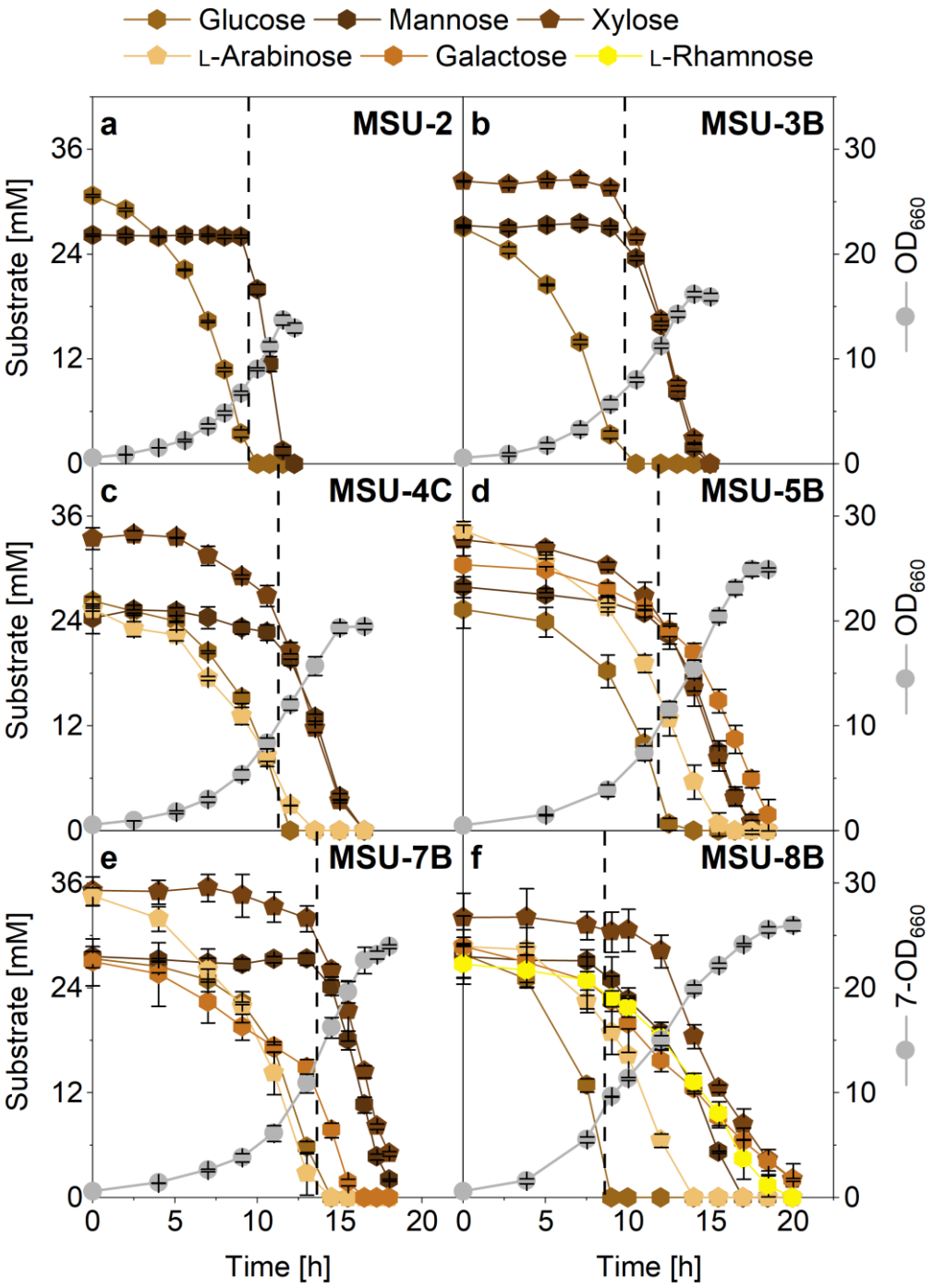

Figure 5-15: Evaluation of the substrate spectrum by the newly created family of genome-engineered *C. glutamicum* strains. The strains comprised MSU-2 (**a**), MSU-3B (**b**), MSU-4C (**c**), MSU-5B (**d**), MSU-7B (**e**), and MSU-8B (**f**). They were all cultivated in shake flasks on a minimal medium with a synthetic sugar mixture. The vertical dashed line indicates the time point of glucose depletion. The data comprise mean values and standard errors from three biological replicates.

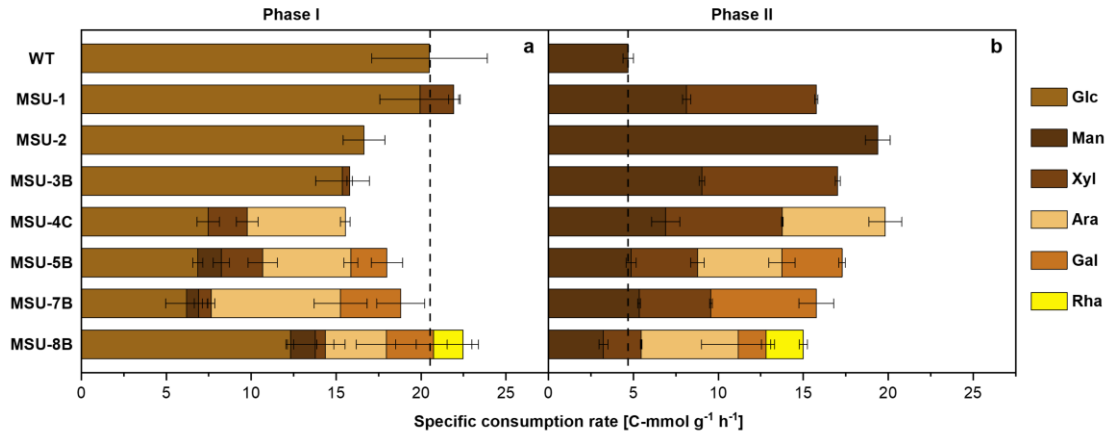

Figure 5-16: Specific sugar consumption rate of different *C. glutamicum* strains on sugar mixtures. The data were estimated from growth of the mutants on synthetic mixtures of sugars, each added in a concentration of 5 g L^{-1}. The sugar spectrum for each strain was adapted to the corresponding native and implemented catabolic pathway repertoire. The data reflect cultures of the wild type (WT) on glucose and mannose, strain MSU-1 (WT pVWEx1 *manA* pEKEx3 *xylA*$_{Xc}$ *xylB*$_{Cg}$) on glucose, xylose, and mannose, strain MSU-2 (WT *P*$_{tuf}$ *manA*) on glucose and mannose, strain MSU-3B (MSU-2 *P*$_{tuf}$ *xylA*$_{Xc}$) on glucose, mannose, and xylose, strain MSU-4C (MSU-3B *P*$_{tuf}$ *araBDAE*$_{Cg}$) on glucose, mannose, xylose, and L-arabinose, strain MSU-5B (MSU-4C *P*$_{tuf}$ *galPMKTE*$_{Ll}$) and MSU-7B (MSU-5B *iolR*) on glucose, mannose, xylose, L-arabinose and galactose, strain MSU-8B (MSU-7B *P*$_{tuf}$ *rhaTBADM*$_{Ec}$) on glucose, mannose, xylose, L-arabinose, galactose and L-rhamnose. The data refer to the culture phases, when glucose was still present (a) and after glucose had been depleted (b). The vertical dashed lines indicate the specific sugar consumption rate of wild type strain. The data comprise mean values and standard errors from three biological replicates.

It appeared interesting to quantify the efficiency of sugar co-consumption, and gain insights into the simultaneous utilization of multiple substrates, which was a highly desirable trait towards efficient processes. To do so on a quantitative basis, we first separated each cultivation into two phases. The first phase (glucose phase, Phase I) represented the period from the beginning of the cultivation until the last time point where glucose was still present in the medium. The second phase (non-glucose phase, Phase II) represented the period after glucose had been fully consumed until the end of the cultivation. We then calculated the specific consumption rates for each sugar during the two phases in three steps (appendix Figure 7-21).

Hereby, the volumetric consumption rate (Q_V) of each sugar was defined as consumed amount of sugar ($\triangle C$) divided by the cultivation time ($\triangle t$) (Eq. 1).

$$Q_V = \frac{\Delta C}{\Delta t} \qquad \text{(Eq. 1)}$$

Second, we estimated the mean biomass concentration (X_M) during the inspected cultivation phase by dividing the area under the biomass concentration curve by the cultivation time.

The two values then allowed to infer the specific consumption rates (Eq. 2).

$$Q_S = \frac{Q_V}{X_M} \qquad \text{(Eq. 2)}$$

As shown in Figure 5-16, the wild type exhibited a high specific glucose consumption rate during Phase I (20.5 C-mmol g^{-1} h^{-1}), while a low specific mannose consumption rate (4.7 C-mmol g^{-1} h^{-1}) was observed for Phase II, matching the poor performance to naturally use the latter sugar. The plasmid-based strain MSU-1 revealed active xylose co-consumption with glucose. When glucose was depleted, the use of xylose sigficantly enhanced. Mannose was only used during the non-glucose phase.

Different to MSU-1, MSU-2 and all further strains were fully genome-based, because of the undesired plasmid burden that was observed for MSU-1. Within the genealogy, MSU-2 was based on the wild type, and additionally engineered for enhanced mannose catabolism. The overexpression of the native *manA* gene boosted the mannose specific consumption rate almost four-fold, underlining the efficiency of this modification. Notably, the genome-based mutant MSU-3B achieved almost the same consumption rates than the plasmid-based counterpart MSU-1, underlining the power of single gene copies to drive heterologous sugar catabolism to high efficiency. The strain used xylose together with glucose, although at a slow rate during Phase I.

Beneficially, the more advanced strains, efficiently utilized other sugars together with glucose, enabling a true co-consumption. Partially, the other sugars even displayed the major fraction of carbon that was assimilated. Therefore, it seemed that the engineered, constitutively expressed catabolisc pathways for L-arabinose, galactose, and L-rhamnose were not subjected to strong carbon catabolite repression by glucose. Likewise, the advanced strains exhibited high total sugar consumption rates resulting from efficient simultaneous utilization of of all sugars. Probably due to the genomic modifications, each strain used the sugars in different ratios.

As another striking observation, strain MSU-5B, as well as strains MSU-7B and MSU-8B co-consumed glucose and mannose. Given the probable inhibition of mannose uptake via the glucose-specific permease PtsG in the present of glucose (Sasaki et al., 2011), it seemed likely that another mechanism enabled the use of mannose. One option was other tranporter which potentially mediated mannose uptake in strain MSU-5B. Galactose permease GalP emerged as possible candidate. In *E. coli* this transporter transports mannose at low affinity (Henderson et al., 1984), and this protein was expressed as part of the galactose pathway in MSU-5B. At this stage, we assume that GalP might funtion as importer for mannose in *C. glutamicum*, while the following phosphorylation of intracellular mannose into mannose 6-phosphate could be catalyzed

by an unknown kinase. It appears interesting to explore the underlying mechanism in more detail.

Impressively, the best cell factory MSU-8B simultaneously utlized all six sugars during in the first culture phase, and co-consumed the remaining five sugars after glucose depletion. This performance was an important step towards the use of biomass-based complex sugar mixtures. Overall, it was interesting to note that the strains exhibited relatively similar values for the total specific consumption rate, indicating a general maximum capacity of sugar uptake. It appears interesting to investigate the reason(s) for the observed upper limit of consumption, eventually allowing to evolve concepts that raise the uptake capacity. Promising options could aim to extend the capacity of other pathways within the central catabolism (Becker et al., 2005a; Becker et al., 2011; Buschke et al., 2013a) or the implementaton of high-flux product pathways that withdraw carbon out of the cell (Becker et al., 2011; Pauli et al., 2023; Rohles et al., 2022; Rohles et al., 2018). All strains tested here were wild-type based and could use all carbon only for growth, eventually providing an upper limit of growth capacity as observed for the wild type on defined media (Grunberger et al., 2013; Unthan et al., 2015).

5.2.2 Benchmarking *C. glutamicum* MSU-8B on a mixture with the seven major biomass sugars

To further evaluate the advanced strain MSU-8B, it was grown on a synthetic mixture of the seven major biomass sugars (Baldoma and Aguilar, 1988; Barrett et al., 2004; Becker et al., 2005a; Jagtap and Rao, 2018; Jiang et al., 2021; Kawaguchi et al., 2009; Kawaguchi et al., 2006; Perez et al., 2002; Pfeifer et al., 2017; Sasaki et al., 2011; Seiboth and Metz, 2011), the hexoses glucose, fructose, mannose, galactose, and L-rhamnose, plus the pentoses xylose and L-arabinose. Each sugar was added in equal amount (Figure 5-17). Notably, strain MSU-8B consumed all seven sugars within less than 30 h, glucose, fructose, and L-arabinose were depleted first, while mannose, xylose, galactose, and L-rhamnose were consumed later. The rapid use of e.g. glucose and fructose during the first culture phase resulted in efficient cell growth. The increased biomass strongly promoted the efficient consumption of the other sugars later, providing a substantial benefit to the created call factory. It was interesting to note that L-rhamnose was metabolized much faster as part of the substrate mixture as compared to its use as sole carbon source (Figure 5-12). Eventually, extra energy and redox power (Becker et al., 2005a; Wittmann et al., 2004), resulting from the metabolization of the other carbon sources provided a benefit to withstand and overcome the toxic side effects caused by lactaldehyde (Baldoma and Aguilar, 1988; Subedi et al., 2008). In this regard, the co-

presence of well-accepted substrate could provide a fitness benefit to the cells, as also observed for *C. glutamicum*, grown on aromatic and sugar mixtures (Becker et al., 2018a; Weiland et al., 2023). Another prominent feature of MSU-8B was the lack of any adaptation phases, when a certain sugar was used up. With the end of one of the substrates, the cells appeared fully unperturbed and simply accelerated the use of other substrates, given the genomically encoded constitutively expressed catabolic pathways.

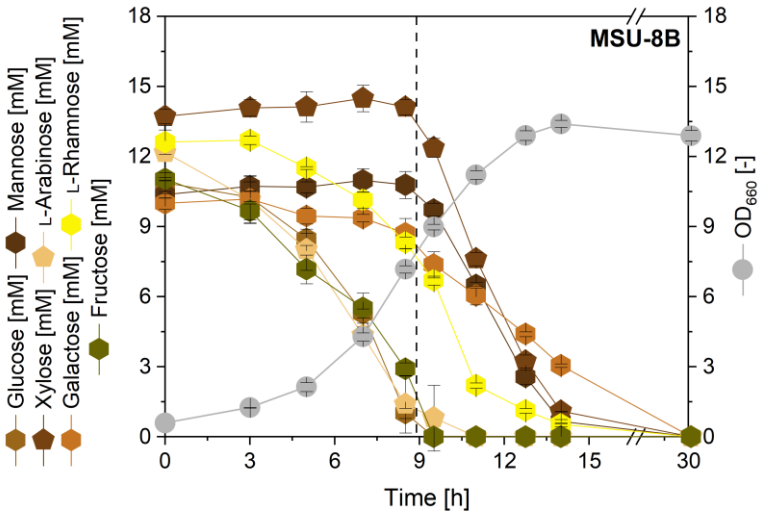

Figure 5-17: Growth of the advanced cell factory *C. glutamicum* MSU-8B on a mixture of seven sugars in shake flasks using minimal medium containing 2 g L^{-1} glucose, 2 g L^{-1} mannose, 2 g L^{-1} xylose, 2 g L^{-1} L-arabinose, 2 g L^{-1} galactose, 2 g L^{-1} L-rhamnose and 2 g L^{-1} fructose. The vertical dashed line indicates the time point of glucose depletion. The data comprise mean values and standard errors from three biological replicates.

Taken together, we tailored the wild type which efficiently consumed only the two first-generation sugars glucose and fructose into a highly flexible multi-substrate-using cell factory after eight rounds of systems metabolic engineering. As shown, the genome-based strain MSU-8B exhibited an expanded and streamlined substrate spectrum that allowed to co-consume glucose, fructose together with the second-generation sugars mannose, xylose, L-arabinose, galactose, and L-rhamnose.

Given its huge relevance and impact for applications in the bioeconomy, the extension of the substrate spectrum of *C. glutamicum* has been addressed in various previous studies strains (Baritugo et al., 2018; Buschke et al., 2013b; Choi et al., 2019). Most of these studies focused on implementing the heterologous use of one or two extra substrates, while to our knowledge, engineered strains have been reported to consume up to only three sugar monomers, i.e. glucose, xylose, and L-arabinose (Gopinath et al.,

2011; Lange et al., 2018; Sasaki et al., 2009). In this regard, our family of multi-substrate-using cell factories displays a milestone towards the valorization of biomass-based substrate mixtures. As shown, it was important to test different alternative modules to find the optimum genetic configuration for high-level expression of the catabolic pathways of interest (appendix Figure 7-22). The designed synthetic operons provided a perfect basis to utilize the second-generation sugar mixtures for future production processes. It appears straightforward to transfer them into previously developed producer strains, such as L-glutamate and L-lysine producers, majorly employing first-generation sugars in current industrial processes to date (Kimura, 2005; Leßmeier et al., 2015). The integration of the best performing synthetic sugar modules into the genome of such producers promises sustainable production from non-food second-generation sugars and feedstocks to be integrated into second-generation biorefineries (Baruah et al., 2018; Malherbe and Cloete, 2002; Sun et al., 2016). Vice versa, the developed chassis strains seem promising to be tailored for the synthesis of novel products, which could then directly be produced in a flexible way from various resources.

5.3 Towards industrial application: Valorization of spent sulfite liquor using the advanced *C. glutamicum* MSU strain family

5.3.1 Metabolically engineered *C. glutamicum* utilizes all sugar-based carbon in spent sulfite liquor

As described above, spent sulfite liquor (SSL) is a globally accumulating waste stream from industrial acid pulping. The liquor contains a wide range of sugars plus inhibitors such as small organic acids (Marques et al., 2009; Sjöström, 1993). As real case proof of value, we first tested our developed multi-substrate-using cell factories for growth on SSL, kindly provided by Borregaard which operates one of the world's largest and most advanced biorefineries, located in Sarpsborg, Norway. To this end, batch cultures on a mix of minerals, trace elements, thiamine and biotin, amended with 20% of SSL-UF were conducted for genome-based engineered strains from all steps of the development. At the start, the medium contained six different sugars at different levels: 113 mM mannose, 68 mM xylose, 44 mM glucose, 27 mM galactose, 19 mM L-arabinose, and 3 mM L-rhamnose. Favorably, all strains achieved the same substrate utilization performance, when grown in SSL-based medium as on the synthetic sugar mixtures.

The mannose-engineered strain MSU-2 consumed glucose and mannose, constituting approximately 60% of the total sugar (Figure 5-18 a). Strain MSU-3B, additionally engineered to utilize xylose, used this pentose as well, and consumed 83% of the SSL

sugars (Figure 5-18 b). The next-level mutant MSU-4B, capable to use also L-arabinose, used four of the six sugars (89% of total sugar) (Figure 5-18 c). Finally, MSU-5B and MSU-7B additionally degraded galactose (Figure 5-18 d, e), while the top strain MSU-8B depleted the entire sugar carbon, including glucose, mannose, xylose, L-arabinose, galactose, and L-rhamnose (Figure 5-18 f) (Figure 5-20 b).

GC-MS analysis of final broth at the end of the cultivation of *C. glutamicum* MSU-8B, confirmed the full consumption sugars (Figure 5-19), confirming the enormous sugar utilization capacity of the created strain. Surprisingly, all engineered strains grew well without significant lag phase, indicating high robustness. The cultivations were completed within 30-36 h, generating considerable amounts of biomass. The cell factories did not reveal any shift in growth phase to the wild type (Figure 5-2 b) and no growth delay, as observed before for the plasmid-based mutant MSU-1 (Figure 5-5 b). Poor utilization of mannose and xylose occurred as long as glucose was present due to carbon catabolite repression, similar to the synthetic sugar mixtures, while L-arabinose, galactose, and L-rhamnose were efficiently co-utilized with glucose. Due to its low abundance in SSL, glucose, was, however, quickly consumed within the first hours of the process, enabling an early on-set of full co-utilization of all available sugar in the medium. An interesting finding was the unexpected decrease of the galactose concentration when cultivating MSU-4C. This mutant didn't contain the heterologous galactose operon, that could have explained the decrease of the sugar level. Notably, the L-arabinose transporter AraE has been shown to transport galactose in some *E. coli* strains, although at lower affinity than the galactose specific permease GalP (Henderson et al., 1984; Weickert and Adhya, 1993). Eventually, the transporter AraE from *C. glutamicum* ATCC 31831, implemented in MSU-4C, might also have such functionality, allowing galactose transport into the cells. However, this hypothesis requires further testing, and it should be noted that, apparently, also strains MSU-2 and MSU-3B revealed low capacity to degrade galactose, which also awaits further clarification. At this point, it seems that the different sugar modules in *C. glutamicum* lead to metabolic crosstalk, due to a certain level of promiscuity. Such mechanisms exist in a range of microbes (Henderson et al., 1984; Morabbi Heravi and Altenbuchner, 2018; Rojas et al., 2021; Weickert and Adhya, 1993).

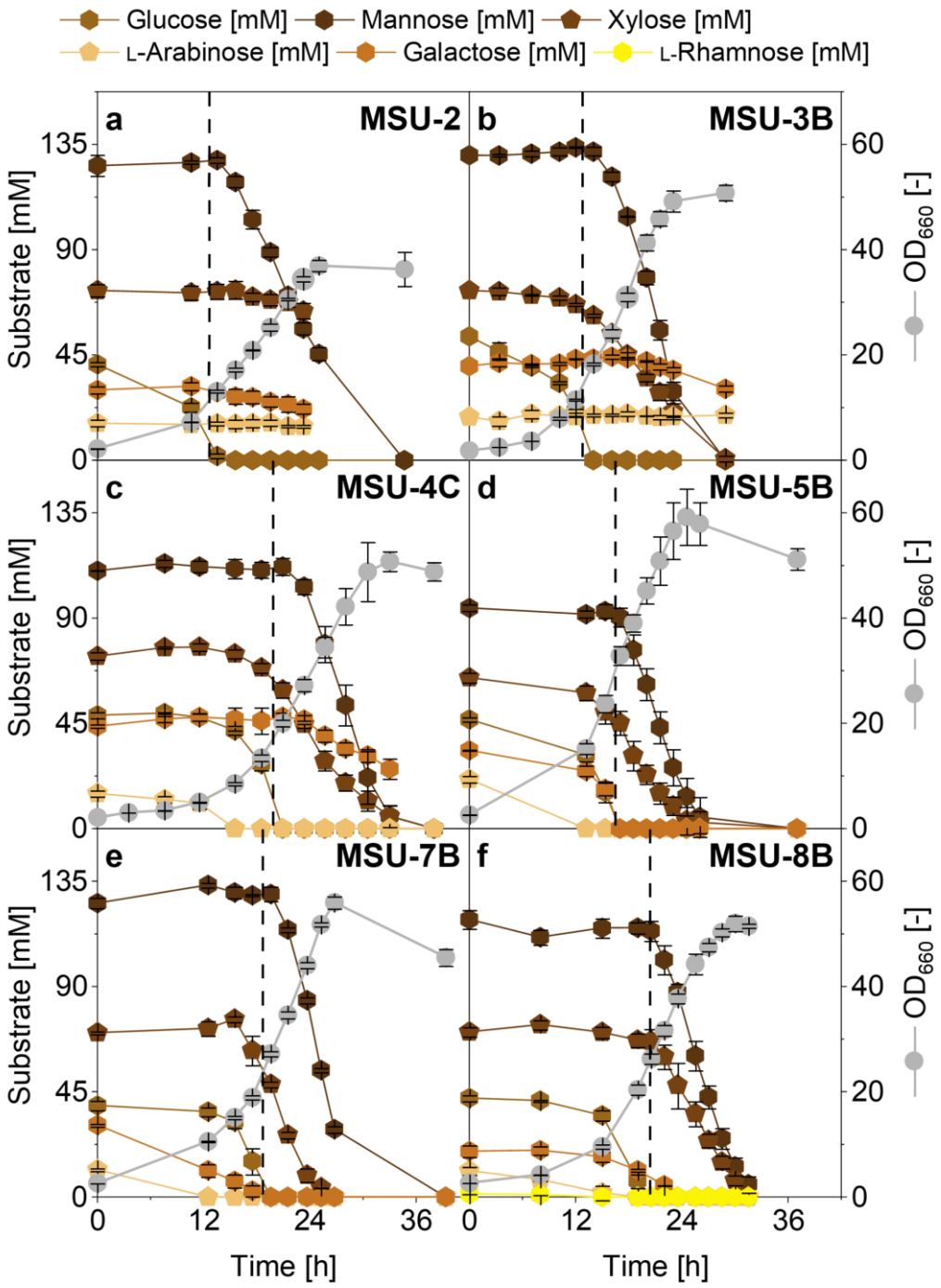

Figure 5-18: Benchmarking the created MSU strain family for growth on spent sulfite liquor medium. The medium contained mineral salts, trace elements, thiamin, biotin, and 20% (v/v) of SSL-UF (Borregaard, Sarpsborg, Norway). The tested genome engineered strains included *C. glutamicum* MSU-2 (**a**), MSU-3B (**b**), MSU-4C (**c**), MSU-5B (**d**), MSU-7B (**e**), and MSU-8B (**f**) in shake flasks using SSL-based medium. L-Rhamnose was present in all cultures at low abundance. Its concentration remained constant for all strain up MSU-7B but is not shown for simplicity. However, the L-rhamnose level is displayed for MSU-8B (**f**). The vertical dashed line indicates the time point of glucose depletion. The data comprise mean values and standard errors from three biological replicates.

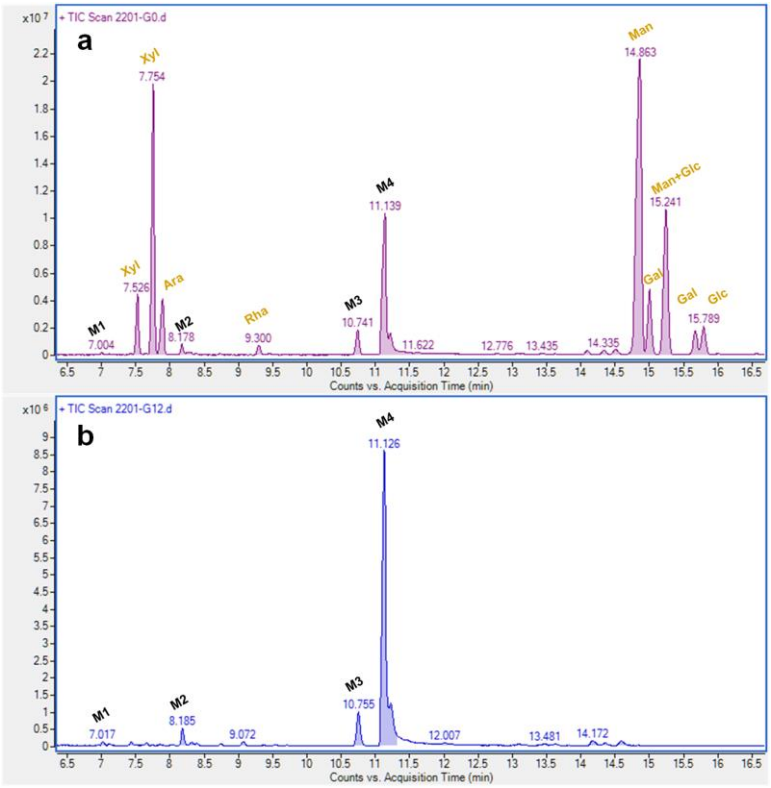

Figure 5-19: Evaluation of the sugar utilization capacity of *C. glutamicum* MSU-8B during growth on SSL-based mineral medium. The data represent the total ion chromatogram (TIC) from GC-MS analysis of samples from the start (**a**) and the end of the cultivation (**b**), shown in Figure 5-18 f. Prior to analysis the sugars were converted into the corresponding trimethylsilyl *O*-methyloximes using a two-step derivatization (Kiefer et al., 2002; Laine and Sweeley, 1971).

Beneficially, systems metabolic engineering substantially increased the overall volumetric consumption sugar rate, as well as the generated biomass (Figure 5-20 a). The metabolic pathway design strategy and the created strain family are summarized in Figure 5-21 and appendix Figure 7-22. The more sugar modules were implemented in a strain, the more sugar was co-consumed, which strongly accelerated overall growth. This engineered feature appeared important, as it promised to enable high volumetric productivities, i.e. space-time yields, when using the novel MSU strain family for SSL-based production purposes. The space time yield is one of the major performance indicators of industrial fermentations. The higher this value, the more product can be formed in a given process time, or the faster a certain target amount of product can be made (Becker et al., 2011; Hoffmann et al., 2021; Pauli et al., 2023; Rohles et al., 2022; Rohles et al., 2018). While this leads to improved performance already in shake flasks, a high space-time-yield beneficially scales in industrial settings. In an existing industrial plant that offers a fixed fermentation volume, an increased space-time-yield enables a higher annual output, as each fermentation cycle is shorter and more cycles can be

conducted over the year (Gasser and Mattanovich, 2007; Westman and Franzen, 2015). This pays off in growing markets which are open to receive additional product at reasonable price (Cooney, 1983; Straathof et al., 2002). On the other hand, when considering building a new plant for a certain annual output that has been projected from business and marketing evaluations, a higher space-time yield enables a smaller plant size and, therefore, lower investment costs (Cooney, 1983; Straathof et al., 2002; Van Dien, 2013).

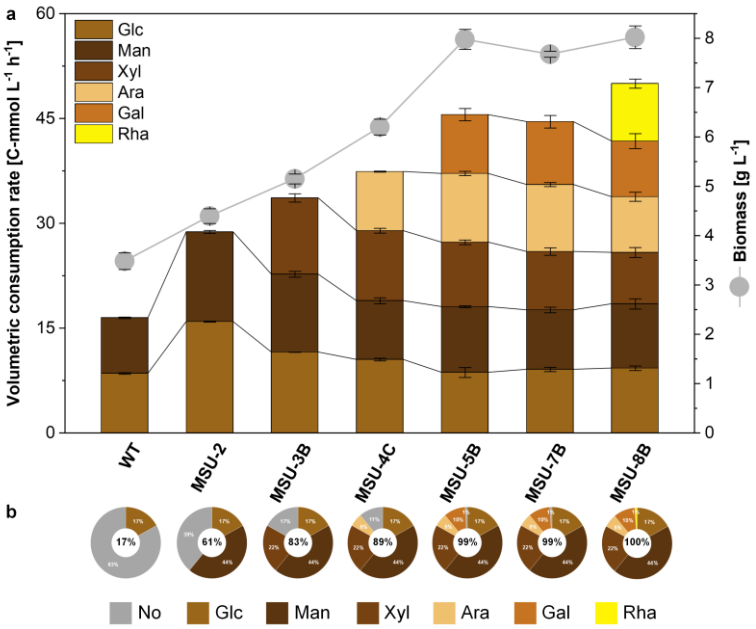

Figure 5-20: Sugar utilization efficiency the created of genome-based *C. glutamicum* MSU strains. In the text only SSL is stated. **a**: Overall volumetric sugar consumption rate and biomass titer on synthetic sugar mixtures. The volumetric consumption rate for each sugar was defined as the amount of consumed sugar divided by the cultivation time. **b**: Completeness of efficiently utilizing sugar-based carbon contained in SSL-UF. No: Not consumed, not efficiently consumed (mannose in the wild type); Glc: Glucose; Man: Mannose; Xyl: Xylose; Ara: L-Arabinose; Gal: Galactose; Rha: L-Rhamnose. The data represent the percentage of the indicated sugars concentration divided by the overall summed sugar concentration.

In addition, the complete use of sugar can be regarded a valuable trait also with regard to yield and titer, as indicated by the higher biomass levels, reached by strain MSU-8B. This feature is particularly attractive for the bulk market, where the raw material displays the major cost driver (Peters, 2007; Rødsrud et al., 2012). A “cleaned-up” broth, depleted from sugar at the end of the fermentation, from biomass after the initial filtration or centrifugation step, and from the target product at the end of the down-stream processing, will be less costly when entering the waste water treatment (Gray, 2004; Nielsen, 2017; Speece, 1983). Moreover, there is not any sugar left that could cause problems during

product purification (Belter et al., 1987; Kalyanpur, 2002; Zydney, 2016). All in all, the advanced chassis strain promised many important benefits.

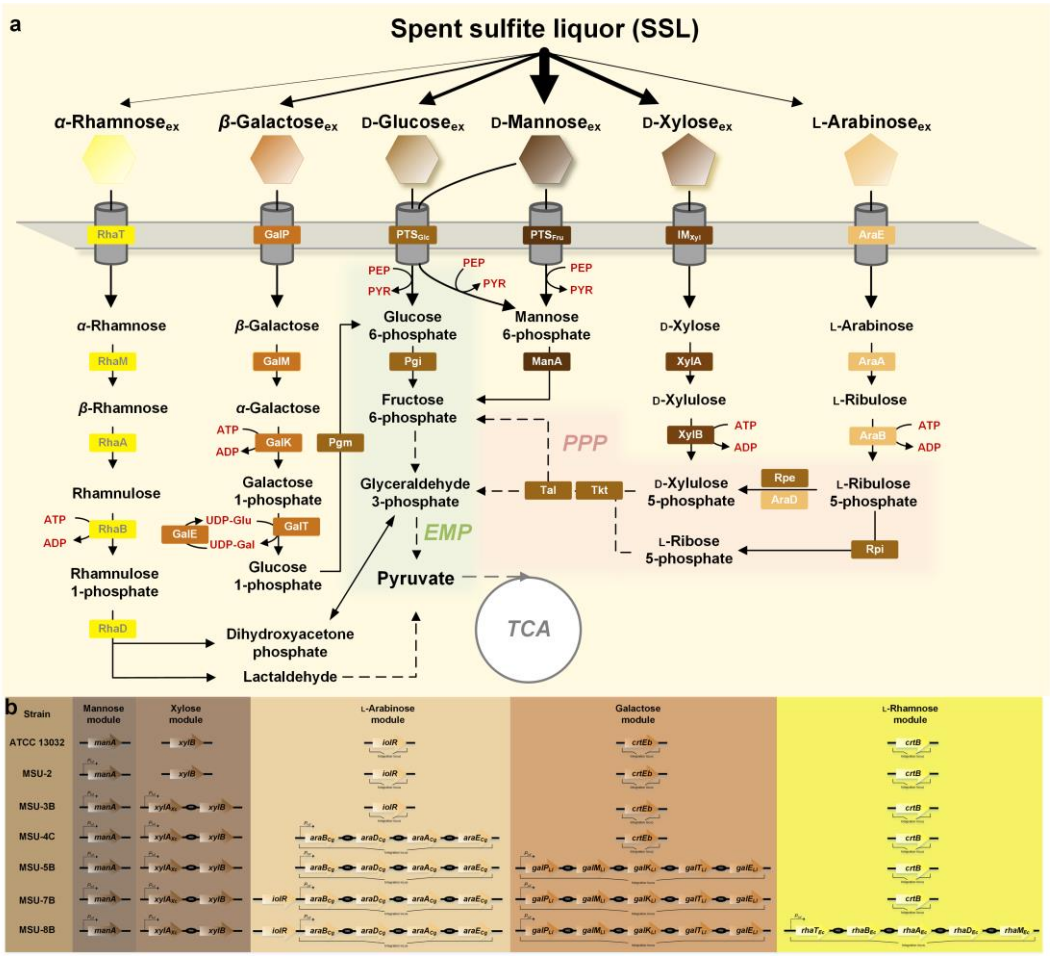

Figure 5-21: Metabolic pathway design for co-utilization of multiple sugars by *C. glutamicum*. The figure shows the newly installed heterologous metabolism, implemented around the native EMP and PP pathways (**a**) and the genomic layout of the created strain family (**b**). AraA: L-arabinose isomerase; AraB: L-ribulokinase; AraD: L-ribulose-5-phosphate 4-epimerase; AraE: L-arabinose-proton symporter; GalE: UDP-glucose 4-epimerase; GalK: galactokinase; GalM: aldose 1-epimerase; GalP: galactose permease; GalT: hexose-1-phosphate uridylyltransferase; IM_{xyl}: xylose symporter; ManA: mannose-6-phosphate isomerase; Pgi: phosphoglucose isomerase; Pgm: phosphoglucomutase; PTS_{Fru}: fructose-specific phosphotransferase system; PTS_{Glc}: glucose-specific phosphotransferase system; RhaA: rhamnose isomerase; RhaB: rhamnulokinase; RhaD: rhamnulose-1-phosphate aldolase; RhaM: rhamnose mutarotase; RhaT: rhamnose-proton symporter; Rpe: ribulose-5-phosphate-3-epimerase; Rpi: ribose-5-phosphate isomerase; Tal: transaldolase; Tkt: transketolase; XylA: xylose isomerase, XylB: xylulokinase. The mannose module comprised overexpression of *manA* (P_{tuf} *manA*). The heterologous xylose module from *X. campestris* was integrated upstream of the native *xylB* locus (P_{tuf} $xylA_{Xc}$ $xylB_{Cg}$). The L-arabinose catabolic operon from *C. glutamicum* ATCC 31831 was installed in the *iolR* locus. Subsequently, *iolR* was recovered due to its importance for efficient sugar metabolization (P_{tuf} $araBDAE_{Cg}$). The heterologous galactose module from *L. lactis* was integrated into the *crtEb* locus (P_{tuf} $galPMKTE_{Ll}$), while the L-rhamnose catabolic operon from *E. coli* was implemented into the into the *crtB* locus (P_{tuf} $rhaTBADM_{Ec}$). All the genetic constructs were stably integrated into the genome of *C. glutamicum*, making all strains fully genome-based, plasmid-free cell factories.

Altogether, we applied systems metabolic engineering to realize the broadest substrate spectrum for *C. glutamicum* that has been ever demonstrated (Figure 5-21 and appendix Figure 7-22) and proved the value of the engineered strains to use all sugar in spent sulfite liquor. While naturally, the wild type was capable of efficiently consuming only 17% of SSL-sugar, *C. glutamicum* MSU-8B utilized 100% (Figure 5-20 b). Given the wide substrate spectrum and the superior robustness of *C. glutamicum* MSU-8B, this strain appears as a suitable platform to utilize diverse feedstocks and raw materials from second-generation biomass towards various applications in the bioeconomy (Baruah et al., 2018; Malherbe and Cloete, 2002; Sun et al., 2016).

5.3.2 Creating a multi-substrate-using cell factory for glutarate-production

Glutarate is an five-carbon building block of commercial value to produce industrial polymers (Li et al., 2020; Napoleon, 1997; Werle et al.; Zheng et al., 2022), as well as bio-degradable cleaning detergents (Diaz, 1997). Its multiple uses explain the great interest to produce the molecule from renewable resources. Previously, our group has created the advanced glutarate producer *C. glutamicum* GTA-4 through rational systems metabolic engineering, setting a benchmark for bio-based glutarate production (Rohles et al., 2018). The GTA-4 strain exhibited high efficiency production, based on 16 genomic traits that were implemented. Nevertheless, the process was based on first-generation substrates, i. e. glucose and molasses (Rohles et al., 2018), unfavorably competing with global land use and food supply (Bhatia et al., 2022; Kuhad and Singh, 1993; Naqvi and Yan). We now aim to merge the traits of the non-producing *C. glutamicum* chassis MSU-8B with that of GTA-4 to create a superior producer for glutarate. To this end, we step-wise implemented the best performing sugar utilization modules, identified during previous strain development, into strain GTA-4. In short, starting from GTA-4, we overexpressed the native *manA* gene under control of the strong constitutive promoter P_{tuf}, leading to strain MSU-10, followed by integration of $xylA_{Xc}$ from *X. campestris* under control of P_{tuf} upstream of the native *xylB* gene (MSU-11). Afterwards, we integrated the catabolic L-arabinose operon $araBDAE_{Cg}$ from *C. glutamicum* ATCC 31831 under control of P_{tuf} into the *iolR* locus (MSU-12). Subsequently, we integrated galactose operon $galPMKTE_{Ll}$ from *L. lactis* under control of P_{tuf} into the *crtEb* locus, which finally yielded *C. glutamicum* MSU-13 (Table 4-1). All steps of the cloning very carefully approved for correctness of the desired mutations by PCR and sequencing. To demonstrate the glutarate production performance, we decided to skip the last round of engineering for L-rhamnose, given the rather low abundance of this sugar in the available industrial liquor

and the fact that we could already show complete L-rhamnose metabolization by integrating a L-rhamnose module.

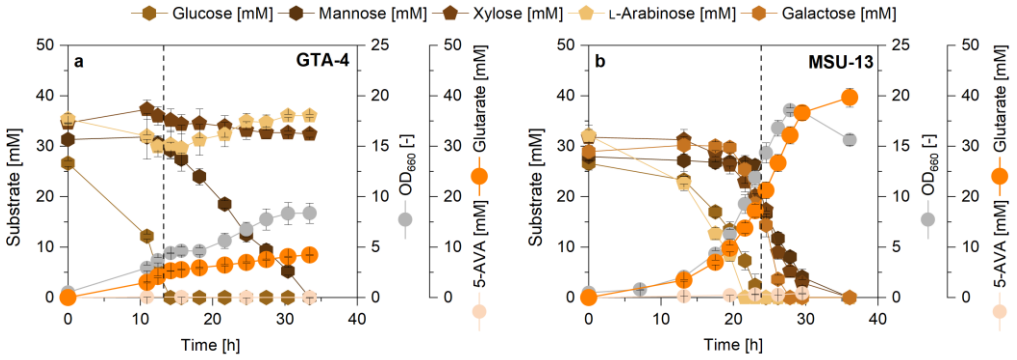

Figure 5-22: Growth and glutarate production performance of strains GTA-4 (**a**) and MSU-13 (**b**) in shake flasks using minimal medium with synthetic sugar mixture as substrate. The concentration of each sugar in the mixture was set to 5 g L^{-1}. The vertical dashed line indicates the time point of glucose depletion. None of strains formed significant amounts of 5-aminovalerate. The data comprise mean values and standard errors from three biological replicates.

Next, the glucose-based producer GTA-4 and the novel strain MSU-13 were evaluated on a synthetic mixture with the five sugars of relevance. Notably, GTA-4 strain metabolized only glucose and, to a weaker extent, mannose. It exhibited clearly diauxic growth with two separated phases. Growth on mannose was very poor and slow, and the cell concentration increased rather linear than exponential. Within 30 h, GTA-4 accumulated 8.6 mM glutarate at a yield 136 C-mmol C-mol^{-1}, when considering only the two sugars that had been utilized (Figure 5-22 a). When producing from glucose alone GTA-4, achieved a 66% higher glutarate yield (226 C-mmol C-mol^{-1}) (Rohles et al., 2018). Obviously, the low efficiency utilization of mannose not only massively extended the process time, but also negatively affected product formation, eventually due to extended maintenance energy requirement (Becker et al., 2005a; Wittmann et al., 2004) or an undesired flux distribution (Buschke et al., 2013a; Hoffmann et al., 2018; Kiefer et al., 2004). When taking all available five sugars into account, the achieved glutarate yield of GTA-4 was as low as 38.5 C-mmol C-mol^{-1}.

In contrast, the advanced strain MSU-13 depleted all five sugars within the same time of 30 h, including glucose, mannose, xylose, L-arabinose, and galactose. Beneficially, the strain revealed neither a growth delay nor a phase of diauxic adaptation (Figure 5-22 b). All sugars were co-consumed. Glutarate was produced throughout the entire cultivation and reached a final titer of 39.7 mM, almost five-fold more than the parental strain. The overall glutarate yield was 211 C-mmol C-mol^{-1}, almost as high as that of GTA-4 on

glucose. The created glutarate cell factory MSU-13 provides an attractive platform to produce glutarate from lignocellulosic biomass and other complex sugar-containing raw materials (Baruah et al., 2018; Malherbe and Cloete, 2002; Sun et al., 2016). In this regard, our strategy to incorporate a range of carefully designed and evaluated sugar utilization modules into an existing glucose-based cell factory, was highly successful. The created cell factory *C. glutamicum* MSU-13 exhibited the extended substrate spectrum of the multi-sugar-using chassis, as well as the superior glutarate production capacity of its glucose-based ancestor, thus synergistically merging all benefits.

This can be taken as a promising potential to be applied to other value-added products, including chemicals, materials, fuels, and healthcare products (Becker et al., 2018b; Becker and Wittmann, 2012a; Becker and Wittmann, 2015). Given the increasing demand for sustainable bio-production from cheap but complex and demanding raw materials, producing strains offer high robustness and a broad substrate spectrum can be assigned a great impact on future production.

5.3.3 Benchmarking glutarate production from spent sulfite liquor in batch and fed-batch processes

Next, we evaluated MSU-13 on SSL. In a first round of experiment, we used shake flask batch cultures. The medium contained 10% SSL-UF together with salts, trace metals, as well as the two vitamins. In addition, we supplied 2 g L^{-1} of yeast extract to support strain growth for the expected long process time under demanding conditions. MSU-13 consumed 99% of all sugar, except the small amount of L-rhamnose (see strain design above). Notably, a final titer of 66.6 mM of glutarate was reached after 60 h (Figure 5-23). Considering the additional carbon from the added yeast extract (Christmann et al., 2023), the achieved overall glutarate yield, based on all fed carbon, was 373.9 C-mmol C-mol. The value was increased by 77%, as compared to that on sugar mixtures. When cultivating MSU-13 on SSL, cell growth was somewhat reduced, directing more carbon flux to product formation. The same beneficial phenomenon was also observed for glucose-based glutarate producers such as *C. glutamicum* GTA-4 strain during fed-batch production. When cell growth slowed down and even ceased during the feed phase, this allowed for a 2.5-fold increase of the glutarate yield (580 C-mmol C-mol) as compared to the batch phase (240 C-mmol C-mol) (Rohles et al., 2018).

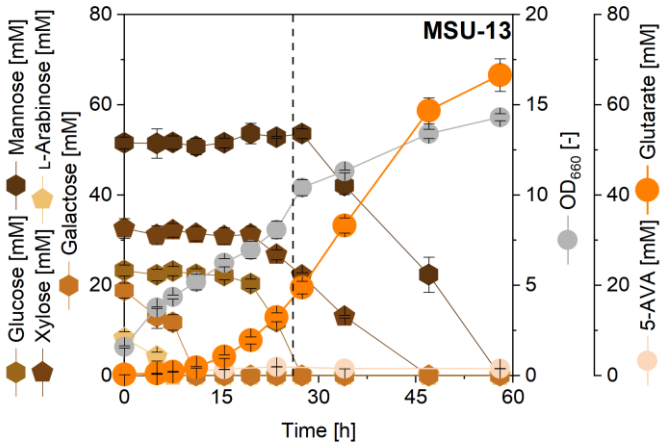

Figure 5-23: Bio-based production of glutarate from SSL. The strain *C. glutamicum* MSU-13 was cultivated on SSL-based medium containing 10% of SSL-UF (Borregaard, Snapsborg, Norway) and 2 g L^{-1} of yeast extract. The vertical dashed line indicates the time point of glucose depletion. The data comprise mean values and standard errors from three biological replicates.

To assess the performance of *C. glutamicum* MSU-13 under industrially relevant conditions, we benchmarked the production in a fed-batch process, using SSL as sole carbon and energy source (Figure 5-24 a). The process was started with a batch phase. The batch medium contained 10% SSL-UF plus 5 g L^{-1} yeast extract (representing about 15% of the SSL-based carbon), minerals, trace metals, and vitamins (pH 6.5) but no further supplements to mimic the lean, cheap set-up envisioned for an economic process. It took about 20 h for the strain to start growing efficiently. Until this point, growth was at least weak, and the cells appeared metabolically active, visible by the complete consumption L-arabinose and galactose. Afterwards, the batched amounts of glucose, xylose, and mannose were consumed. After about 55 h, the initial sugars were nearly depleted, indicated by the increasing dissolved oxygen (DO) level and the decreasing carbon dioxide concentration in the exhaust gas (XCO_2). At this time point, the first pulse of pure SSL-UF was given, which brought back the medium to an SSL concentration of 10%. The feed addition resulted in an immediate decrease of the DO signal and increased respiration activity indicating the direct on-set of sugar metabolism. It should be noted the extra shot resulted in an accumulation all compounds that were contained in SSL but not degraded by the cells, containing partially toxic chemicals (Holmgren and Sellstedt, 2008; Marques et al., 2009; Palmqvist and Hahn-Hägerdal, 2000b). Nevertheless, the obvious accumulated xylose and mannose were eventually depleted. In this regard, the glutarate producing *C. glutamicum* MSU-13, equipped with efficient pathways to catabolize the various carbon sources, handled all sugars in SSL very well,

even after 6 feed-pulses. In addition, acetate contained in SSL was co-consumed together with glucose during the batch phase, while rapid uptake of acetate was observed during the feeding phase.

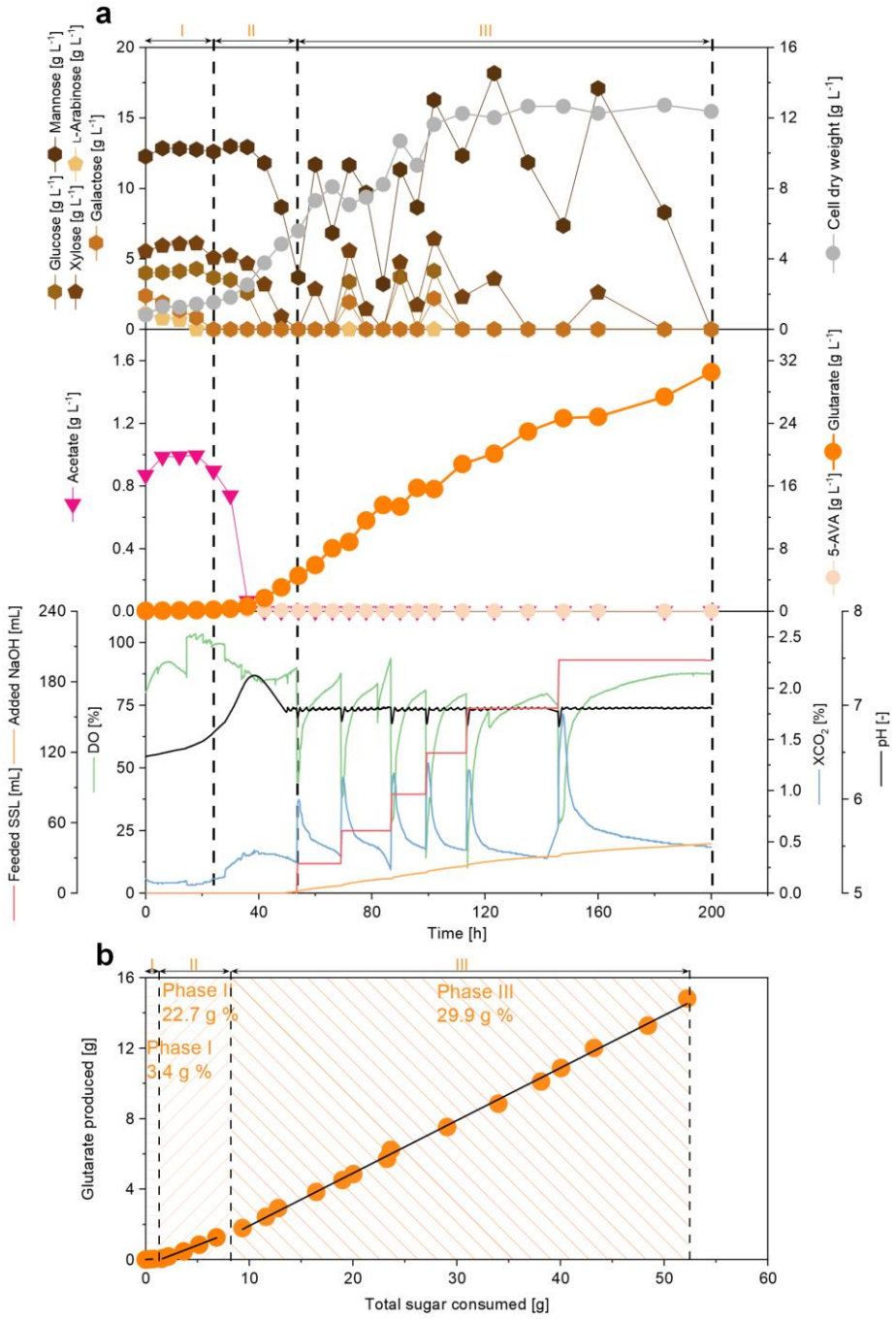

Figure 5-24: Fed-batch production of glutarate by metabolically engineered *C. glutamicum* MSU-13 from industrial waste stream-spent sulfite liquor. Fermentation profile (**a**) and glutarate yield (**b**) during whole process. The total sugar consumed is given as sum of the mass of all substrates, including glucose, mannose, xylose, L-arabinose, galactose, and acetate.

Glutarate production started when cells started to grow and reached a concentration of 5 g L^{-1} at the end of second phase (II), while the product was formed at a yield of 0.23 g g^{-1}. Further on, the glutarate level increased to a final titer of 30 g L^{-1}, encouragingly coupled to increased glutarate yield of 0.30 g g^{-1} (Figure 5-24 b). The cells produced glutarate almost exclusively, whereas the formation of the potential by-product 5-aminovalerate was negligible. Overall, the novel MSU-13 producer enabled glutarate production from all SSL-sugar for the first time, thereby revealing a remarkable performance. The product yield was lower as compared to a fed-batch process on a glucose-molasses medium (0.51 g g^{-1}) (Rohles et al., 2018), leaving space for improvement. Considering the excellent production performance of MSU-13 on synthetic sugar mixtures, the prolonged fermentation in the SSL-based process seemed to be due to the toxicity of the raw material suggesting to try to improve the tolerance of the producer by further rounds of metabolic engineering and/or streamlining the process by additional detoxifying raw material pre-treatment steps (Chandel et al., 2013; Mussatto and Roberto, 2004). Additionally, further strain engineering could aim to relax the carbon catabolite repression for the use of mannose and xylose. This might allow to consume all sugars simultaneously. Nevertheless, the *C. glutamicum* strain MSU-13 equipped with 20 genomic traits, including 16 modifications for glutarate production (Figure 3-2) and 4 modifications for extending substrate spectrum (Figure 5-21), exhibited stable productivity to valorize the industrial waste stream SSL to glutarate after 6 feed-pulses and 200 h fermentation, indicating excellent performance and robustness of the novel cell factory. This achievement demonstrates the power of systems metabolic engineering toward attractive biorefinery processes that valorize SSL. Moreover, given the successfully demonstrated purification of bio-based glutarate and its polymerization into nylon-6,5 (Rohles et al., 2018), the integration of these downstream processes to the developed fermentation process would enable the use of SSL for green nylon production.

Taken together, systems metabolic engineering *C. glutamicum* created the non-producing chassis strain MSU-8B which harnessed all six sugars in SSL. Furthermore, transferring the best multi-sugar blocks into a previously derived gluatarate-producing strain appeared as straightforward strategy to yield *C. glutamicum* MSU-13 as an efficient and robust glutarate production host from SSL. As an important proof of concept, our strategy demonstrated the valorization of sugars in spent sulfite liquor, the industrial waste stream from pulp and paper industry, to produce the bulk chemical glutarate using tailor-made *C. glutamicum* strains.

5.4 Production of the antimicrobial peptide pediocin PA-1 from spent sulfite liquor

5.4.1 Re-engineering of the multi-substrate use in a genome-reduced *C. glutamicum* chassis

The high-value antimicrobial peptide pediocin PA-1 is a potent bacteriocin for food preservation (Papagianni and Anastasiadou, 2009; Rodriguez et al., 2002). Recently, production of this peptide has been demonstrated using the robust industrial workhorse *C. glutamicum* by heterologous expression of a codon-optimized version of the pediocin PA-1 cluster $pedACD^{Cg}$ from *P. acidilactici* (Christmann et al., 2023; Goldbeck et al., 2021). Interestingly, the genome-reduced strain CR099 was used for the pediocin PA-1 production, in which three prophages (CGP1, CGP2, and CGP3) and all copies of two insertion sequence elements (ISCg1 and ISCg2) in the genome of wild type strain ATCC 13032 were deleted (Baumgart et al., 2018). We were interested in assessing the growth differences between the genome-reduced strain and the wild type strain. The strain CR099 exhibited a growth rate of 0.49 h^{-1} and specific consumption rate of 38.0 C-mmol g^{-1} h^{-1} on glucose, suggesting superior growth characteristics compared to that of the strain ATCC 13032 (Table 5-2). To evaluate the performance of the genome-reduced strain on SSL, we engineered CR099 towards the extended substrate spectrum. The best performing sugar utilization modules were implemented, following the same strategy, as described for the glutarate producing strain. Starting from CR099: overexpression of the native gene *manA* obtained the strain MSU-14; following integration of the gene $xylA_{Xc}$ obtained the strain MSU-15; afterwards, integration of the L-arabinose catabolic operon $araBDAE_{Cg}$ generated the strain MSU-16; subsequently, integration of the galactose catabolic operon $galPMKTE_{Ll}$ yielded the strain MSU-17 (Table 4-1).

MSU-17 was grown on SSL-based medium, containing 20% SSL-UF (Figure 5-25). This strain utilized almost 99 % sugars in SSL in about 30 h, including glucose, mannose, xylose, L-arabinose, and galactose. In terms of growth and substrate consumption on SSL, CR099 behaved like the ATCC 13032-derived strain. While genome-reduced strains were found more robust against several stresses, e.g., pH stress, oxidative stress, osmotic stress, and phosphate limitation, revealing improved growth and cells fitness (Baumgart et al., 2018; Baumgart et al., 2013), the genome-reduced strain did not provide increased robustness to handle with SSL.

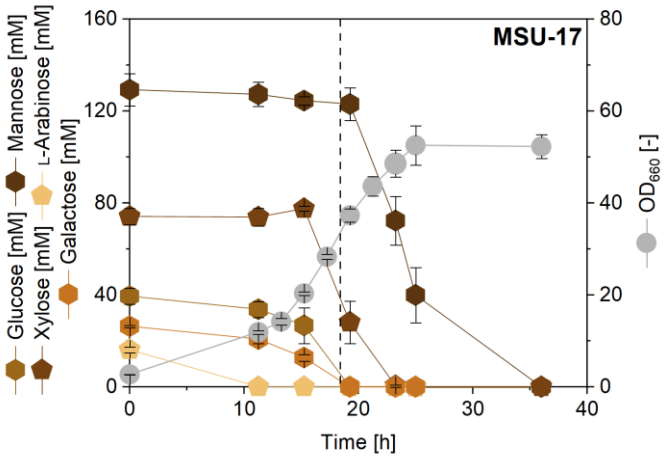

Figure 5-25: The growth performance of genome-reduced *C. glutamicum* MSU-17 on SSL-based medium containing 20% (v/v) SSL-UF. The vertical dashed line indicates the time point of glucose depletion. The data comprise mean values and standard errors from three biological replicates.

5.4.2 Pediocin production from spent sulfite liquor

So far, the production of pediocin PA-1 using *C. glutamicum* mainly relied on complex rich media containg high level of expensive yeast exact and peptone (Christmann et al., 2023; Goldbeck et al., 2021), while the optimized minimal medium still required glucose and 10 g L^{-1} additional yeast extract (Christmann et al., 2023). To construct a pediocin PA-1 producer strain with extended substrate spectrum for a cheaper and sustainable process, the plasmid pXMJ19-*pedACD*^{Cg} harboring the pediocin PA-1 cluster was transformed into MSU-17, and the resulting strain was designated *C. glutamicum* MSU-18. We tested the engineered strain MSU-18 on SSL-based medium containing 10% SSL-UF, and a reduced amount of 5 g L^{-1} yeast extract (Aasen et al., 2000). As shown in Figure 5-26, production of pediocin PA-1 from SSL using engineered *C. glutamicum* strain was achieved for the first time. Regarding sugar utilization, the strain MSU-18 behaved the same as parental strain MSU-17, consuming about 99 % sugars in SSL. Unexpectedly, the cells exhibited a clear diauxic growth. Within the initial 20 h, the strain consumed L-arabinose, galactose, and glucose to grow and produce pediocin PA-1 continuously, reaching a pediocin PA-1 titer of 10188 BU mL^{-1}. In later phase, the slow utilization of xylose and mannose led to a growth shift and subsequent linear cells growth up to a final OD_{660} of 19.3. In addition, the cells appeared to stop producing pediocin PA-1 between 20-40 h, while production restarted after 40 h, reaching a final pediocin PA-1 titer of 16582 BU mL^{-1} in about 50 h. Since the growth and the global transcriptional machinery of *C. glutamicum* were previously found to be unaffected by the expression of pediocin PA-1 cluster, as well as the product pediocin PA-1 (Christmann et al., 2023),

the plasmid burden of course cannot be excluded, but the slow growth and sugar utilization of strain MSU-18 on SSL were most likely due to the oxygen limiting conditions. Lactate, the predominant by-product under oxygen limiting conditions of *C. glutamicum* (Zahoor et al., 2012), was accumulated up to 40 mM in initial 20 h, while the secretion of lactate significantly reduced afterwards, observing a maximum concentration of 49 mM in 40 h. Given the toxicity of lactate to microbes, it is obvious that the lactate formation was detrimental to the process. Additionally, the pH value during the whole process was above 7.0, an unfavorable condition for the pediocin PA-1 formation which required acidic conditions, such as pH 5.9 and pH 6.0, for optimal production (Christmann et al., 2023). Other process parameters could also be optimized to further boost the pediocin PA-1 production on SSL, e.g., fine-tuning of oxygen supply, and addition of calcium chloride (Christmann et al., 2023). It is also interesting to benchmark this cell factory under fed-batch conditions using SSL as substrate. In sum, despite the poor production performance, we demonstrated the pediocin PA-1 production in *C. glutamicum* using SSL as substrate, reflecting the impressive capability of *C. glutamicum* to produce high-value active ingredients from toxic industrial waste stream. Again, this is another proof of concept to valorize SSL into high-value antimicrobial peptide, providing significant evidence for the generalizability of our strategy.

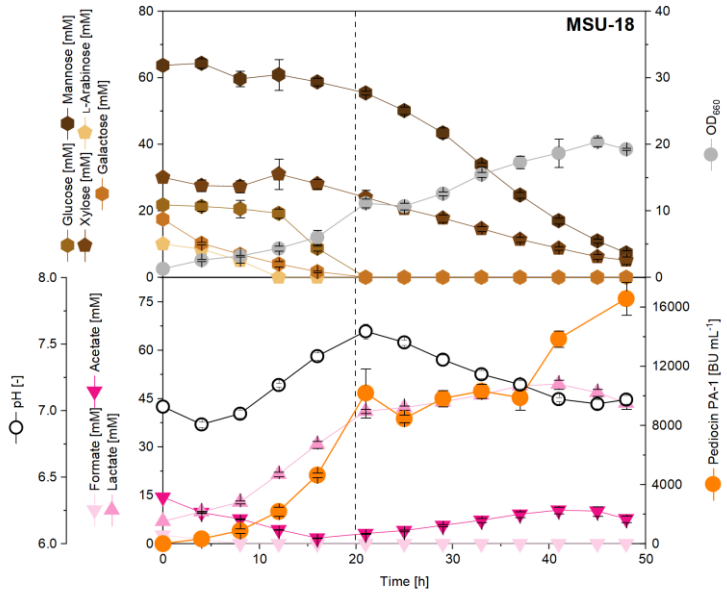

Figure 5-26: Bio-based production of pediocin from SSL. The strain MSU-18 was cultivated on SSL-based medium containing 10% (v/v) SSL-UF. 5 g L^{-1} yeast exact was added. The vertical dashed line indicates the time point of glucose depletion. The data comprise mean values and standard errors from three biological replicates. Jens Christmann conducted this experiment.

5.5 Selective recovery of high-value sugars from spent sulfite liquor using *C. glutamicum* cell factories with a fine-tuned substrate spectrum

Notably, several of the sugars, present in SSL, have a recognized commercial value. As example, mannose is used as auxiliary moisturizing agent in cosmetics, feed additive, treatment for urinary tract infections (UTIs), while galactose, also called the “brain sugar” due to its impact to support early human development and prevent diseases, is used as dietary supplement, and L-rhamnose is used as precursor for synthesis of the aroma furaneol and cardiac drugs. In the previous chapters, the fermentative use of these sugars, together with glucose, xylose, and L-arabinose, was demonstrated. It appeared as an interesting concept to alternatively purify mannose, galactose and L-rhamnose from the complex SSL waste stream.

First, we aimed at direct purification of the sugars from SSL-UF using flash and preparative ion exchange chromatography. Different resins were applied in a set of experiments, as described above. They all yielded similar separation performance. When processing SSL samples, three major eluting fractions were observed (appendix Figure 7-24). The fractions, collected over the first 17 minutes, appeared colourless and clear. Then, brownish compounds from the SSL eluted between 18-28 minutes. Afterwards, the eluting liquid became clear again. Subsequently, the sugar content in all fractions was analyzed, as exemplified for a Ca^{2+} loaded resin (appendix Figure 7-23). Almost no sugar eluted over the first 28 minutes. Unfavorably, owing to structural similarity, all sugars co-eluted over a long- and similar-time window, causing mixed sugars in almost every fraction. Using chromatography, the separation of related two sugar-mixtures, such as glucose and mannose (Caruel et al., 1991), glucose and xylose (Caruel et al., 1991; Sjöman et al., 2007), xylose and L-arabinose (Caruel et al., 1991), respectively, could be demonstrated before. However, the complex composition of SSL appeared to demanding to allow straightforward isolation of single sugars. More sophisticated processes or additional rounds of processing individual fractions could eventually provide a solution but would suffer from high efforts and high costs. Moreover, they probably would suffer from expectable fluctuations in the sugar. While xylose enriched liquors (more than 70%) from hardwood hydrolysates are industrially processed to recover xylose, whereby only minor amounts of other sugars and byproducts have to be removed (Rafiqul and Sakinah, 2012; Rødsrud et al., 2012; Zhang et al., 2014). Applying this to SSL, containing 50% mannose and other 5 sugars, suggests that a direct separation of mannose might be possible but difficult, while a recovery of other sugars in this stream is certainly challenging to achieve. Although it is possible to use several and larger columns to extensively improve separation performance (Geerdes et al., 1954;

Vaňková and Polakovič, 2010), the economic cost couldn't be ignored. Apparently, the structural similarity and the unfavorable, complex sugar composition of SSL markedly hindered the separation, allowing only an inefficient and laborious sugar recovery.

Given successful tailoring of the substrate spectrum of *C. glutamicum*, shown above, it appeared promising to adapt it for selective microbial conversion (Funk, 1975) to selectively degrade unattractive sugars by streamlined bacteria, while retaining a high-value sugar of interest (Funk, 1975). Towards this, we aimed for a selective recovery of mannose, galactose, and L-rhamnose from SSL, respectively, using tailor-made *C. glutamicum* strains.

5.5.1 Recovery of mannose, a supplement to treat and prevent urinary tract infections

To enable the selective recovery of mannose from SSL, a novel mutant, capable of consuming all sugars except mannose, was apparently needed. Towards this goal, a possible option was to block the mannose uptake into the cells, considering the existing catabolic mannose pathway in *C. glutamicum* (Lee et al., 1994; Sasaki et al., 2011). Since PtsG and PtsF were known as functional transporters of mannose (Sasaki et al., 2011), the deletion of the gene *ptsH*, encoding the histidine-containing phosphocarrier protein (HPr) of the PTS, essential for the uptake of all PTS-coupled sugars, appeared promising (Sasaki et al., 2011). We therefore deleted the *ptsH* gene in *C. glutamicum* MSU-7B which comprised catabolic pathways for glucose, mannose, xylose, L-arabinose, and galactose. After verification by PCR and sequencing, the obtained mutant was designated *C. glutamicum* MAN-1A (MSU-7B *ΔptsH*). Secondly, the deletion of *manA*, encoding mannose 6-phosphate isomerase, appeared promising to to disrupt the mannose catabolism (Sasaki et al., 2011). To this end, *manA* was deleted in MSU-7B, generating *C. glutamicum* MAN-1B (MSU-7B *ΔmanA*).

Growth tests of MAN-1A and MAN-1B were performed in minimal medium, containing glucose and mannose. Surprisingly, MAN-1A consumed glucose and mannose completely, thereby exhibiting diauxic growth. Glucose was first consumed, while mannose was consumed only after glucose had been depleted (Figure 5-27 a). This behaviour was unexpected. The mannose uptake should have been blocked due to disruption of the PTS (Sasaki et al., 2011). This finding suggested the presence of another transporter in strain MAN-1A, capable of transporting mannose. Given the multiple functions of the galactose permease GalP shown in *E. coli*, including activities

related to the transport of glucose and mannose (Henderson et al., 1984) and the presence of this protein in MAN-1A, of its potential role should be clarified.

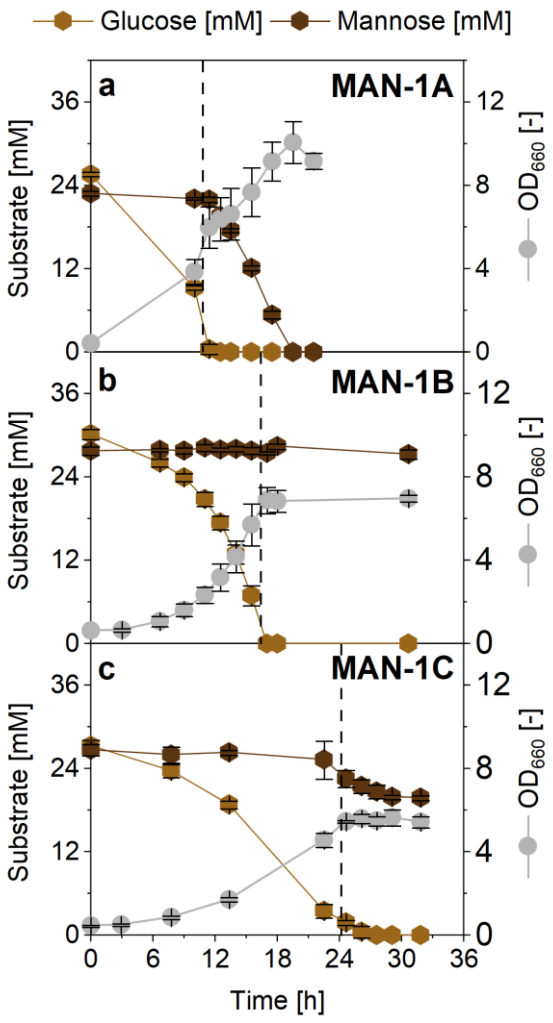

Figure 5-27: Growth characteristics of *C. glutamicum* MAN-1A (MSU-7B *ΔptsH*) (**a**), MAN-1B (MSU-7B *ΔmanA*) (**b**) and MAN-1C (MSU-7A *ΔptsH*) (**c**) in minimal medium containing 5 g L^{-1} glucose and 5 g L^{-1} mannose. The vertical dashed line indicates the time point of glucose depletion. The data comprise mean values and standard errors from three biological replicates.

Accordingly, we deleted the *ptsH* gene in *C. glutamicum* MSU-7A which lacked the catabolic galactose operon, yielding *C. glutamicum* MAN-1C (MSU-7A *ΔptsH*). Notably, when growing MAN-1C on a mixture of glucose and mannose, glucose was fully consumed, while the mannose concentration decreased only slightly (Figure 5-27 c). This indicated that the galactose operon from *L. lactis* was involved in mannose uptake and utilization, providing an explanation for the simultaneous consumption of glucose and mannose in the strains MSU-5B, MSU-7B and MSU-8B, described above (Figure 5-

16). Additionally, the growth rate of MAN-1C on glucose during the initial phase (0.11 h^{-1}) was severely reduced, as compared to MAN-1A (0.22 h^{-1}), further revealing a contribution of GalP to glucose uptake. The remaining glucose uptake in MAN-1C seemed to be mediated via other non-PTS permease, e.g. myo-inositol permeases and β-glucoside-PTS permease in *C. glutamicum* (Lindner et al., 2011; Ruan et al., 2020). These non-PTS permeases might also be able to import mannose considering the structural similarity between glucose and mannose, resulting in the observed slight mannose decrease. Given the interference between the different transport systems and the promiscouity of the involved transporters, a selective block of the uptake of mannose by transporter engineering appeared challenging, if not even infeasible, and was therefore not further considered.

In contrast, we expected the other strain, MAN-1B, which lacked mannose 6-phosphate isomerase activity. Favorably, mannose remained untouched during the whole cultivation, while only glucose was utilized (Figure 5-27 b). The growth rate of MAN-1B was slightly reduced, as compared to the parent strain, eventually caused by the role of mannose 6-phosphate in the synthesis of GDP-mannose as cell wall building block (Sasaki et al., 2011). Nevertheless, the deletion of *manA* gene appeared as a suitable, if not the only, option to abolish mannose utilization. The deletion of *galE* was no alternative because the *C. glutamicum* strain had to exhibit galactose utilization capacity to enable the selective enrichment of mannose.

Next, strain MSU-8B, capable to metabolize all sugars in SSL was streamlined by deleting *manA* to remove the capacity to use mannose. Ideally, the generated mutant *C. glutamicum* MAN-2 (MAN-8B *ΔmanA*) was supposed to enable to selective recovery of mannose from the waste stream. When growing MAN-2 in shake flasks on 20% SSL-UF medium, the desired feature could be proven. The strain consumed all sugars except mannose, while the level of the latter remained constant (Figure 7-28 a). The successful enrichment of mannose was proven by GC-MS analysis of SSL-UF (Figure 7-28 b) and the culture supernatant after 40 h of cultivation (Figure 7-28 c). As shown, only mannose remained.

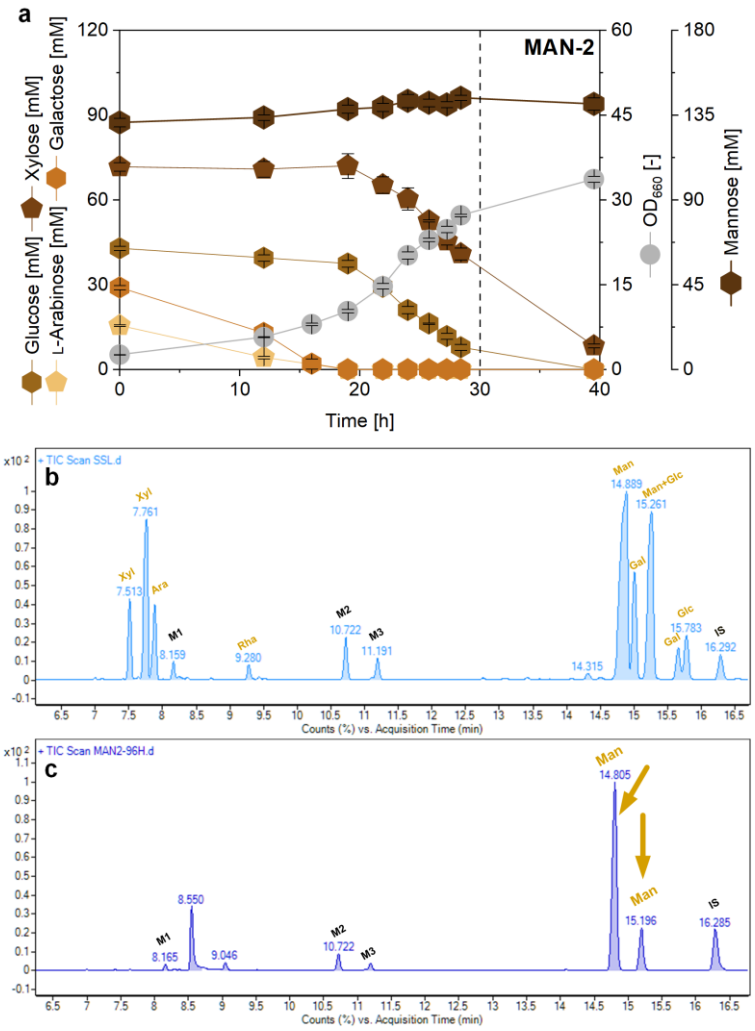

Figure 5-28: Recovery of mannose from SSL by engineered *C. glutamicum* MAN-2 (MAN-8B *ΔmanA*). The strain MAN-2 was cultivated in SSL-based medium containing 20% (v/v) SSL-UF (**a**). L-Rhamnose data is not shown due to its low concentration. The vertical dashed line indicates the time point of glucose depletion. The data comprise mean values and standard errors from three biological replicates. Chromatogram on GC-MS of SSL-UF sample (**b**) and shake-flask cultivation sample of MAN-2 (**c**).

Next, we benchmarked MAN-2 in a fed-batch process, using buffered SSL medium (Figure 5-29). In brief, the cells were grown on 20% SSL-UF as substrate during the batch phase, and pure SSL-UF was used for feeding, as described above. During the batch phase, the strain MAN-2 grew exponentially and consumed L-arabinose, L-rhamnose, galactose, glucose, and xylose, while the mannose concentration remained constant. After about 25 h, the feed was manually added to start the feed phase. The sugars from the first feed-pulse allowed the cells to grow again, reaching a maximum cell dry mass of 15 g L^{-1}, whereas a stationary phase was observed after the second feed-pulse. Notably, all sugars, except mannose, were completely depleted. However, it took about 100 h to deplete the remaining xylose (9 g L^{-1}). Xylose, at low level, seemed

to be inefficiently consumed by recombinant *C. glutamicum* strains, as previously demonstrated (Kawaguchi et al., 2006; Sasaki et al., 2009). Interestingly, a co-utilization ratio of glucose to xylose close to 1 mol mol^{-1} was observed, suggesting a markedly improvement of the simultaneous consumption of glucose and xylose due to the *manA* deletion, which indicated an unknown regulation between the *manA* gene and xylose utilization. Given the contribution of the myo-inositol proton symporter IolT1 to xylose uptake (Brusseler et al., 2018), as well as the role of the *ptsG* gene for xylose utilization (Wang et al., 2014), the xylose catabolism in *C. glutamicum* seemed regulated via many genes, requiring more studies to understand the underlying mechanisms. Mannose reached a titer of 60 g L^{-1} after the second feed-pulse. Previous attempts to separate mannose from SSL used laborious low-efficiency routes. First, monomeric mannose was converted into the bisulfite adduct in the mixture, followed by crystallization, separation, and regeneration of mannose (Timell, 1975). Second, separation was based on glycosidation concurrent with methanolysis, followed by crystallization and separation of the obtained methyl mannoside, again needing final regeneration of mannose (Timell, 1975). Here, the straightforward microbial conversion process provided an attractive alternative given its excellent selectivity and simplicity. In sum, the developed *C. glutamicum* MAN-2 strain selectively recovered mannose from the complex sugar mixture SSL, successfully providing a high-level broth of mannose without further sugars.

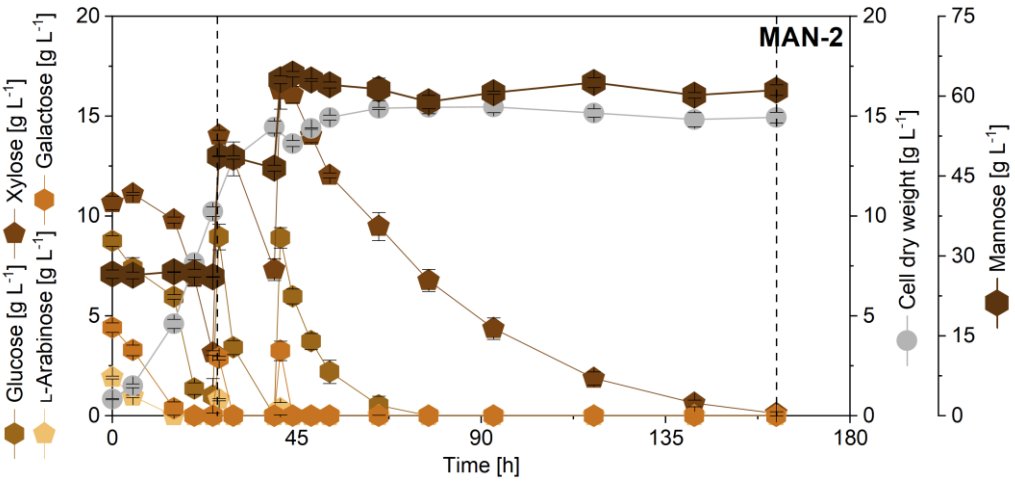

Figure 5-29: Fed-batch fermentation for the recovery of mannose from industrial waste stream-spent sulfite liquor by metabolically engineered *C. glutamicum* MAN-2. L-Rhamnose data is not shown due to its low concentration. The data represents mean values and standard errors from two biological replicates.

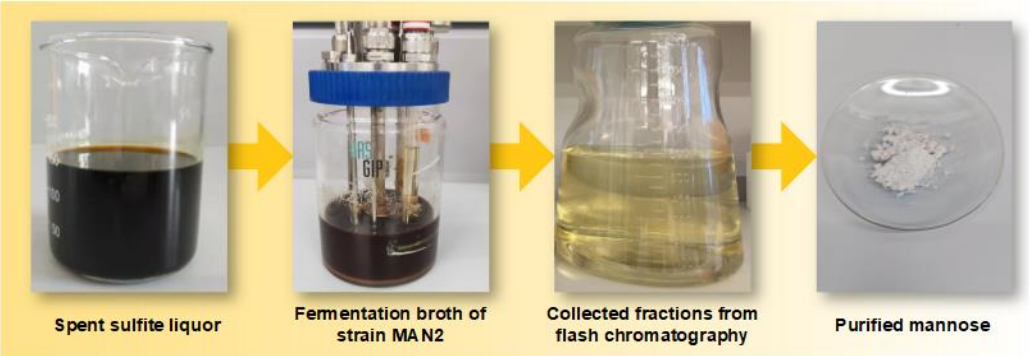

Figure 5-30: Cascaded recovery and purification of mannose from industrial waste stream-spent sulfite liquor by *C. glutamicum* MAN-2 with streamline substrate spectrum.

To demonstrate the entire value chain, the obtained mannose-containing fermentation broth was used for downstream separation and purification. Using ion exchange chromatography, three different phases, the beginning phase, the brownish color phase, and the late phase were observed for fermentation broth as for pure SSL-UF stream (see above) (appendix Figure 7-24). Obviously, mannose was the only sugar contained in the later fractions (appendix Figure 7-25). These were collected, followed by mannose crystallization. After color removal and evaporation of water, concentrated mannose was obtained. Following washing of the crystals in ethanol, evaporation and lyophilization, yielded a white crystalline powder. In this regard, the cascaded valorization of the industrial waste stream SSL provided pure mannose, a high-value supplement to treat and prevent urinary tract infections (Figure 5-30).

5.5.2 Recovery of galactose, a dietary supplement

To selectively recover galactose from SSL, the desired *C. glutamicum* strain should correspondingly utilize all sugars, except galactose. To obtain the desired genotype, we implemented the best performing L-rhamnose operon, $rhaTBADM_{Ec}$, into the genome of *C. glutamicum* MSU-7A. The mutant was supposed to use glucose, mannose, xylose, L-arabinose, and L-rhamnose. It was designated *C. glutamicum* GAL-1 (MSU-7A P_{tuf} $rhaTBADM_{Ec}$). The strain was grown in shake flasks on 20% SSL-UF medium. It revealed complete consumption of glucose, mannose, xylose, L-arabinose and L-rhamnose, whereas galactose remained in the cultivation broth (Figure 5-31). Unexpectably, the galactose concentration remained stable over the initial process phase, but decreased toward the end of the process, enabling selective enrichment but linked to a loss of product.

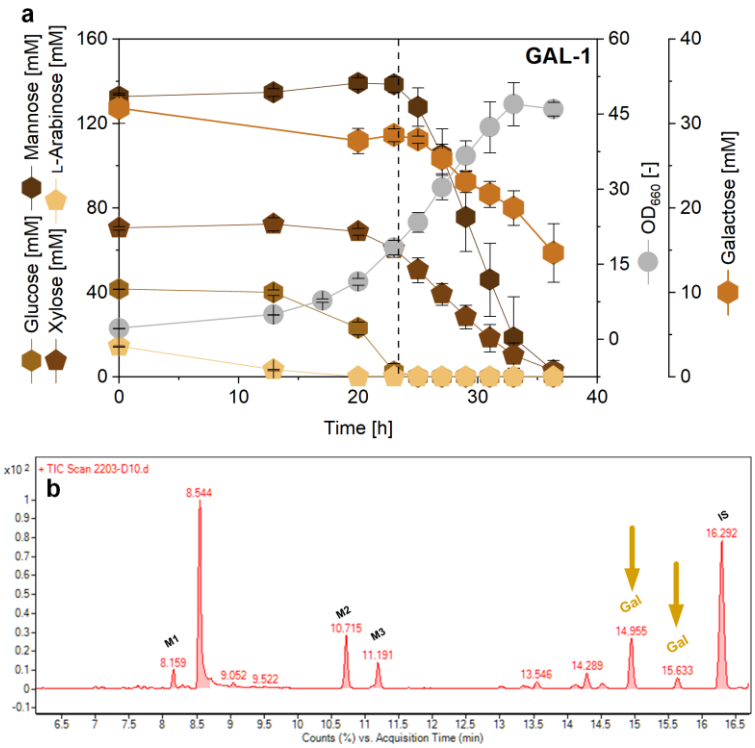

Figure 5-31: Recovery of galactose from SSL by engineered *C. glutamicum* GAL-1 (MSU-7A P_{tuf} *rhaTBADM*$_{Ec}$). The strain GAL-1 was cultivated in SSL-based medium containing 20% (v/v) SSL-UF (**a**). L-Rhamnose data is not shown due to its low concentration. The vertical dashed line indicates the time point of glucose depletion. The data comprise mean values and standard errors from three biological replicates. Chromatogram on GC-MS of shake-flask cultivation sample of GAL-1 (**b**).

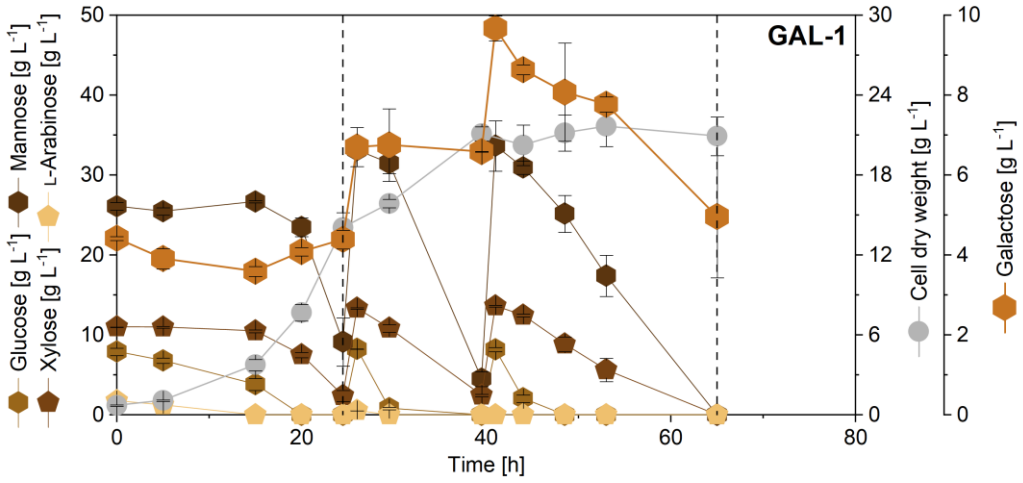

Figure 5-32: Fed-batch fermentation for the recovery of galactose from industrial waste stream-spent sulfite liquor by metabolically engineered *C. glutamicum* GAL-1. L-Rhamnose data is not shown due to its low concentration. The data represents mean values and standard errors from two biological replicates.

Subsequently, we performed a fed-batch process of GAL-1 using buffered SSL-based medium (Figure 5-32). In brief, 20% SSL-UF was used as substrate during the batch phase, and pure SSL-UF was used as the feed. GAL-1 grew exponentially during the batch phase, whereby L-arabinose, L-rhamnose, glucose, xylose and mannose were consumed, leaving galactose. Supported by the first feed-pulse, the cells exhibited a diauxic growth and reached a maximum cell dry weight of 21 g L^{-1}, whereas no cell growth was obtained after the second feed-pulse. Furthermore, GAL-1 strain efficiently consumed all sugars in SSL except galactose. Regarding galactose, it reached a maximum level of 10 g L^{-1} after the second feed-pulse, but then decreased.

Considering the low activity of the L-arabinose transporter AraE from *E. coli* to transport galactose (Henderson et al., 1984; Weickert and Adhya, 1993), the introduced AraE from *C. glutamicum* ATCC 31831 in MSU-4C strain appeared to be a candidate which eventually caused the consumption of galactose. By selectively introducing the galactose catabolic genes without *galP* in strain MSU-4C, the possibility of AraE to transport galactose could be verified. Moreover, a closer look at the Leloir pathway revealed the presence of multiple enzymes in *C. glutamicum* ATCC 13032, such as aldose 1-epimerase (GalM, NCgl2246), galactokinase (GalK, NCgl2152), and UDP-glucose 4-epimerase (GalE, NCgl1846). It is possible that the inherited enzymes were also functional, contributing to galactose catabolism.

To systematically investigate the galactose uptake and catabolism in *C. glutamicum*, the catabolic genes *galMKTE* (without *galP*) from *L. lactis* were inserted into the episomal vector pClik 5a MCS (Buschke et al., 2011; Hoffmann et al., 2018), yielding pClik 5a MCS *galMKTE*. In addition, the *galP* gene from *L. lactis* was individually expressed under control of the *tuf* promoter, generating the vector pClik 5a MCS *galP*. Subsequently, the transformation of vectors pClik 5a MCS, pClik 5a MCS *galP*, and pClik 5a MCS *galMKTE* into ATCC 13032 yielded *C. glutamicum* GAL-2A, GAL-2B, and GAL-2C, respectively, while the transformation of pClik 5a MCS *galMKTE* into MSU-4C yielded *C. glutamicum* GAL-2D.

All strains were plated on minimal medium agarose plates containing 10 g L^{-1} galactose as sole carbon source (Figure 5-33). Surprisingly, despite the lack of *galP* gene, the strain GAL-2C exhibited growth on galactose as a result of expression of galactose catabolic genes (Figure 5-33 b). Without doubt, this indicated the presence of a so far unidentified endogenous galactose transporter in the wild type. Interestingly, galactose was successfully used as an inducer of the IPTG inducible P_{tac} promoter in *C. glutamicum*, suggesting the general ability of *C. glutamicum* to transport galactose (Cheng et al., 2016). Likewise, growth of GAL-2D on galactose was observed, however, significantly

slower than that of GAL-2C, likely because the introduced heterologous genes caused detrimental effects (Figure 5-33 b). The other strains exhibited no growth on galactose, although small colonies were noticed for ATCC 13032 and GAL-2A from day 24, which seemed to be due to mutation (Figure 5-33). The potential function of AraE from ATCC 31831 for galactose uptake could not be confirmed. However, the native galactose transport into the cells seemed to be the major reason for the observed galactose decrease. This also provided an explanation for the decreased galactose level of the strains MSU-2, MSU-3B and MSU-4B on SSL, described above (Figure 5-18). Moreover, given the presence of several native transporters in *C. glutamicum* for different sugars, including hexoses glucose, fructose, and mannose (Baritugo et al., 2018; Leßmeier et al., 2015; Sasaki et al., 2011), as well as pentoses, xylose and L-arabinose (Kawaguchi et al., 2008; Kawaguchi et al., 2006), our findings about the existing of endogenous galactose transporter further proved the robustness and versatility of *C. glutamicum*, making it as an attractive chassis strain for utilizing a variety of carbon sources.

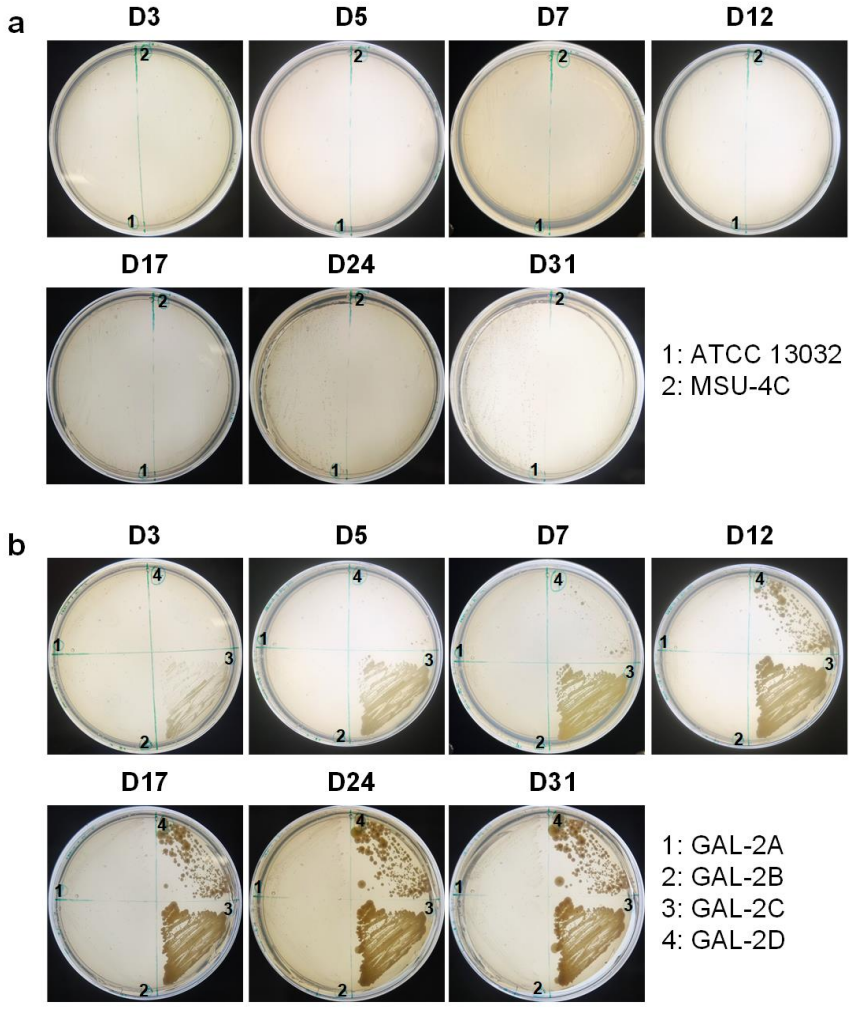

Figure 5-33: *C. glutamicum* strains growth on minimal medium plates with 2% agarose (20 g L^{-1}) instead of agar. A minimal medium containing 10 g L^{-1} galactose as carbon source was applied. D: Day.

5.5.3 Enrichment of L-rhamnose, a precursor in the flavor and perfume industry, along with glutarate production

Toward enrichment of L-rhamnose from SSL by *C. glutamicum*, a recombinant strain capable of utilizing all sugars except L-rhamnose was desired. Here, the above developed glutarate producing strain MSU-13, reaching high-level glutarate production from glucose, mannose, xylose, L-arabinose, and galactose in SSL, was selected as the parental strain. The native gene *iolR* of MSU-13 was recovered as previously described, providing *C. glutamicum* RHA-1 (MSU-13 *iolR*). When cultivated in shake flasks containing 10% SSL-UF, RHA-1 could utilize glucose, mannose, xylose, L-arabinose, and galactose completely, leaving only L-rhamnose (Figure 5-34 a), reflected by the GC/MS analysis of the cultivation broth (Figure 5-34 b). In addition, the concentration of L-rhamnose remained stable during the whole process. Glutarate was secreted continuously by RHA-1 strain, accumulating to a final glutarate level of 69 mM.

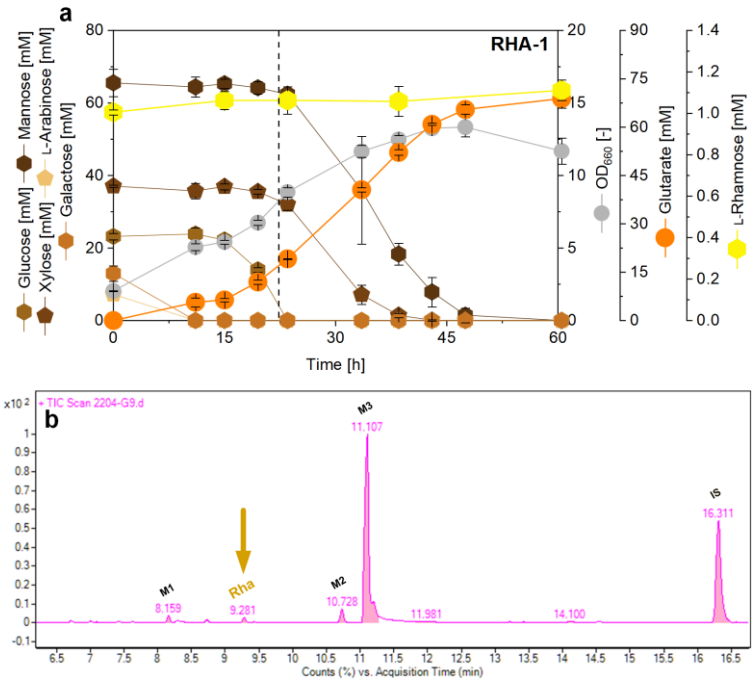

Figure 5-34: Recovery of L-rhamnose from SSL by engineered *C. glutamicum* RHA-1 (MSU-13 *iolR*). The strain RHA-1 was cultivated in SSL-based medium containing 10% (v/v) SSL-UF (**a**). The vertical dashed line indicates the time point of glucose depletion. The data comprise mean values and standard errors from three biological replicates. Chromatogram on GC-MS of shake-flask cultivation sample of RHA-1 (**b**).

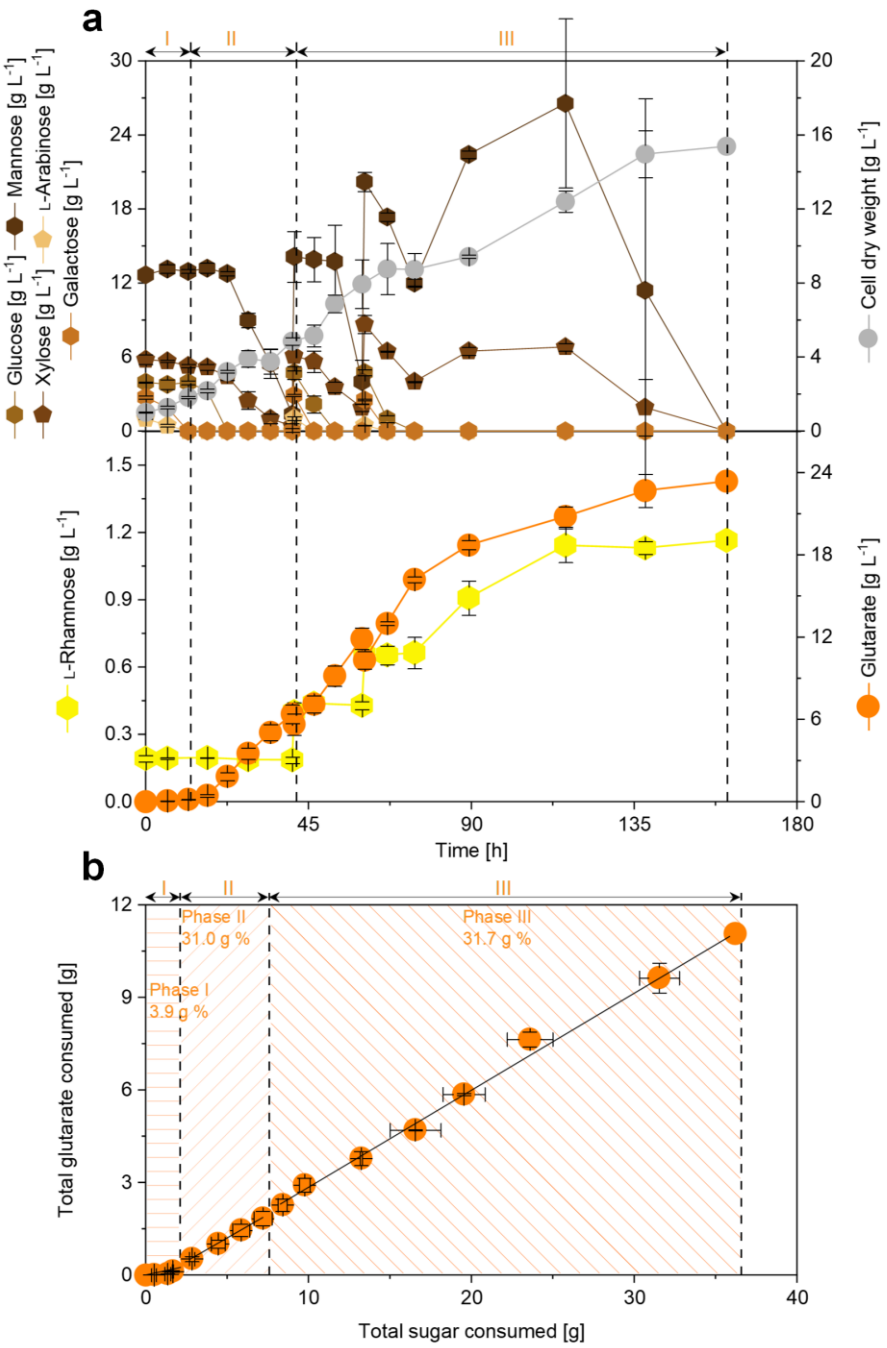

Figure 5-35: Fed-batch fermentation for the recovery of L-rhamnose and production of glutarate from industrial waste stream-spent sulfite liquor by metabolically engineered *C. glutamicum* RHA-1. Fermentation profile (**a**) and product yield (**b**). The data represents mean values and standard errors from two biological replicates. The total sugar consumed is given as sum of the mass of all substrates, including glucose, mannose, xylose, L-arabinose, galactose, and acetate.

Furthermore, we performed a fed-batch process using RHA-1 to enrich L-rhamnose from SSL (Figure 5-35). In brief, 10% SSL-UF was used as substrate in SSL-based medium with MOPS buffer during the batch phase, and the pure SSL-UF was used as the only

feed to reach the level of 10% again after each feed-pulse. Same to the parental strain MSU-13, three phases, including lag phase (I), batch phase (II), and feed phase (III), were observed. The RHA-1 strain first consumed L-arabinose, galactose, and glucose, then xylose and mannose during the lag phase (I) and batch phase (II), while L-rhamnose apparently remained stable as in shake flasks cultivation. In the feed phase (III), despite 4 times feed-pulse, RHA-1 equipped with effective catabolic pathway for glucose, mannose, xylose, L-arabinose, and galactose, completely utilized all sugars except L-rhamnose in 160 h. Stepwise enrichment of L-rhamnose following feed-pulse was observed, reaching a final titer of 1.1 g L^{-1}, 5-fold higher than that on 10% SSL-UF. In addition, a glutarate yield of 0.04 g g^{-1} was obtained during the lag phase (I), which increased up to 0.31 g g^{-1} in the batch phase (II) and 0.32 g g^{-1} in the feed phase (III), leading to a final glutarate titer of 23.4 g L^{-1}. Other known by-products were negligible.

Theoretically, the recovered sugar level described above, including mannose, galactose, and L-rhamnose, could be multiplied by adding several more feed-pulse. However, when conducting fed-batch fermentation processes of MAN-2 and GAL-1 (20% SSL-UF level after feed-pulse), cell growth decreased after several additional feed-pulses (data not shown). Given the existing inhibitors in SSL, such as furfural, 5-hydroxyfurfural, and particularly high level sulfite (Chandel et al., 2012b; Palmqvist and Hahn-Hägerdal, 2000b), this effect could be be due to the accumulation of inhibitors. Pretreatment and detoxification, e.g. by physical, chemical, and biological methods (Chandel et al., 2012b; Mussatto and Roberto, 2004; Palmqvist and Hahn-Hägerdal, 2000a), appeared promising to alleviate inhibitory effects. Alternatively, other raw materials and various feed-stocks, e.g. sugarcane bagasse (Chandel et al., 2012a; Pandey et al., 2000; Rumbold et al., 2009), wheat straw (Huang et al., 2021; Rumbold et al., 2009; Tian et al., 2018), corn stover (Rumbold et al., 2009; Zhao et al., 2018), which contain relevant valuable sugars, appear promising to recover selective sugars of interest. In addition, novel strains capable of selectively recovering xylose or L-arabinose could be easily obtained through one additional round of deletion of the responsible sugar utilization genes based on strain MSU-8B. Deletion of the fructose utilization genes could enable *C. glutamicum* to recover fructose from fructose-rich raw materials, such as molasses (Wittmann and Becker, 2007) and high-fructose corn syrup (Kay et al., 2010; Vuilleumier, 1993).

Furthermore, engineering *C. glutamicum* for the synthesis of valuable products appears promising. Here, the L-rhamnose recovering strain RHA-1 was demonstrated to produce glutarate with appealing performance, adding more value to the overall process. Without doubt, the glutarate synthetic module, as well as other biosynthetic pathways to produce

high value amino acids, chemicals, fuels, materials and healthcare products in *C. glutamicum* (Becker et al., 2018b; Becker and Wittmann, 2012a; Becker and Wittmann, 2015), could be conveniently applied in our robust chassis strains with extended substrate spectrum, allowing concurrent sugar recovery and production instead of only biomass formation. Taken together, we established *C. glutamicum* as platform for recovery of valuable sugars, including mannose, galactose, and L-rhamnose, from SSL streams with excellent selectivity, providing an attractive alternative for traditional separation process.

6 Conclusion and Outlook

Given the global climate change and environmental problems caused by the massive industrial use of fossil resources, biorefineries have gained increasing attention for sustainable production of chemicals, materials, and fuels (Cherubini, 2010; Ohara, 2003). The development of cell factories towards cheap feedstocks, particularly second-generation lignocellulosic biomass, appears crucial for environmentally sustainable and economically feasible future (Lee and Lavoie, 2013; Malherbe and Cloete, 2002).

This work focused on systems metabolic engineering *C. glutamicum* towards a broadened substrate spectrum. Starting from the wild type *C. glutamicum* ATCC 13032 which could only utilize glucose and fructose efficiently, a range of carefully designed synthetic sugar utilization modules, for mannose, xylose, L-arabinose, galactose, and L-rhamnose, were successfully implemented, and multiple rounds of iterative optimization were conducted. The finally created *C. glutamicum* MSU-8B co-utilized seven biomass sugars, i.e., glucose, fructose, mannose, xylose, L-arabinose, galactose, and L-rhamnose. In this regard, MSU-8B appeared as the first chassis strain capable of utilizing seven sugars and can be regarded as a promising platform for second-generation biorefineries. Beneficially, MSU-8B could efficiently harness 100% sugars in spent sulfite liquor (SSL), displaying high robustness towards the industrial waste stream. Subsequently, the streamlined sugar modules were successfully transferred into a superior glutarate producer, generating *C. glutamicum* MSU-13 which allowed glutarate production from complex sugar mixtures. During a fed-batch fermentation process using SSL as sole substrate, MSU-13 reached a glutarate titer up to 30 g L^{-1}. In addition, production of the high-value antimicrobial peptide pediocin PA-1 from SSL was demonstrated by adopting the strategy. Furthermore, recovery of single high-value sugars from SSL, including mannose, galactose, and L-rhamnose, using engineered *C. glutamicum* strains with streamlined substrate spectrum were established, providing the attractive microbial conversion processes for single sugar recovery from complex mixtures. Hereby, different processes were developed towards valorization of SSL using the industrial workhorse *C. glutamicum.*

In terms of substrate utilization, metabolic engineering to further optimize sugar utilization by evaluation of catabolic genes and transporters from other donors (Baritugo et al., 2018), and fine-tuned adjustment of gene expression (Li et al., 2022), can be expected to reach efficient and simultaneous utilization of all sugars. Additionally, the substrate spectrum of *C. glutamicum* MSU-8B could be further extended towards other raw materials and feedstocks (Baritugo et al., 2018). Given that lactose is composed of glucose and galactose, introducing lactose permease and β-galactosidase, which

mediate lactose uptake and breakdown (Brabetz et al., 1991), should enable complete utilization of lactose, providing cell factory to valorize whey, a waste product of the dairy industry, rich in lactose (Siso, 1996). Streamlining *C. glutamicum* to utilize glycerol, a main by-product from biodiesel industry, is promising to valorize crude glycerol (Rittmann et al., 2008). Engineering the mannitol catabolism, which makes up to 30% of dry weight in brown seaweeds, could open the use of seaweed biomass for third-generation biorefineries (Hoffmann et al., 2018; Hoffmann et al., 2021). Beside these units, direct utilization of polysaccharides, such as starch (Tateno et al., 2007a), cellulose (Tsuchidate et al., 2011), and hemicellulose (Yim et al., 2016), is of high interest to simplify overall process and reduce cost.

Another key field is production based on a broad substrate spectrum. Here, the glutarate production and pediocin PA-1 production have been demonstrated. In this regard, the streamlined sugar modules could be easily implemented to other value-added products derived from *C. glutamicum*, such as L-lysine (Eggeling and Bott, 2015; Wittmann and Becker, 2007), 5-aminovalerate (Rohles et al., 2022; Rohles et al., 2016), L-pipecolic acid (Pauli et al., 2023), ectoine (Becker et al., 2013; Giesselmann et al., 2019), hydroxyectoine (Jungmann et al., 2022), and diaminopentane (Kind et al., 2010). However, this straightforward ‘copy and paste’ strategy may result in undesirable product formation when using alternative substrates (Hoffmann et al., 2018). Without doubt, in-depth analysis of the metabolism from different substrates should be performed to gain a better understanding of the underlying mechanism towards optimal cell growth and product formation (Becker et al., 2011; Buschke et al., 2013a; Hoffmann et al., 2018), eventually yielding attractive *C. glutamicum* cell factories to efficiently produce a variety of products from a broad substrate spectrum. On this basis, the potential of industrial workhorse *C. glutamicum* could be fully exploited, realizing the biorefinery concept and achieving a more sustainable and economically friendly bio-production.

7 Appendix

7.1 Primers

Primers used in this work are listed in Table 7-1.

Table 7-1: Specific primers sequences used for the construction of the integrative transformation vectors.

Primer	Sequence	Plasmid
PeftumanA01	CTGCGTTAATTAACAATTGGTATTTCCGACCGCTTGGAAC	pClik int *sacB* P_{tuf}*manA*
PeftumanA02	CATTCGCAGGGTAACGGCCATTACAAGTCCTTTTCTTCAATGG	
PeftumanA03	CCATTGAAGAAAAGGACTTGTAATGGCCGTTACCCTGCGAATG	
PeftumanA04	GTGAGCCTTCCAATAGCTCCATTGTATGTCCTCCTGGACTTC	
PeftumanA05	GAAGTCCAGGAGGACATACAATGGAGCTATTGGAAGGCTCAC	
PeftumanA06	AATCCCGGGTCTAGAGGATCAGGGATTCTTCCTCGTTGTC	
PintxylA05	CTGCGTTAATTAACAATTGGCCACGTTGGAGTCTTTGG	pClik int *sacB* P_{tuf}*xylA*$_{Xc}$; pClik int *sacB* P_{tac}*xylA*$_{Xc}$
PintxylA06	TGAAAACGGTGTTGCTCATTGTATGTCCTCCTGGACTTC	
PintxylA07	GAAGTCCAGGAGGACATACAATGAGCAACACCGTTTTCA	
PintxylA08	TGTATGTCCTCCTGGACTTCTCAACGCGTCAGGTACTGAT	
PintxylA09	ATCAGTACCTGACGCGTTGAGAAGTCCAGGAGGACATACA	
PintxylA10	AATCCCGGGTCTAGAGGATCGTAGTAGCCCGTTCCAGAA	
PintxylA11	AGCCGATGATTAATTGTCAACTTAAAAATCCTCTTCCGTT	
PintxylA12	AACGGAAGAGGATTTTTAAGTTGACAATTAATCATCGGCT	
PintxylA13	TGTATGTCCTCCTGGACTTCCTAGTACCAACCCTGCGTTG	
Pintara01	CTGCGTTAATTAACAATTGGACCCTCACGATCGCATGTC	pClik int *sacB* Δ*iolR*; pClik int *sacB* int_*iolR*
PdeliolR01	GAATTATCCAATGCAACGCGTCTTCGAGGCGTTGGGCTACT	
PdeliolR02	AGTAGCCCAACGCCTCGAAGACGCGTTGCATTGGATAATTC	
PdeliolR03	AATCCCGGGTCTAGAGGATCTCTCCATCCGCTGGACCA	
PintiolR01	CATTCGCAGGGTAACGGCCATTACCTGGCCACCAGAGTGG	
PintiolR02	CCACTCTGGTGGCCAGGTAATGGCCGTTACCCTGCGAATG	
PintiolR03	AATCCCGGGTCTAGAGGATCGAGTGAGTAGCTCCAGTGGC	

7.2 Codon optimization

To optimize heterologous gene expression, codon optimization was conducted to adapt the codon usage of *C. glutamicum*. Codon optimization was performed by Biocat GmbH (Heidelberg, Germany) or GenScript Biotech (Rijswijk, Netherlands), using the company's bioinformatics algorithms, and sequences are shown in the following figures.

```
XylAXc_nt 1     ATGAGCAACACCGTTTTCATCGGCGCGAAAGAATACTTCCCCGGCATCGGCAAGATCGGCTTCGAAGGCCGCGATTCGGACAACCCGCTCGCATTCAAGGTGTACGACGC
XylAXc_co 1     ...TC.........C...........A..G..G........A.....................................C..T.....A..G...........C........

XylAXc_nt 111   CAACAAGCAGGTCGCCGGCAAGTCCATGGCCGAACACCTGCGCTTTGCGGTGGCCTACTGGCACAGCTTCTGCGGCAATGGCGCCGATCCGTTCGGCCCGGGCACGCGTG
XylAXc_co 111   T...........G..T..............A..............C..A.....A.........TC............C.....T..C..A........A.....C....

XylAXc_nt 221   CGTATCCGTGGGACGTAGGCAACACCGCGCTGGCGCGTGCCGAAGCCAAGTCCGATGCCGCGTTCGAATTCTTCACCAAGCTCGGCGTGCCGTATTACTGCTTTCACGAC
XylAXc_co 221   .A..C..A.....T..C...........A.....T..C..A..G..T...........A..T.....G.............G.....C..A..C........C.....T

XylAXc_nt 331   ATCGACCTGGCGCCGGATGCGGACGACATCGGCGAGTACGAAAACAACCTCAAGCACATGGTGCGCATTGCCAAGCAGCGCCAGGCCGACACCGGCGTCAAGCTGCTGTG
XylAXc_co 331   ...........A..A..C..A..T..T.......................G...........C.....C..A..............T.......................

XylAXc_nt 441   GGGCACCGCCAATCTGTTCTCGCACCCGCGCTACATGAATGGTGCCTCCACTAATCCGGACTTCAACGTCGTGGCGCGCGCCGCGGTGCAGGTCAAGGCGGCGATCGATG
XylAXc_co 441   .........A..C........C.....A...........C..C..A.....C..C..A..T........G.....T.....T..A..............A..T.......

XylAXc_nt 551   CCACGGTGGAGCTGGGCGGGGAAAACTACGTGTTCTGGGGCGGTCGCGAAGGCTACGCCTGCCTGCACAACACGCAAATGAAGCGCGAGCAGGACAACATGGCGCGCTTC
XylAXc_co 551   .T..C..C...........C.......................C.....G........A.....T........C..G...........A.....T........A......

XylAXc_nt 661   CTGACCCTGGCGCGCGACTACGGGCGTGCGATTGGCTTTACCGGCAACTTCCTGATCGAGCCCAAGCCCATGGAGCCGATGAAGCACCAGTACGACTTCGACAGCGCCAC
XylAXc_co 661   ...........A...........C..C..A..C.....C.....................A..A.....A........A.......................TTC...A..

XylAXc_nt 771   GGTGATCGGCTTCCTGCACCAGCACGGCCTGGACCAGGATTTCAAGCTCAATATCGAAGCCAACCACGCCACGCTGTCGGGCCACAGCTTCGAGCACGACCTGCAGGTGG
XylAXc_co 771   C..C.............................................G..C.....G..A........A..C.....C......TC............T........C.

XylAXc_nt 881   CCAGCGATGCCGGCCTGCTCGGCAGCATCGATGCCAACCGCGGCAACCCGCAGAACGGCTGGGATACCGACCAGTTCCCAACCGACCTGTACGACACCGTCGGCGCGATG
XylAXc_co 881   .TTC......A........G...TC.........T..............A.....................T..............T.....................T...

XylAXc_nt 991   CTGGTGGTGCTGCGTCAGGGCGGGCTGGCACCGGGCGGGCTGAACTTCGATGCCAAGGTGCGGCGTGAATCGTCCGACCCGCAGGACCTGTTCCTGGCCCACATCGGCGG
XylAXc_co 991   ........C.....C........C........A..T..T..T...........T.....C..C..C..G..C.....T..A.................A...........

XylAXc_nt 1101  CATGGACGCGTTCGCACGCGGGCTGGAAGTGGCCGACGCGCTGCTGACCTCTTCGCCCCTGGAAACCTGGCGCGCGCAGCGTTACGCCAGCTTCGACAGCGGCGCGGGCG
XylAXc_co 1101  .........A.....T.....C...........A..T..A...........C..C..A.................T.....C.....ATC.......TC......T....

XylAXc_nt 1211  CGGACTTTGCCAACGGCACCAGCACGCTGGCGGACCTGGCCAAGTACGCCGCCGGCAGGGGCGAGCCGACGCAAGTCAGCGGCCGCCAGGAGGCCTACGAGAACCTGATC
XylAXc_co 1211  .A.....C..T.........TC...C.....A..T.....A........T..T...C.C.....A..A..C..G..GTC...T........A..T..............

XylAXc_nt 1321  AATCAGTACCTGACGCGTTGA
XylAXc_co 1321  ..C...........C..C.A.
```

Figure 7-1: Alignment of the native *xylA_Xc_na* gene sequence from *X. campestris* pv. *campestris* ATCC33913 and the codon-optimized *xylA_Xc_co* gene sequence. The upper row represents the native *xylA_Xc_na* gene sequence from *X. campestris* pv. *campestris* ATCC33913, while the lower row represents the codon-optimized *xylA_Xc_co* gene sequence. Identical sequence was shown as '.', while the changed sequence was indicated as letters. The alignment was performed in Snapgene using local alignment (Smith-Waterman).

Figure 7-2: Alignment of the native *araA_Cg_na* gene sequence from *C. glutamicum* ATCC 31831 and the codon-optimized *araA_ Cg_co* gene sequence. The upper row represents the native *araA_Cg_na* gene sequence from *C. glutamicum* ATCC 31831, while the lower row represents the codon-optimized *araA_ Cg_co* gene sequence. Identical sequence was shown as '.', while the changed sequence was indicated as letters. The alignment was performed in Snapgene using local alignment (Smith-Waterman).

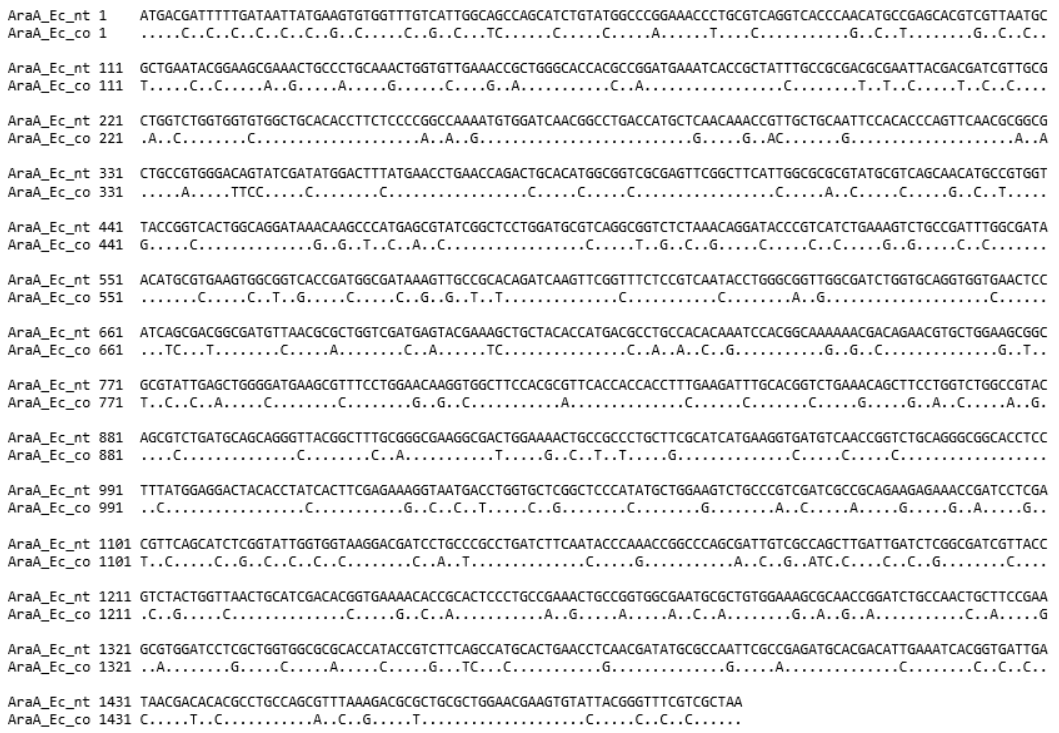

Figure 7-3: Alignment of the native *araA_Ec_na* gene sequence from *E. coli* MG1655 and the codon-optimized *araA_ Ec_co* gene sequence. The upper row represents the native *araA_Ec_na* gene sequence from *E. coli* MG1655, while the lower row represents the codon-optimized *araA_ Ec_co* gene sequence.

Identical sequence was shown as '.', while the changed sequence was indicated as letters. The alignment was performed in Snapgene using local alignment (Smith-Waterman).

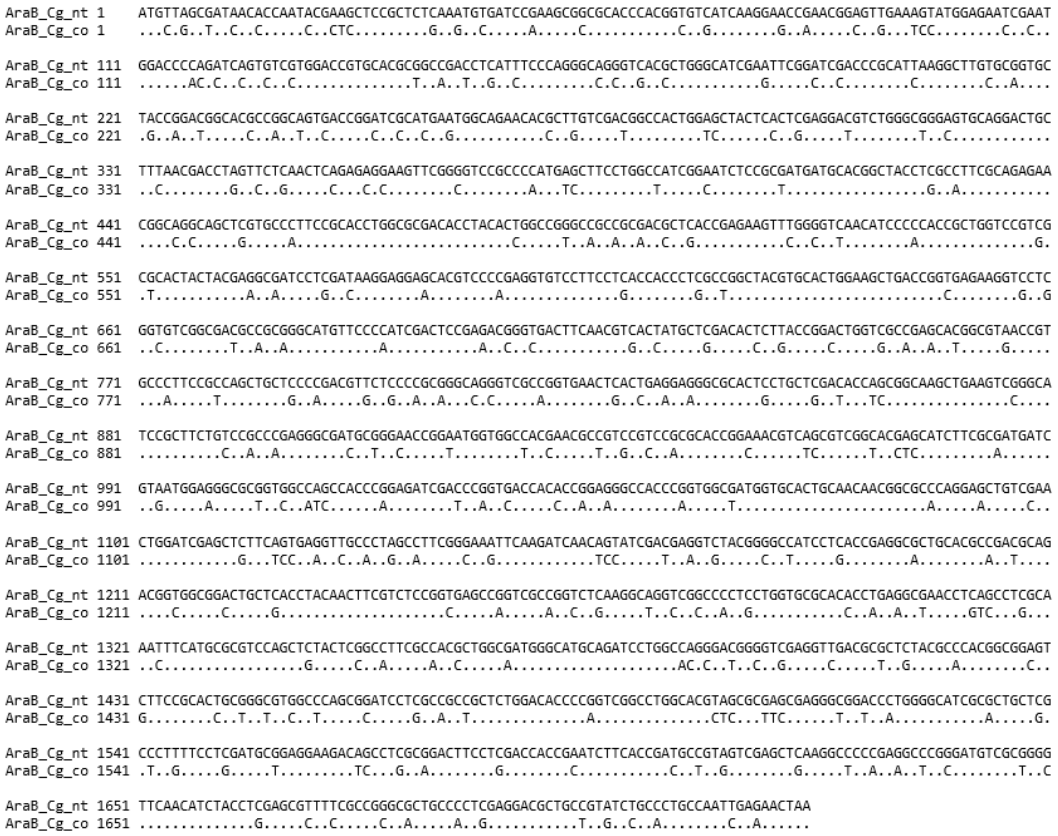

Figure 7-4: Alignment of the native *araB_Cg_na* gene sequence from *C. glutamicum* ATCC 31831 and the codon-optimized *araB_ Cg_co* gene sequence. The upper row represents the native *araB_Cg_na* gene sequence from *C. glutamicum* ATCC 31831, while the lower row represents the codon-optimized *araB_ Cg_co* gene sequence. Identical sequence was shown as '.', while the changed sequence was indicated as letters. The alignment was performed in Snapgene using local alignment (Smith-Waterman).

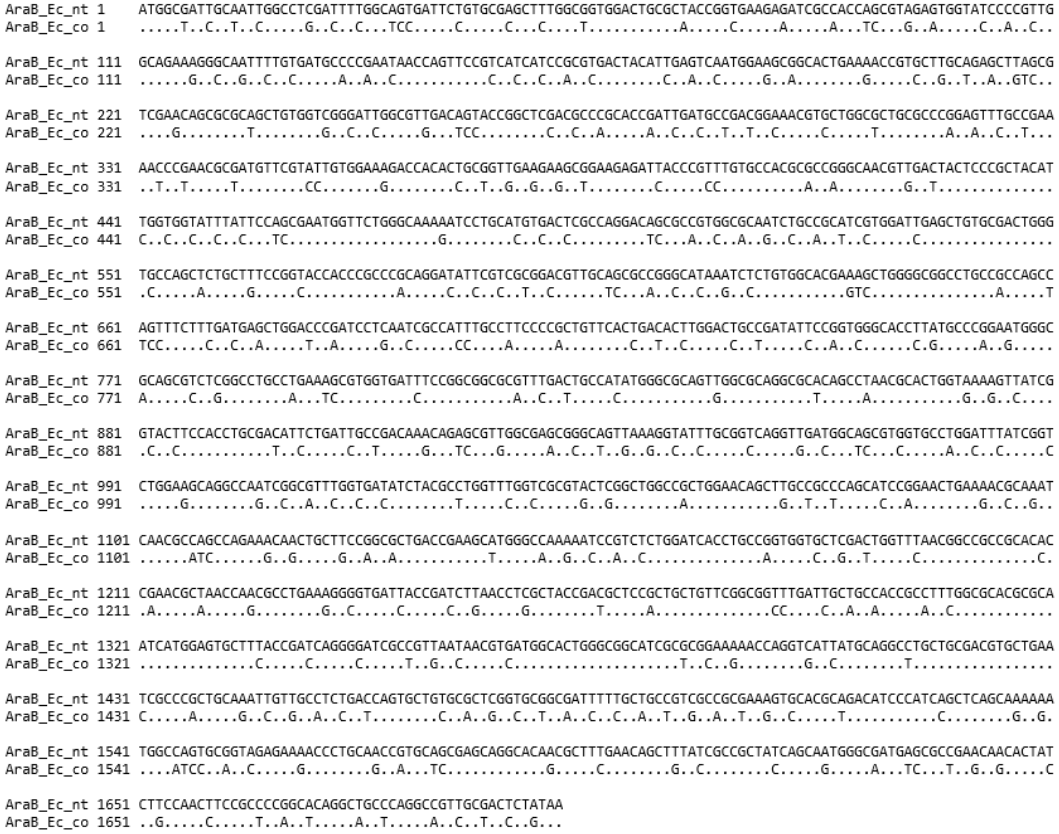

Figure 7-5: Alignment of the native *araB_Ec_na* gene sequence from *E. coli* MG1655 and the codon-optimized *araB_ Ec_co* gene sequence. The upper row represents the native *araB_Ec_na* gene sequence from *E. coli* MG1655, while the lower row represents the codon-optimized *araB_ Ec_co* gene sequence. Identical sequence was shown as '.', while the changed sequence was indicated as letters. The alignment was performed in Snapgene using local alignment (Smith-Waterman).

Figure 7-6: Alignment of the native *araD_Cg_na* gene sequence from *C. glutamicum* ATCC 31831 and the codon-optimized *araD_ Cg_co* gene sequence. The upper row represents the native *araD_Cg_na* gene sequence from *C. glutamicum* ATCC 31831, while the lower row represents the codon-optimized *araD_ Cg_co* gene sequence. Identical sequence was shown as '.', while the changed sequence was indicated as letters. The alignment was performed in Snapgene using local alignment (Smith-Waterman).

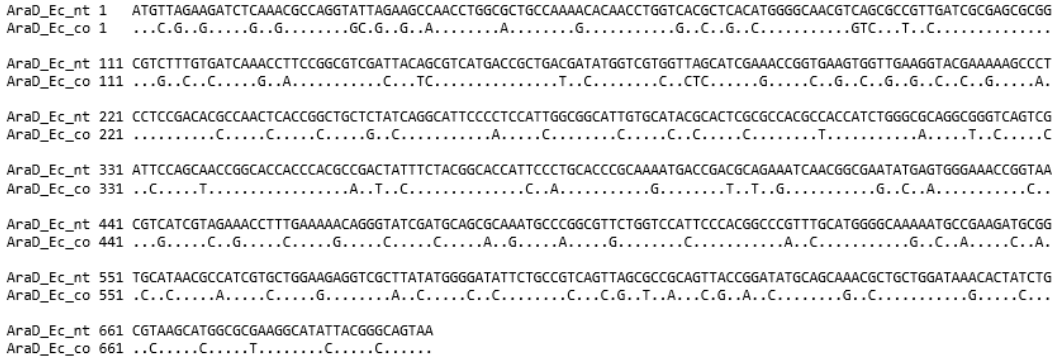

Figure 7-7: Alignment of the native *araD_Ec_na* gene sequence from *E. coli* MG1655 and the codon-optimized *araD_ Ec_co* gene sequence. The upper row represents the native *araD_Ec_na* gene sequence from *E. coli* MG1655, while the lower row represents the codon-optimized *araD_ Ec_co* gene sequence. Identical sequence was shown as '.', while the changed sequence was indicated as letters. The alignment was performed in Snapgene using local alignment (Smith-Waterman).

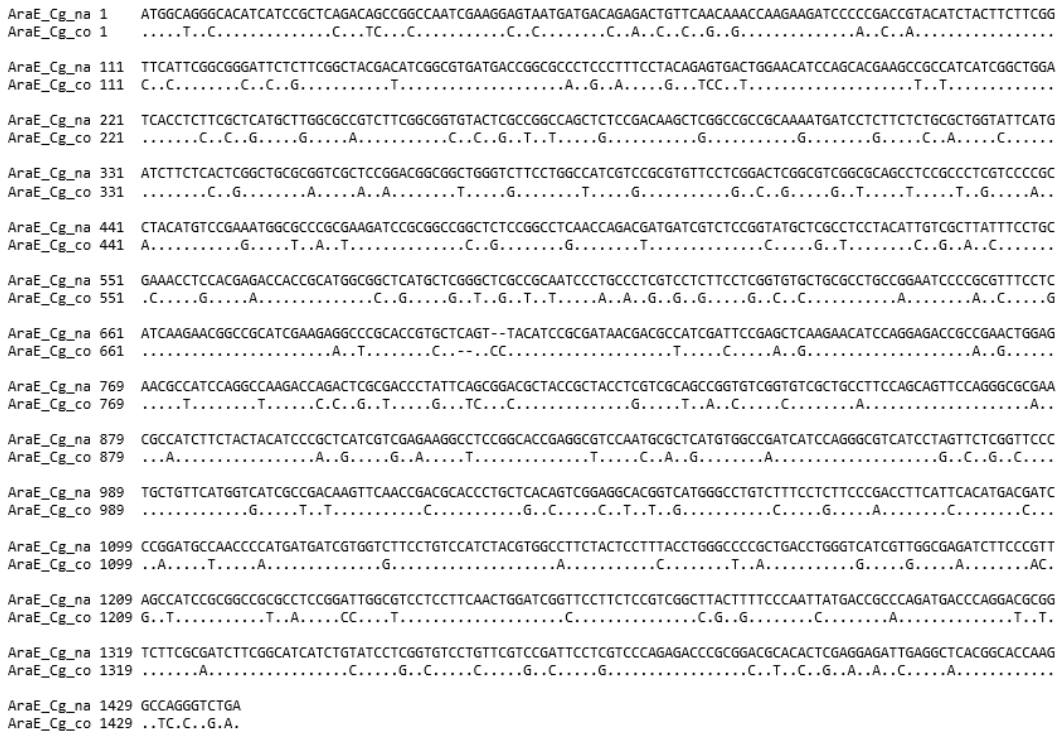

Figure 7-8: Alignment of the native *araE_Cg_na* gene sequence from *C. glutamicum* ATCC 31831 and the codon-optimized *araE_ Cg_co* gene sequence. The upper row represents the native *araE_Cg_na* gene sequence from *C. glutamicum* ATCC 31831, while the lower row represents the codon-optimized *araE_ Cg_co* gene sequence. Identical sequence was shown as '.', while the changed sequence was indicated as letters. The alignment was performed in Snapgene using local alignment (Smith-Waterman).

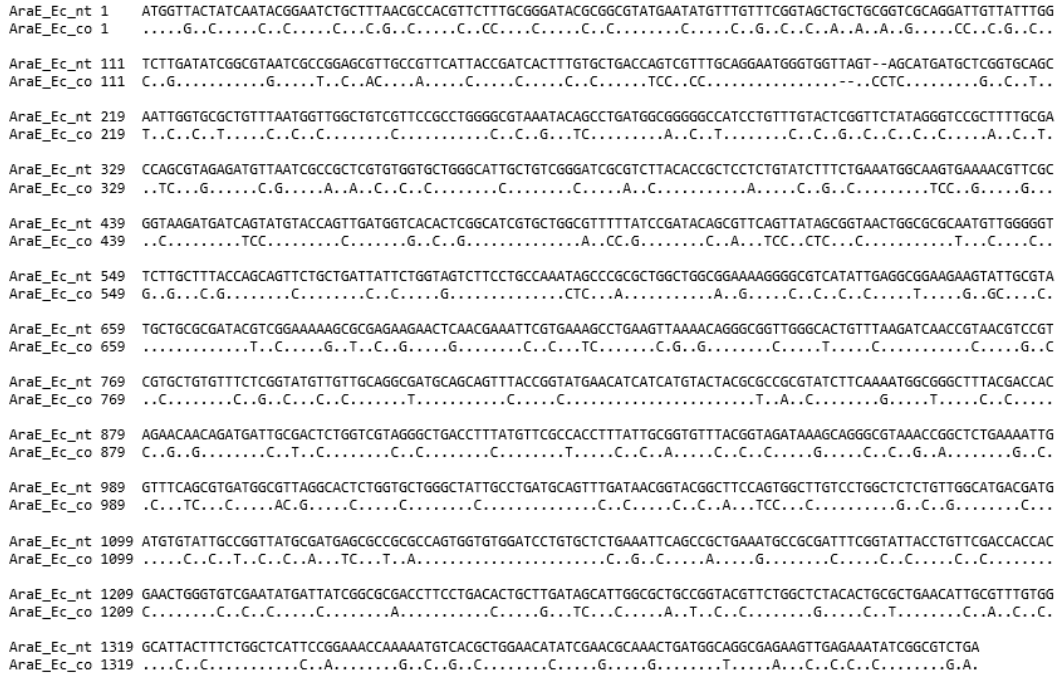

Figure 7-9: Alignment of the native *araE_Ec_na* gene sequence from *E. coli* MG1655 and the codon-optimized *araE_ Ec_co* gene sequence. The upper row represents the native *araE_Ec_na* gene sequence from *E. coli* MG1655, while the lower row represents the codon-optimized *araE_ Ec_co* gene sequence. Identical sequence was shown as '.', while the changed sequence was indicated as letters. The alignment was performed in Snapgene using local alignment (Smith-Waterman).

Figure 7-10: Alignment of the native *galE_Ll_na* gene sequence from *L. lactis* subsp. *cremoris* MG1363 and the codon-optimized *galE_Ll_co* gene sequence. The upper row represents the native *galE_Ll_na* gene sequence from *L. lactis* subsp. *cremoris* MG1363, while the lower row represents the codon-optimized *galE_Ll_co* gene sequence. Identical sequence was shown as '.', while the changed sequence was indicated as letters. The alignment was performed in Snapgene using local alignment (Smith-Waterman).

Figure 7-11: Alignment of the native *galM_Ll_na* gene sequence from *L. lactis* subsp. *cremoris* MG1363 and the codon-optimized *galM_Ll_co* gene sequence. The upper row represents the native *galM_Ll_na* gene sequence from *L. lactis* subsp. *cremoris* MG1363, while the lower row represents the codon-optimized *galM_Ll_co* gene sequence. Identical sequence was shown as '.', while the changed sequence was indicated as letters. The alignment was performed in Snapgene using local alignment (Smith-Waterman).

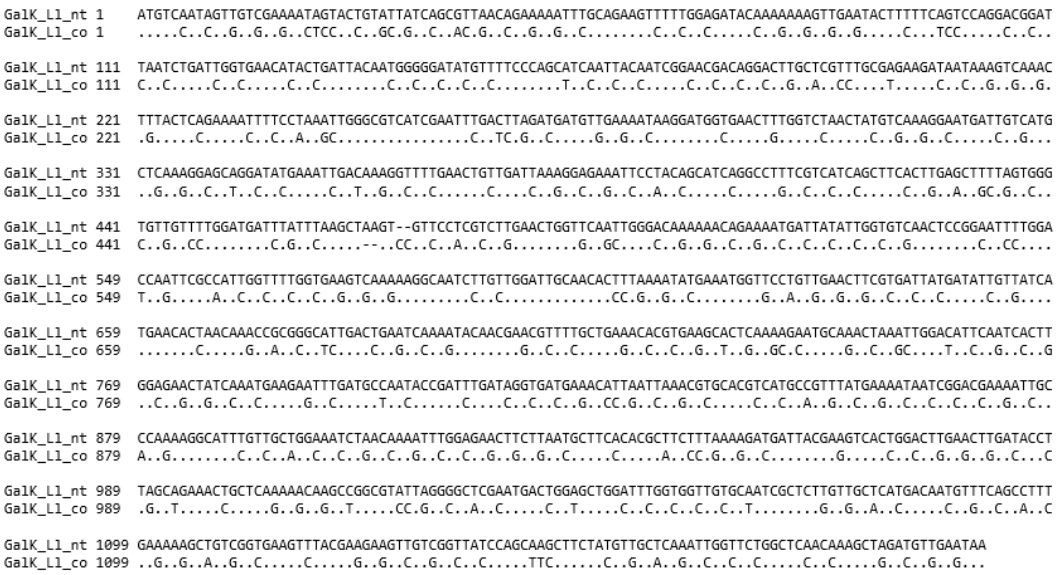

Figure 7-12: Alignment of the native *galK_Ll_na* gene sequence from *L. lactis* subsp. *cremoris* MG1363 and the codon-optimized *galK_Ll_co* gene sequence. The upper row represents the native *galK_Ll_na* gene sequence from *L. lactis* subsp. *cremoris* MG1363, while the lower row represents the codon-optimized *galK_Ll_co* gene sequence. Identical sequence was shown as '.', while the changed sequence was indicated as letters. The alignment was performed in Snapgene using local alignment (Smith-Waterman).

Figure 7-13: Alignment of the native *galP_Ll_na* gene sequence from *L. lactis* subsp. *cremoris* MG1363 and the codon-optimized *galP_Ll_co* gene sequence. The upper row represents the native *galP_Ll_na* gene sequence from *L. lactis* subsp. *cremoris* MG1363, while the lower row represents the codon-optimized *galP_Ll_co* gene sequence. Identical sequence was shown as '.', while the changed sequence was indicated as letters. The alignment was performed in Snapgene using local alignment (Smith-Waterman).

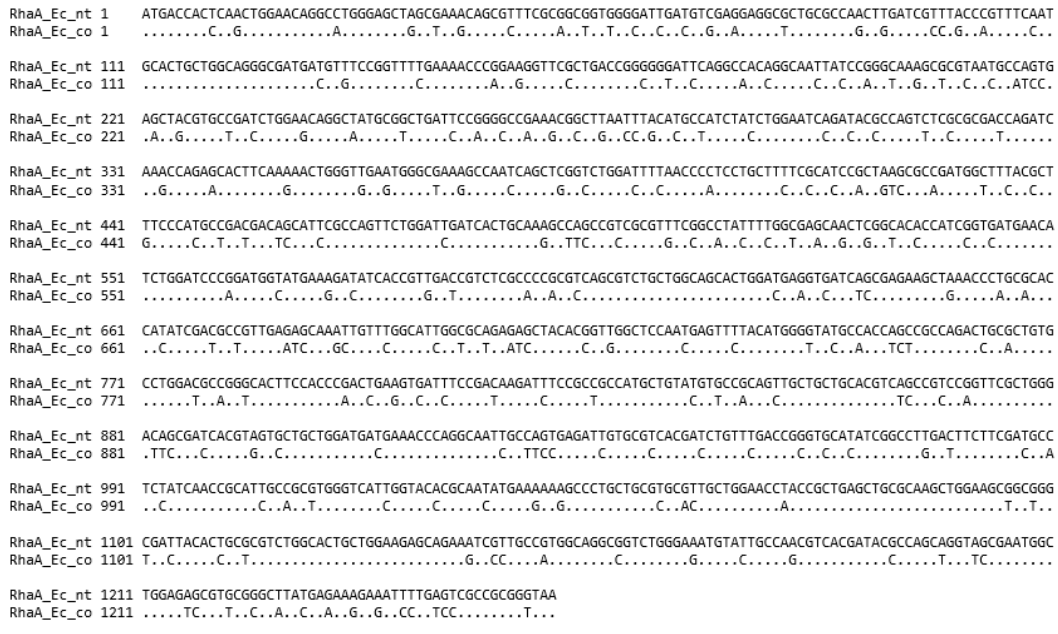

Figure 7-14: Alignment of the native *rhaA_Ec_na* gene sequence from *E. coli* MG1655 and the codon-optimized *rhaA_Ec_co* gene sequence. The upper row represents the native *rhaA_Ec_na* gene sequence from *E. coli* MG1655, while the lower row represents the codon-optimized *rhaA_Ec_co* gene sequence. Identical sequence was shown as '.', while the changed sequence was indicated as letters. The alignment was performed in Snapgene using local alignment (Smith-Waterman).

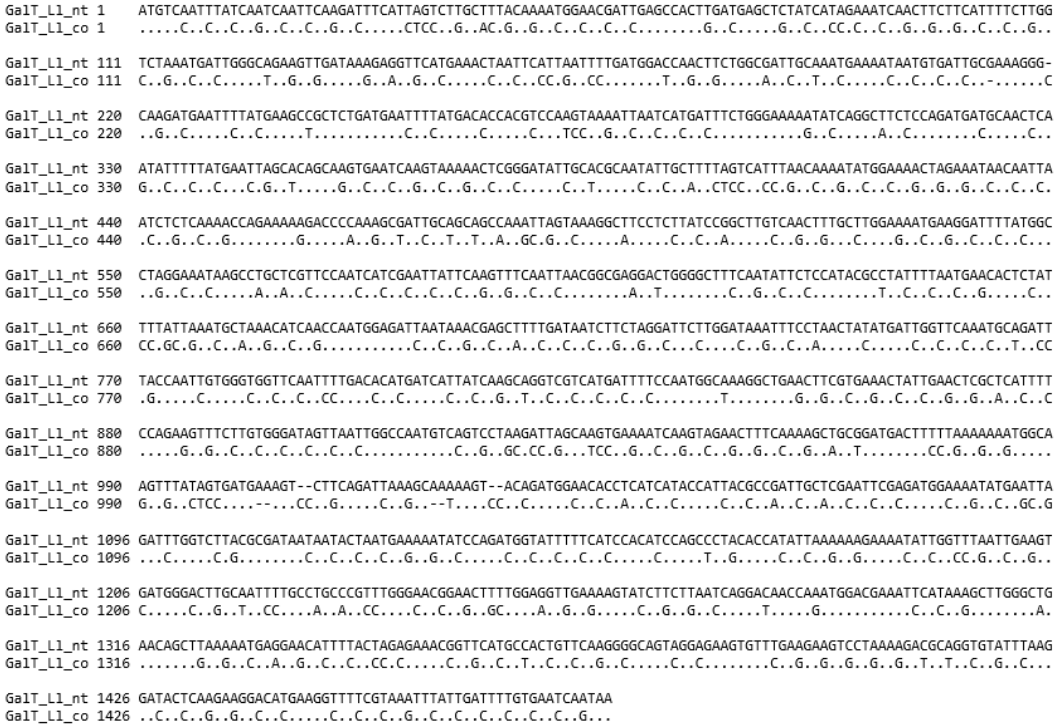

Figure 7-15: Alignment of the native *galT_Ll_na* gene sequence from *L. lactis* subsp. *cremoris* MG1363 and the codon-optimized *galT_Ll_co* gene sequence. The upper row represents the native *galT_Ll_na* gene sequence from *L. lactis* subsp. *cremoris* MG1363, while the lower row represents the codon-optimized *galT_Ll_co* gene sequence. Identical sequence was shown as '.', while the changed sequence was indicated as letters. The alignment was performed in Snapgene using local alignment (Smith-Waterman).

Figure 7-16: Alignment of the native *rhaD_Ec_na* gene sequence from *E. coli* MG1655 and the codon-optimized *rhaD_Ec_co* gene sequence. The upper row represents the native *rhaD_Ec_na* gene sequence from *E. coli* MG1655, while the lower row represents the codon-optimized *rhaD_Ec_co* gene sequence. Identical sequence was shown as '.', while the changed sequence was indicated as letters. The alignment was performed in Snapgene using local alignment (Smith-Waterman).

Figure 7-17: Alignment of the native *rhaB_Ec_na* gene sequence from *E. coli* MG1655 and the codon-optimized *rhaB_Ec_co* gene sequence. The upper row represents the native *rhaB_Ec_na* gene sequence from *E. coli* MG1655, while the lower row represents the codon-optimized *rhaB_Ec_co* gene sequence. Identical sequence was shown as '.', while the changed sequence was indicated as letters. The alignment was performed in Snapgene using local alignment (Smith-Waterman).

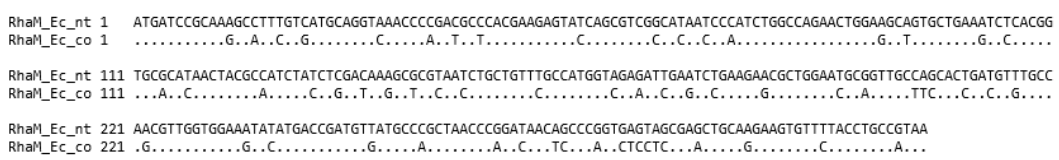

Figure 7-18: Alignment of the native *rhaM_Ec_na* gene sequence from *E. coli* MG1655 and the codon-optimized *rhaM_Ec_co* gene sequence. The upper row represents the native *rhaM_Ec_na* gene sequence from *E. coli* MG1655, while the lower row represents the codon-optimized *rhaM_Ec_co* gene sequence. Identical sequence was shown as '.', while the changed sequence was indicated as letters. The alignment was performed in Snapgene using local alignment (Smith-Waterman).

Figure 7-19: Alignment of the native *rhaT_Ec_na* gene sequence from *E. coli* MG1655 and the codon-optimized *rhaT_Ec_co* gene sequence. The upper row represents the native *rhaT_Ec_na* gene sequence from *E. coli* MG1655, while the lower row represents the codon-optimized *rhaT_Ec_co* gene sequence. Identical sequence was shown as '.', while the changed sequence was indicated as letters. The alignment was performed in Snapgene using local alignment (Smith-Waterman).

7.3 Detoxification of furfural, 5-HMF, and sulfite by *C. glutamicum*

To characterize the inhibitory effects of inhibitors contained in SSL on *C. glutamicum*, growth tests in the presence of furfural, 5-HMF, and sulfite were conducted. In this regard, the wild type *C. glutamicum* ATCC 13032 was cultivated in shake flasks using minimal medium with glucose as substrate, adding 10 mM furfural, 10 mM 5-HMF, and 30 mM sulfite, respectively. Meanwhile, the experiments were also performed under abiotic conditions where *C. glutamicum* cells were not inoculated. This experiment was conducted by Dr.-Ing. Susanne Schwechheimer.

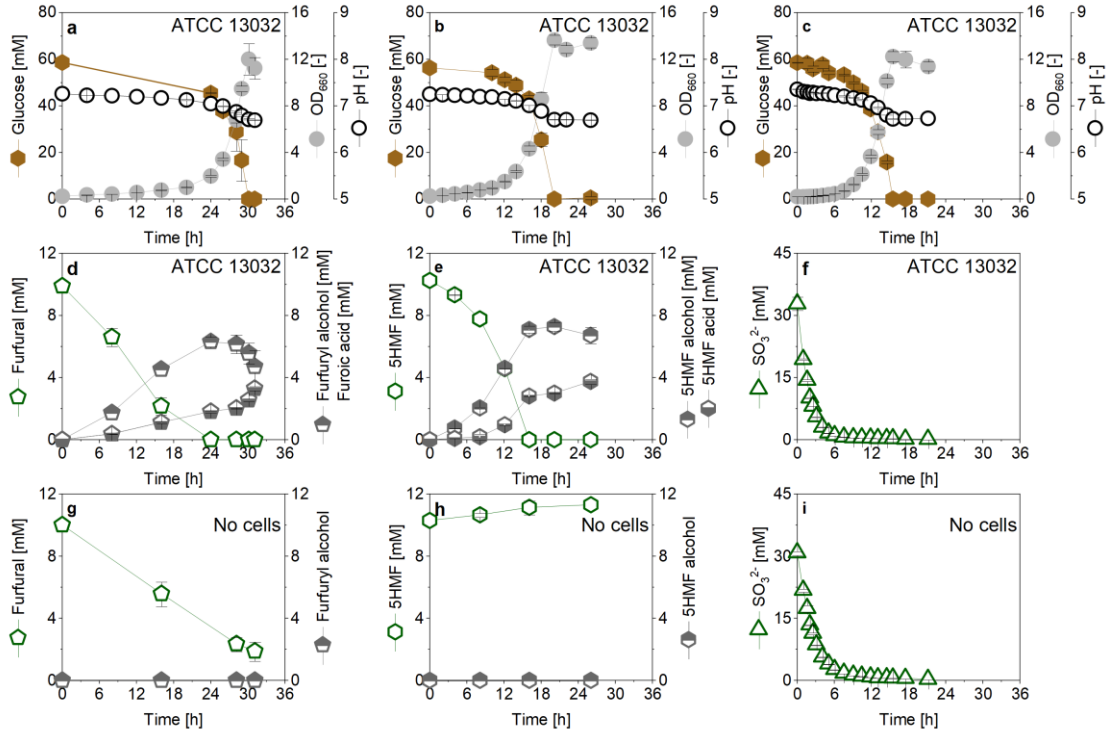

Figure 7-20: The growth test of *C. glutamicum* ATCC 13032 in the presence of 10 mM furfural (**a**, **d**), 10 mM 5-HMF (**b**, **e**), and 30 mM sulfite (**c**, **f**), respectively, in shake flasks using minimal medium with 10 g L^{-1} glucose as substrate. The degradation of furfural (**g**), 5-HMF (**h**), and sulfite (**i**), respectively, under abiotic conditions where no *C. glutamicum* cells were added. The data comprise mean values and standard errors from three biological replicates.

7.4 Calculation of specific consumption rate on synthetic sugar mixture

To evaluate the utilization characteristics of each sugar on synthetic sugar mixture, two phases were defined: phase I is glucose phase from the beginning of cultivation until the last time point that glucose is still present in the medium; phase II is non-glucose phase from the time point that glucose is fully consumed until the end of cultivation, and a specific consumption rate of each sugar on each phase was calculated as shown below.

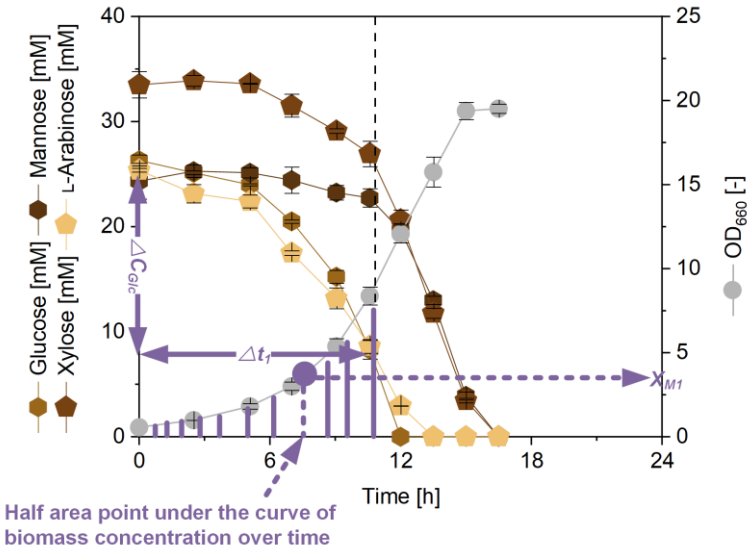

Figure 7-21: Example to calculate the glucose specific consumption rate in phase I. The vertical dashed line indicates the time point of glucose depletion. $\triangle C_{Glc}$ (mmol L^{-1}) represents the consumed glucose concentration in phase I, $\triangle t_1$ (h) represents the cultivation time during phase I, X_{M1} (g L^{-1}) represents the mean biomass concentration in phase I (the corresponding biomass concentration is obtained via multiplication of the optical density value in the plot by a factor of 0.32).

The volumetric glucose consumption rate Q_{V_Glc} (mmol L^{-1} h^{-1}) in phase I was first calculated based on Eq. 1.

$$Q_V = \frac{\Delta C}{\Delta t} \qquad \text{(Eq. 1)}$$

Then, the mean biomass concentration X_{M1} (g L^{-1}) is calculated when the biomass concentration that reaches half of the area under the curve of biomass concentration over cultivation time in phase I using polynomial trend line.

Last, the glucose specific consumption rate Q_{S_Glc} (mmol g^{-1} h^{-1}) in phase I was calculated based on Eq. 2.

$$Q_S = \frac{Q_V}{X_M} \qquad \text{(Eq. 2)}$$

The corresponding sugar C-molar rate (C-mmol g^{-1} h^{-1}) is obtained by multiplication of a factor of 6 or 5.

7.5 The genomic layout of the created *C. glutamiucm* strain family

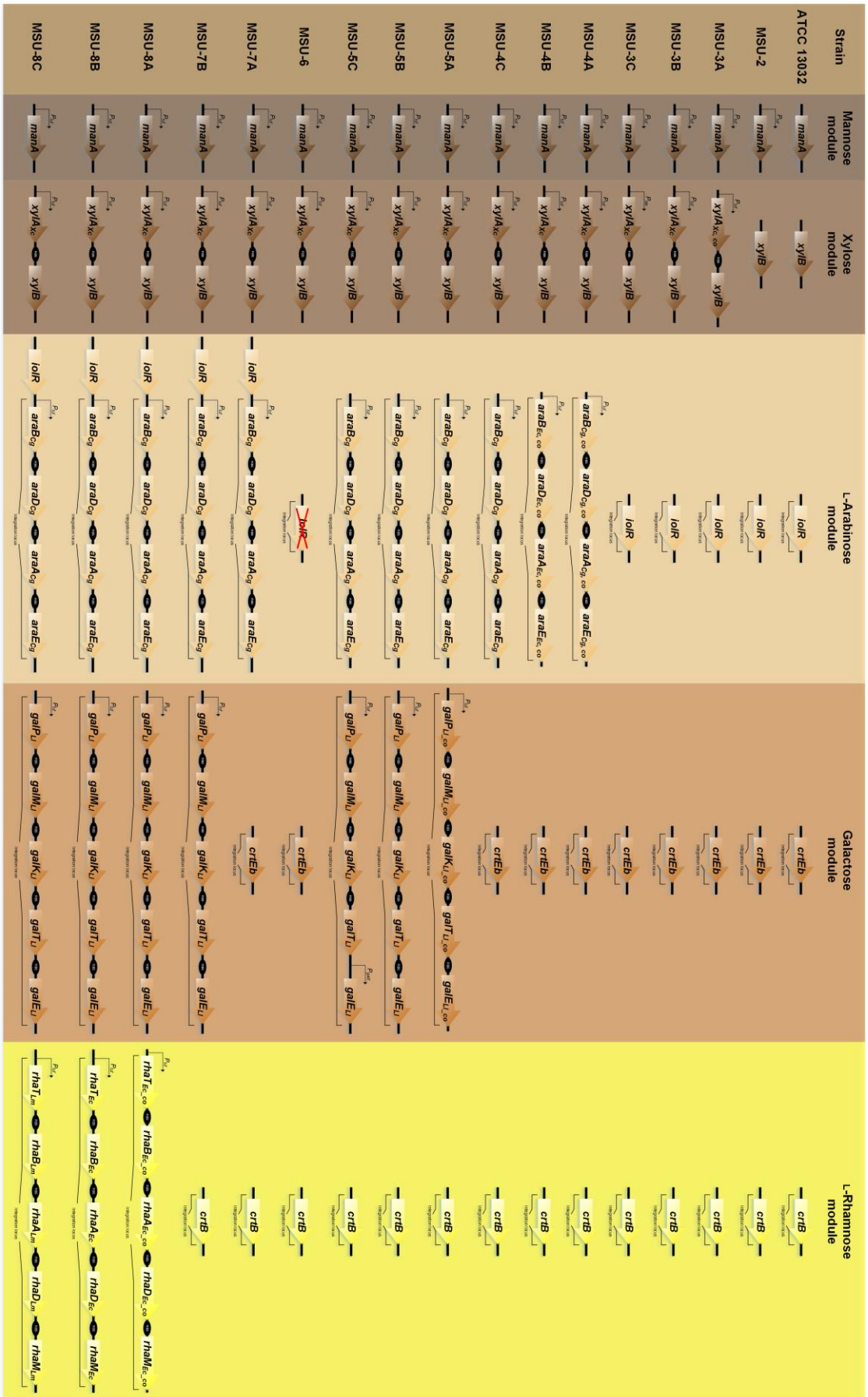

Figure 7-22: The figure shows the genomic layout of the created genome-based *C. glutamicum* strain family. The mannose module comprised overexpression of *manA* under control of the *tuf* promoter (Pt_{uf} *manA*). The three heterologous xylose modules using $xylA_{Xc}$ gene from *X. campestris* were integrated upstream of the native *xylB* locus: (i) P_{tuf} $xylA_{Xc,\ co}$ included the codon-optimized (co) version $xylA_{Xc,\ co}$ under control of the *tuf* promoter, (ii) P_{tuf} $xylA_{Xc}$ contained the native $xylA_{Xc}$ gene under control of the *tuf* promoter, and (iii) P_{tac} $xylA_{Xc}$ based on the native $xylA_{Xc}$ under control of the IPTG-inducible *tac* promoter. The three L-arabinose catabolic operons were installed in the *iolR* locus: (i) codon optimized version of P_{tuf} $araBDAE_{Cg,\ co}$ from *C. glutamicum* ATCC 31831, (ii) L-arabinose operon P_{tuf} $araBDAE_{Ec,\ co}$ from *E. coli* in codon-optimized form, and (iii) native codon usage P_{tuf} $araBDAE_{Cg}$ from *C. glutamicum* ATCC 31831. The three heterologous galactose modules from *L. lactis* was integrated into the *crtEb* locus: (i) codon optimized version of P_{tuf} $galPMKTE_{Ll,\ co}$, (ii) native codon usage P_{tuf} $galPMKTE_{Ll}$, and (iii) bicistronic design P_{tuf} $galPMKT_{Ll}$ P_{galE} $galE_{Ll}$ where *galE* gene was expressed under its native promotor. IolR was recovered in its original locus due to its importance for efficient sugar metabolization (P_{tuf} $araBDAE_{Cg}$). The three L-rhamnose catabolic operons was implemented into the into the *crtB* locus: (i) codon optimized version of P_{tuf} $rhaTBADM_{Ec,\ co}$ from *E. coli*, (ii) native codon usage P_{tuf} $rhaTBADM_{Ec}$ from *E. coli*, and (iii) native codon usage P_{tuf} $rhaTBADM_{Lm}$ from *L. monocytogenes*. All the genetic constructs were stably integrated into the genome of *C. glutamicum*, making all strains fully genome-based, plasmid-free cell factories.

7.6 Separation results using flash and preparative ion exchange chromatography

The separation results of SSL samples using preparative ion exchange chromatography were shown below. The experiment was conducted by Melanie Fox from MyBiotech GmbH (Überherrn, Germany).

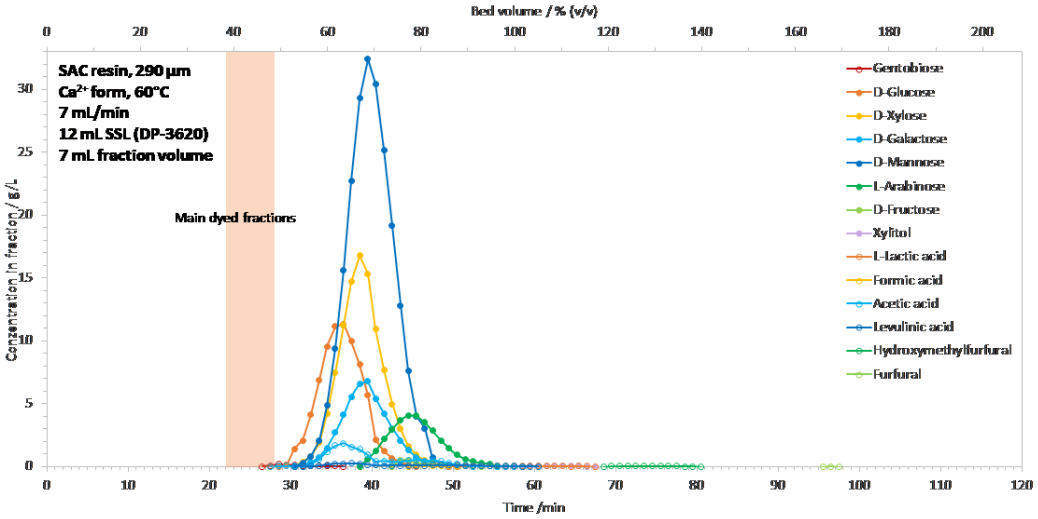

Figure 7-23: Ion exchange chromatography of pure SSL-UF sample using Lewatit MDS 1268 Ca290.

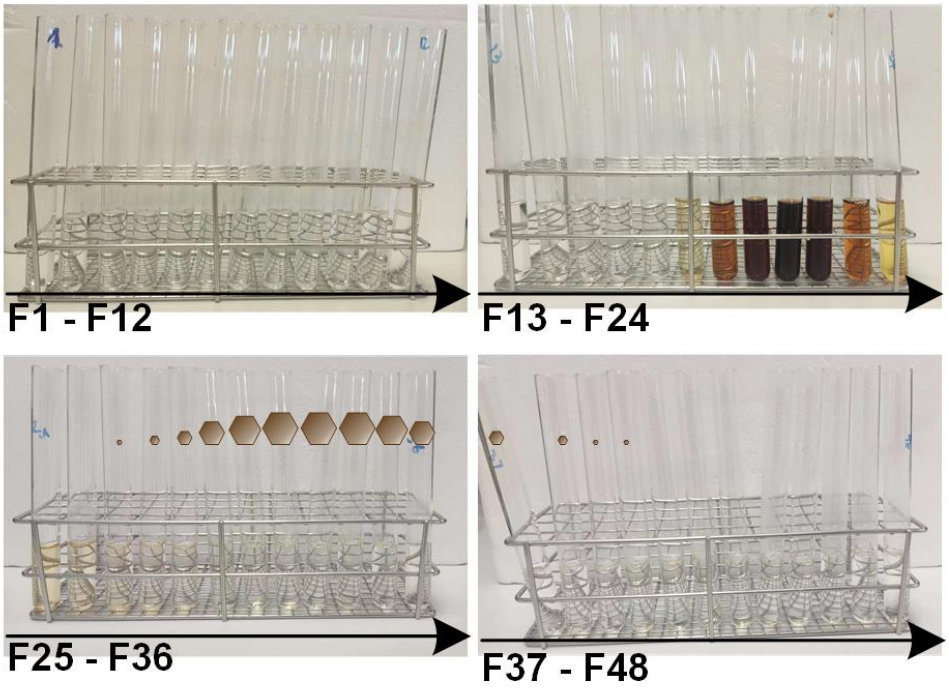

Figure 7-24: Collected fractions F1 – F48 using preparative ion exchange chromatography to separate mannose from fermentation broth sample of the strain MAN-2. Hexagons represent mannose, which was contained in collected fractions, where the area of hexagons represents the concentration of mannose as shown in Figure 7-25. Similar separation patterns were observed for SSL-UF samples, where the colourless fractions were collected over the first 17 minutes, brownish compounds from the SSL were eluted between 18-28 minutes, and the later eluting liquid became clear again.

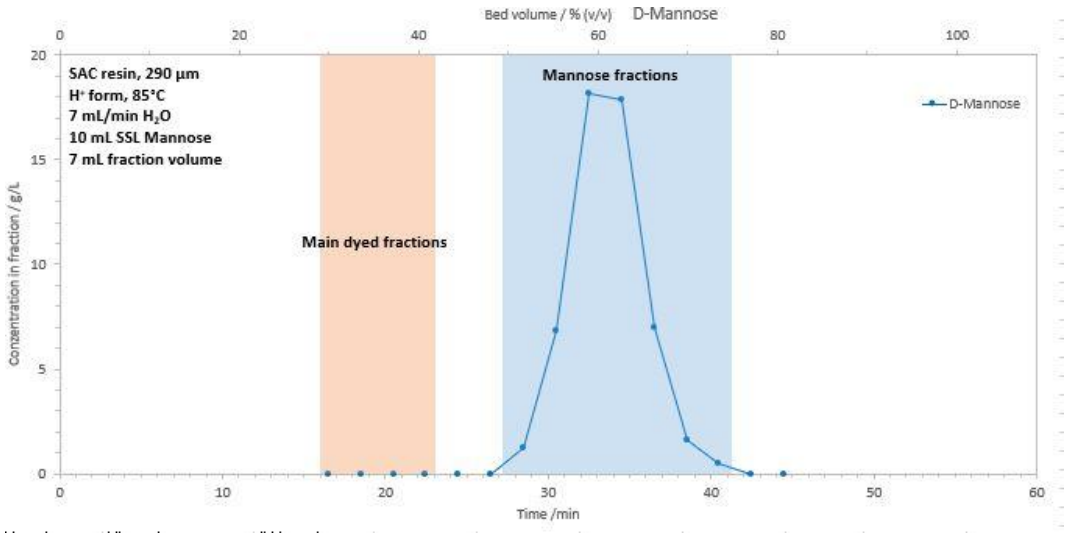

Figure 7-25: Ion exchange chromatography of fermentation broth sample of the strain MAN-2.

8 Abbreviations and Symbols

Abbreviations

Ack	ATP-dependent acetate kinase
AcsA	Acetyl-CoA synthetase
Amy	α-Amylase
AraA	Arabinose isomerase
AraB	Ribulokinase
AraD	Ribulose-5-phosphate 4-epimerase
AraE	Arabinose-proton symporter
araR	Gene, encoding repressor of the arabinose catabolic genes
ATCC	American Type Culture Collection
AVA	5-Aminovalerate
BglA	Phospho-β-glucosidase
BglF	β-Glucoside-specific permease
BHI	Brain heart infusion
BHI++	Brain heart infusion with $(NH4)_2SO_4$ and glucose
BHIS	Brain heart infusion with sorbitol
BSTFA	N, O-Bis(trimethylsilyl)trifluoroacetamide
CBP	Consolidated bioprocessing
CbpA	Scaffolding protein
CDW	Cell dry weight
CelE	Endoglucanase
CM	Complex medium
co	Codon-optimized
crtB	Gene, encoding phytoene synthase
crtEb	Gene, encoding lycopene elongase
dapB	Gene, encoding dihydrodipicolinate reducatase
DavA	5-Aminovaleramide amidase
DavB	Lysine 2-monooxygenase
DavD	Glutarate semialdehyde dehydrogenase
DavT	5-Aminovalerate aminotransferase
ddh	Gene, encoding diaminopimelate dehydrogenase
DHB	3,4-Dihydroxybenzoic acid
Dld	Quinone-dependent D-Lactate dehydrogenase
DMSO	Dimethyl sulfoxide
DNA	Deoxyribonucleic acid
dNTP	Deoxynucleoside triphosphate
DSMZ	Deutsche Sammlung von Mikroorganismen und Zellkulturen
DTT	Dithiothreitol
EDTA	Ethylenediaminetetraacetic acid
ELSD	Evaporative light scattering detector
EMP	Embden–Meyerhof–Parnas
FAO	Food and Agriculture Organization
fbp	Gene, encoding fructose 1, 6-bisphosphatase
FDA	Food and Drug Administration

gabD	Gene, encoding Glutarate semialdehyde dehydrogenase
gabP	Gene, encoding γ-aminobutyrate permease
gabT	Gene, encoding 5-aminovalerate transaminase
GalE	UDP-glucose 4-epimerase
GalK	Galactokinase
GalM	Aldose 1-epimerase
GalP	Galactose permease
GalT	Hexose-1-phosphate uridylyltransferase
GC-MS	Gas chromatography–mass spectrometry
Glk	Glucokinase
GlpD	Glycerol 3-phosphate dehydrogenase
GlpF	Glycerol transport facilitator
GlpK	Glycerokinase
GMO	Genetically modified organism
gnd	Gene, encoding 6-phosphogluconate dehydrogenase
GRAS	Generally recognized as safe
HMF	5-Hydroxymethylfurfural
hom	Gene, encoding homeserine dehydrogenase
HPLC	High-performance liquid chromatography
HPr	Histidine-containing phosphocarrier protein
icd	Gene, encoding isocitrate dehydrogenase
IMxyl	Xylose symporter
iolR	Gene, encoding transcriptional regulator
IolT1	Myo-inositol transporter 1
IolT2	Myo-inositol transporter 2
IPTG	Isopropyl β-D-1-thiogalactopyranoside
IS	Internal standard
kan^R	kanamycin resistance
LAB	Lactic acid bacteria
LacS	Lactose permease
LacY	Lactose permease
LacZ	β-Galactosidase
ldh	Gene, encoding NAD^+-dependent lactate dehydrogenase
LldD	Quinone-dependent L-lactate dehydrogenase
lysA	Gene, encoding diaminopimelate decarboxylase
lysC	Gene, encoding aspartate kinase
lysE	Gene, encoding lysine permease
MalE	Malic enzyme
ManA	Mannose-6-phosphate isomerase
MctC	Monocarboxylic acid transporter
MSTFA	N-methyl-N-(trimethylsilyl)trifluoroacetamide
MtlD	Mannitol-2-dehydrogenase
mtlR	Gene, encoding autoregulatory transcriptional repressor
MtlT	Mannitol transporter
NAD(P)	Nicotinamide adenine dinucleotide (phosphate), oxidized
NAD(P)H	Nicotinamide adenine dinucleotide (phosphate), reduced
OD	Optical density

OPA	O-Phthalaldehyde
ORI	Origin of replication
pck	Gene, encoding phophpenolpyruvate carboxykinase
PCR	Polymerase chain reaction
pedA	Gene for ribosomal synthesis of pre-pediocin
pedB	Gene, encoding immunity protein
pedC	Gene for processing, cleavage and secretion of mature pediocin
pedD	Gene for processing, cleavage and secretion of mature pediocin
PfkA	6-Phosphofructokinase
PfkB	1-Phosphofructokinase
Pgi	Phosphoglucose isomerase
Pgm	Phosphoglucomutase
PHB	Polyhydroxybutyrate
PLA	Polylactic acid
PP	Pentose Phosphate
Pta	Phosphotransacetylase
PTS	Phosphotransferase system
ptsF	Gene, encoding fructose transporter
PTSFru	Fructose-specific phosphotransferase system
ptsG	Gene, encoding glucose transporter
PTSGlc	Glucose-specific phosphotransferase system
ptsH	Gene, encoding phosphocarrier protein HPr
PTSSuc	Sucrose-specific phosphotransferase system
pyc	Gene, encoding pyruvate carboxylase
RBS	Ribosomal binding site
RhaA	Rhamnose isomerase
RhaB	Rhamnulokinase
RhaD	Rhamnulose 1-phosphate aldolase
RhaM	Rhamnose mutarotase
RhaT	Rhamnose-proton symporter
Rpe	Ribulose-5-phosphate-3-epimerase
Rpi	Ribose 5-phosphate isomerase
sacB	Gene, encoding levansucrase
ScrB	Sucrose-6-phosphate hydrolase
ScrK	Fructokinase
SSL	Spent sulfite liquor
SSL UF	Spent sulfite liquor ultrafiltration
SugR	Transcriptional regulator
TAE	Buffer containing of Tris, acetic acid and EDTA
Tal	Transaldolase
tet^R	tetracycline resistance
Tkt	Transketolase
tkt-operon	Genes, encoding transketolase operon
tuf	Gene, encoding elongation factor tu
UDP	Uridine diphosphate
UTI	Urinary Tract Infection
xdh	Gene, encoding xylose dehydrogenase

XDH	Xylitol dehydrogenase
XI	Xylose isomerase
XK	Xylulokinase
XlnA	Endoxylanase
XR	Xylose reductase
XylA	Xylose isomerase
XylB	Xylulokinase
xylC	Gene, encoding xylonolactonase
xylE	Gene, encoding xylose-proton symporter
xylXABCD-operon	Genes, encoding enzymes for Weimberg pathway
XynB	Xylosidase
zwf	Gene, encoding glucose-6-phosphate dehydrogenase

Symbols

μ	Specific growth rate
C	Substrate concentration
Q_S	Specific substrate consumption rate
Q_V	Volumetric substrate consumption rate
t	Time
X_M	Mean biomass concentration
$Y_{X/S}$	Biomass yield

9 References

Aasen, I. M., Moretro, T., Katla, T., Axelsson, L., Storro, I. (2000). Influence of complex nutrients, temperature and pH on bacteriocin production by *Lactobacillus sakei* CCUG 42687. *Appl Microbiol Biotechnol*, 53, 159-66.

Adachi, N., Takahashi, C., Ono-Murota, N., Yamaguchi, R., Tanaka, T., Kondo, A. (2013). Direct L-lysine production from cellobiose by *Corynebacterium glutamicum* displaying beta-glucosidase on its cell surface. *Appl Microbiol Biotechnol*, 97, 7165-72.

Adkins, J., Jordan, J., Nielsen, D. R. (2013). Engineering *Escherichia coli* for renewable production of the 5-carbon polyamide building-blocks 5-aminovalerate and glutarate. *Biotechnol Bioeng*, 110, 1726-34.

Alexandri, M., Papapostolou, H., Stragier, L., Verstraete, W., Papanikolaou, S., Koutinas, A. A. (2017). Succinic acid production by immobilized cultures using spent sulphite liquor as fermentation medium. *Bioresour Technol*, 238, 214-222.

Almeida, J. R., Modig, T., Petersson, A., Hähn-Hägerdal, B., Lidén, G., Gorwa-Grauslund, M. F. (2007). Increased tolerance and conversion of inhibitors in lignocellulosic hydrolysates by *Saccharomyces cerevisiae*. *Journal of Chemical Technology & Biotechnology*, 82, 340-349.

Amartey, S., Jeffries, T. (1996). An improvement in *Pichia stipitis* fermentation of acid-hydrolysed hemicellulose achieved by overliming (calcium hydroxide treatment) and strain adaptation. *World J Microbiol Biotechnol*, 12, 281-3.

Annergren, G., Germgard, U. (2014). Process aspects for sulfite pulping. *Appita : Technology, Innovation, Manufacturing, Environment*, 67, 270-276.

Anusree, M., Wendisch, V. F., Nampoothiri, K. M. (2016). Co-expression of endoglucanase and beta-glucosidase in *Corynebacterium glutamicum* DM1729 towards direct lysine fermentation from cellulose. *Bioresour Technol*, 213, 239-244.

Arndt, A., Auchter, M., Ishige, T., Wendisch, V. F., Eikmanns, B. J. (2008). Ethanol catabolism in *Corynebacterium glutamicum*. *J Mol Microbiol Biotechnol*, 15, 222-33.

Aro, T., Fatehi, P. (2017). Production and Application of Lignosulfonates and Sulfonated Lignin. *ChemSusChem*, 10, 1861-1877.

Attfield, P. V., Bell, P. J. (2006). Use of population genetics to derive nonrecombinant *Saccharomyces cerevisiae* strains that grow using xylose as a sole carbon source. *FEMS Yeast Res*, 6, 862-8.

Bajwa, P. K., Shireen, T., D'Aoust, F., Pinel, D., Martin, V. J., Trevors, J. T., Lee, H. (2009). Mutants of the pentose-fermenting yeast *Pichia stipitis* with improved tolerance to inhibitors in hardwood spent sulfite liquor. *Biotechnol Bioeng*, 104, 892-900.

Baldoma, L., Aguilar, J. (1988). Metabolism of L-fucose and L-rhamnose in *Escherichia coli*: aerobic-anaerobic regulation of L-lactaldehyde dissimilation. *J Bacteriol*, 170, 416-21.

Baritugo, K.-A. G., Kim, H. T., David, Y. C., Choi, J. H., Choi, J.-i., Kim, T. W., Park, C., Hong, S. H., Na, J.-G., Jeong, K. J., Joo, J. C., Park, S. J. (2018). Recent advances in metabolic engineering of *Corynebacterium glutamicum* as a potential platform microorganism for biorefinery. *Biofuels, Bioproducts and Biorefining*, 12, 899-925.

Barrett, E., Stanton, C., Zelder, O., Fitzgerald, G., Ross, R. P. (2004). Heterologous expression of lactose- and galactose-utilizing pathways from lactic acid bacteria in *Corynebacterium glutamicum* for production of lysine in whey. *Appl Environ Microbiol*, 70, 2861-6.

Barton, N., Horbal, L., Starck, S., Kohlstedt, M., Luzhetskyy, A., Wittmann, C. (2018). Enabling the valorization of guaiacol-based lignin: Integrated chemical and

biochemical production of cis,cis-muconic acid using metabolically engineered *Amycolatopsis* sp ATCC 39116. *Metab Eng*, 45, 200-210.

Baruah, J., Nath, B. K., Sharma, R., Kumar, S., Deka, R. C., Baruah, D. C., Kalita, E. (2018). Recent Trends in the Pretreatment of Lignocellulosic Biomass for Value-Added Products. *Frontiers in Energy Research*, 6.

Batt, C. A., Caryallo, S., Easson, D. D., Jr., Akedo, M., Sinskey, A. J. (1986). Direct evidence for a xylose metabolic pathway in *Saccharomyces cerevisiae*. *Biotechnol Bioeng*, 28, 549-53.

Baumchen, C., Krings, E., Bringer, S., Eggeling, L., Sahm, H. (2009). Myo-inositol facilitators IolT1 and IolT2 enhance D-mannitol formation from D-fructose in *Corynebacterium glutamicum*. *FEMS Microbiol Lett*, 290, 227-35.

Baumgart, M., Unthan, S., Kloss, R., Radek, A., Polen, T., Tenhaef, N., Muller, M. F., Kuberl, A., Siebert, D., Bruhl, N., Marin, K., Hans, S., Kramer, R., Bott, M., Kalinowski, J., Wiechert, W., Seibold, G., Frunzke, J., Ruckert, C., Wendisch, V. F., Noack, S. (2018). *Corynebacterium glutamicum* Chassis C1*: Building and Testing a Novel Platform Host for Synthetic Biology and Industrial Biotechnology. *ACS Synth Biol*, 7, 132-144.

Baumgart, M., Unthan, S., Ruckert, C., Sivalingam, J., Grunberger, A., Kalinowski, J., Bott, M., Noack, S., Frunzke, J. (2013). Construction of a prophage-free variant of *Corynebacterium glutamicum* ATCC 13032 for use as a platform strain for basic research and industrial biotechnology. *Appl Environ Microbiol*, 79, 6006-15.

Becker, J., Klopprogge, C., Zelder, O., Heinzle, E., Wittmann, C. (2005a). Amplified expression of fructose 1,6-bisphosphatase in *Corynebacterium glutamicum* increases in vivo flux through the pentose phosphate pathway and lysine production on different carbon sources. *Appl Environ Microbiol*, 71, 8587-96.

Becker, J., Klopprogge, C., Zelder, O., Heinzle, E., Wittmann, C. (2005b). Amplified expression of fructose 1,6-bisphosphatase in *Corynebacterium glutamicum* increases in vivo flux through the pentose phosphate pathway and lysine production on different carbon sources. *Applied and environmental microbiology*, 71, 8587-8596.

Becker, J., Kuhl, M., Kohlstedt, M., Starck, S., Wittmann, C. (2018a). Metabolic engineering of Corynebacterium glutamicum for the production of cis, cis-muconic acid from lignin. *Microb Cell Fact*, 17, 115.

Becker, J., Rohles, C. M., Wittmann, C. (2018b). Metabolically engineered Corynebacterium glutamicum for bio-based production of chemicals, fuels, materials, and healthcare products. *Metab Eng*, 50, 122-141.

Becker, J., Schafer, R., Kohlstedt, M., Harder, B. J., Borchert, N. S., Stoveken, N., Bremer, E., Wittmann, C. (2013). Systems metabolic engineering of *Corynebacterium glutamicum* for production of the chemical chaperone ectoine. *Microb Cell Fact*, 12, 110.

Becker, J., Wittmann, C. (2012a). Bio-based production of chemicals, materials and fuels -*Corynebacterium glutamicum* as versatile cell factory. *Curr Opin Biotechnol*, 23, 631-40.

Becker, J., Wittmann, C. (2012b). Systems and synthetic metabolic engineering for amino acid production - the heartbeat of industrial strain development. *Curr Opin Biotechnol*, 23, 718-26.

Becker, J., Wittmann, C. (2015). Advanced biotechnology: metabolically engineered cells for the bio-based production of chemicals and fuels, materials, and health-care products. *Angew Chem Int Ed Engl*, 54, 3328-50.

Becker, J., Wittmann, C. (2017). Industrial microorganisms: *Corynebacterium glutamicum*. *Industrial biotechnology: microorganisms*, 1, 183-220.

Becker, J., Wittmann, C. (2019). A field of dreams: Lignin valorization into chemicals, materials, fuels, and health-care products. *Biotechnol Adv*, 37, 107360.

Becker, J., Zelder, O., Hafner, S., Schroder, H., Wittmann, C. (2011). From zero to hero--design-based systems metabolic engineering of *Corynebacterium glutamicum* for L-lysine production. *Metab Eng*, 13, 159-68.

Beguin, P., Aubert, J. P. (1994). The biological degradation of cellulose. *FEMS Microbiol Rev*, 13, 25-58.

Belter, P. A., Cussler, E. L., Hu, W. (1987). Bioseparations: Downstream processing for biotechnology. *John Wiley and Sons Inc.,New York, NY*, United States.

Bengtsson, O., Hahn-Hagerdal, B., Gorwa-Grauslund, M. F. (2009). Xylose reductase from *Pichia stipitis* with altered coenzyme preference improves ethanolic xylose fermentation by recombinant *Saccharomyces cerevisiae*. *Biotechnol Biofuels*, 2, 9.

Bhatia, L., Bachheti, R. K., Garlapati, V. K., Chandel, A. K. (2022). Third-generation biorefineries: a sustainable platform for food, clean energy, and nutraceuticals production. *Biomass Conversion and Biorefinery*, 12, 4215-4230.

Biermann, C. J. (1996). Handbook of pulping and papermaking. *Elsevier*.

Björling, T., Lindman, B. (1989). Evaluation of xylose-fermenting yeasts for ethanol production from spent sulfite liquor. *Enzyme and Microbial Technology*, 11, 240-246.

Bjørsvik, H.-R., Minisci, F. (1999). Fine Chemicals from Lignosulfonates. 1. Synthesis of Vanillin by Oxidation of Lignosulfonates. *Organic Process Research & Development*, 3, 330-340.

Blombach, B., Schreiner, M. E., Holatko, J., Bartek, T., Oldiges, M., Eikmanns, B. J. (2007). L-Valine production with pyruvate dehydrogenase complex-deficient *Corynebacterium glutamicum*. *Appl Environ Microbiol*, 73, 2079-84.

Blombach, B., Seibold, G. M. (2010). Carbohydrate metabolism in Corynebacterium glutamicum and applications for the metabolic engineering of L-lysine production strains. *Appl Microbiol Biotechnol*, 86, 1313-22.

Bolten, C. J. (2010). Bio-based Production of L-methionine in *Corynebacterium Glutamicum*. *Cuvillier*.

Brabetz, W., Liebl, W., Schleifer, K. H. (1991). Studies on the utilization of lactose by *Corynebacterium glutamicum*, bearing the lactose operon of *Escherichia coli*. *Arch Microbiol*, 155, 607-12.

Branco, R. H. R., Serafim, L. S., Xavier, A. M. R. B. (2019). Second Generation Bioethanol Production: On the Use of Pulp and Paper Industry Wastes as Feedstock. *Fermentation*, 5, 4.

Brown, L., Thomas, R. (1983). Comparison of the inotropic potencies of some synthetic and naturally occurring cardiac glycosides using isolated left atrium of guinea pig. *Arzneimittelforschung*, 33, 814-7.

Brown, M. R. (1991). The amino-acid and sugar composition of 16 species of microalgae used in mariculture. *Journal of experimental marine biology and ecology*, 145, 79-99.

Brusseler, C., Radek, A., Tenhaef, N., Krumbach, K., Noack, S., Marienhagen, J. (2018). The myo-inositol/proton symporter IolT1 contributes to D-xylose uptake in *Corynebacterium glutamicum*. *Bioresour Technol*, 249, 953-961.

Bull, H. B., Breese, K., Ferguson, G. L., Swenson, C. A. (1964). The pH of urea solutions. *Arch Biochem Biophys*, 104, 297-304.

Burgardt, A., Moustafa, A., Persicke, M., Spross, J., Patschkowski, T., Risse, J. M., Peters-Wendisch, P., Lee, J. H., Wendisch, V. F. (2021). Coenzyme Q_{10} Biosynthesis Established in the Non-Ubiquinone Containing *Corynebacterium glutamicum* by Metabolic Engineering. *Frontiers in Bioengineering and Biotechnology*, 9, 650961.

Buschke, N., Becker, J., Schafer, R., Kiefer, P., Biedendieck, R., Wittmann, C. (2013a). Systems metabolic engineering of xylose-utilizing *Corynebacterium glutamicum* for production of 1,5-diaminopentane. *Biotechnol J*, 8, 557-70.

Buschke, N., Schafer, R., Becker, J., Wittmann, C. (2013b). Metabolic engineering of industrial platform microorganisms for biorefinery applications--optimization of

substrate spectrum and process robustness by rational and evolutive strategies. *Bioresour Technol*, 135, 544-54.

Buschke, N., Schroder, H., Wittmann, C. (2011). Metabolic engineering of Corynebacterium glutamicum for production of 1,5-diaminopentane from hemicellulose. *Biotechnol J*, 6, 306-17.

Caruel, H., Rigal, L., Gaset, A. (1991). Carbohydrate separation by ligand-exchange liquid chromatography: Correlation between the formation of sugar-cation complexes and the elution order. *Journal of Chromatography A*, 558, 89-104.

Castillo Martinez, F. A., Balciunas, E. M., Salgado, J. M., Domínguez González, J. M., Converti, A., Oliveira, R. P. d. S. (2013). Lactic acid properties, applications and production: A review. *Trends in Food Science & Technology*, 30, 70-83.

Chandel, A. K., da Silva, S. S., Carvalho, W., Singh, O. V. (2012a). Sugarcane bagasse and leaves: foreseeable biomass of biofuel and bio-products. *Journal of Chemical Technology & Biotechnology*, 87, 11-20.

Chandel, A. K., da Silva, S. S., Singh, O. V. (2012b). Detoxification of Lignocellulose Hydrolysates: Biochemical and Metabolic Engineering Toward White Biotechnology. *BioEnergy Research*, 6, 388-401.

Chandel, A. K., da Silva, S. S., Singh, O. V. (2013). Detoxification of Lignocellulose Hydrolysates: Biochemical and Metabolic Engineering Toward White Biotechnology. *BioEnergy Research*, 6, 388-401.

Chang, Z., Dai, W., Mao, Y., Cui, Z., Wang, Z., Chen, T. (2020). Engineering Corynebacterium glutamicum for the Efficient Production of 3-Hydroxypropionic Acid from a Mixture of Glucose and Acetate via the Malonyl-CoA Pathway. *Catalysts*, 10, 203.

Chen, C., Li, Y., Hu, J., Dong, X., Wang, X. (2015). Metabolic engineering of *Corynebacterium glutamicum* ATCC13869 for L-valine production. *Metab Eng*, 29, 66-75.

Chen, T., Zhu, N., Xia, H. (2014). Aerobic production of succinate from arabinose by metabolically engineered *Corynebacterium glutamicum*. *Bioresour Technol*, 151, 411-4.

Chen, Z., Huang, J., Wu, Y., Wu, W., Zhang, Y., Liu, D. (2017). Metabolic engineering of *Corynebacterium glutamicum* for the production of 3-hydroxypropionic acid from glucose and xylose. *Metab Eng*, 39, 151-158.

Cheng, F., Gong, Q., Yu, H., Stephanopoulos, G. (2016). High-titer biosynthesis of hyaluronic acid by recombinant *Corynebacterium glutamicum*. *Biotechnol J*, 11, 574-84.

Cherubini, F. (2010). The biorefinery concept: using biomass instead of oil for producing energy and chemicals. *Energy conversion and management*, 51, 1412-1421.

Cho, D. H., Lee, Y. J., Um, Y., Sang, B. I., Kim, Y. H. (2009). Detoxification of model phenolic compounds in lignocellulosic hydrolysates with peroxidase for butanol production from *Clostridium beijerinckii*. *Appl Microbiol Biotechnol*, 83, 1035-43.

Choi, J. W., Jeon, E. J., Jeong, K. J. (2019). Recent advances in engineering *Corynebacterium glutamicum* for utilization of hemicellulosic biomass. *Curr Opin Biotechnol*, 57, 17-24.

Christmann, J., Cao, P., Becker, J., Desiderato, C. K., Goldbeck, O., Riedel, C. U., Kohlstedt, M., Wittmann, C. (2023). High-efficiency production of the antimicrobial peptide pediocin PA-1 in metabolically engineered *Corynebacterium glutamicum* using a microaerobic process at acidic pH and elevated levels of bivalent calcium ions. *Microb Cell Fact*, 22, 41.

Chung, S. C., Park, J. S., Yun, J., Park, J. H. (2017). Improvement of succinate production by release of end-product inhibition in *Corynebacterium glutamicum*. *Metab Eng*, 40, 157-164.

Coelho, A. I., Berry, G. T., Rubio-Gozalbo, M. E. (2015). Galactose metabolism and health. *Curr Opin Clin Nutr Metab Care*, 18, 422-7.

Converti, A., Domínguez, J. M., Perego, P., da Silva, S. S., Zilli, M. (2000). Wood Hydrolysis and Hydrolyzate Detoxification for Subsequent Xylitol Production. *Chemical Engineering & Technology*, 23, 1013-1020.

Cooney, C. L. (1983). Bioreactors: design and operation. *Science*, 219, 728-33.

Daniel, L. A. F., Susana, R. P., Luísa, S. S., Dmitry, V. E., Ana, M. R. B. X. (2012). Second Generation Bioethanol from Lignocellulosics: Processing of Hardwood Sulphite Spent Liquor. In: Marco Aurelio Pinheiro, L., Alexandra Pardo Policastro, N., Eds.), Bioethanol. *IntechOpen*, Rijeka, pp. Ch. 6.

Dashko, S., Zhou, N., Compagno, C., Piskur, J. (2014). Why, when, and how did yeast evolve alcoholic fermentation? *FEMS Yeast Res*, 14, 826-32.

Dashtban, M., Gilbert, A., Fatehi, P. (2012). Production of furfural: overview and challenges. *J. Sci. Technol. Forest Prod. Process*, 2, 44-53.

De Nunzio, C., Bartoletti, R., Tubaro, A., Simonato, A., Ficarra, V. (2021). Role of D-Mannose in the Prevention of Recurrent Uncomplicated Cystitis: State of the Art and Future Perspectives. *Antibiotics (Basel)*, 10.

Delgenes, J. P., Moletta, R., Navarro, J. M. (1996). Effects of lignocellulose degradation products on ethanol fermentations of glucose and xylose by *Saccharomyces cerevisiae*, *Zymomonas mobilis*, *Pichia stipitis*, and *Candida shehatae*. *Enzyme and Microbial Technology*, 19, 220-225.

Dessbesell, L., Paleologou, M., Leitch, M., Pulkki, R., Xu, C. (2020). Global lignin supply overview and kraft lignin potential as an alternative for petroleum-based polymers. *Renewable and Sustainable Energy Reviews*, 123, 109768.

Diaz, I. M. S., MA), Gummeson, Joel Jeffry (Belchertown, MA), Heininger, Mark Weir (Springfield, MA) Water based dimethyl ester cleaning solution. *Monsanto Company (St. Louis, MO)*, United States, (1997).

Domingues, R., Bondar, M., Palolo, I., Queirós, O., de Almeida, C. D., Cesário, M. T. (2021). Xylose Metabolism in Bacteria—Opportunities and Challenges towards Efficient Lignocellulosic Biomass-Based Biorefineries. *Applied Sciences*, 11, 8112.

Dominguez, H., Cocaign-Bousquet, M., Lindley, N. D. (1997). Simultaneous consumption of glucose and fructose from sugar mixtures during batch growth of *Corynebacterium glutamicum*. *Appl Microbiol Biotechnol*, 47, 600-603.

Dominguez, H., Lindley, N. D. (1996). Complete Sucrose Metabolism Requires Fructose Phosphotransferase Activity in *Corynebacterium glutamicum* To Ensure Phosphorylation of Liberated Fructose. *Appl Environ Microbiol*, 62, 3878-80.

Dominguez, H., Rollin, C., Guyonvarch, A., Guerquin-Kern, J. L., Cocaign-Bousquet, M., Lindley, N. D. (1998). Carbon-flux distribution in the central metabolic pathways of *Corynebacterium glutamicum* during growth on fructose. *Eur J Biochem*, 254, 96-102.

Dunlop, A. P. (1948). Furfural Formation and Behavior. *Industrial & Engineering Chemistry*, 40, 204-209.

Eggeling, L., Bott, M. (2005). Handbook of *Corynebacterium glutamicum*. *CRC press*.

Eggeling, L., Bott, M. (2015). A giant market and a powerful metabolism: L-lysine provided by *Corynebacterium glutamicum*. *Appl Microbiol Biotechnol*, 99, 3387-94.

Ek, M., Gellerstedt, G., Henriksson, G. (2009). Pulping chemistry and technology. *Walter de Gruyter*.

Engels, V., Georgi, T., Wendisch, V. F. (2008). ScrB (Cg2927) is a sucrose-6-phosphate hydrolase essential for sucrose utilization by *Corynebacterium glutamicum*. *FEMS Microbiol Lett*, 289, 80-9.

Engels, V., Wendisch, V. F. (2007). The DeoR-type regulator SugR represses expression of *ptsG* in *Corynebacterium glutamicum*. *J Bacteriol*, 189, 2955-66.

Ennahar, S., Aoude-Werner, D., Sorokine, O., Van Dorsselaer, A., Bringel, F., Hubert, J. C., Hasselmann, C. (1996). Production of pediocin AcH by *Lactobacillus plantarum* WHE 92 isolated from cheese. *Appl Environ Microbiol*, 62, 4381-7.

Ensley, B. D. (1986). Stability of recombinant plasmids in industrial microorganisms. *Critical Reviews in Biotechnology*, 4, 263-277.

FAO Forest products = Produits forestiers = Productos forestales. FAO forestry series = Collection FAO Forêts, (2019), pp. 258-393.

Fatehi, P., Ni, Y. (2011). Integrated Forest Biorefinery − Sulfite Process. Sustainable Production of Fuels, Chemicals, and Fibers from Forest Biomass. vol. 1067. *American Chemical Society*, pp. 409-441.

Felipe, M. G., Vieira, D. C., Vitolo, M., Silva, S. S., Roberto, I. C., Manchilha, I. M. (1995). Effect of acetic acid on xylose fermentation to xylitol by *Candida guilliermondii*. *J Basic Microbiol*, 35, 171-7.

Ferreira, J. A., Agnihotri, S., Taherzadeh, M. J. (2019). Chapter 3 - Waste Biorefinery. In: Taherzadeh, M. J., Bolton, K., Wong, J., Pandey, A., Eds.), Sustainable Resource Recovery and Zero Waste Approaches. *Elsevier*, pp. 35-52.

Fieseler, L., Schmitter, S., Teiserskas, J., Loessner, M. J. (2012). Rhamnose-inducible gene expression in *Listeria monocytogenes*. *PLoS One*, 7, e43444.

Funk, H. F. Recovery of pentoses and hexoses from wood and other material containing hemicellulose and further processing of C5-and C6-components. (1975).

Galbe, M., Zacchi, G. (2002). A review of the production of ethanol from softwood. *Appl Microbiol Biotechnol*, 59, 618-28.

Gancedo, J. M. (1998). Yeast carbon catabolite repression. *Microbiol Mol Biol Rev*, 62, 334-61.

Gasser, B., Mattanovich, D. (2007). Antibody production with yeasts and filamentous fungi: on the road to large scale? *Biotechnol Lett*, 29, 201-12.

Geerdes, J. D., Lewis, B. A., Montgomery, R., Smith, F. (1954). Chromatographic Separation of Sugars with Hydrocellulose. *Analytical Chemistry*, 26, 264-266.

Gerstmeir, R., Wendisch, V. F., Schnicke, S., Ruan, H., Farwick, M., Reinscheid, D., Eikmanns, B. J. (2003). Acetate metabolism and its regulation in *Corynebacterium glutamicum*. *J Biotechnol*, 104, 99-122.

Giesselmann, G., Dietrich, D., Jungmann, L., Kohlstedt, M., Jeon, E. J., Yim, S. S., Sommer, F., Zimmer, D., Muhlhaus, T., Schroda, M., Jeong, K. J., Becker, J., Wittmann, C. (2019). Metabolic Engineering of *Corynebacterium glutamicum* for High-Level Ectoine Production: Design, Combinatorial Assembly, and Implementation of a Transcriptionally Balanced Heterologous Ectoine Pathway. *Biotechnol J*, 14, e1800417.

Goldbeck, O., Desef, D. N., Ovchinnikov, K. V., Perez-Garcia, F., Christmann, J., Sinner, P., Crauwels, P., Weixler, D., Cao, P., Becker, J., Kohlstedt, M., Kager, J., Eikmanns, B. J., Seibold, G. M., Herwig, C., Wittmann, C., Bar, N. S., Diep, D. B., Riedel, C. U. (2021). Establishing recombinant production of pediocin PA-1 in *Corynebacterium glutamicum*. *Metab Eng*, 68, 34-45.

Gonçalves, S., Ferra, J., Paiva, N., Martins, J., Carvalho, L. H., Magalhães, F. D. (2021). Lignosulphonates as an Alternative to Non-Renewable Binders in Wood-Based Materials. *Polymers*, 13, 4196.

Gopinath, V., Meiswinkel, T. M., Wendisch, V. F., Nampoothiri, K. M. (2011). Amino acid production from rice straw and wheat bran hydrolysates by recombinant pentose-utilizing *Corynebacterium glutamicum*. *Appl Microbiol Biotechnol*, 92, 985-96.

Gray, K. A., Zhao, L., Emptage, M. (2006). Bioethanol. *Curr Opin Chem Biol*, 10, 141-6.

Gray, N. F. (2004). Biology of wastewater treatment. *World Scientific*.

Grossiord, B. P., Luesink, E. J., Vaughan, E. E., Arnaud, A., de Vos, W. M. (2003). Characterization, expression, and mutation of the *Lactococcus lactis galPMKTE* genes, involved in galactose utilization via the Leloir pathway. *J Bacteriol*, 185, 870-8.

Grunberger, A., van Ooyen, J., Paczia, N., Rohe, P., Schiendzielorz, G., Eggeling, L., Wiechert, W., Kohlheyer, D., Noack, S. (2013). Beyond growth rate 0.6: *Corynebacterium glutamicum* cultivated in highly diluted environments. *Biotechnol Bioeng*, 110, 220-8.

Hahn-Hagerdal, B., Karhumaa, K., Fonseca, C., Spencer-Martins, I., Gorwa-Grauslund, M. F. (2007). Towards industrial pentose-fermenting yeast strains. *Appl Microbiol Biotechnol*, 74, 937-53.

Han, T., Kim, G. B., Lee, S. Y. (2020). Glutaric acid production by systems metabolic engineering of an L-lysine-overproducing *Corynebacterium glutamicum*. *Proc Natl Acad Sci U S A*, 117, 30328-30334.

Hansen, L. H., Knudsen, S., Sorensen, S. J. (1998). The effect of the *lacY* gene on the induction of IPTG inducible promoters, studied in *Escherichia coli* and *Pseudomonas fluorescens*. *Curr Microbiol*, 36, 341-7.

Hecquet, L., Bolte, J., Demuynck, C. (1996). Enzymatic synthesis of "natural-labeled" 6-deoxy-L-sorbose precursor of an important food flavor. *Tetrahedron*, 52, 8223-8232.

Heer, D., Sauer, U. (2008). Identification of furfural as a key toxin in lignocellulosic hydrolysates and evolution of a tolerant yeast strain. *Microb Biotechnol*, 1, 497-506.

Heider, S. A., Peters-Wendisch, P., Wendisch, V. F. (2012). Carotenoid biosynthesis and overproduction in *Corynebacterium glutamicum*. *BMC Microbiol*, 12, 198.

Heipieper, H. J., Weber, F. J., Sikkema, J., Keweloh, H., de Bont, J. A. M. (1994). Mechanisms of resistance of whole cells to toxic organic solvents. *Trends in Biotechnology*, 12, 409-415.

Helle, S. S., Lin, T., Duff, S. J. B. (2008). Optimization of spent sulfite liquor fermentation. *Enzyme and Microbial Technology*, 42, 259-264.

Helle, S. S., Murray, A., Lam, J., Cameron, D. R., Duff, S. J. (2004). Xylose fermentation by genetically modified *Saccharomyces cerevisiae* 259ST in spent sulfite liquor. *Bioresour Technol*, 92, 163-71.

Henderson, P. J., Bradley, S., Macpherson, A. J., Horne, P., Davis, E. O., Daruwalla, K. R., Jones-Mortimer, M. C. (1984). Sugar-proton transport systems of *Escherichia coli*. *Biochem Soc Trans*, 12, 146-8.

Henke, N. A., Wendisch, V. F. (2019). Improved Astaxanthin Production with *Corynebacterium glutamicum* by Application of a Membrane Fusion Protein. *Mar Drugs*, 17.

Henke, N. A., Wichmann, J., Baier, T., Frohwitter, J., Lauersen, K. J., Risse, J. M., Peters-Wendisch, P., Kruse, O., Wendisch, V. F. (2018). Patchoulol Production with Metabolically Engineered *Corynebacterium glutamicum*. *Genes (Basel)*, 9.

Henriques, T. M., Pereira, S. R., Serafim, L. S., Xavier, A. M. R. B. (2018). Two-Stage Aeration Fermentation Strategy to Improve Bioethanol Production by *Scheffersomyces stipitis*. *Fermentation*, 4, 97.

Hermann, T., Pfefferle, W., Baumann, C., Busker, E., Schaffer, S., Bott, M., Sahm, H., Dusch, N., Kalinowski, J., Puhler, A., Bendt, A. K., Kramer, R., Burkovski, A. (2001). Proteome analysis of *Corynebacterium glutamicum*. *Electrophoresis*, 22, 1712-23.

Hochster, R. M., Watson, R. W. (1954). Enzymatic isomerization of D-xylose to D-xylulose. *Arch Biochem Biophys*, 48, 120-9.

Hocking, M. B. (1997). Vanillin: Synthetic Flavoring from Spent Sulfite Liquor. *Journal of Chemical Education*, 74, 1055.

Hoffmann, S. L., Jungmann, L., Schiefelbein, S., Peyriga, L., Cahoreau, E., Portais, J. C., Becker, J., Wittmann, C. (2018). Lysine production from the sugar alcohol mannitol: Design of the cell factory Corynebacterium glutamicum SEA-3 through integrated analysis and engineering of metabolic pathway fluxes. *Metab Eng*, 47, 475-487.

Hoffmann, S. L., Kohlstedt, M., Jungmann, L., Hutter, M., Poblete-Castro, I., Becker, J., Wittmann, C. (2021). Cascaded valorization of brown seaweed to produce L-lysine and value-added products using *Corynebacterium glutamicum* streamlined by systems metabolic engineering. *Metab Eng*, 67, 293-307.

Höglund, H. (2009). Mechanical pulping. *Pulping chemistry and technology*, 57.

Holmgren, M., Sellstedt, A. (2008). Identification of white-rot and soft-rot fungi increasing ethanol production from spent sulfite liquor in co-culture with *Saccharomyces cerevisiae*. *J Appl Microbiol*, 105, 134-40.

Holo, H., Nilssen, O., Nes, I. F. (1991). Lactococcin A, a new bacteriocin from *Lactococcus lactis* subsp. *cremoris*: isolation and characterization of the protein and its gene. *J Bacteriol*, 173, 3879-87.

Hu, B., Li, H., Wang, Q., Tan, Y., Chen, R., Li, J., Ban, W., Liang, L. (2018). Production and utilization of L-arabinose in China. *World Journal of Engineering and Technology*, 6, 24-36.

Hu, X., Shi, Y., Zhang, P., Miao, M., Zhang, T., Jiang, B. (2016). D-Mannose: Properties, Production, and Applications: An Overview. *Compr Rev Food Sci Food Saf*, 15, 773-785.

Huang, C. F., Lin, T. H., Guo, G. L., Hwang, W. S. (2009). Enhanced ethanol production by fermentation of rice straw hydrolysate without detoxification using a newly adapted strain of *Pichia stipitis*. *Bioresour Technol*, 100, 3914-20.

Huang, L.-Z., Ma, M.-G., Ji, X.-X., Choi, S.-E., Si, C. (2021). Recent Developments and Applications of Hemicellulose from wheat straw: A review. *Frontiers in Bioengineering and Biotechnology*, 9, 440.

Hueck, C. J., Hillen, W. (1995). Catabolite repression in *Bacillus subtilis*: a global regulatory mechanism for the gram-positive bacteria? *Mol Microbiol*, 15, 395-401.

Hyeon, J. E., Jeon, W. J., Whang, S. Y., Han, S. O. (2011). Production of minicellulosomes for the enhanced hydrolysis of cellulosic substrates by recombinant *Corynebacterium glutamicum*. *Enzyme and Microbial Technology*, 48, 371-7.

Ikeda, K. (2002). New seasonings. *Chem Senses*, 27, 847-9.

Ikeda, M. (2003). Amino acid production processes. *Adv Biochem Eng Biotechnol*, 79, 1-35.

Ikeda, M. (2012). Sugar transport systems in *Corynebacterium glutamicum*: features and applications to strain development. *Appl Microbiol Biotechnol*, 96, 1191-200.

Ikeda, M., Katsumata, R. (1999). Hyperproduction of tryptophan by *Corynebacterium glutamicum* with the modified pentose phosphate pathway. *Appl Environ Microbiol*, 65, 2497-502.

Ikeda, M., Mizuno, Y., Awane, S., Hayashi, M., Mitsuhashi, S., Takeno, S. (2011). Identification and application of a different glucose uptake system that functions as an alternative to the phosphotransferase system in *Corynebacterium glutamicum*. *Appl Microbiol Biotechnol*, 90, 1443-51.

Ikeda, M., Nakagawa, S. (2003). The *Corynebacterium glutamicum* genome: features and impacts on biotechnological processes. *Appl Microbiol Biotechnol*, 62, 99-109.

Inui, M., Kawaguchi, H., Murakami, S., Vertes, A. A., Yukawa, H. (2004). Metabolic engineering of *Corynebacterium glutamicum* for fuel ethanol production under oxygen-deprivation conditions. *J Mol Microbiol Biotechnol*, 8, 243-54.

Iwamoto, K., Shiraiwa, Y. (2005). Salt-regulated mannitol metabolism in algae. *Mar Biotechnol (NY)*, 7, 407-15.

Jager, W., Schafer, A., Puhler, A., Labes, G., Wohlleben, W. (1992). Expression of the *Bacillus subtilis sacB* gene leads to sucrose sensitivity in the gram-positive bacterium *Corynebacterium glutamicum* but not in *Streptomyces lividans*. *J Bacteriol*, 174, 5462-5.

Jagtap, S. S., Rao, C. V. (2018). Microbial conversion of xylose into useful bioproducts. *Appl Microbiol Biotechnol*, 102, 9015-9036.

Jeppsson, M., Bengtsson, O., Franke, K., Lee, H., Hahn-Hagerdal, B., Gorwa-Grauslund, M. F. (2006). The expression of a *Pichia stipitis* xylose reductase mutant with higher K_M for NADPH increases ethanol production from xylose in recombinant *Saccharomyces cerevisiae*. *Biotechnol Bioeng*, 93, 665-73.

Jiang, N., Dillon, F. M., Silva, A., Gomez-Cano, L., Grotewold, E. (2021). Rhamnose in plants - from biosynthesis to diverse functions. *Plant Sci*, 302, 110687.

Jo, S., Yoon, J., Lee, S. M., Um, Y., Han, S. O., Woo, H. M. (2017). Modular pathway engineering of *Corynebacterium glutamicum* to improve xylose utilization and succinate production. *J Biotechnol*, 258, 69-78.

Johansson, E., Brandberg, T., Larsson, C. (2011). Influence of cultivation procedure for *Saccharomyces cerevisiae* used as pitching agent in industrial spent sulphite liquor fermentations. *J Ind Microbiol Biotechnol*, 38, 1787-92.

Johansson, E., Xiros, C., Larsson, C. (2014). Fermentation performance and physiology of two strains of *Saccharomyces cerevisiae* during growth in high gravity spruce hydrolysate and spent sulphite liquor. *BMC Biotechnol*, 14, 47.

Jojima, T., Fujii, M., Mori, E., Inui, M., Yukawa, H. (2010). Engineering of sugar metabolism of *Corynebacterium glutamicum* for production of amino acid L-alanine under oxygen deprivation. *Appl Microbiol Biotechnol*, 87, 159-65.

Jojima, T., Noburyu, R., Sasaki, M., Tajima, T., Suda, M., Yukawa, H., Inui, M. (2015). Metabolic engineering for improved production of ethanol by *Corynebacterium glutamicum*. *Appl Microbiol Biotechnol*, 99, 1165-72.

Jolkver, E., Emer, D., Ballan, S., Kramer, R., Eikmanns, B. J., Marin, K. (2009). Identification and characterization of a bacterial transport system for the uptake of pyruvate, propionate, and acetate in *Corynebacterium glutamicum*. *J Bacteriol*, 191, 940-8.

Jorge, J. M., Leggewie, C., Wendisch, V. F. (2016). A new metabolic route for the production of gamma-aminobutyric acid by *Corynebacterium glutamicum* from glucose. *Amino Acids*, 48, 2519-2531.

Jorge, J. M., Nguyen, A. Q., Perez-Garcia, F., Kind, S., Wendisch, V. F. (2017). Improved fermentative production of gamma-aminobutyric acid via the putrescine route: Systems metabolic engineering for production from glucose, amino sugars, and xylose. *Biotechnol Bioeng*, 114, 862-873.

Jungmann, L., Hoffmann, S. L., Lang, C., De Agazio, R., Becker, J., Kohlstedt, M., Wittmann, C. (2022). High-efficiency production of 5-hydroxyectoine using metabolically engineered *Corynebacterium glutamicum*. *Microb Cell Fact*, 21, 274.

Kalinowski, J., Bathe, B., Bartels, D., Bischoff, N., Bott, M., Burkovski, A., Dusch, N., Eggeling, L., Eikmanns, B. J., Gaigalat, L., Goesmann, A., Hartmann, M., Huthmacher, K., Kramer, R., Linke, B., McHardy, A. C., Meyer, F., Mockel, B., Pfefferle, W., Puhler, A., Rey, D. A., Ruckert, C., Rupp, O., Sahm, H., Wendisch, V. F., Wiegrabe, I., Tauch, A. (2003). The complete *Corynebacterium glutamicum* ATCC 13032 genome sequence and its impact on the production of L-aspartate-derived amino acids and vitamins. *J Biotechnol*, 104, 5-25.

Kallscheuer, N., Menezes, R., Foito, A., da Silva, M. H., Braga, A., Dekker, W., Sevillano, D. M., Rosado-Ramos, R., Jardim, C., Oliveira, J., Ferreira, P., Rocha, I., Silva, A. R., Sousa, M., Allwood, J. W., Bott, M., Faria, N., Stewart, D., Ottens, M., Naesby, M., Nunes Dos Santos, C., Marienhagen, J. (2019). Identification and Microbial Production of the Raspberry Phenol Salidroside that Is Active against Huntington's Disease. *Plant Physiol*, 179, 969-985.

Kallscheuer, N., Vogt, M., Bott, M., Marienhagen, J. (2017). Functional expression of plant-derived *O*-methyltransferase, flavanone 3-hydroxylase, and flavonol synthase in *Corynebacterium glutamicum* for production of pterostilbene, kaempferol, and quercetin. *J Biotechnol*, 258, 190-196.

Kalyanpur, M. (2002). Downstream processing in the biotechnology industry. *Mol Biotechnol*, 22, 87-98.

Karhumaa, K., Hahn-Hagerdal, B., Gorwa-Grauslund, M. F. (2005). Investigation of limiting metabolic steps in the utilization of xylose by recombinant *Saccharomyces cerevisiae* using metabolic engineering. *Yeast*, 22, 359-68.

Karim, A. S., Curran, K. A., Alper, H. S. (2013). Characterization of plasmid burden and copy number in *Saccharomyces cerevisiae* for optimization of metabolic engineering applications. *FEMS Yeast Res*, 13, 107-16.

Kato, O., Youn, J. W., Stansen, K. C., Matsui, D., Oikawa, T., Wendisch, V. F. (2010). Quinone-dependent D-lactate dehydrogenase Dld (Cg1027) is essential for growth of *Corynebacterium glutamicum* on D-lactate. *BMC Microbiol*, 10, 321.

Kawaguchi, H., Sasaki, M., Vertes, A. A., Inui, M., Yukawa, H. (2008). Engineering of an L-arabinose metabolic pathway in *Corynebacterium glutamicum*. *Appl Microbiol Biotechnol*, 77, 1053-62.

Kawaguchi, H., Sasaki, M., Vertes, A. A., Inui, M., Yukawa, H. (2009). Identification and functional analysis of the gene cluster for L-arabinose utilization in *Corynebacterium glutamicum*. *Appl Environ Microbiol*, 75, 3419-29.

Kawaguchi, H., Vertes, A. A., Okino, S., Inui, M., Yukawa, H. (2006). Engineering of a xylose metabolic pathway in Corynebacterium glutamicum. *Appl Environ Microbiol*, 72, 3418-28.

Kawaguchi, H., Yoshihara, K., Hara, K. Y., Hasunuma, T., Ogino, C., Kondo, A. (2018). Metabolome analysis-based design and engineering of a metabolic pathway in *Corynebacterium glutamicum* to match rates of simultaneous utilization of D-glucose and L-arabinose. *Microb Cell Fact*, 17, 76.

Kay, P., Michelle, S., Veronica, C. N. (2010). High fructose corn syrup: production, uses and public health concerns. *Biotechnology and Molecular Biology Reviews*, 5, 71-78.

Kiefer, D., Merkel, M., Lilge, L., Hausmann, R., Henkel, M. (2021). High cell density cultivation of *Corynebacterium glutamicum* on bio-based lignocellulosic acetate using pH-coupled online feeding control. *Bioresour Technol*, 340, 125666.

Kiefer, P., Heinzle, E., Wittmann, C. (2002). Influence of glucose, fructose and sucrose as carbon sources on kinetics and stoichiometry of lysine production by Corynebacterium glutamicum. *J Ind Microbiol Biotechnol*, 28, 338-43.

Kiefer, P., Heinzle, E., Zelder, O., Wittmann, C. (2004). Comparative metabolic flux analysis of lysine-producing *Corynebacterium glutamicum* cultured on glucose or fructose. *Appl Environ Microbiol*, 70, 229-39.

Kim, H. T., Baritugo, K.-A., Oh, Y. H., Hyun, S. M., Khang, T. U., Kang, K. H., Jung, S. H., Song, B. K., Park, K., Kim, I.-K., Lee, M. O., Kam, Y., Hwang, Y. T., Park, S. J., Joo, J. C. (2018). Metabolic Engineering of *Corynebacterium glutamicum* for the High-Level Production of Cadaverine That Can Be Used for the Synthesis of Biopolyamide 510. *ACS Sustainable Chemistry & Engineering*, 6, 5296-5305.

Kim, H. T., Khang, T. U., Baritugo, K. A., Hyun, S. M., Kang, K. H., Jung, S. H., Song, B. K., Park, K., Oh, M. K., Kim, G. B., Kim, H. U., Lee, S. Y., Park, S. J., Joo, J. C. (2019). Metabolic engineering of *Corynebacterium glutamicum* for the production of glutaric acid, a C5 dicarboxylic acid platform chemical. *Metab Eng*, 51, 99-109.

Kimura, E. (2005). 19 L-glutamate production. *Handbook of Corynebacterium glutamicum (Boca Raton, FL)*, 439.

Kind, S., Jeong, W. K., Schroder, H., Wittmann, C. (2010). Systems-wide metabolic pathway engineering in *Corynebacterium glutamicum* for bio-based production of diaminopentane. *Metab Eng*, 12, 341-51.

Kinoshita, S., Udaka, S., Shimono, M. (1957). Studies on the amino acid fermentation Part I. Production of L-glutamic acid by various microorganisms. *The Journal of general and applied microbiology*, 3, 193-205.

Klaffl, S., Brocker, M., Kalinowski, J., Eikmanns, B. J., Bott, M. (2013). Complex regulation of the phosphoenolpyruvate carboxykinase gene pck and characterization of its GntR-type regulator IolR as a repressor of myo-inositol utilization genes in *Corynebacterium glutamicum*. *J Bacteriol*, 195, 4283-96.

Klinke, H. B., Thomsen, A. B., Ahring, B. K. (2004). Inhibition of ethanol-producing yeast and bacteria by degradation products produced during pre-treatment of biomass. *Appl Microbiol Biotechnol*, 66, 10-26.

Koch, D. J., Ruckert, C., Rey, D. A., Mix, A., Puhler, A., Kalinowski, J. (2005). Role of the ssu and seu genes of *Corynebacterium glutamicum* ATCC 13032 in utilization of sulfonates and sulfonate esters as sulfur sources. *Appl Environ Microbiol*, 71, 6104-14.

Kohlstedt, M., Starck, S., Barton, N., Stolzenberger, J., Selzer, M., Mehlmann, K., Schneider, R., Pleissner, D., Rinkel, J., Dickschat, J. S., Venus, J., J, B. J. H. v. D., Wittmann, C. (2018). From lignin to nylon: Cascaded chemical and biochemical conversion using metabolically engineered *Pseudomonas putida*. *Metab Eng*, 47, 279-293.

Kohlstedt, M., Weimer, A., Weiland, F., Stolzenberger, J., Selzer, M., Sanz, M., Kramps, L., Wittmann, C. (2022). Biobased PET from lignin using an engineered cis, cis-muconate-producing *Pseudomonas putida* strain with superior robustness, energy and redox properties. *Metab Eng*, 72, 337-352.

Kornberg, H. L., Lambourne, L. T. (1992). Role of the phosphoenolpyruvate-dependent fructose phosphotransferase system in the utilization of mannose by *Escherichia coli*. *Proc Biol Sci*, 250, 51-5.

Kotrba, P., Inui, M., Yukawa, H. (2003). A single V317A or V317M substitution in Enzyme II of a newly identified beta-glucoside phosphotransferase and utilization system of *Corynebacterium glutamicum* R extends its specificity towards cellobiose. *Microbiology*, 149, 1569-1580.

Krahn, I., Bonder, D., Torregrosa-Barragan, L., Stoppel, D., Krause, J. P., Rosenfeldt, N., Meiswinkel, T. M., Seibold, G. M., Wendisch, V. F., Lindner, S. N. (2021). Evolving a New Efficient Mode of Fructose Utilization for Improved Bioproduction in *Corynebacterium glutamicum*. *Frontiers in Bioengineering and Biotechnology*, 9, 669093.

Kranjcec, B., Papes, D., Altarac, S. (2014). D-Mannose powder for prophylaxis of recurrent urinary tract infections in women: a randomized clinical trial. *World J Urol*, 32, 79-84.

Krause, F. S., Henrich, A., Blombach, B., Kramer, R., Eikmanns, B. J., Seibold, G. M. (2010). Increased glucose utilization in *Corynebacterium glutamicum* by use of maltose, and its application for the improvement of L-valine productivity. *Appl Environ Microbiol*, 76, 370-4.

Kremling, A., Kremling, S., Bettenbrock, K. (2009). Catabolite repression in *Escherichia coli*- a comparison of modelling approaches. *Febs J*, 276, 594-602.

Kromer, J. O., Sorgenfrei, O., Klopprogge, K., Heinzle, E., Wittmann, C. (2004). In-depth profiling of lysine-producing *Corynebacterium glutamicum* by combined analysis of the transcriptome, metabolome, and fluxome. *J Bacteriol*, 186, 1769-84.

Kuhad, R. C., Singh, A. (1993). Lignocellulose biotechnology: current and future prospects. *Critical Reviews in Biotechnology*, 13, 151-172.

Kumagai, H. (2000). Microbial production of amino acids in Japan. *History of Modern Biotechnology I*, 71-85.

Kuyper, M., Harhangi, H. R., Stave, A. K., Winkler, A. A., Jetten, M. S., de Laat, W. T., den Ridder, J. J., Op den Camp, H. J., van Dijken, J. P., Pronk, J. T. (2003). High-level functional expression of a fungal xylose isomerase: the key to efficient ethanolic fermentation of xylose by *Saccharomyces cerevisiae*? *FEMS Yeast Res*, 4, 69-78.

Ladakis, D., Michailidi, K., Vlysidis, A., Koutinas, A., Kookos, I. K. (2018). Valorization of spent sulphite liquor for succinic acid production via continuous fermentation system. *Biochemical Engineering Journal*, 137, 262-272.

Lai, L., Bura, R. (2012). The sulfite mill as a sugar-flexible future biorefinery. *Tappi Journal*, 11, 27-35.

Laine, R. A., Sweeley, C. C. (1971). Analysis of trimethylsilyl *O*-methyloximes of carbohydrates by combined gas-liquid chromatography-mass spectrometry. *Anal Biochem*, 43, 533-8.

Lange, J., Muller, F., Bernecker, K., Dahmen, N., Takors, R., Blombach, B. (2017). Valorization of pyrolysis water: a biorefinery side stream, for 1,2-propanediol

production with engineered *Corynebacterium glutamicum*. *Biotechnol Biofuels*, 10, 277.

Lange, J., Muller, F., Takors, R., Blombach, B. (2018). Harnessing novel chromosomal integration loci to utilize an organosolv-derived hemicellulose fraction for isobutanol production with engineered *Corynebacterium glutamicum*. *Microb Biotechnol*, 11, 257-263.

Larsson, S., Palmqvist, E., Hahn-Hägerdal, B., Tengborg, C., Stenberg, K., Zacchi, G., Nilvebrant, N.-O. (1999a). The generation of fermentation inhibitors during dilute acid hydrolysis of softwood. *Enzyme and Microbial Technology*, 24, 151-159.

Larsson, S., Quintana-Sainz, A., Reimann, A., Nilvebrant, N. O., Jonsson, L. J. (2000). Influence of lignocellulose-derived aromatic compounds on oxygen-limited growth and ethanolic fermentation by *Saccharomyces cerevisiae*. *Appl Biochem Biotechnol*, 84-86, 617-32.

Larsson, S., Reimann, A., Nilvebrant, N.-O., Jönsson, L. J. (1999b). Comparison of different methods for the detoxification of lignocellulose hydrolyzates of spruce. *Appl Biochem Biotechnol*, 77, 91-103.

Laslo, T., von Zaluskowski, P., Gabris, C., Lodd, E., Ruckert, C., Dangel, P., Kalinowski, J., Auchter, M., Seibold, G., Eikmanns, B. J. (2012). Arabitol metabolism of *Corynebacterium glutamicum* and its regulation by AtlR. *J Bacteriol*, 194, 941-55.

Lawford, H. G., Rousseau, J. D. (1993). Production of ethanol from pulp mill hardwood and softwood spent sulfite liquors by genetically engineered E. coli. *Appl Biochem Biotechnol*, 39-40, 667-85.

Lee, J. K., Sung, M. H., Yoon, K. H., Yu, J. H., Oh, T. K. (1994). Nucleotide sequence of the gene encoding the *Corynebacterium glutamicum* mannose enzyme II and analyses of the deduced protein sequence. *FEMS Microbiol Lett*, 119, 137-45.

Lee, J. Y., Na, Y. A., Kim, E., Lee, H. S., Kim, P. (2016). The Actinobacterium *Corynebacterium glutamicum*, an Industrial Workhorse. *J Microbiol Biotechnol*, 26, 807-22.

Lee, R. A., Lavoie, J.-M. (2013). From first-to third-generation biofuels: Challenges of producing a commodity from a biomass of increasing complexity. *Animal Frontiers*, 3, 6-11.

Leßmeier, L., Zahoor ul Hassan, A., Lindner, S., Wendisch, V. F. (2015). Metabolic engineering of *Corynebacterium glutamicum* for alternative carbon source utilization. Corynebacterium glutamicum: From Systems Biology to Biotechnological Applications.

Levin, G. V. (2002). Tagatose, the new GRAS sweetener and health product. *J Med Food*, 5, 23-36.

Li, C., Jiang, T., Li, M., Zou, Y., Yan, Y. (2022). Fine-tuning gene expression for improved biosynthesis of natural products: From transcriptional to post-translational regulation. *Biotechnol Adv*, 54, 107853.

Li, G., Huang, D., Sui, X., Li, S., Huang, B., Zhang, X., Wu, H., Deng, Y. (2020). Advances in microbial production of medium-chain dicarboxylic acids for nylon materials. *Reaction Chemistry & Engineering*, 5, 221-238.

Li, Y., Cong, H., Liu, B., Song, J., Sun, X., Zhang, J., Yang, Q. (2016). Metabolic engineering of *Corynebacterium glutamicum* for methionine production by removing feedback inhibition and increasing NADPH level. *Antonie Van Leeuwenhoek*, 109, 1185-97.

Li, Z., Shen, Y. P., Jiang, X. L., Feng, L. S., Liu, J. Z. (2018). Metabolic evolution and a comparative omics analysis of *Corynebacterium glutamicum* for putrescine production. *J Ind Microbiol Biotechnol*, 45, 123-139.

Liebl, W. (2005). *Corynebacterium* taxonomy. *Handbook of Corynebacterium glutamicum. CRC Press, Boca Raton, FL*, 9-34.

Lindemann, B., Ogiwara, Y., Ninomiya, Y. (2002). The discovery of umami. *Chem Senses*, 27, 843-4.

Lindner, S. N., Petrov, D. P., Hagmann, C. T., Henrich, A., Kramer, R., Eikmanns, B. J., Wendisch, V. F., Seibold, G. M. (2013). Phosphotransferase system-mediated glucose uptake is repressed in phosphoglucoisomerase-deficient *Corynebacterium glutamicum* strains. *Appl Environ Microbiol*, 79, 2588-95.

Lindner, S. N., Seibold, G. M., Henrich, A., Kramer, R., Wendisch, V. F. (2011). Phosphotransferase system-independent glucose utilization in *Corynebacterium glutamicum* by inositol permeases and glucokinases. *Appl Environ Microbiol*, 77, 3571-81.

Lira-Parada, P. A., Sinner, P., Kohlstedt, M., Kager, J., Wittmann, C., Herwig, C., Bar, N. (2022). Linking process and metabolic modelling for the estimation of carbon flux distribution in *Corynebacterium glutamicum* growth in spent sulfite liquor. *IFAC-PapersOnLine*, 55, 228-233.

Litsanov, B., Brocker, M., Bott, M. (2013). Glycerol as a substrate for aerobic succinate production in minimal medium with *Corynebacterium glutamicum*. *Microb Biotechnol*, 6, 189-95.

Liu, Y. (2020). A code within the genetic code: codon usage regulates co-translational protein folding. *Cell Commun Signal*, 18, 145.

Lopez, M. J., Nichols, N. N., Dien, B. S., Moreno, J., Bothast, R. J. (2004). Isolation of microorganisms for biological detoxification of lignocellulosic hydrolysates. *Appl Microbiol Biotechnol*, 64, 125-31.

Lora, J. (2008). Chapter 10 - Industrial Commercial Lignins: Sources, Properties and Applications. In: Belgacem, M. N., Gandini, A., Eds.), Monomers, Polymers and Composites from Renewable Resources. *Elsevier*, Amsterdam, pp. 225-241.

Lynd, L. R., van Zyl, W. H., McBride, J. E., Laser, M. (2005). Consolidated bioprocessing of cellulosic biomass: an update. *Curr Opin Biotechnol*, 16, 577-83.

Lynd, L. R., Weimer, P. J., van Zyl, W. H., Pretorius, I. S. (2002). Microbial cellulose utilization: fundamentals and biotechnology. *Microbiol Mol Biol Rev*, 66, 506-77, table of contents.

Ma, M., Liu, Z. L. (2010). Mechanisms of ethanol tolerance in *Saccharomyces cerevisiae*. *Appl Microbiol Biotechnol*, 87, 829-45.

Malherbe, S., Cloete, T. E. (2002). Lignocellulose biodegradation: fundamentals and applications. *Reviews in Environmental Science and Biotechnology*, 1, 105-114.

Malin, G. M., Bourd, G. I. (1991). Phosphotransferase-dependent glucose transport in *Corynebacterium glutamicum*. *Journal of Applied Bacteriology*, 71, 517-523.

Mao, Y., Li, G., Chang, Z., Tao, R., Cui, Z., Wang, Z., Tang, Y. J., Chen, T., Zhao, X. (2018). Metabolic engineering of *Corynebacterium glutamicum* for efficient production of succinate from lignocellulosic hydrolysate. *Biotechnol Biofuels*, 11, 95.

Marques, A. P., Evtuguin, D. V., Magina, S., Amado, F. M. L., Prates, A. (2009). Chemical Composition of Spent Liquors from Acidic Magnesium–Based Sulphite Pulping of Eucalyptus globulus. *Journal of Wood Chemistry and Technology*, 29, 322-336.

Martín, C., Galbe, M., Wahlbom, C. F., Hahn-Hägerdal, B., Jönsson, L. J. (2002). Ethanol production from enzymatic hydrolysates of sugarcane bagasse using recombinant xylose-utilising *Saccharomyces cerevisiae*. *Enzyme and Microbial Technology*, 31, 274-282.

Martinez, A., Rodriguez, M. E., Wells, M. L., York, S. W., Preston, J. F., Ingram, L. O. (2001). Detoxification of dilute acid hydrolysates of lignocellulose with lime. *Biotechnol Prog*, 17, 287-93.

Martinez, A., Rodriguez, M. E., York, S. W., Preston, J. F., Ingram, L. O. (2000). Effects of $Ca(OH)_2$ treatments ("overliming") on the composition and toxicity of bagasse hemicellulose hydrolysates. *Biotechnol Bioeng*, 69, 526-36.

Marugg, J. D., Gonzalez, C. F., Kunka, B. S., Ledeboer, A. M., Pucci, M. J., Toonen, M. Y., Walker, S. A., Zoetmulder, L. C., Vandenbergh, P. A. (1992). Cloning, expression, and nucleotide sequence of genes involved in production of pediocin PA-1, and bacteriocin from *Pediococcus acidilactici* PAC1.0. *Appl Environ Microbiol*, 58, 2360-7.

Marwaha, S. S., Kennedy, J. F. (1988). Whey—pollution problem and potential utilization. *International Journal of Food Science & Technology*, 23, 323-336.

Matar, S., Hatch, L. F. (2001). Chemistry of petrochemical processes. *Elsevier*.

Matsushika, A., Goshima, T., Fujii, T., Inoue, H., Sawayama, S., Yano, S. (2012). Characterization of non-oxidative transaldolase and transketolase enzymes in the pentose phosphate pathway with regard to xylose utilization by recombinant *Saccharomyces cerevisiae*. *Enzyme and Microbial Technology*, 51, 16-25.

Matsuura, R., Kishida, M., Konishi, R., Hirata, Y., Adachi, N., Segawa, S., Imao, K., Tanaka, T., Kondo, A. (2019). Metabolic engineering to improve 1,5-diaminopentane production from cellobiose using beta-glucosidase-secreting *Corynebacterium glutamicum*. *Biotechnol Bioeng*, 116, 2640-2651.

McClintock, M. K., Zhang, K. (2017). Xylose metabolism and its metabolic engineering applications. *Engineering Microbial Metabolism for Chemical Synthesis; World Scientific (Europe): Hackensack, NJ, USA*, 209-235.

Meiswinkel, T. M., Gopinath, V., Lindner, S. N., Nampoothiri, K. M., Wendisch, V. F. (2013a). Accelerated pentose utilization by *Corynebacterium glutamicum* for accelerated production of lysine, glutamate, ornithine and putrescine. *Microb Biotechnol*, 6, 131-40.

Meiswinkel, T. M., Rittmann, D., Lindner, S. N., Wendisch, V. F. (2013b). Crude glycerol-based production of amino acids and putrescine by *Corynebacterium glutamicum*. *Bioresour Technol*, 145, 254-8.

Mikkola, J. P., Salmi, T., Sjöholm, R., Mäki-Arvela, P., Vainio, H. (2000). Hydrogenation of xylose to xylitol: three-phase catalysis by promoted raney nickel, catalyst deactivation and in-situ sonochemical catalyst rejuvenation. In: Corma, A., Melo, F. V., Mendioroz, S., Fierro, J. L. G., Eds.), Studies in Surface Science and Catalysis. vol. 130. *Elsevier*, pp. 2027-2032.

Miura, M., Shimotori, Y., Nakatani, H., Harada, A., Aoyama, M. (2015). Bioconversion of Birch Wood Hemicellulose Hydrolyzate to Xylitol. *Appl Biochem Biotechnol*, 176, 947-55.

Mizukami, T., Hamu, A., Ikeda, M., Oka, T., Katsumata, R. (1994). Cloning of the ATP phosphoribosyl transferase gene of *Corynebacterium glutamicum* and application of the gene to L-histidine production. *Biosci Biotechnol Biochem*, 58, 635-8.

Montastruc, L., Ajao, O., Marinova, M., Barreto, C., Domenech, S. Hemicellulose Biorefinery For Furfural Production Energy Requirement Analysis and Minimization. (2011).

Monteiro, M. R., Kugelmeier, C. L., Pinheiro, R. S., Batalha, M. O., da Silva César, A. (2018). Glycerol from biodiesel production: Technological paths for sustainability. *Renewable and Sustainable Energy Reviews*, 88, 109-122.

Moon, M. W., Kim, H. J., Oh, T. K., Shin, C. S., Lee, J. S., Kim, S. J., Lee, J. K. (2005). Analyses of enzyme II gene mutants for sugar transport and heterologous expression of fructokinase gene in *Corynebacterium glutamicum* ATCC 13032. *FEMS Microbiol Lett*, 244, 259-66.

Moon, M. W., Park, S. Y., Choi, S. K., Lee, J. K. (2007). The phosphotransferase system of *Corynebacterium glutamicum*: features of sugar transport and carbon regulation. *J Mol Microbiol Biotechnol*, 12, 43-50.

Mora-Lugo, R., Stegmuller, J., Mack, M. (2019). Metabolic engineering of roseoflavin-overproducing microorganisms. *Microb Cell Fact*, 18, 146.

Morabbi Heravi, K., Altenbuchner, J. (2018). Cross Talk among Transporters of the Phosphoenolpyruvate-Dependent Phosphotransferase System in *Bacillus subtilis*. *J Bacteriol*, 200.

Mussatto, S. I., Roberto, I. C. (2004). Alternatives for detoxification of diluted-acid lignocellulosic hydrolyzates for use in fermentative processes: a review. *Bioresour Technol*, 93, 1-10.

Napoleon, E. R. (1997). Improving the receptivity of PVC articles toward water-based inks, coatings, or adhesives. *Journal of Vinyl and Additive Technology*, 3, 145-150.

Naqvi, M., Yan, J. (2015). First-Generation Biofuels. Handbook of Clean Energy Systems. pp. 1-18.

Nentwich, S. S., Brinkrolf, K., Gaigalat, L., Huser, A. T., Rey, D. A., Mohrbach, T., Marin, K., Puhler, A., Tauch, A., Kalinowski, J. (2009). Characterization of the LacI-type transcriptional repressor RbsR controlling ribose transport in *Corynebacterium glutamicum* ATCC 13032. *Microbiology*, 155, 150-164.

Neuner, A., Heinzle, E. (2011). Mixed glucose and lactate uptake by *Corynebacterium glutamicum* through metabolic engineering. *Biotechnol J*, 6, 318-29.

Neuner, A., Wagner, I., Sieker, T., Ulber, R., Schneider, K., Peifer, S., Heinzle, E. (2013). Production of L-lysine on different silage juices using genetically engineered *Corynebacterium glutamicum*. *J Biotechnol*, 163, 217-24.

Nie, L., He, Y., Hu, L., Zhu, X., Wu, X., Zhang, B. (2022). Improvement in L-ornithine production from mannitol via transcriptome-guided genetic engineering in *Corynebacterium glutamicum*. *Biotechnol Biofuels Bioprod*, 15, 97.

Nielsen, P. H. (2017). Microbial biotechnology and circular economy in wastewater treatment. *Microb Biotechnol*, 10, 1102-1105.

Nigam, J. N. (2001). Ethanol production from wheat straw hemicellulose hydrolysate by *Pichia stipitis*. *J Biotechnol*, 87, 17-27.

Oh, E. J., Jin, Y. S. (2020). Engineering of *Saccharomyces cerevisiae* for efficient fermentation of cellulose. *FEMS Yeast Res*, 20.

Ohara, H. (2003). Biorefinery. *Appl Microbiol Biotechnol*, 62, 474-477.

Olson, D. G., McBride, J. E., Shaw, A. J., Lynd, L. R. (2012). Recent progress in consolidated bioprocessing. *Curr Opin Biotechnol*, 23, 396-405.

Pabby, A. K., Rizvi, S. S., Requena, A. M. S. (2008). Handbook of membrane separations: chemical, pharmaceutical, food, and biotechnological applications. *CRC press*.

Palmqvist, E., Grage, H., Meinander, N. Q., Hahn-Hagerdal, B. (1999). Main and interaction effects of acetic acid, furfural, and p-hydroxybenzoic acid on growth and ethanol productivity of yeasts. *Biotechnol Bioeng*, 63, 46-55.

Palmqvist, E., Hahn-Hägerdal, B. (2000a). Fermentation of lignocellulosic hydrolysates. I: inhibition and detoxification. *Bioresour Technol*, 74, 17-24.

Palmqvist, E., Hahn-Hägerdal, B. (2000b). Fermentation of lignocellulosic hydrolysates. II: inhibitors and mechanisms of inhibition. *Bioresour Technol*, 74, 25-33.

Palmqvist, E., Hahn-Hägerdal, B., Szengyel, Z., Zacchi, G., Rèczey, K. (1997). Simultaneous detoxification and enzyme production of hemicellulose hydrolysates obtained after steam pretreatment. *Enzyme and Microbial Technology*, 20, 286-293.

Pandey, A., Soccol, C. R., Nigam, P., Soccol, V. T. (2000). Biotechnological potential of agro-industrial residues. I: sugarcane bagasse. *Bioresour Technol*, 74, 69-80.

Papagianni, M., Anastasiadou, S. (2009). Pediocins: The bacteriocins of Pediococci. Sources, production, properties and applications. *Microb Cell Fact*, 8, 3.

Parajó, J. C., Dominguez, H., Domínguez, J. M. (1997). Improved xylitol production with *Debaryomyces hansenii* Y-7426 from raw or detoxified wood hydrolysates. *Enzyme and Microbial Technology*, 21, 18-24.

Parche, S., Burkovski, A., Sprenger, G. A., Weil, B., Krämer, R., Titgemeyer, F. (2001). *Corynebacterium glutamicum*: a dissection of the PTS. *J Mol Microbiol Biotechnol*, 3, 423-428.

Paris, G., Berlinguet, L., Gaudry, R., English Jr., J., Dayan, J. E. (2003). Glutaric Acid and Glutarimide. Organic Syntheses. pp. 47-47.

Park, S. D., Lee, J. Y., Sim, S. Y., Kim, Y., Lee, H. S. (2007). Characteristics of methionine production by an engineered *Corynebacterium glutamicum* strain. *Metab Eng*, 9, 327-36.

Park, S. J., Kim, E. Y., Noh, W., Park, H. M., Oh, Y. H., Lee, S. H., Song, B. K., Jegal, J., Lee, S. Y. (2013). Metabolic engineering of *Escherichia coli* for the production of 5-aminovalerate and glutarate as C5 platform chemicals. *Metab Eng*, 16, 42-7.

Pauli, S., Kohlstedt, M., Lamber, J., Weiland, F., Becker, J., Wittmann, C. (2023). Systems metabolic engineering upgrades *Corynebacterium glutamicum* for selective high-level production of the chiral drug precursor and cell-protective extremolyte L-pipecolic acid. *Metab Eng*.

Peng, X., Okai, N., Vertes, A. A., Inatomi, K., Inui, M., Yukawa, H. (2011). Characterization of the mannitol catabolic operon of *Corynebacterium glutamicum*. *Appl Microbiol Biotechnol*, 91, 1375-87.

Pereira, S. R., Ivanusa, S., Evtuguin, D. V., Serafim, L. S., Xavier, A. M. (2012). Biological treatment of eucalypt spent sulphite liquors: a way to boost the production of second generation bioethanol. *Bioresour Technol*, 103, 131-5.

Pereira, S. R., Portugal-Nunes, D. J., Evtuguin, D. V., Serafim, L. S., Xavier, A. M. R. B. (2013). Advances in ethanol production from hardwood spent sulphite liquors. *Process Biochemistry*, 48, 272-282.

Pereira, S. R., Sanchez, I. N. V., Frazao, C. J., Serafim, L. S., Gorwa-Grauslund, M. F., Xavier, A. M. (2015). Adaptation of *Scheffersomyces stipitis* to hardwood spent sulfite liquor by evolutionary engineering. *Biotechnol Biofuels*, 8, 50.

Perez-Garcia, F., Burgardt, A., Kallman, D. R., Wendisch, V. F., Bar, N. (2021). Dynamic Co-Cultivation Process of Corynebacterium glutamicum Strains for the Fermentative Production of Riboflavin. *Fermentation-Basel*, 7.

Perez-Garcia, F., Max Risse, J., Friehs, K., Wendisch, V. F. (2017a). Fermentative production of L-pipecolic acid from glucose and alternative carbon sources. *Biotechnol J*, 12.

Perez-Garcia, F., Ziert, C., Risse, J. M., Wendisch, V. F. (2017b). Improved fermentative production of the compatible solute ectoine by *Corynebacterium glutamicum* from glucose and alternative carbon sources. *J Biotechnol*, 258, 59-68.

Perez, J., Munoz-Dorado, J., de la Rubia, T., Martinez, J. (2002). Biodegradation and biological treatments of cellulose, hemicellulose and lignin: an overview. *Int Microbiol*, 5, 53-63.

Peters, D. (2007). Raw materials. *Adv Biochem Eng Biotechnol*, 105, 1-30.

Pfeifer, E., Gatgens, C., Polen, T., Frunzke, J. (2017). Adaptive laboratory evolution of *Corynebacterium glutamicum* towards higher growth rates on glucose minimal medium. *Sci Rep*, 7, 16780.

Pitkanen, J. P., Rintala, E., Aristidou, A., Ruohonen, L., Penttila, M. (2005). Xylose chemostat isolates of *Saccharomyces cerevisiae* show altered metabolite and enzyme levels compared with xylose, glucose, and ethanol metabolism of the original strain. *Appl Microbiol Biotechnol*, 67, 827-37.

Poblete-Castro, I., Hoffmann, S. L., Becker, J., Wittmann, C. (2020). Cascaded valorization of seaweed using microbial cell factories. *Curr Opin Biotechnol*, 65, 102-113.

Porru, D., Parmigiani, A., Tinelli, C., Barletta, D., Choussos, D., Di Franco, C., Bobbi, V., Bassi, S., Miller, O., Gardella, B. (2014). Oral D-mannose in recurrent urinary tract infections in women: A pilot study. *Journal of Clinical Urology*, 7, 208-213.

Power, J. (1967). The L-rhamnose genetic system in *Escherichia coli* K-12. *Genetics*, 55, 557-68.

Prassas, I., Diamandis, E. P. (2008). Novel therapeutic applications of cardiac glycosides. *Nat Rev Drug Discov*, 7, 926-35.

Qin, L., Liu, Z. H., Li, B. Z., Dale, B. E., Yuan, Y. J. (2012). Mass balance and transformation of corn stover by pretreatment with different dilute organic acids. *Bioresour Technol*, 112, 319-26.

Radek, A., Krumbach, K., Gatgens, J., Wendisch, V. F., Wiechert, W., Bott, M., Noack, S., Marienhagen, J. (2014). Engineering of *Corynebacterium glutamicum* for minimized carbon loss during utilization of D-xylose containing substrates. *J Biotechnol*, 192 Pt A, 156-60.

Radek, A., Tenhaef, N., Muller, M. F., Brusseler, C., Wiechert, W., Marienhagen, J., Polen, T., Noack, S. (2017). Miniaturized and automated adaptive laboratory evolution: Evolving *Corynebacterium glutamicum* towards an improved D-xylose utilization. *Bioresour Technol*, 245, 1377-1385.

Rafiqul, I., Sakinah, A. M. (2012). Design of process parameters for the production of xylose from wood sawdust. *Chemical Engineering Research and Design*, 90, 1307-1312.

Reinscheid, D. J., Schnicke, S., Rittmann, D., Zahnow, U., Sahm, H., Eikmanns, B. J. (1999). Cloning, sequence analysis, expression and inactivation of the *Corynebacterium glutamicum pta-ack* operon encoding phosphotransacetylase and acetate kinase. *Microbiology*, 145 (Pt 2), 503-513.

Rennie, E. A., Scheller, H. V. (2014). Xylan biosynthesis. *Curr Opin Biotechnol*, 26, 100-7.

Restolho, J. A., Prates, A., de Pinho, M. N., Afonso, M. D. (2009). Sugars and lignosulphonates recovery from eucalyptus spent sulphite liquor by membrane processes. *Biomass and Bioenergy*, 33, 1558-1566.

Revelles, O., Espinosa-Urgel, M., Fuhrer, T., Sauer, U., Ramos, J. L. (2005). Multiple and interconnected pathways for L-lysine catabolism in *Pseudomonas putida* KT2440. *J Bacteriol*, 187, 7500-10.

Rittmann, D., Lindner, S. N., Wendisch, V. F. (2008). Engineering of a glycerol utilization pathway for amino acid production by *Corynebacterium glutamicum*. *Appl Environ Microbiol*, 74, 6216-22.

Rodrigues, R. C. L. B., Lu, C., Lin, B., Jeffries, T. W. Fermentation Kinetics for Xylitol Production by a *Pichia stipitis* D-Xylulokinase Mutant Previously Grown in Spent Sulfite Liquor. In: Adney, W. S., McMillan, J. D., Mielenz, J., Klasson, K. T., Eds.), Biotechnology for Fuels and Chemicals. *Humana Press*, Totowa, NJ, (2008), pp. 717-727.

Rodriguez, J. M., Martinez, M. I., Kok, J. (2002). Pediocin PA-1, a wide-spectrum bacteriocin from lactic acid bacteria. *Crit Rev Food Sci Nutr*, 42, 91-121.

Rødsrud, G., Lersch, M., Sjöde, A. (2012). History and future of world's most advanced biorefinery in operation. *Biomass and Bioenergy*, 46, 46-59.

Rohles, C., Pauli, S., Giesselmann, G., Kohlstedt, M., Becker, J., Wittmann, C. (2022). Systems metabolic engineering of *Corynebacterium glutamicum* eliminates all by-products for selective and high-yield production of the platform chemical 5-aminovalerate. *Metab Eng*, 73, 168-181.

Rohles, C. M., Giesselmann, G., Kohlstedt, M., Wittmann, C., Becker, J. (2016). Systems metabolic engineering of *Corynebacterium glutamicum* for the production of the carbon-5 platform chemicals 5-aminovalerate and glutarate. *Microb Cell Fact*, 15, 154.

Rohles, C. M., Gläser, L., Kohlstedt, M., Gießelmann, G., Pearson, S., del Campo, A., Becker, J., Wittmann, C. (2018). A bio-based route to the carbon-5 chemical glutaric acid and to bionylon-6,5 using metabolically engineered *Corynebacterium glutamicum*. *Green Chemistry*, 20, 4662-4674.

Rojas, S. A. T., Schadeweg, V., Kirchner, F., Boles, E., Oreb, M. (2021). Identification of a glucose-insensitive variant of Gal2 from *Saccharomyces cerevisiae* exhibiting a high pentose transport capacity. *Sci Rep*, 11, 24404.

Roser, M., Josic, D., Kontou, M., Mosetter, K., Maurer, P., Reutter, W. (2009). Metabolism of galactose in the brain and liver of rats and its conversion into glutamate and other amino acids. *J Neural Transm (Vienna)*, 116, 131-9.

Ruan, H., Yu, H., Xu, J. (2020). The glucose uptake systems in *Corynebacterium glutamicum*: a review. *World J Microbiol Biotechnol*, 36, 126.

Rueda, C., Calvo, P. A., Moncalián, G., Ruiz, G., Coz, A. (2015). Biorefinery options to valorize the spent liquor from sulfite pulping. *Journal of Chemical Technology & Biotechnology*, 90, 2218-2226.

Rumbold, K., van Buijsen, H. J., Overkamp, K. M., van Groenestijn, J. W., Punt, P. J., van der Werf, M. J. (2009). Microbial production host selection for converting second-generation feedstocks into bioproducts. *Microb Cell Fact*, 8, 64.

Ryu, K. S., Kim, C., Kim, I., Yoo, S., Choi, B. S., Park, C. (2004). NMR application probes a novel and ubiquitous family of enzymes that alter monosaccharide configuration. *J Biol Chem*, 279, 25544-8.

Salkovic-Petrisic, M., Osmanovic-Barilar, J., Knezovic, A., Hoyer, S., Mosetter, K., Reutter, W. (2014). Long-term oral galactose treatment prevents cognitive deficits in male Wistar rats treated intracerebroventricularly with streptozotocin. *Neuropharmacology*, 77, 68-80.

Sasaki, M., Jojima, T., Inui, M., Yukawa, H. (2008). Simultaneous utilization of D-cellobiose, D-glucose, and D-xylose by recombinant *Corynebacterium glutamicum* under oxygen-deprived conditions. *Appl Microbiol Biotechnol*, 81, 691-9.

Sasaki, M., Jojima, T., Kawaguchi, H., Inui, M., Yukawa, H. (2009). Engineering of pentose transport in *Corynebacterium glutamicum* to improve simultaneous utilization of mixed sugars. *Appl Microbiol Biotechnol*, 85, 105-15.

Sasaki, M., Teramoto, H., Inui, M., Yukawa, H. (2011). Identification of mannose uptake and catabolism genes in *Corynebacterium glutamicum* and genetic engineering for simultaneous utilization of mannose and glucose. *Appl Microbiol Biotechnol*, 89, 1905-16.

Sato, N., Kishida, M., Nakano, M., Hirata, Y., Tanaka, T. (2020). Metabolic Engineering of Shikimic Acid-Producing *Corynebacterium glutamicum* From Glucose and Cellobiose Retaining Its Phosphotransferase System Function and Pyruvate Kinase Activities. *Frontiers in Bioengineering and Biotechnology*, 8, 569406.

Sawada, H., Takagi, Y. (1964). The Metabolism of L-Rhamnose in *Escherichia Coli*. 3. L-Rhamulose-Phosphate Aldolase. *Biochim Biophys Acta*, 92, 26-32.

Schafer, A., Schwarzer, A., Kalinowski, J., Puhler, A. (1994). Cloning and characterization of a DNA region encoding a stress-sensitive restriction system from *Corynebacterium glutamicum* ATCC 13032 and analysis of its role in intergeneric conjugation with *Escherichia coli*. *J Bacteriol*, 176, 7309-19.

Schaffer, S., Weil, B., Nguyen, V. D., Dongmann, G., Gunther, K., Nickolaus, M., Hermann, T., Bott, M. (2001). A high-resolution reference map for cytoplasmic and membrane-associated proteins of *Corynebacterium glutamicum*. *Electrophoresis*, 22, 4404-22.

Scheer, E., Eggeling, L., Sahm, H. (1988). Improved D,L-α-hydroxybutyrate conversion to L-isoleucine with *Corynebacterium glutamicum* mutants with increased D-lactate utilization. *Appl Microbiol Biotechnol*, 28, 474-477.

Schneider, J., Niermann, K., Wendisch, V. F. (2011). Production of the amino acids L-glutamate, L-lysine, L-ornithine and L-arginine from arabinose by recombinant *Corynebacterium glutamicum*. *J Biotechnol*, 154, 191-8.

Schwarzer, A., Puhler, A. (1991). Manipulation of *Corynebacterium glutamicum* by gene disruption and replacement. *Biotechnology (N Y)*, 9, 84-7.

Seibold, G., Auchter, M., Berens, S., Kalinowski, J., Eikmanns, B. J. (2006). Utilization of soluble starch by a recombinant *Corynebacterium glutamicum* strain: growth and lysine production. *J Biotechnol*, 124, 381-91.

Seibold, G. M., Wurst, M., Eikmanns, B. J. (2009). Roles of maltodextrin and glycogen phosphorylases in maltose utilization and glycogen metabolism in *Corynebacterium glutamicum*. *Microbiology*, 155, 347-358.

Seiboth, B., Metz, B. (2011). Fungal arabinan and L-arabinose metabolism. *Appl Microbiol Biotechnol*, 89, 1665-73.

Sharkey, M. A., Maher, M. A., Guyonvarch, A., Engel, P. C. (2011). Kinetic characterisation of recombinant *Corynebacterium glutamicum* NAD^+-dependent LDH over-expressed in *E. coli* and its rescue of an *lldD*$^-$ phenotype in *C. glutamicum*: the issue of reversibility re-examined. *Arch Microbiol*, 193, 731-40.

Shaw, A. J., Lam, F. H., Hamilton, M., Consiglio, A., MacEwen, K., Brevnova, E. E., Greenhagen, E., LaTouf, W. G., South, C. R., van Dijken, H., Stephanopoulos, G. (2016). Metabolic engineering of microbial competitive advantage for industrial fermentation processes. *Science*, 353, 583-6.

Shen, J., Chen, J., Jensen, P. R., Solem, C. (2019). Development of a novel, robust and cost-efficient process for valorizing dairy waste exemplified by ethanol production. *Microb Cell Fact*, 18, 51.

Shen, X.-H., Huang, Y., Liu, S.-J. (2005). Genomic analysis and identification of catabolic pathways for aromatic compounds in *Corynebacterium glutamicum*. *Microbes and environments*, 20, 160-167.

Sheng, Q., Wu, X., Jiang, Y., Li, Z., Wang, F., Zhang, B. (2021). Highly efficient biosynthesis of L-ornithine from mannitol by using recombinant *Corynebacterium glutamicum*. *Bioresour Technol*, 327, 124799.

Siebert, D., Wendisch, V. F. (2015). Metabolic pathway engineering for production of 1,2-propanediol and 1-propanol by *Corynebacterium glutamicum*. *Biotechnol Biofuels*, 8, 91.

Silva, M. M., Lidon, F. (2016). Food preservatives – An overview on applications and side effects. *Emirates Journal of Food and Agriculture*, 28, 366-373.

Siso, M. I. G. (1996). The biotechnological utilization of cheese whey: A review. *Bioresour Technol*, 57, 1-11.

Sjöman, E., Mänttäri, M., Nyström, M., Koivikko, H., Heikkilä, H. (2007). Separation of xylose from glucose by nanofiltration from concentrated monosaccharide solutions. *Journal of Membrane Science*, 292, 106-115.

Sjöström, E. (1993). Chapter 10 - Wood-based Chemicals and Pulping By-products. In: Sjöström, E., (Ed.), Wood Chemistry (Second Edition). *Academic Press*, San Diego, pp. 225-248.

Song, Y., Matsumoto, K., Tanaka, T., Kondo, A., Taguchi, S. (2013). Single-step production of polyhydroxybutyrate from starch by using alpha-amylase cell-surface displaying system of *Corynebacterium glutamicum*. *J Biosci Bioeng*, 115, 12-4.

Speece, R. E. (1983). Anaerobic biotechnology for industrial wastewater treatment. *Environmental Science & Technology*, 17, 416A-427A.

Stackebrandt, E., Rainey, F. A., Ward-Rainey, N. L. (1997). Proposal for a new hierarchic classification system, Actinobacteria classis nov. *International journal of systematic bacteriology*, 47, 479-491.

Stansen, C., Uy, D., Delaunay, S., Eggeling, L., Goergen, J. L., Wendisch, V. F. (2005). Characterization of a *Corynebacterium glutamicum* lactate utilization operon induced during temperature-triggered glutamate production. *Appl Environ Microbiol*, 71, 5920-8.

Straathof, A. J., Panke, S., Schmid, A. (2002). The production of fine chemicals by biotransformations. *Curr Opin Biotechnol*, 13, 548-56.

Strelkov, S., von Elstermann, M., Schomburg, D. (2004). Comprehensive analysis of metabolites in *Corynebacterium glutamicum* by gas chromatography/mass spectrometry. *Biol Chem*, 385, 853-61.

Subedi, K. P., Kim, I., Kim, J., Min, B., Park, C. (2008). Role of GldA in dihydroxyacetone and methylglyoxal metabolism of *Escherichia coli* K12. *FEMS Microbiol Lett*, 279, 180-7.

Sun, S., Cao, X., Sun, R. (2016). The role of pretreatment in improving the enzymatic hydrolysis of lignocellulosic materials. *Bioresour Technol*, 199, 49-58.

Sun, T., Altenbuchner, J. (2010). Characterization of a mannose utilization system in *Bacillus subtilis*. *J Bacteriol*, 192, 2128-39.

Takagi, Y., Sawada, H. (1964a). The Metabolism of L-Rhamnose in *Escherichia Coli*. I. L-Rhamnose Isomerase. *Biochim Biophys Acta*, 92, 10-7.

Takagi, Y., Sawada, H. (1964b). The Metabolism of L-Rhamnose in *Escherichia Coli*. Ii. L-Rhamnulose Kinase. *Biochim Biophys Acta*, 92, 18-25.

Takahashi, H., Kobayashi, Y., Kaneko, N. (1983). Conformational studies of DL-lactaldehyde by ^{1}H-NMR, Raman and i.r. spectroscopy. *Spectrochimica Acta Part A: Molecular Spectroscopy*, 39, 569-572.

Takahashi, S., Tanifuji, K., Shiell, K., Fatehi, P., Jahan, M. S., Ohi, H., Ni, Y. (2013). Removal of Acetic Acid from Spent Sulfite Liquor Using Anion Exchange Resin for Effective Xylose Fermentation with *Pichia stipitis*. *Bioresources*, 8, 2417-2428.

Tangney, M., Mitchell, W. J. (2000). Analysis of a catabolic operon for sucrose transport and metabolism in *Clostridium acetobutylicum* ATCC 824. *J Mol Microbiol Biotechnol*, 2, 71-80.

Tate, C. G., Muiry, J., Henderson, P. (1992). Mapping, cloning, expression, and sequencing of the *rhaT* gene, which encodes a novel L-rhamnose-H^{+} transport protein in *Salmonella typhimurium* and *Escherichia coli*. *Journal of Biological Chemistry*, 267, 6923-6932.

Tateno, T., Fukuda, H., Kondo, A. (2007a). Direct production of L-lysine from raw corn starch by *Corynebacterium glutamicum* secreting *Streptococcus bovis* alpha-amylase using *cspB* promoter and signal sequence. *Appl Microbiol Biotechnol*, 77, 533-41.

Tateno, T., Fukuda, H., Kondo, A. (2007b). Production of L-lysine from starch by *Corynebacterium glutamicum* displaying alpha-amylase on its cell surface. *Appl Microbiol Biotechnol*, 74, 1213-20.

Tchieu, J. H., Norris, V., Edwards, J. S., Saier, M. H., Jr. (2001). The complete phosphotransferase system in *Escherichia coli*. *J Mol Microbiol Biotechnol*, 3, 329-46.

Thompson, J., Chassy, B. M. (1981). Uptake and metabolism of sucrose by *Streptococcus lactis*. *J Bacteriol*, 147, 543-51.

Tian, S.-Q., Zhao, R.-Y., Chen, Z.-C. (2018). Review of the pretreatment and bioconversion of lignocellulosic biomass from wheat straw materials. *Renewable and Sustainable Energy Reviews*, 91, 483-489.

Timell, T. Proceedings of the Eighth Cellulose Conference I. Wood Chemicals-A Future Challenge. *JOHN WILEY & SONS* New York, (1975).

Tsuchidate, T., Tateno, T., Okai, N., Tanaka, T., Ogino, C., Kondo, A. (2011). Glutamate production from beta-glucan using endoglucanase-secreting *Corynebacterium glutamicum*. *Appl Microbiol Biotechnol*, 90, 895-901.

Tsuge, Y., Hori, Y., Kudou, M., Ishii, J., Hasunuma, T., Kondo, A. (2014). Detoxification of furfural in *Corynebacterium glutamicum* under aerobic and anaerobic conditions. *Appl Microbiol Biotechnol*, 98, 8675-83.

Tsuge, Y., Yamamoto, S., Kato, N., Suda, M., Vertes, A. A., Yukawa, H., Inui, M. (2015). Overexpression of the phosphofructokinase encoding gene is crucial for achieving high production of D-lactate in *Corynebacterium glutamicum* under oxygen deprivation. *Appl Microbiol Biotechnol*, 99, 4679-89.

Tsunogai, S. (1971). Oxidation rate of sulfite in water and its bearing on the origin of sulfate in meteoric precipitation. *GEOCHEMICAL JOURNAL*, 5, 175-185.

Udaka, S. (1960). Screening method for microorganisms accumulating metabolites and its use in the isolation of *Micrococcus glutamicus*. *J Bacteriol*, 79, 754-5.

Ulbricht, R., J., Northup, S., J., Thomas, J., A. (1984). A Review of 5-Hydroxymethylfurfural (HMF) in Parenteral Solutions. *Toxicological Sciences*, 4, 843-853.

Umu, O. C. O., Rudi, K., Diep, D. B. (2017). Modulation of the gut microbiota by prebiotic fibres and bacteriocins. *Microb Ecol Health Dis*, 28, 1348886.

Unthan, S., Baumgart, M., Radek, A., Herbst, M., Siebert, D., Bruhl, N., Bartsch, A., Bott, M., Wiechert, W., Marin, K., Hans, S., Kramer, R., Seibold, G., Frunzke, J., Kalinowski, J., Ruckert, C., Wendisch, V. F., Noack, S. (2015). Chassis organism from *Corynebacterium glutamicum*--a top-down approach to identify and delete irrelevant gene clusters. *Biotechnol J*, 10, 290-301.

Ur-Rehman, S., Mushtaq, Z., Zahoor, T., Jamil, A., Murtaza, M. A. (2015). Xylitol: a review on bioproduction, application, health benefits, and related safety issues. *Crit Rev Food Sci Nutr*, 55, 1514-28.

Vafaeezadeh, M., Hashemi, M. M. (2016). A non-cyanide route for glutaric acid synthesis from oxidation of cyclopentene in the ionic liquid media. *Process Safety and Environmental Protection*, 100, 203-207.

Van Dien, S. (2013). From the first drop to the first truckload: commercialization of microbial processes for renewable chemicals. *Curr Opin Biotechnol*, 24, 1061-8.

Vaňková, K., Polakovič, M. (2010). Optimization of single-column chromatographic separation of fructooligosaccharides. *Process Biochemistry*, 45, 1325-1329.

Venema, K., Kok, J., Marugg, J. D., Toonen, M. Y., Ledeboer, A. M., Venema, G., Chikindas, M. L. (1995). Functional analysis of the pediocin operon of *Pediococcus acidilactici* PAC1.0: PedB is the immunity protein and PedD is the precursor processing enzyme. *Mol Microbiol*, 17, 515-22.

Vishtal, A. G., Kraslawski, A. (2011). Challenges in industrial applications of technical lignins. *Bioresources*, 6, 3547-3568.

Vuilleumier, S. (1993). Worldwide production of high-fructose syrup and crystalline fructose. *The American journal of clinical nutrition*, 58, 733S-736S.

Wan, Y., Kertesz, M., Spitale, R. C., Segal, E., Chang, H. Y. (2011). Understanding the transcriptome through RNA structure. *Nat Rev Genet*, 12, 641-55.

Wang, C., Cai, H., Zhou, Z., Zhang, K., Chen, Z., Chen, Y., Wan, H., Ouyang, P. (2014). Investigation of *ptsG* gene in response to xylose utilization in *Corynebacterium glutamicum*. *J Ind Microbiol Biotechnol*, 41, 1249-58.

Wang, Z., Chan, S. H. J., Sudarsan, S., Blank, L. M., Jensen, P. R., Solem, C. (2016). Elucidation of the regulatory role of the fructose operon reveals a novel target for enhancing the NADPH supply in *Corynebacterium glutamicum*. *Metab Eng*, 38, 344-357.

Watson, N. E., Prior, B. A., Lategan, P. M., Lussi, M. (1984). Factors in acid treated bagasse inhibiting ethanol production from D-xylose by *Pachysolen tannophilus*. *Enzyme and Microbial Technology*, 6, 451-456.

Weickert, M. J., Adhya, S. (1993). The galactose regulon of *Escherichia coli*. *Mol Microbiol*, 10, 245-51.

Weiland, F., Barton, N., Kohlstedt, M., Becker, J., Wittmann, C. (2023). Systems metabolic engineering upgrades *Corynebacterium glutamicum* to high-efficiency cis, cis-muconic acid production from lignin-based aromatics. *Metab Eng*, 75, 153-169.

Weiland, F., Kohlstedt, M., Wittmann, C. (2022). Guiding stars to the field of dreams: Metabolically engineered pathways and microbial platforms for a sustainable lignin-based industry. *Metab Eng*, 71, 13-41.

Weimberg, R. (1961). Pentose Oxidation by *Pseudomonas fragi*. *Journal of Biological Chemistry*, 236, 629-635.

Weissgram, M., Gstottner, J., Lorantfy, B., Tenhaken, R., Herwig, C., Weber, H. K. (2015). Generation of PHB from Spent Sulfite Liquor Using Halophilic Microorganisms. *Microorganisms*, 3, 268-89.

Weixler, D., Berghoff, M., Ovchinnikov, K. V., Reich, S., Goldbeck, O., Seibold, G. M., Wittmann, C., Bar, N. S., Eikmanns, B. J., Diep, D. B., Riedel, C. U. (2022). Recombinant production of the lantibiotic nisin using *Corynebacterium glutamicum* in a two-step process. *Microb Cell Fact*, 21, 11.

Wendisch, V. F. (2003). Genome-wide expression analysis in *Corynebacterium glutamicum* using DNA microarrays. *J Biotechnol*, 104, 273-85.

Wendisch, V. F., de Graaf, A. A., Sahm, H., Eikmanns, B. J. (2000). Quantitative determination of metabolic fluxes during coutilization of two carbon sources: comparative analyses with *Corynebacterium glutamicum* during growth on acetate and/or glucose. *J Bacteriol*, 182, 3088-96.

Werle, P., Morawietz, M., Lundmark, S., Sörensen, K., Karvinen, E., Lehtonen, J. (2000). Alcohols, Polyhydric. Ullmann's Encyclopedia of Industrial Chemistry.

Westman, J. O., Franzen, C. J. (2015). Current progress in high cell density yeast bioprocesses for bioethanol production. *Biotechnol J*, 10, 1185-95.

Winkler, C., Frick, B., Schroecksnadel, K., Schennach, H., Fuchs, D. (2006). Food preservatives sodium sulfite and sorbic acid suppress mitogen-stimulated peripheral blood mononuclear cells. *Food Chem Toxicol*, 44, 2003-7.

Wittmann, C., Becker, J. (2007). The L-lysine story: from metabolic pathways to industrial production. Amino Acid Biosynthesis~ Pathways, Regulation and Metabolic Engineering. *Springer*, pp. 39-70.

Wittmann, C., Heinzle, E. (2001). Modeling and experimental design for metabolic flux analysis of lysine-producing *Corynebacteria* by mass spectrometry. *Metab Eng*, 3, 173-91.

Wittmann, C., Kiefer, P., Zelder, O. (2004). Metabolic fluxes in Corynebacterium glutamicum during lysine production with sucrose as carbon source. *Appl Environ Microbiol*, 70, 7277-87.

Wittmann, C., Weber, J., Betiku, E., Kromer, J., Bohm, D., Rinas, U. (2007). Response of fluxome and metabolome to temperature-induced recombinant protein synthesis in *Escherichia coli*. *J Biotechnol*, 132, 375-84.

Wittmann, C., Zeng, A. P., Deckwer, W. D. (1995). Growth inhibition by ammonia and use of a pH-controlled feeding strategy for the effective cultivation of *Mycobacterium chlorophenolicum*. *Appl Microbiol Biotechnol*, 44, 519-25.

Wolf, S., Becker, J., Tsuge, Y., Kawaguchi, H., Kondo, A., Marienhagen, J., Bott, M., Wendisch, V. F., Wittmann, C. (2021). Advances in metabolic engineering of *Corynebacterium glutamicum* to produce high-value active ingredients for food, feed, human health, and well-being. *Essays Biochem*, 65, 197-212.

Xavier, A. M., Correia, M. F., Pereira, S. R., Evtuguin, D. V. (2010). Second-generation bioethanol from eucalypt sulphite spent liquor. *Bioresour Technol*, 101, 2755-61.

Xing, R., Qi, W., Huber, G. W. (2011). Production of furfural and carboxylic acids from waste aqueous hemicellulose solutions from the pulp and paper and cellulosic ethanol industries. *Energy and Environmental Science*, 4, 2193-2205.

Xu, J., Zhang, J., Liu, D., Zhang, W. (2016). Increased glucose utilization and cell growth of Corynebacterium glutamicum by modifying the glucose-specific phosphotransferase system (PTS^{Glc}) genes. *Can J Microbiol*, 62, 983-992.

Xu, J. Z., Ruan, H. Z., Yu, H. B., Liu, L. M., Zhang, W. (2020). Metabolic engineering of carbohydrate metabolism systems in *Corynebacterium glutamicum* for improving the efficiency of L-lysine production from mixed sugar. *Microb Cell Fact*, 19, 39.

Xu, P., Luo, M. (2012). Xylose: Production, Consumption, and Health Benefits. *Nova Science Publishers*.

Yamamoto, S., Suda, M., Niimi, S., Inui, M., Yukawa, H. (2013). Strain optimization for efficient isobutanol production using *Corynebacterium glutamicum* under oxygen deprivation. *Biotechnol Bioeng*, 110, 2938-48.

Yang, F., Hanna, M. A., Sun, R. (2012). Value-added uses for crude glycerol--a byproduct of biodiesel production. *Biotechnol Biofuels*, 5, 13.

Yang, S. T., Silva, E. M. (1995). Novel products and new technologies for use of a familiar carbohydrate, milk lactose. *J Dairy Sci*, 78, 2541-62.

Yao, W., Chu, C., Deng, X., Zhang, Y., Liu, M., Zheng, P., Sun, Z. (2009). Display of alpha-amylase on the surface of *Corynebacterium glutamicum* cells by using NCgl1221 as the anchoring protein, and production of glutamate from starch. *Arch Microbiol*, 191, 751-9.

Yim, S. S., Choi, J. W., Lee, S. H., Jeon, E. J., Chung, W. J., Jeong, K. J. (2017). Engineering of *Corynebacterium glutamicum* for Consolidated Conversion of Hemicellulosic Biomass into Xylonic Acid. *Biotechnol J*, 12.

Yim, S. S., Choi, J. W., Lee, S. H., Jeong, K. J. (2016). Modular Optimization of a Hemicellulose-Utilizing Pathway in *Corynebacterium glutamicum* for Consolidated Bioprocessing of Hemicellulosic Biomass. *ACS Synth Biol*, 5, 334-43.

Yin, L., Hu, X., Xu, D., Ning, J., Chen, J., Wang, X. (2012). Co-expression of feedback-resistant threonine dehydratase and acetohydroxy acid synthase increase L-isoleucine production in *Corynebacterium glutamicum*. *Metab Eng*, 14, 542-50.

Yu, S., Wayman, M., Parekh, S. K. (1987). Fermentation to ethanol of pentose-containing spent sulphite liquor. *Biotechnol Bioeng*, 29, 1144-50.

Zahoor, A., Lindner, S. N., Wendisch, V. F. (2012). Metabolic engineering of *Corynebacterium glutamicum* aimed at alternative carbon sources and new products. *Comput Struct Biotechnol J*, 3, e201210004.

Zeitsch, K. J. (2000). The chemistry and technology of furfural and its many by-products. *Elsevier*.

Zha, J., Zang, Y., Mattozzi, M., Plassmeier, J., Gupta, M., Wu, X., Clarkson, S., Koffas, M. A. G. (2018). Metabolic engineering of *Corynebacterium glutamicum* for anthocyanin production. *Microb Cell Fact*, 17, 143.

Zhang, H. J., Fan, X. G., Qiu, X. L., Zhang, Q. X., Wang, W. Y., Li, S. X., Deng, L. H., Koffas, M. A., Wei, D. S., Yuan, Q. P. (2014). A novel cleaning process for industrial production of xylose in pilot scale from corncob by using screw-steam-explosive extruder. *Bioprocess Biosyst Eng*, 37, 2425-36.

Zhang, J., Geng, A., Yao, C., Lu, Y., Li, Q. (2012). Effects of lignin-derived phenolic compounds on xylitol production and key enzyme activities by a xylose utilizing yeast *Candida athensensis* SB18. *Bioresour Technol*, 121, 369-78.

Zhang, X., Yao, L., Xu, G., Zhu, J., Zhang, X., Shi, J., Xu, Z. (2017). Enhancement of fructose utilization from sucrose in the cell for improved L-serine production in engineered *Corynebacterium glutamicum*. *Biochemical Engineering Journal*, 118, 113-122.

Zhang, Z., Kuipers, G., Niemiec, L., Baumgarten, T., Slotboom, D. J., de Gier, J. W., Hjelm, A. (2015). High-level production of membrane proteins in *E. coli* BL21(DE3) by omitting the inducer IPTG. *Microb Cell Fact*, 14, 142.

Zhao, Y., Damgaard, A., Christensen, T. H. (2018). Bioethanol from corn stover–a review and technical assessment of alternative biotechnologies. *Progress in Energy and Combustion Science*, 67, 275-291.

Zheng, L., McClelland, D. J., Rehmann, K. M. S., Barnett, K. J., Huber, G. W., Klier, J. (2022). Bio-based 1,5-Pentanediol as a Replacement for Petroleum-Derived 1,6-Hexanediol for Polyester Polyols, Coatings, and Adhesives. *ACS Sustainable Chemistry & Engineering*, 10, 5781-5791.

Zhou, H., Cheng, J. S., Wang, B. L., Fink, G. R., Stephanopoulos, G. (2012). Xylose isomerase overexpression along with engineering of the pentose phosphate pathway and evolutionary engineering enable rapid xylose utilization and ethanol production by *Saccharomyces cerevisiae*. *Metab Eng*, 14, 611-22.

Zhu, N., Xia, H., Wang, Z., Zhao, X., Chen, T. (2013). Engineering of acetate recycling and citrate synthase to improve aerobic succinate production in *Corynebacterium glutamicum*. *PLoS One*, 8, e60659.

Zhu, Q., Zhang, X., Luo, Y., Guo, W., Xu, G., Shi, J., Xu, Z. (2015). L-Serine overproduction with minimization of by-product synthesis by engineered *Corynebacterium glutamicum*. *Appl Microbiol Biotechnol*, 99, 1665-73.

Zydney, A. L. (2016). Continuous downstream processing for high value biological products: A Review. *Biotechnol Bioeng*, 113, 465-75.